

NORTHWESTERN UNIVERSITY

Investigating How Membrane Mechanical Properties Affect the Expression, Folding, and Function of a Model
Mechanosensitive Channel Protein

A DISSERTATION

SUBMITTED TO THE GRADUATE SCHOOL

IN PARTIAL FULFILLMENT OF THE REQUIREMENTS

for the degree

DOCTOR OF PHILOSOPHY

Field of Interdisciplinary Biological Sciences

By

Miranda Lynn Jacobs

EVANSTON, ILLINOIS

June 2022

Abstract

Mechanosensation is an essential behavior for cellular health that depends on the interactions between the plasma membrane and stretch-activated ion channels. To date, a few studies have measured the effect of membrane composition on protein behaviors from folding to function. However, the relationship between membrane mechanical properties and these behaviors remains poorly understood. The objective of this thesis is to uncover the relationship between membrane properties and protein behavior. My central hypothesis is that by decreasing membrane elastic moduli, protein folding efficiency may be improved and the activation sensitivity of a model mechanosensitive channel may be decreased, and that this property can be modulated with membrane amphiphiles. To investigate this relationship, we turned to the mechanosensitive channel of large conductance (MscL). As MscL is activated by membrane tension, MscL activity is expected to be altered by membrane mechanical properties that alter tension propagation. First, we determined the relationship between membrane elasticity and membrane protein folding using cell-free protein expression systems, and synthetic vesicles constructed from non-natural amphiphiles to modify membrane properties. Through this study, we found that by decreasing the area expansion modulus of the membrane, MscL folding was improved. We then wondered how certain natural amphiphiles modulate membrane mechanical properties. Using micropipette aspiration techniques, we determined that polyunsaturated fatty acids decrease the area expansion modulus of pure phospholipid membranes. However, in the presence of high amounts of cholesterol, this relationship depends on fatty acid identity. Finally, we wondered how membrane mechanical properties impact MscL behavior. Using patch-clamp electrophysiology with an integrated pressure-transducer, we determined that MscL sensitivity was decreased in the presence of amphiphiles that decrease membrane area expansion modulus. The results of these studies contribute to a critical unmet need in the field of membrane mechanobiology and highlight the role of membrane area expansion modulus on membrane protein folding and function. Together, the studies in this thesis demonstrate an important role of membrane amphiphiles in modulating membrane biophysical properties through affecting membrane protein folding and function.

Acknowledgments

I would first like to thank my advisor, Prof. Neha Kamat for taking the risk of having me as her first student in the lab. When I joined, the lab was filled with so much hope but uncertainty as we all embarked on this journey together in science. Through Neha's guidance I learned many skills and topics that I would likely have not had the opportunity to learn otherwise. I joined the lab knowing barely anything about lipids or polymers and now I feel confident as a lipid membrane expert. I really enjoyed her mentorship style which gave the guidance to not get lost in the science but the freedom to choose what projects to pursue while holding me to a high standard which constantly challenged me. I also thank Neha for patiently mentoring me in other skills such as writing, making figures, and presenting. She really took the time to get me ready for anything I may need in my future career outside of graduate school. After going through many rotations and working in a couple labs before graduate school, I can easily say that Neha was the best fit for me as an advisor and I am so grateful I had the opportunity to be in her lab.

Next, I would like to thank individuals from my undergraduate research experiences who prepared me for graduate school. I can confidently say that I would not be in this position today without their mentorship. I thank Prof. Oscar Colamonici and Prof. John P. O'Bryan. I next would like to thank Dr. Mathew Perez-Neut and Emiliano Huesca who mentored me while I was in the Colamonici Lab, especially Mat who recommended me to Oscar and taught me many lab skills. I next want to thank the postdocs and graduate students of the O'Bryan lab who mentored me when I was preparing for graduate school applications. Thank you to Dr. Russell Spencer Smith, Dr. Angela Russo, Dr. Jacquelin Cobbert, Dr. Erika Herrero-Garcia, Priyanka Gajwani, and Dianicha Santana.

I would next like to thank my lab mates who have provided me with many good times and support through my PhD. I still remember attending my first campus event as the only student of the lab and feeling lonely as all my friends were spending time bonding with their lab mates. Shortly after this event, the lab began to

grow, and I was joined by Maggie Boyd, Justin Peruzzi and a year later, Tim Vu. Thank you all for making my graduate experience special and having many thoughtful scientific and non-scientific conversations. Through many happy hours, conferences, and events these people brought a lot of joy to my PhD experience. We were later joined by Taylor Gunnells, Dr. Jan Steinkühler, Citlayi Villaseñor, Vivian Hu, Mary Kelly, and Beth Dibiase who all brought their unique personalities and perspectives to the lab. Thanks to everyone in the Kamat lab for enhancing my PhD experience. I can easily say that I have learned something from each of you that I will take with me for the rest of my life. I would also like to thank one of our undergrads who served as an amazing support system to me during my PhD, Claire Hilburger. Even as an undergrad, she served as a mentor and great friend through the many challenges of graduate school.

I also want to thank Paul DeCaen for serving as a second mentor to me in my PhD and hosting me in his lab for the last three years to do electrophysiology. I would not have been able to complete my last paper without his guidance. I also want to thank all members of the DeCaen lab, Dr. Thuy Vien, Dr. Leo C.T. Ng, Dr. My Chau Ta, Megan Larmore, Dr. Louise Kimura, Dr. Ohri Esarte Palomero, and Eddie Guadarrama for welcoming me into their lab community and making me feel like I had a second home downtown.

I would next like to thank my friends in and out of graduate school. My friends at Northwestern have enriched my experience through scientific conversations and generally good times. Thank you to Luyi Cheng, Clare Harper, Megan Larmore, Deanna Badong, Chris Koo, Soo Ro, Candy Zhu, Nic Daffern, Brandon Liauw, Michael Schamber, and Clarence Chan for being the ones I could go to when I wanted to have fun, a fancy dinner, a wild concert, a good workout class, or when I just needed some support. I wanted to give a special shoutout to Chris who recommended I reach out to Neha when I was deciding which lab to join which changed the outcome of my PhD in ways I never imagined.

I would also like to thank my non-science friends for keeping me grounded. I would recommend to everyone to have friends outside of science as they really put what matters into perspective. Thank you to Dani

Convey, Evanne Offenbacker, and Maddie Archer-Burton for playing this role in my life. Finally, I would like to thank Vas for supporting me through my PhD. He was always there when I needed someone to talk to and was very patient when I was stressed but was always ready to celebrate even the smallest wins with me.

When I was choosing which university to pursue my PhD at, being close to my family was extremely important to me. I was elated to find out I was accepted into Northwestern's IBiS program because it meant I was able to live near my family. It was amazing having my parents and siblings nearby during graduate school so I could go home for a night or go to Costco on a random weekend. Last, I thank my grandparents for supporting me and always being proud of me. When I published my first paper my grandma had my aunt print it out for her so she could show her friends. I also thank my grandpa who was looking forward to reading this thesis but passed away before it was completed.

I am extremely grateful to have such an amazing support system in my mentors, peers, friends, and family and I could not have completed this thesis without this support system.

For my parents and grandparents

Table of Contents

| | |
|--|-----------|
| Abstract | 2 |
| Acknowledgments | 3 |
| List of Figures | 13 |
| List of Tables | 17 |
| 1. Introduction | 18 |
| 1.1 The plasma membrane as an active interface..... | 18 |
| Membrane mechanical properties are important for biological function..... | 18 |
| Bilayer vesicles as model systems to study biological membranes | 20 |
| Non-natural amphiphiles as lipid mimics | 21 |
| Membrane protein folding <i>in vivo</i> | 23 |
| Membrane protein folding in minimal systems for understanding protein folding <i>in vivo</i> | 24 |
| 1.2 Mechanosensitive channels | 25 |
| Stretch-activated ion channels are essential components of force sensing..... | 25 |
| The force-from-lipids mechanism of mechanosensitive channel activation | 29 |
| 1.3 Specific Aims | 30 |
| 1.4 Description of Thesis | 31 |
| 2. The role of membrane properties in membrane protein folding and function: a closer look at mechanosensitive channels | 36 |
| 2.1 Membrane composition controls membrane properties | 37 |

| | |
|---|-----------|
| Membrane organization to achieve heterogenous membrane properties within a single cell..... | 41 |
| 2.2 Membrane properties and protein folding..... | 44 |
| <i>In vitro</i> studies reveal membrane properties that are important for membrane protein folding..... | 44 |
| How <i>in vitro</i> studies relate to <i>in vivo</i> protein folding | 46 |
| 2.3 Membrane mechanical properties influence ion channel behavior..... | 47 |
| Bacterial mechanosensitive channels | 48 |
| Eukaryotic mechanosensitive channels | 50 |
| Piezo1 – a model mammalian mechanosensitive channel | 51 |
| 2.4 The relationship between optimal membrane composition in membrane protein folding and activity | 53 |
| 2.5 Conclusion..... | 58 |
| 3. Methods for lipid/polymer hybrid membrane preparation and co-translational insertion of a membrane protein..... | 59 |
| 3.1 Introduction..... | 60 |
| 3.2 Materials..... | 62 |
| 3.2.1 Hybrid vesicle preparation..... | 62 |
| 3.2.2 Vesicle purification | 63 |
| 3.2.3 Cell-free expression of a GFP-membrane protein into hybrid vesicles | 63 |
| 3.2.4 Assessment of membrane protein activity | 63 |
| 3.3 Methods..... | 64 |
| 3.3.1 Hybrid vesicle preparation..... | 64 |
| 3.3.2 Vesicle purification | 65 |
| 3.3.3 Cell-free expression of a GFP-membrane protein into hybrid vesicles | 66 |

| | |
|--|-----------|
| | 9 |
| 3.3.4 Assessment of membrane protein activity | 68 |
| 3.4 Notes | 70 |
| 3.5 Acknowledgements | 76 |
| 4. Determination of the role of membrane area expansion modulus and defects on the folding of the mechanosensitive channel of large conductance using hybrid membranes composed of diblock copolymers and phospholipids | 77 |
| 4.1 Significance | 78 |
| 4.2 Introduction..... | 79 |
| 4.3 Materials and Methods | 80 |
| 4.4 Results..... | 85 |
| Lipid vesicles increase production of a membrane protein. | 85 |
| Diblock copolymers enhance MscLGFP folding during cell-free protein synthesis..... | 88 |
| Increasing membrane elasticity improves membrane protein folding. | 97 |
| PEG headgroups prevent MscLGFP folding and insertion into membranes..... | 102 |
| The role of membrane defects in protein folding..... | 105 |
| 4.5 Discussion | 109 |
| 4.6 Acknowledgements | 116 |
| 5. The effect of polyunsaturated fatty acids on membrane mechanical properties | |
| 117 | |
| 5.1 Introduction..... | 118 |
| 5.2 Materials and Methods | 120 |

| | |
|--|------------|
| | 10 |
| 5.3 Results..... | 128 |
| ω -3 fatty acids increase membrane elasticity in the absence of cholesterol | 128 |
| EPA and DHA differentially affect membrane elasticity in the presence of high levels of cholesterol | 139 |
| Membrane phase-segregation behavior impacts elasticity with an alternate phospholipid composition | 154 |
| 5.4 Discussion | 156 |
| 5.5 Conclusion..... | 160 |
| 5.6 Acknowledgements | 161 |
| 6. Methods of membrane protein integration into giant bilayer vesicles for patch-clamp electrophysiology and micropipette aspiration techniques | 162 |
| 6.1 Cell-free protein synthesis into synthetic giant unilamellar vesicles | 163 |
| Protein production | 163 |
| GUV electroformation from SUVs containing protein | 163 |
| Challenges of using GUVs in high-pressure patch-clamp electrophysiology applications..... | 164 |
| 6.2 Giant spheroplasts..... | 165 |
| Spheroplast formation methods | 165 |
| Patch-clamp electrophysiology with pressure control for mechanosensitive channel activity measurements | 168 |
| Challenges of measuring MscL activation in spheroplasts | 170 |
| 6.3 Giant plasma membrane vesicles | 170 |
| 7. Probing the force-from-lipid mechanism with synthetic polymers | 172 |
| 7.1 Introduction..... | 173 |

| | |
|---|------------|
| | 11 |
| 7.2 Results..... | 175 |
| Poloxamer P124 desensitizes MscL | 187 |
| A detergent confirms the relationship between membrane properties and MscL activation | 193 |
| Various poloxamers reveal a relationship between K_A , k_c and MscL activation sensitivity | 197 |
| P124 does not alter MscL activity through pore occlusion or changes in membrane thickness | 197 |
| Trek1 confirms the relationship between K_A , k_c and <i>force-from-lipids</i> gating of mechanosensitive channels..... | 208 |
| 7.3 Discussion | 214 |
| 7.4 Conclusion..... | 217 |
| 7.5 Materials and Methods | 218 |
| Materials..... | 218 |
| Methods | 218 |
| 7.6 Acknowledgements | 223 |
| 8. Conclusions and future work..... | 225 |
| 8.1 Specific Aims | 225 |
| 8.2 Conclusions..... | 226 |
| Membrane elasticity is important for membrane protein folding..... | 226 |
| Polyunsaturated fatty acids reduce membrane elastic moduli | 227 |
| Membrane elastic properties are important for mechanosensitive channel function | 228 |
| 8.3 Future work..... | 229 |
| Membrane composition and membrane mechanical properties | 229 |
| The role of membrane properties in membrane protein folding | 230 |
| The relationship between mechanosensitive channels and membrane mechanical properties | 231 |

Membrane composition and the behavior of predominantly non-mechanosensitive membrane proteins
..... 233

References235

List of Figures

| | |
|---|----|
| Figure 1.1 K_A , k_c , and fluidity are important membrane properties in biological function..... | 20 |
| Figure 1.2 Nonnatural amphiphiles mimic phospholipids | 22 |
| Figure 1.3 Structure of MscL and MscS in a bilayer | 27 |
| Figure 1.4 Schematic outline of thesis..... | 32 |
| Figure 2.1. Membrane properties do not always equal the sum of their parts measured individually | 39 |
| Figure 2.2 Lipid rafts organize lipids and produce dynamic regions of differing membrane properties..... | 43 |
| Figure 2.3 Membrane protein insertion and folding prefers a softer, thinner, more fluid membrane environment..... | 46 |
| Figure 2.4 MscL activation is predominantly affected by membrane thickness..... | 49 |
| Figure 2.5 Piezo1 inactivation sensitivity is modulated by PUFAs | 52 |
| Figure 2.6 Protein trafficking is determined by transmembrane domain length..... | 56 |
| Figure 3.1 Vesicle purification schematic | 66 |
| Figure 3.2 Sample vesicle purification elution curve..... | 67 |
| Figure 3.3 MTSET calcein release assay | 68 |
| Figure 3.4 GFP fluorescence allows the observation of protein production and folding..... | 70 |
| Figure 4.1 Lipid vesicles improve the production of MscL during cell-free protein synthesis. | 86 |
| Figure 4.2 Lipid vesicles improve the folding of MscL during cell-free protein synthesis. | 87 |
| Figure 4.3 MscLGFP is active in lipid vesicles..... | 89 |
| Figure 4.4 PEO-b-PBD 1.8 kDa polymers aid MscLGFP folding..... | 90 |
| Figure 4.5 PEO-b-PBD 1.8 kDa and DOPC blend uniformly in hybrid vesicles..... | 91 |
| Figure 4.6 PEO-b-PBD 1.05 kDa improves MscLGFP folding in DOPC vesicles..... | 92 |
| Figure 4.7 MscLGFP yield varies with MscLGFP folding in a cell-free reaction containing vesicles. | 94 |
| Figure 4.8 Micropipette aspiration of hybrid polymer/lipid vesicles..... | 95 |
| Figure 4.9 Elastic moduli of DOPC vesicles containing various amphiphiles. | 98 |

| | |
|--|-----|
| Figure 4.10 Increasing membrane elasticity with a membrane-additive improves MscLGFP folding..... | 99 |
| Figure 4.11 Calcein leakage assay to assess vesicle stability. | 100 |
| Figure 4.12 C ₁₂ E ₈ alone does not facilitate membrane protein folding and at high concentrations disrupts vesicle formation..... | 101 |
| Figure 4.13 PEG-modified lipids decrease MscLGFP folding efficiency..... | 103 |
| Figure 4.14 Cholesterol incorporation in DOPC vesicles decreases MscLGFP folding. | 104 |
| Figure 4.15 Hybrid membranes contain a larger fraction of membrane defects..... | 106 |
| Figure 4.16 Example kinetic traces for NBD dithionite quenching membrane permeability assay..... | 107 |
| Figure 4.17 NBD photobleaching control in the absence of sodium dithionite | 108 |
| Figure 4.18 PEO-b-PBD 1.8 kDa decreases membrane fluidity..... | 110 |
| Figure 4.19 MscLGFP folding into vesicle membranes depends on the available folding area and steric repulsion. | 113 |
| Figure 4.20 Channelrhodopsin-2 GFP (ChR2GFP) folding improves with PEO-b-PBD 1.8 kDa. | 114 |
| Figure 5.1 Apparent area expansion moduli (K_{app}) of model membranes containing non-esterified fatty acids..... | 130 |
| Figure 5.2 Spectroscopic analysis of fatty acid oxidation. | 132 |
| Figure 5.3 Sample micropipette aspiration stress/ strain curve. | 133 |
| Figure 5.4 Fatty acid incorporation amounts differ based on fatty acid identity..... | 134 |
| Figure 5.5 Effect of the number and position of unsaturated bonds in non-esterified PUFAs on K_{app} | 137 |
| Figure 5.6 Fatty acids increase membrane fluidity. | 138 |
| Figure 5.7 DHA and EPA have distinct effects on the K_{app} of membranes with cholesterol nanodomains | 141 |
| Figure 5.8 FRET standard curve used to calculate relative surface area changes in vesicles..... | 142 |
| Figure 5.9 In the absence of domains, EPA and DHA affect vesicle surface area similarly..... | 142 |
| Figure 5.10 Determination of membrane fatty acid composition in ternary mixtures with POPC and cholesterol. | 146 |

| | |
|--|-----|
| Figure 5.11 Cholesterol is similarly incorporated into membranes containing different fatty acids. | 147 |
| Figure 5.12 Melting temperature of membranes is below ambient temperature and a phase transition is not expected during aspiration measurements | 148 |
| Figure 5.13 DHA increases the fluidity of membranes containing cholesterol..... | 151 |
| Figure 5.14 Assessing the generality of the effect of cholesterol content on FFA-induced changes in K_{app} | 155 |
| Figure 6.1 GUVs formed from the dry dot method incorporate proteins expressed into SUVs in cell-free reactions. | 164 |
| Figure 6.2 Fluorescence images of spheroplasts overexpressing MscLGFP..... | 167 |
| Figure 6.3 Patch clamp electrophysiology demonstrates activity of MscLGFP overexpressed in spheroplasts. | 169 |
| Figure 7.1 Patch-clamp electrophysiology of giant plasma membrane vesicles (GPMVs) measures MscL pressure sensitivity. | 177 |
| Figure 7.2 U2OS cell lines stably expressing MscLGFP | 178 |
| Figure 7.3 GPMVs budding off U2OS cells | 179 |
| Figure 7.4 Schematic and properties of amphiphiles used in this study..... | 180 |
| Figure 7.5 Sample data analysis workflow | 182 |
| Figure 7.6 Example results of full traces of MscL and no MscL recordings..... | 183 |
| Figure 7.7 MscL(G22S)mEGFP reduces the pressure required for activation compared to MscLmEGFP (WT), but does not change channel conductance | 184 |
| Figure 7.8 Differing GPMV formation methods yield similar MscL activation pressures, but crosslinking reagents reduce the probability of channel opening | 185 |
| Figure 7.9 Lysophosphatidylcholine (LPC) activation confirms MscL behavior in GPMVs formed from U2OS cells..... | 186 |
| Figure 7.10 Poloxamer P124 decreases MscL sensitivity. | 188 |
| Figure 7.11 P124 prevents MscL activation at high concentrations | 189 |

| | |
|---|-----|
| Figure 7.12 Micropipette sample aspiration curve of a GPMV membrane | 190 |
| Figure 7.13 Poloxamer incubation time alters poloxamer effect on membrane properties..... | 191 |
| Figure 7.14 P124 Effect on membrane fluidity..... | 192 |
| Figure 7.15 Poloxamer P124 alters GPMV mechanical properties | 194 |
| Figure 7.16 C ₁₂ E ₈ effect on MscL activation pressure, K _A , k _c , and fluidity | 195 |
| Figure 7.17 A non-ionic detergent decreases MscL sensitivity and alters membrane properties similar to poloxamer | 196 |
| Figure 7.18 Poloxamer effect on membrane stability | 198 |
| Figure 7.19 MscL activation sensitivity in the presence of various alternate poloxamers | 199 |
| Figure 7.20 Other poloxamer effect on K _A k _c and fluidity | 200 |
| Figure 7.21 Membrane area expansion modulus and bending rigidity are good predictors for MscL pressure sensitivity | 201 |
| Figure 7.22 Poloxamer does not impact MscL through pore occlusion or membrane thickness changes | 202 |
| Figure 7.23 Validation of GPMV calcium influx assay | 204 |
| Figure 7.24 MscL(G22C)GFP pressure sensitivity is restored in the presence of DTT | 205 |
| Figure 7.25 GPMV diameter increases in the presence of various poloxamers and a detergent..... | 207 |
| Figure 7.26 Trek-1 activation is also predicted by membrane properties. | 210 |
| Figure 7.27 U2OS cells stably expressing mTrek1..... | 211 |
| Figure 7.28 Trek1 GFP is retained in GPMV membranes | 212 |
| Figure 7.29 Trek1 mechanosensitive currents are only observed in GPMVs formed from stable cells expressing Trek1 | 213 |

List of Tables

| | |
|--|-----|
| Table 2.1 Common membrane amphiphiles and their impact on membrane structure and properties | 40 |
| Table 4.1 Area expansion moduli of giant unilamellar vesicles. | 96 |
| Table 5.1 Lipidomic analysis quantifies membrane compositions used for micropipette aspiration. | 131 |
| Table 5.2 K_{app} values of fatty acid/ DOPC blended membranes..... | 136 |
| Table 5.3 K_{app} values for DOPC membranes containing fatty acids and cholesterol domains. | 140 |
| Table 5.4 Comparison of phase transition temperatures for vesicles composed of DOPC and 1:1 DOPC and cholesterol | 149 |
| Table 5.5 k_c values for fatty acid and cholesterol-containing membranes. | 152 |
| Table 5.6 Comparison of k_c measurements obtained by the flickering spectroscopy method and micropipette aspiration..... | 153 |
| Table 5.7 K_{app} values of POPC, cholesterol, and fatty acid membranes..... | 156 |

Chapter 1

1. Introduction

1.1 The plasma membrane as an active interface

The cellular plasma membrane is an active participant in cellular function. Through various concerted interactions between lipids and proteins, the plasma membrane is able to sense and respond to internal and external stimuli to protect the needs of the cell. It was originally assumed that proteins were the sole active molecules in these processes and were scaffolded by the lipid bilayer. However, the importance of lipids in these processes has been increasingly demonstrated. Recent advances have revealed that lipids modulate a variety of membrane proteins through folding and localization to proper function. The work in this thesis explores this relationship with a goal of deepening the understanding of how lipids impact membrane properties and how these changes influence protein behavior.

Membrane mechanical properties are important for biological function

Mechanical stress occurs during many cellular processes such as motility and cell division. In order to communicate over long ranges within the cell, membrane tension is propagated in some cell types (1). As

a result of this tension propagation, the transduction of mechanical signals into biochemical outputs occurs through various mechanosensory proteins. The influence of the membrane environment on these interactions has highlighted the importance of lipid composition in cellular homeostasis and has drawn attention to the influence of membrane mechanics on various behaviors of membrane proteins (2).

Membrane properties are tightly controlled in biological systems to confer mechanical stability and modulate how the membrane interacts with its surroundings. Cells sense and control their membrane compositions through membrane proteins such as flippases and floppases, fatty acid transporters and cholesterol sensors such as SCAP (3). The control of membrane properties is presumed to be important for various cellular processes such as membrane protein folding and mechanotransduction. In addition to the interactions with mechanosensory proteins, the membrane environment is also known to influence the behavior of non-mechanosensory membrane proteins through specific and non-specific interactions (4). A more detailed description of membrane properties and the influence of membrane amphiphiles can be found in **Chapter 2** but it is important to note that membrane composition and properties are critical for the proper function of the cell.

The cell membrane is comprised of a very diverse lipidome and these lipids together determine the material properties of the bilayer (5). The primary membrane components are phospholipids, sterols, and sphingolipids. Sterols were presumed to be the primary modulator of membrane properties through interactions with phospholipids (6, 7). However, recent evidence has demonstrated that other amphiphiles in the bilayer play a role in modulating membrane properties. One class of such amphiphiles are polyunsaturated fatty acids (PUFAs) which are found in high abundance in organisms which reside in cold environments and are hypothesized to be important for maintaining membrane properties within biological ranges at extreme temperatures. Some properties that PUFAs have been hypothesized to alter include increased membrane fluidity and membrane elastic properties such as area expansion modulus (K_A) and bending stiffness (k_c) (Figure 1.1) (8). However, the direct impact of these amphiphiles on membrane

properties has been poorly characterized. One goal of this thesis is to measure how changes in PUFAs impact membrane mechanics which are important for biological functions such as protein folding and ion channel activity.

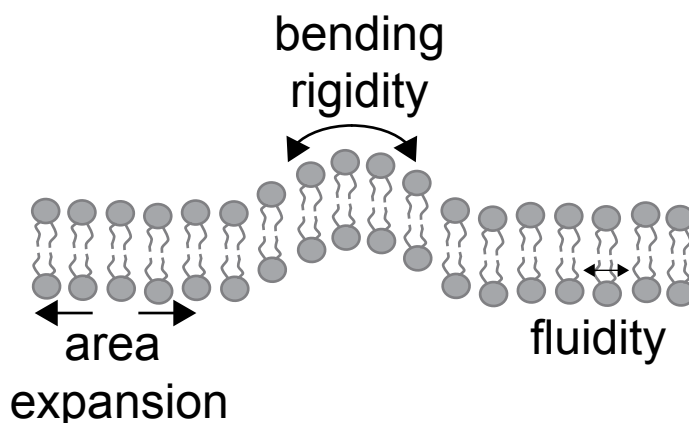


Figure 1.1 K_A , k_c , and fluidity are important membrane properties in biological function

Membrane properties which are important for cellular behavior include area expansion (K_A), bending stiffness (k_c), and fluidity. These properties are expected to influence the interactions between the membrane and embedded proteins to modulate protein activity. The work in this thesis explores the relationship between these membrane properties and membrane protein folding and the function of mechanosensitive channels.

Bilayer vesicles as model systems to study biological membranes

Bilayer vesicles mimic the basic structure of a cellular membrane and are often used in the characterization of proteins in minimal membrane environment. Bilayer vesicles can be comprised of pure phospholipids or mixtures of cell-extracted lipids and offer complete tunability of membrane composition. As cellular membranes are often integrated with the cytoskeleton and extracellular matrix in mammalian cells or contain a cell wall in bacterial and plant cells, contributions from the bilayer alone are difficult to discern. However, bilayer vesicles lack these interactions and are useful in determining the mechanical properties of the bilayer and direct interactions between the bilayer and an embedded protein.

Membrane mechanical properties are readily measured in bilayer vesicles due to their spherical structure. Laplace's law states that the pressure inside a sphere is inversely proportional to the radius as long as the surface tension is presumed to change minimally. Vesicle membrane tension may be calculated using the following equation,

$$T = \frac{Pr}{2}$$

Where T is membrane tension, P is pressure applied to the membrane and r is vesicle or cylinder radius. Through this equation, membrane elastic properties can be calculated such as K_A , k_C , and lytic tension.

Non-natural amphiphiles as lipid mimics

Non-natural amphiphiles which self-assemble into bilayers allow for membrane properties to be modulated in new and unique ways. These amphiphiles offer increased chemical and physical stability and can be used to probe the effects of membrane properties in ways that lipids do not allow. In addition, non-natural amphiphiles are chemically distinct from lipids which enables the study of global membrane properties on biological functions aside from direct binding interactions. The non-natural amphiphiles used in this thesis include diblock copolymers and triblock copolymers (Ploxamers) which offer distinct features in the observation of the effect of membrane properties on protein behavior (Figure 1.2). First, diblock copolymers can self-assemble into bilayers and can mimic a membrane without lipids because of their cylindrical molecular shape (9). Diblock copolymers can also form hybrid membranes which have hybrid material properties such as the biological specificity of lipids with increased stability and a K_A much lower than what is possible with lipids alone (10). In this thesis, diblock copolymers were used to observe the impact of K_A on membrane protein folding in a minimal system and demonstrated the ability of a protein to fold directly into a non-natural membrane. In contrast, triblock copolymers do not usually form bilayer structures alone but act more similar to a detergent and can insert into preformed bilayers and are hypothesized to modulate membrane properties (11). This behavior enables the integration of this non-natural amphiphile into cellular membranes which is a feature that is not possible with diblock copolymers. In this thesis, triblock

copolymers were used to modulate the membrane composition of cell-extracted bilayer vesicles, a process which would have otherwise required metabolic mutations.

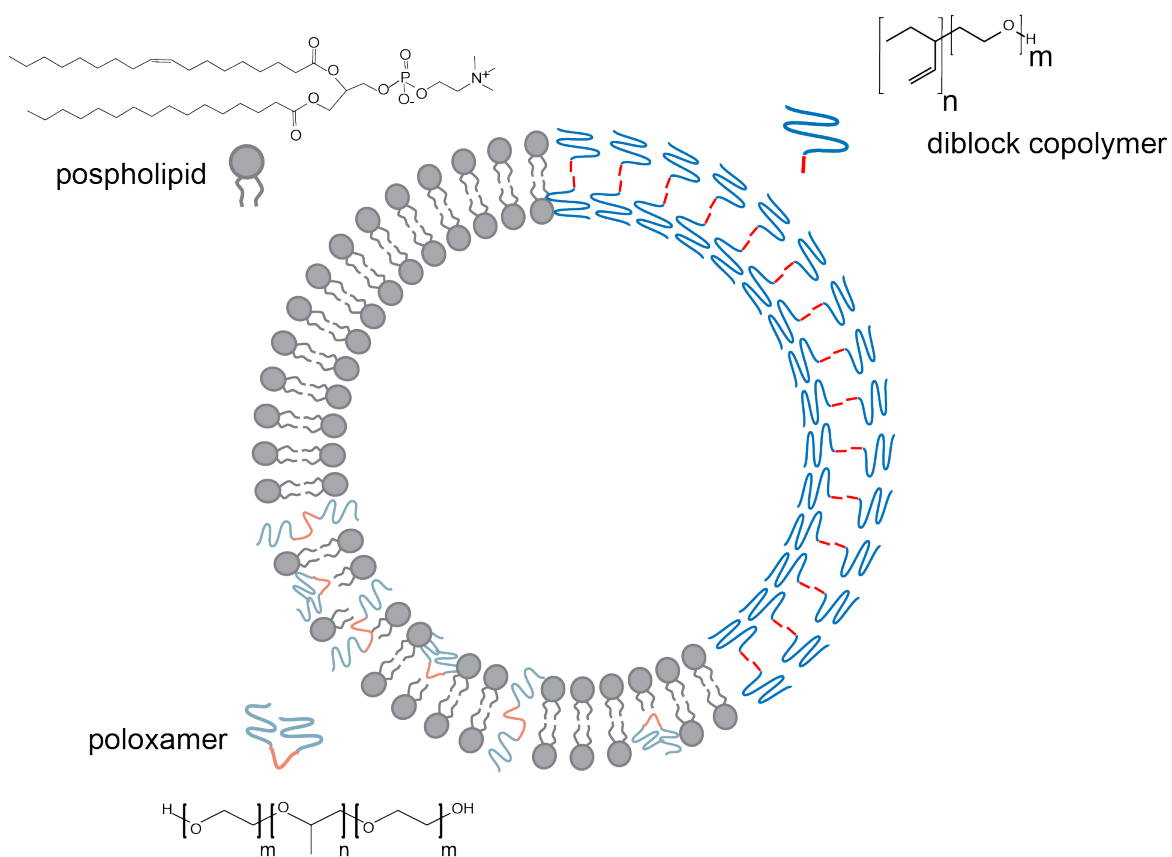


Figure 1.2 Nonnatural amphiphiles mimic phospholipids

Diblock copolymers and poloxamers are amphiphilic molecules that can be used to mimic phospholipids. Diblock copolymers can form standalone bilayer membranes with properties such as increased stability and elasticity. In contrast, poloxamer does not usually form a standalone membrane but can insert into preformed membrane to exert similar stability improvements as diblock copolymers.

Membrane protein folding *in vivo*

Production and folding is a critical first step in the life cycle of a protein. Membrane proteins are often folded through interactions with various chaperones and this process is similar in all domains of life from bacteria to mammalian cells. *E. coli* are commonly used as model bacteria and are beneficial in protein production and purification applications. This gram-negative bacterial species is comprised of two membranes and a thin peptidoglycan cell-wall in the periplasmic space. The outer membrane primarily functions to protect the inner membrane from external stressors such as physical force and antibiotics. An interesting feature of the outer membrane of gram-negative bacteria is the presence of porins which are membrane channel proteins that allow passive diffusion of small hydrophilic molecules into the periplasm. As such, the outer membrane is considered more permeable than the inner membrane. In contrast, the inner membrane is believed to be the true barrier which protects the cytoplasm and is less permeable. The proteome of each of these membranes is distinct due to the differing functions of each membrane. In addition, the structures of proteins in the inner membrane compared to the outer membrane have differing features. Specifically, inner membrane proteins are primarily α -helical while outer membrane proteins are β -barrels.

The mechanism of how proteins fold relies on their secondary structure. α -helical proteins fold co-translationally either with or without a chaperone (12, 13). Most inner membrane proteins are α -helical and have access to the inner membrane during translation and are inserted into the bilayer by either the SEC translocon or YidC insertase (13). In contrast, β -barrel proteins are synthesized completely prior to folding and then are folded or secreted to the outer membrane with a chaperone. β -barrel proteins likely require chaperones because it is energetically unfavorable for a protein to cross the inner membrane and exit the membrane to enter the outer membrane.

Membrane protein folding in minimal systems for understanding protein folding *in vivo*

Protein folding has been increasingly studied *in vitro* to understand the basic principles of protein folding. These studies utilize measurements of the energy of unfolding, refolding efficiency after denaturation, or co-translational folding in cell free systems. Through the observation of protein folding using each of these techniques, the importance of the membrane and its lipid composition in this process has emerged. A detailed overview of the importance of lipid composition and membrane properties in membrane protein folding can be found in **Chapter 2**.

Despite chaperone assistance during membrane protein folding *in vivo*, both α -helical and β -barrel proteins have been demonstrated to directly insert into bilayers without a chaperone (12, 14, 15). This observation suggests that α -helical membrane proteins may fold directly into the inner membrane during translation while β -barrel proteins may be secreted through the Sec-translocon into the periplasm and may fold spontaneously into the outer membrane from there. While these mechanisms suggest that chaperones are not required for protein folding it is important to note that chaperones do play a large role in protein folding but the membrane may be important as well. These mechanisms support the possibility that either the membrane aids protein folding along with chaperones, or some proteins may spontaneously insert into the membrane while other proteins require chaperones.

Spontaneous insertion into the bilayer may be important for proteins which evolved earlier than chaperones or in the folding of chaperones themselves. Towards this idea, Eaglesfield et al found that proteorhodopsin (PR) contains a hydrophobic N-terminal domain that promoted co-translational spontaneous insertion by directing the ribosome to the membrane during translation (16). As PR is expected to have evolved prior to translocation machinery and SRP guides, this N-terminal domain is expected to promote spontaneous insertion in the absence of chaperones. This finding suggests that co-translational insertion may be directed by an N-terminal hydrophobic domain in primitive membrane proteins. In addition, the prevalence of protein

folding and insertion directly into membranes has been demonstrated through thermodynamic measurements of polypeptides showed that some proteins will favor the membrane surface over the translocon and will likely fold into the membrane and bypass the translocon (13, 17). Accordingly, a growing body of research supports the finding that membrane proteins prefer some lipid compositions (18), suggesting a role of the membrane and its composition in protein folding. Together, these observations demonstrate that direct interactions with the membrane may be important for protein folding even in the presence of chaperones and this behavior is likely important for protein folding in eukaryotes as well as bacteria.

While bacteria lack compartmentalization, eukaryotic cells are divided into organelles which serve to compartmentalize incompatible cellular functions. The endoplasmic reticulum (ER) is the organelle in which proteins fold, and contains similar chaperoning systems as bacteria to facilitate the folding of the higher volume of proteins which are folded in eukaryotic cells. ER membranes are hypothesized to have lipid compositions which promote protein folding such as low concentrations of cholesterol (19). As various conditions such as temperature and metabolic diseases may alter membrane properties and bacteria and eukaryotic systems respectively, the relationship between the membrane and membrane protein folding is important for overall biological function.

1.2 Mechanosensitive channels

Stretch-activated ion channels are essential components of force sensing

Mechanotransduction is the process by which cells sense and respond to physical stimuli. One class of mechanosensory proteins that are found in all domains of life are mechanosensitive channels. As they are activated by forces in the membrane, mechanosensitive channels have been increasingly shown to be modulated by membrane composition. In higher organisms, stretch activated-channels sense and respond

to various stimuli from touch and hearing sensation in neurons to shear stress in endothelial cells (20). In contrast, prokaryotic mechanosensitive channels have simpler functions of relieving excess membrane tension to prevent cell lysis. Because of these simpler functions, prokaryotic mechanosensitive channels are used as model mechanosensitive channels. Two of such channels are well-characterized and have served as foundational research targets for future studies of more advanced mechanosensitive channels in higher organisms.

The bacterial mechanosensitive channels, Large-Conductance Mechanosensitive Channel (MscL) (PDB: 2OAR) (21) and the Small-Conductance Mechanosensitive Channel (MscS) (PDB: 6PWP) (22) were the first stretch-activated channels to be discovered. These ion channels differ in structure (Figure 1.3) but are non-selective in the molecules they can transport and have similar proposed functions of preventing cell lysis during osmotic stress. Both of these channels activates in response to membrane tension through *force-from-lipids* (23). MscS has a smaller conductance and poses a lesser risk of cell dehydration from prolonged activation and activates at lower membrane tensions (24). MscL was the first mechanosensitive channel to be discovered and has a large conducting pore which activates at near-lytic membrane tensions (1-10 mN/m). It is hypothesized that MscS and MscL work together in the prevention of cell lysis where MscS activates first and if it cannot relieve enough tension then MscL activates just before cell lysis would occur (24). These channels have been used as model mechanosensitive channels in understanding the general mechanisms of mechanosensitive channel behavior and have been studied in response to the effects of membrane composition effects on mechanosensitive channels (25–28). A detailed overview of how membrane composition and properties affect MscL and MscS can be found in **Chapter 2**.

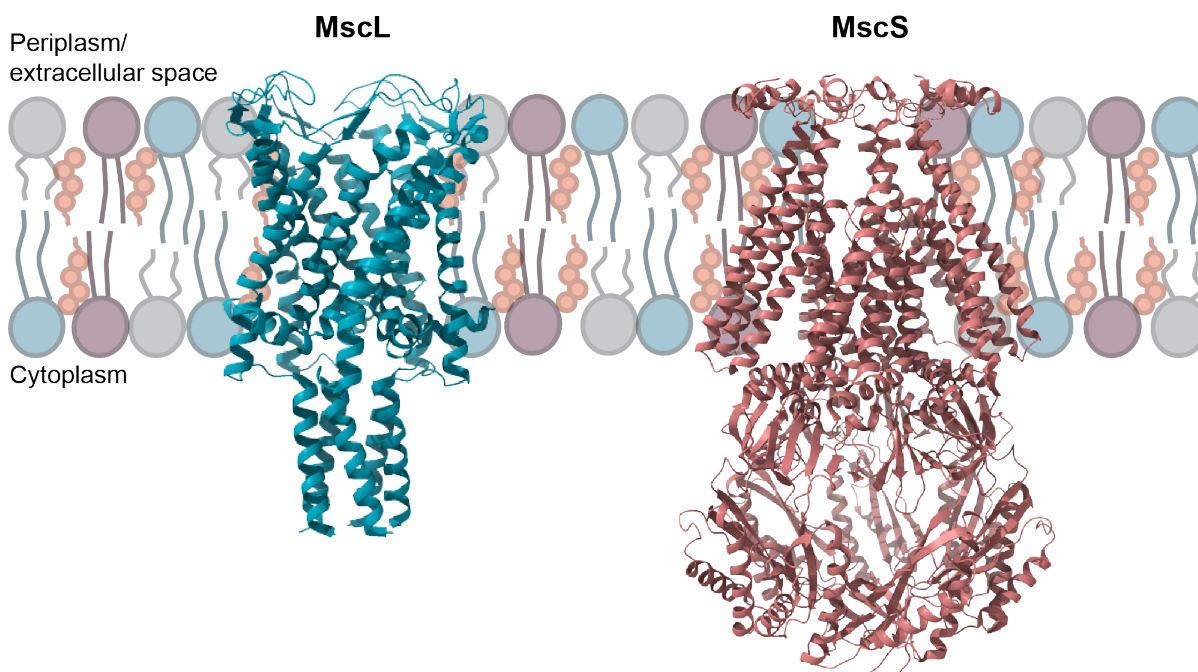


Figure 1.3 Structure of MscL and MscS in a bilayer

MscL and MscS are bacterial mechanosensitive channels found in various organisms including *E. coli*. These channels have similar functions of protecting the cell from lysis under osmotic stress but have unique structural features. MscL PDB: 2OAR, MscS PDB: 6PWP

The Piezo family of mechanosensitive channels, Piezo1 and 2, are cation channels found in diverse eukaryotic cell types (29). This class of mechanosensitive channels is important for calcium signaling in response to various physical forces. Piezo 1 is found in diverse non-neuronal cell types and plays various important roles from maintaining cell volume and sensing of shear stress to bone density regulation (30). The other channel in this family, Piezo2, plays an important role in sensory neurons where it is involved in touch and hearing sensation (30). In red blood cells, Piezo1 controls cellular volume and impacts microvascular tone through ATP release.^{11,12} Recently, Piezo1 was found to display altered activity in endothelial cells in response to PUFA exposure (31, 32). The activity shift was hypothesized to occur due to changes in membrane biophysical properties that accompanied fatty acid uptake.¹³ In addition, stiffer

membranes, like those present in hypercholesterolemia-associated cells¹, have been found to inhibit Piezo1 activation (31, 32), which drastically inhibits RBC function.¹¹ Taken together, these results suggest membrane properties influence Piezo1 activity,^{6,14} but these properties have not been identified or measured directly.¹³ This is a critical gap in knowledge that we hypothesize is significant to understanding RBC regulation of the endothelial environment. RBCs are a highly deformable cell type which increases their sensitivity to external membrane forces,¹⁵ and suggests that mechanotransduction plays an important role in RBC function. An outline of the effect of membrane properties on Piezo1 behavior is outlined further in **Chapter 2**.

While MscL/ MscS and Piezo1/ 2 are the most common mechanosensitive channels found in bacteria and eukaryotes, respectively, there are many other mechanosensitive channels which are used by cells to sense their surroundings. Many of these channels have been characterized to be sensitive to various mechanical stimuli but their functions are poorly understood. For example, TRPV4 is a mechanosensitive channel which is not activated by membrane stretching as it has a delayed activation to cellular forces (33). In addition, mTrek1 and hTRAAK are neuronal mechanosensitive potassium channels which are important for maintaining membrane potential and have been shown to directly activate in response to membrane stretching (34). These examples describe the presence of mechanosensitive channels in various cell types but there are many more channels which are believed to be mechanosensitive. It is believed that these channels work in conjunction with lipids, both locally and globally, to modulate their activation. While the prevalence of mechanosensitive channels has increasingly demonstrated, their physiological activation mechanisms and roles in cellular physiology are poorly understood.

The force-from-lipids mechanism of mechanosensitive channel activation

The force-from-lipid mechanism is the most accepted theory for mechanosensitive channel gating, especially in prokaryotic mechanosensitive channels. Through this mechanism, mechanosensitive channels are gated by forces propagated through the membrane which are broadly dispersed and induce conformational changes to stretch-activated channels. The foundations of the force-from-lipids mechanism were originally demonstrated through the reconstitution and activation of mechanosensitive channels in model bilayers which were demonstrated to be gated solely by forces pulling on the lipids and not through ligand or voltage gating. While this theory is the most accepted opening mechanism in prokaryotes, eukaryotic mechanosensitive channels have confounding cellular structures, like the cytoskeleton and extracellular matrix which are tethered to mechanosensitive channels and are also expected to influence activity. However, it has been hypothesized that most mechanosensitive channels, even eukaryotic channels, are gated at least partially by force-from-lipids (2).

Despite the presence of membrane tethering structures such as the cytoskeleton, the force-from-lipids theory is hypothesized to be the primary mode of mechanosensitive channel activation. The key distinction between simple force-from-lipids and force-from-filament channel activation is the primary perturbation of the membrane. This perturbation may come from either a force directly acting on the membrane or a reactive force from the protein after a small conformational change induced by a filament which then acts back on the channel of interest and causes it to open or close. The lipid pressure profile maintains the channels in either the open or closed state and the channels themselves can exert forces on the bilayer which can change the lipid pressure profile. Therefore, when a cytoskeletal or ECM connection to a membrane protein causes a change in channel position within the bilayer this will exert a force on the bilayer which changes the lipid pressure profile and thus acts back on that channel and causes channel activation or deactivation. As the membrane lipid composition is important for membrane properties and force-transmission, the impact of lipid composition on bilayer properties is necessary for the fundamental understanding of mechanosensitive channel gating and cellular mechanosensation. This force sharing

principle dictates that other types of channels, especially those not considered to be mechanosensitive may be modulated by the membrane and its lipid composition through changes in the lipid pressure profile upon activity dynamics. Even channels that are not mechanically activated like MscL may be mechanically sensitive to bilayer composition and perturbations.

As the force-from-lipids theory relies on interactions between the membrane and embedded proteins, membrane composition is expected to influence these interactions. A few studies have explored this relationship, however, the generality of membrane composition and the impact on membrane properties needs to be explored further. A review of the studies which outline the impact of membrane properties on mechanosensitive channels is described in **Chapter 2**.

1.3 Specific Aims

Aim 1: Observe MscL folding in response to membrane composition and properties altered by diblock copolymers. Our hypothesis is that decreases in the area expansion modulus of membranes enhances the cotranslational folding efficiency and synthesis of an alpha helical, mechanosensitive channel protein. Using the mechanosensitive channel of large conductance (MscL) expressed as a fusion protein with monomeric enhanced green fluorescent protein (mEGFP) on the c-terminus, we will measure MscL folding in the presence of synthetic lipid vesicles. We will use diblock copolymers to alter the mechanical properties of the vesicles.

Aim 2: Quantify the effects of non-esterified fatty acids and cholesterol on membrane mechanical properties. My next aim will explore a class of amphiphiles that have known effects on mechanosensitive channels, but whose mode of action remains unclear. My hypothesis is that PUFAs change membrane elasticity as a function of PUFA chemical structure and membrane cholesterol content. Using micropipette

aspiration techniques on model lipid membranes, we will measure changes in membrane physical properties as a function of PUFA identity and composition.

Aim 3: Measure changes in mechanosensitive channel activity and membrane mechanical properties in response to membrane composition altered by the incorporation of synthetic amphiphiles. My hypothesis is that amphiphiles that increase membrane elasticity (decrease the area expansion modulus) will increase the threshold pressure required to activate mechanosensitive channels. Using patch-clamp electrophysiology with an integrated pressure controller and giant plasma membrane vesicles (GPMVs), we will measure changes in the ion channel activity of MscL to single-channel resolution in response to the addition of triblock copolymers (Ploxamers). In addition, micropipette aspiration techniques will be used to measure changes in membrane mechanical properties in response to Ploxamers. We will use these techniques to measure the impact of Ploxamers on MscL activation pressure and determine the relationship between MscL activation and membrane mechanical properties.

1.4 Description of Thesis

The work in this thesis consists of eight chapters which describe the effect of membrane properties on membrane protein behavior from folding to function. **Chapter 2** describes a literature review and perspective of these topics. This chapter begins with a description of how membrane amphiphiles are expected to alter membrane properties and behavior. Next, this chapter discusses the effect of membrane properties on membrane protein folding. We then describe how membrane amphiphiles have been used to begin to uncover the role of membrane properties in mechanosensitive channel function. Finally, this chapter offers a perspective on the relationship between membrane properties on membrane protein folding and function and the importance of spatially segregating these processes in biological systems. The remaining chapters in this thesis present work regarding these topics (Figure 1.4).

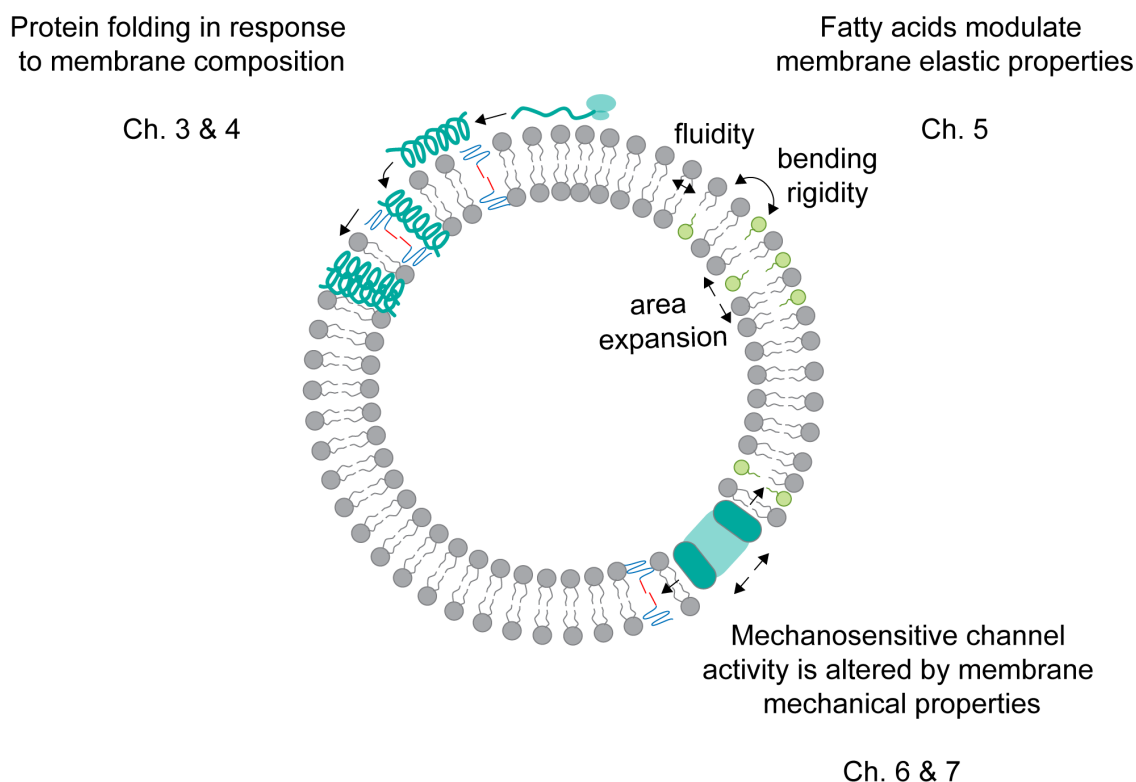


Figure 1.4 Schematic outline of thesis

This thesis consists of three major sections which address the topic of understanding how membrane mechanical properties impact protein behavior through folding and function. **Chapters 3 and 4** describe how protein folding responds to alterations of membrane area expansion modulus using diblock copolymers. **Chapter 5** demonstrates the impact of fatty acids on membrane mechanical properties and proposes a mechanism of how biological systems alter membrane properties. Finally, **Chapters 6 and 7** probe the force-from-lipids mechanism of mechanosensitive channel activation using a triblock copolymer which demonstrates the importance of membrane mechanical properties in mechanosensitive channel activation.

The first topic of this thesis focuses on membrane protein folding which spans **Chapters 3 and 4**. **Chapter 3** describes a method for the observation of membrane protein folding in the presence of hybrid model membranes constructed from phospholipids and diblock copolymers. In this chapter, a method for *in vitro* detection of protein expression through a fluorescent protein reporter is described as well as the construction of hybrid model membranes as a platform for protein expression. The methods outlined in this

chapter serve as a guideline for *in vitro* protein folding studies into any suspended membrane platform. In addition, this chapter offers a detailed description of the technique for constructing bilayer vesicles from lipids and diblock copolymers which has been performed in few studies to date. This platform has the potential to offer biological compatibility imparted by lipids combined with structural stability and unique mechanical properties of diblock copolymers. The application of these methods is described in **Chapter 4** where they are used to uncover the role of membrane properties on membrane protein folding.

Membrane protein folding is expected to rely on membrane properties as the direct folding of proteins into membranes has been increasingly demonstrated. However, the role of membrane elasticity and specifically, the area expansion modulus has not been described due to challenges of using natural lipids to alter this property. **Chapter 4** describes how we overcame these challenges by incorporating non-natural amphiphiles into lipid membranes which allows the observation of alterations of membrane protein folding as a function of membrane elasticity. In addition, the role of membrane defects in membrane protein folding is discussed. This study provides *in vitro* evidence for how membrane mechanical properties are important for membrane protein folding and highlights how the properties of the endoplasmic reticulum membrane may have evolved to consist of softer membranes to promote protein folding *in vivo*.

Inspired by these results, **Chapter 5** addresses a potential mechanism of how cells modulate their membrane elastic properties. Polyunsaturated fatty acids are hypothesized to be important for membrane properties because of their abundance in species which reside in cold temperatures and the observation of their impact on mechanosensitive channel behavior. Despite these observations, membrane mechanical properties have not been measured in systems containing these amphiphiles. In this chapter, the impact of polyunsaturated fatty acids on membrane properties in the presence and absence of cholesterol is described. This work proposes a mechanism of how different fatty acids alter membrane properties in unique ways and describes how membrane phase separation may be used to modulate cellular membrane

properties. These observations also highlight the importance of measuring membrane properties directly as membrane properties are not additive in complex mixtures of lipids.

As we demonstrate the importance of measuring membrane properties directly, **Chapter 6** describes methods for the construction of membrane platforms which are suitable for both membrane property measurements and quantitative ion channel activity detection techniques. Such platforms include model bilayer giant unilamellar vesicles (GUVs), giant spheroplasts, and giant plasma membrane vesicles (GPMVs). The benefits and challenges of each system is listed and the justification for the use of GPMVs for studying membrane properties and mechanosensitive channel activation is described. This platform, which enables the use of the complementary methods of micropipette aspiration and patch-clamp electrophysiology, has the power to uncover the role of membrane properties in ion channel behavior.

Chapter 7 demonstrates the use of GPMVs treated with triblock copolymers for the observation of membrane property modulation of mechanosensitive channel behavior. As the canonical activation mechanism of many mechanosensitive channels is through force-from-lipids, membrane properties are expected to alter mechanosensitive channel behavior. Here, the direct measurement of membrane properties and mechanosensitive channel pressure sensitivity is described. Through this study, the force-from-lipids mechanism is supported and the relationship between membrane properties and channel behavior is directly compared. This study demonstrates the role of membrane elastic properties such as area expansion and bending stiffness in the activation of a model mechanosensitive channel.

Finally, **Chapter 8** describes the conclusions and implications of this work and the outlook on future studies to be completed. Membrane mechanical properties are important for the function of various ion channels, and it is hypothesized that while all channels may not be mechanically gated, many are sensitive to changes in mechanical properties but have not been characterized in this way. This thesis outlines the importance of membrane properties on membrane proteins from folding to function and proposes a reasoning for the

evolution of the membrane composition of organelles and the presence of lipids rafts which may promote these behaviors. This work highlights the implication of altering membrane properties through exposure to household products, dietary consumption of certain lipids, and the impact these changes may have on protein function and eventually health and disease.

Chapter 2

2. The role of membrane properties in membrane protein folding and function: a closer look at mechanosensitive channels

Cellular membranes function to compartmentalize the cell and its organelles and serve as active sensors to transduce various signals across these membranes. In these processes, membrane lipids are commonly assumed to be a scaffold to house proteins which confer the active roles of the membrane. However, membrane lipids have been increasingly shown to play an active role in the function of the cell membrane through specific and nonspecific interactions with membrane proteins. These interactions may affect proteins through modulation of activity through specific binding, nonspecific effects through modulation of membrane properties and the modification of protein organization within the membrane through lipid rafts. Various mechanosensitive channels, one of the fastest-responding signal transducers, are known to be

modulated by these interactions with lipids, which has sparked interest in the effect of membrane composition on mechanosensitive channel behavior. Here, we review lipids and their effect on membrane properties and mechanosensitive channels from folding to function and propose connections between these processes.

2.1 Membrane composition controls membrane properties

All biological membranes have similar bilayer structures and are comprised of primarily phospholipids, sterols, and sphingolipids. Despite these similarities, the composition of each biological membrane is unique and varies depending on cell type and organelle. As an example, bacterial membranes have vastly different lipid compositions from mammalian cell membranes (35) which may be attributed to differences in cell wall presence and differing cytoskeletal structures which confer differing mechanical needs of the membrane. Similarly, mammalian cells have differing lipid compositions based on the organism or tissue type (5, 36) which may be necessary to allow for differing cellular functions depending on the physiological location of the cell. In addition, organelle membranes within cells have varying lipid compositions and these compositions are presumed to be important for the unique function of each organelle (19, 36).

Membranes are composed of various molecules which uniquely contribute to membrane structure and properties. Some common lipids include phospholipids such as phosphatidylethanolamine (PE) and phosphatidylcholine (PC) and sterols which are commonly found in mammalian cells in the form of cholesterol and in bacteria as hopanoids (37). The regulation of cellular membrane composition is important to maintain proper cellular function. This regulation is achieved through lipid metabolism pathways which are out of the scope of this review but have been outlined in previous reviews by Van Meer et al., Magnuson et al, and Sampath et al. and Vance, among others (19, 36, 38, 39). Bacteria are known to alter membrane composition in response to their environment (37, 40). Similarly, cells can combat external changes in membrane composition (41) and without this regulation, cell viability is lost (42).

Each lipid species within a cell membrane imparts unique properties and specificity on the membrane. As an example, phospholipids are the most common molecule found in membranes (36) and are used to create the bilayer structure of the membrane through self-assembly (43). Fatty acids, which are commonly grouped with phospholipids, are known to alter membrane properties based on chain saturation whether they are esterified into phospholipids (6, 7, 44, 45) or exist as single-chain molecules (46–49). Sterols are also important membrane molecules as they improve membrane stability (6) and are found in high abundance in lipid rafts (50). It is important to note that the properties of a membrane are not additive when looking at individual amphiphiles as differences in physicochemical interactions between molecules can alter the resultant bulk membrane properties (Figure 2.1) (46, 51–55). However, a basic understanding of how different membrane amphiphiles contribute to the global properties of a membrane sheds light on the functional importance of distinct lipids on biological systems. Table 2.1 demonstrates a general overview of the contribution of different amphiphiles on membrane properties.

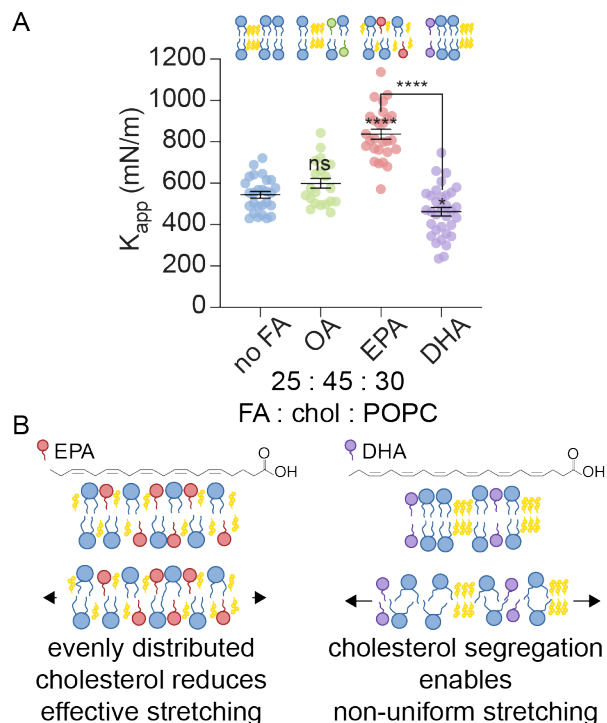


Figure 2.1. Membrane properties do not always equal the sum of their parts measured individually

A) Micropipette aspiration measurements of mixed lipid vesicles demonstrated membrane K_{app} is not predicted by contributions from amphiphiles alone. EPA and DHA when measured independently exhibited similar K_{app} values but mixing with high concentrations of cholesterol gave rise to different relationship. B) The observed differences in K_{app} between EPA and DHA may be explained by differences in the propensity of these mixtures to phase separate. EPA is less likely to phase separate which increases K_{app} . In contrast, DHA induces more or larger cholesterol domains which may decrease the effective K_{app} .

original source: Jacobs *et al. Biophys. J.* 2021

| Lipid class | specific lipid example | impact on membrane structure or properties |
|---------------|---|---|
| phospholipids | PE | zwitterionic pH 7.4, promotes fusion (56) |
| | PC | zwitterionic, most common phospholipid in mammals (19), allows bilayer structure self-assembly (43) |
| | PI | anionic, able to be phosphorylated, role in lipid signaling and membrane trafficking (57) |
| | PS, PA, PG | net anionic |
| | cardiolipin (CL) | net anionic, decreases membrane packing and stability (58), found only in bacteria and mitochondria (35) |
| fatty acids* | DHA, EPA (polyunsaturated) | increase membrane fluidity (47), decrease area expansion modulus (45, 46), increase stability of lipid rafts (47, 59–61) |
| | palmitic acid (found in DPPC), stearic acid (found in DSPC) (saturated) | decrease membrane fluidity (62), increase area expansion modulus (6, 45) |
| sphingolipids | sphingomyelin | promotes lipid raft formation (6, 63), increases membrane thickness (64), reduces membrane fluidity (65) |
| sterols | cholesterol | increases membrane stiffness (51, 55, 66), stability (6), decrease fluidity (67), promotes lipid raft formation (50, 68–70), promotes fusion (56) |

Table 2.1 Common membrane amphiphiles and their impact on membrane structure and properties

*Fatty acids are commonly conjugated through covalent bonds as phospholipid tails and exhibit similar properties in either form (45, 46).

Membrane organization to achieve heterogenous membrane properties within a single cell

Organelles are expected to have unique membrane properties due to differences in lipid composition, which relates to their functions (5, 71). Following the protein trafficking pathway from the ER to the plasma membrane, organelle membranes have compositions which gives rise to membranes that are increasingly thicker, more ordered, and stiffer (19, 36, 64). Indeed, the plasma membrane has the highest concentration of cholesterol and sphingomyelin while the ER membrane has the lowest concentration of these amphiphiles (35). The resultant properties of these membranes are expected to differ greatly where the ER is thinner, softer, and more fluid which may benefit its function of protein folding (72) while the plasma membrane is stiffer and thicker which may serve to protect the cell (58, 73). These functional connections between organelle function and lipid composition demonstrate that cells have tight control over their membrane composition between membranes within the cell and this may be necessary for the unique function of each organelle.

Besides organelles, cells also have spatial control of their lipid composition and properties within each membrane (Figure 2.2A). Membranes have different compositions between leaflets through asymmetry (74) or across the lateral plane of the membrane as lipid rafts. Lipid rafts, or phase-separated domains are known to be present in membranes ranging from bacteria (75) to mammalian cells (76). In bacteria, they function to sort bacterial signaling proteins in the absence of organelles, which often serve this function in higher ordered systems (75). Similarly, lipid rafts are believed to sort membrane proteins in eukaryotic cells to cluster proteins or to optimize the local membrane composition around each protein (77, 78). Domains are usually described as one of two categories, liquid ordered (L_o), which is referred to as the "raft" domain, and liquid disordered (L_d), or "non-raft" domain (63, 79). The formation of these distinct phase-separated domains is driven by membrane composition (60, 76, 78, 80, 81). Specifically, sterols and sphingolipids promote raft formation through self-assembly into phase-separated L_o domains (6, 82). In addition, there have been cases of certain phospholipids or fatty acids with polyunsaturated chains which exist in L_d domains and promote or destabilize L_o domains through incompatibility of membrane order between sterols

and polyunsaturated chains (47, 59, 60). Lipid raft and non-raft domains have distinct physical properties (Figure 2.2B). L_d domains consist of regions with lower cholesterol concentration and higher concentrations of unsaturated phospholipids (83) and therefore are expected to be more disordered and fluid (47, 67) and have lower bending stiffness (84) and a lower area expansion modulus (7, 46, 85). In contrast, L_o domains have higher amounts of cholesterol and sphingolipids (6, 82) and are expected to be less fluid (67), thicker (64, 84), and have a higher bending rigidity (84) and area expansion modulus (6, 85). Raft and non-raft domains are used by cells to organize proteins and provide unique environments for proteins that are localized within an organelle membrane.

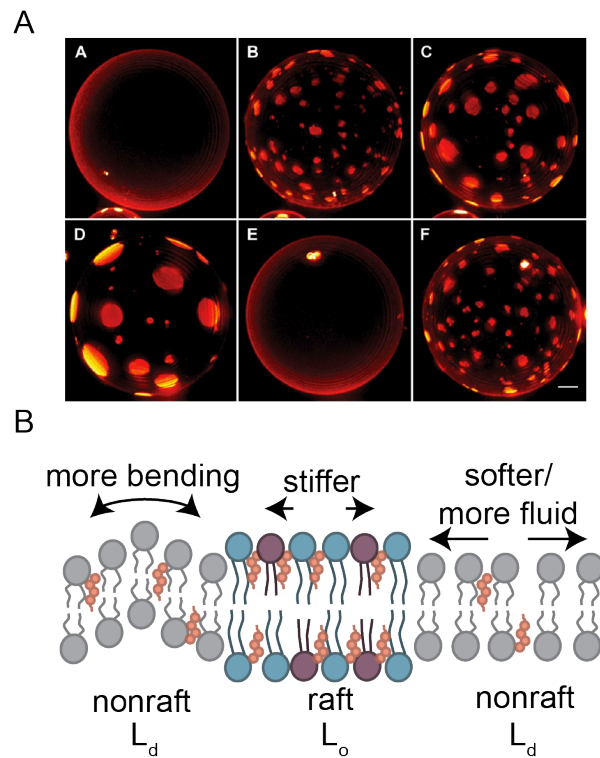


Figure 2.2 Lipid rafts organize lipids and produce dynamic regions of differing membrane properties

A) Time lapse of a GUV undergoing oscillatory phase separation (reproduced under CC-BY-4.0 <https://creativecommons.org/licenses/by/4.0/> original source: Oglęcka *et al. elife* 2014). B) lipid rafts give rise to regions of differing membrane properties. Nonraft (L_d) phases comparatively are expected to have a reduced K_A and k_c with enhanced fluidity. Raft (L_o) domains are expected to be less fluid and stiffer with a higher K_A and k_c .

2.2 Membrane properties and protein folding

One cellular process that relies on membrane composition and properties is membrane protein folding (86). While cellular systems contain chaperones to facilitate membrane protein folding, mounting evidence suggests that the membrane plays a role in this process as well. Primitive membrane proteins likely required the ability to fold into the membrane without the aid of translocation machinery as membrane proteins existed prior to translocon evolution (16). Free energy calculations determined that membrane proteins favor insertion into the membrane (13, 87) and follow the same folding pathway with or without a translocon (17). In addition, membrane protein folding with a translocon may be tuned by membrane properties through modulating the translocon activity directly (88). Various *in vitro* studies have demonstrated that membrane protein folding occurs in model membranes in the absence of translocation machinery (12, 15, 16). The understanding of how membrane mechanical properties affect protein folding *in vitro* will further the understanding of the mechanisms of protein folding *in vivo*.

***In vitro* studies reveal membrane properties that are important for membrane protein folding**

Membrane composition is important for membrane protein folding. As mentioned in the previous section, the endoplasmic reticulum (ER) is the location where protein folding occurs within a cell and this organelle has a distinct membrane composition and physical properties. While the ability to study the how the properties of ER membranes affect protein folding remains a challenge, there have been several *in vitro* studies that have outlined different membrane properties which promote membrane protein folding. The effect of membrane composition on membrane protein folding was originally characterized using unfolding and refolding studies to isolate the interactions of the protein directly with the membrane (18, 89, 90). Recent advances have allowed co-translational protein folding studies to determine the direct effect on

folding in a manner more similar to the native pathway which utilize cell-free protein expression systems (12, 91).

Membrane protein unfolding and refolding studies have been used since the 1990's to determine which lipids preferentially interact with membrane proteins. Various studies from the Booth group focused on the refolding or unfolding rates of a model α -helical protein, Bacteriorhodopsin (BR). These studies demonstrated that membrane properties such as increased curvature strain (18), reduced bending stiffness (92) and decreased chain pressure (93) increased BR folding. In contrast, an unfolding study demonstrated that chain pressure increased the free energy of unfolding, stabilizing the folded state of BR (94). Refolding studies of model β -barrel proteins highlighted that reduced bending stiffness (14), increased membrane fluidity (89, 95), membrane defects (86), reduced membrane thickness, and increased curvature strain promoted β -barrel refolding in bilayer vesicles (95).

Similar to refolding studies, peptide insertion studies were used to mimic the folding and insertion of an unfolded protein into a membrane. A study using a peptide which inserts under certain pH conditions demonstrated that reduced membrane thickness and bending stiffness improves the insertion step of membrane protein folding, however, unlike the results of protein refolding studies, membrane fluidity did not impact helix formation or peptide insertion (96). The similarities of the results of these studies demonstrate that there are key trends which promote membrane protein insertion for both α -helical and β -barrel membrane proteins.

Recently, cell-free protein synthesis has allowed for the observation of co-translational membrane protein folding. These studies allow for the evaluation of folding efficiency through a pathway more similar to *in vitro* protein folding. Through co-translational observation of protein folding, the importance of the area expansion modulus was revealed where decreased K_A improved the folding of a model α -helical mechanosensitive channel (10). In addition, the results from refolding and unfolding studies were confirmed

where decreased membrane thickness (97), increased fluidity (10), reduced bending stiffness (98), and reduced headgroup pressure (12, 91) promoted co-translational protein folding (Figure 2.3). These similarities highlight that while unfolding and refolding studies were useful before the development of other methods for studying protein folding, newer methods have provided more context into how proteins may fold *in vivo*.

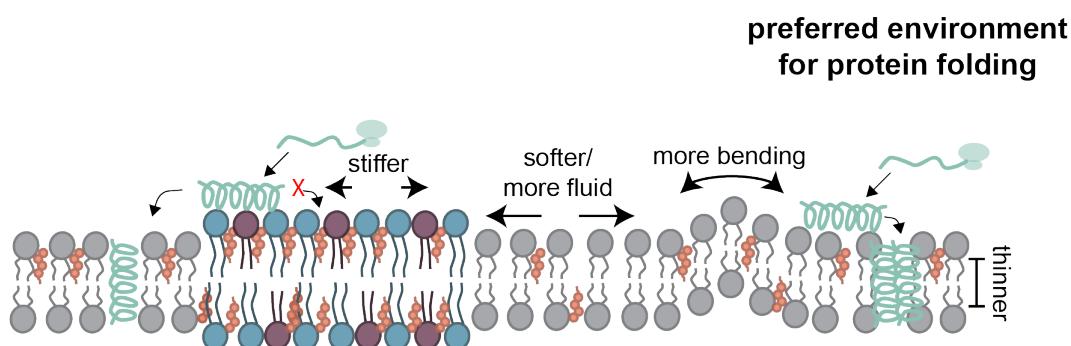


Figure 2.3 Membrane protein insertion and folding prefers a softer, thinner, more fluid membrane environment

Through various protein folding studies, the impact of membrane properties on protein spontaneous insertion and folding was revealed. Membranes which are thinner, more flexible to bending, and softer promote protein folding.

How *in vitro* studies relate to *in vivo* protein folding

The membrane composition and resultant physical properties of the ER are important for protein folding as this is the location of membrane protein folding in eukaryotes. The relationship between membrane properties and protein folding are demonstrated by the function of Ire1, which is a membrane protein that senses the lipid composition of the ER and initiates the unfolded protein response (UPR) (99). In addition, Ire1 activates in response to saturated fatty acids, which indicates that alterations in membrane properties such as decreased fluidity and increases in bending rigidity and area expansion modulus are unfavorable for membrane protein folding (100). The existence of this sensor which links membrane protein folding and

ER membrane composition and initiates the unfolded protein response highlights the importance of membrane composition in membrane protein folding *in vivo*. This connection supports the work of *in vitro* protein folding assays which demonstrated that membrane protein folding relies on membrane composition. Indeed, the ER membrane is thinner than the plasma membrane or other organelles (64) which is expected to promote protein folding. The ER membrane also has a lower cholesterol and sphingomyelin (36, 64) concentration such that we would expect a decreased bending rigidity (51) and area expansion modulus (6, 46) and increased fluidity which are properties hypothesized to promote membrane protein folding. In addition, the ER has a large surface area organized through membrane folds which is expected to facilitate the folding of the high volume of membrane proteins required for the entire cell (10). These estimations highlight that membrane properties which are important for protein folding *in vitro* may also be important for membrane protein folding *in vivo*.

2.3 Membrane mechanical properties influence ion channel behavior

Membrane proteins require specific lipid compositions and therefore specific membrane properties to function. This relationship is especially important for mechanosensitive channels which activate through force-from-lipids. The effect of membrane composition on the activity of bacterial mechanosensitive channels has been studied extensively and this information is used as a model for more advanced eukaryotic mechanosensitive channels. These bacterial mechanosensitive channels are useful because they are solely activated by force-from-lipids as they are not expected to be tethered to the cytoskeleton or extracellular matrix, as observed in many eukaryotic channels. Despite the prevalence of use as a model mechanosensor, even similar bacterial mechanosensitive channels exhibit distinct behaviors in response to changes in lipid composition. Through these studies using model membranes with tightly controlled membrane compositions, the impact of membrane properties on mechanosensitive channel behavior could be estimated. However, most of these studies do not measure the mechanical properties of their exact

system and rely on estimates of membrane mechanical properties from measurements that were established previously in similar systems.

Bacterial mechanosensitive channels

Bacterial mechanosensitive channels served as model mechanosensors in the initial studies of mechanosensitive channel behavior. These initial studies aimed to demonstrate which membrane composition are favorable for mechanosensitive channel behavior in order to predict the importance of membrane properties in mechanosensitive channel activation. First, the Large-Conductance Mechanosensitive Channel (MscL) has been demonstrated to be activated by reductions in membrane thickness (27) and local curvature strain (24). In addition, the presence of cholesterol is known to decrease activation sensitivity (24) which highlights other mechanical properties such as bending stiffness, fluidity or area expansion modulus may be important as well, but more studies need to be performed to isolate the role of these properties. In contrast, the Small-Conductance Mechanosensitive Channel (MscS), is not affected by changes in membrane thickness nor bending stiffness but its activation is reduced in the presence of PE lipids which may increase membrane area expansion modulus (26), but this has not been measured directly (101). Similar to MscL, cholesterol decreases the pressure sensitivity of MscS but this effect is greater for MscS (24). Taken together, these results suggest that MscL requires a membrane with a specific thickness (Figure 2.4), while MscS is less sensitive to thickness but may require the membrane to have a specific area expansion modulus. These studies have introduced the effect of various membrane mechanical properties on mechanosensitive channel activation; however, more studies will be needed in the future to directly determine which membrane properties modulate mechanosensitive channel force-from-lipids.

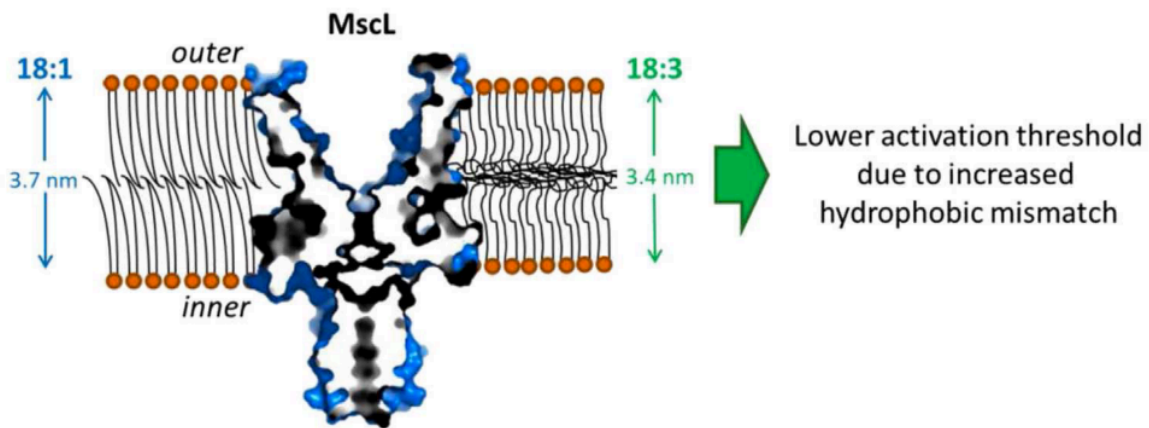


Figure 2.4 MscL activation is predominantly affected by membrane thickness

MscL activation was measured in the presence of various membrane amphiphiles which are expected to alter membrane properties. The property which consistently affected MscL activation was membrane hydrophobic thickness as helical tilt is promoted in thinner membranes thus reducing the force to activate the channel (reproduced with permission, license #5278980197400 original source: Ridone *et al. Journal of the Mechanical Behavior of Biomedical Materials* 2018).

Eukaryotic mechanosensitive channels

A major challenge of isolating the effects of membrane properties on eukaryotic mechanosensitive channels in cellular environments is due to the unknown effects of added amphiphiles on the complex environment of the cell and the inability to isolate differences between membrane mechanics and the contribution of cytoskeletal forces. In addition, the techniques commonly used to measure membrane properties of cells, such as atomic force microscopy (AFM), do not exclude the impact of cytoskeletal forces. A large portion of the work that has been done to determine eukaryotic mechanosensitive channel sensitivity has been performed using exogenous addition of fatty acids or cholesterol to cellular membranes. The effect of these molecules on membrane mechanics may be predicted as described in Table 1, however, the impact in a cellular context may not be as reliable as in model membrane systems. as an example, cholesterol is known to stiffen model membranes as measured through area expansion modulus, bending stiffness, and fluidity (51, 55, 66, 67). However, when cholesterol is added to cellular membranes and cell stiffness is measured by AFM, cholesterol addition is perceived to soften membranes (102). These observations may signify two possibilities, 1) live cells perform extensive remodeling and soften their cytoskeleton and membranes simultaneously upon cholesterol addition. Or 2) measurements of cell properties may largely measure cytoskeletal contributions and the addition of cholesterol may affect both the cytoskeleton and membrane mechanics.

Despite these challenges, the body of research attempting to determine the role of membrane properties on eukaryotic mechanosensitive channels has been increasing. As eukaryotic systems contain more complex signaling pathways, various ion channels have been proposed to be mechanosensitive. Some of such channels have been demonstrated to be activated by force-from-lipids and their behavior is modulated by the incorporation of different membrane amphiphiles (34). However, other channels such as transient receptor potential cation channel subfamily V member 4 (TRPV4) are insensitive to membrane stretch (103) yet activate in cell swelling conditions thus the activation mechanism remains elusive but this channel is presumed to be indirectly mechanosensitive (33). Despite the uncertainty in the mechanosensitivity of

TRPV4, the Vasquez group observed a connection between membrane mechanical properties and TRPV4 activation. This study suggested that in the presence of a polyunsaturated fatty acid, TRPV4 activation is increased which was attributed to reduced membrane bending stiffness and increased fluidity (104). These studies suggest that membrane mechanical properties play a role in mechanosensation through the modulation of channels which are directly and indirectly activated by membrane tension.

Piezo1 – a model mammalian mechanosensitive channel

A mechanosensitive channel which has gained interest recently is Piezo Type Mechanosensitive Ion Channel Component 1 (Piezo1) due to its prevalence in red blood cells and many human tissues such as bladder and lungs. Piezo1 is one of the most well-studied mammalian mechanosensitive channels in terms of structure and functional response to changes in membrane lipid composition. This channel has a unique two-part behavior where channel *activation* and programmed *inactivation* are distinct features of this channel, and each behavior responds differently to cellular and membrane mechanical properties. Another study by the Vasquez group demonstrated that stiffer environments measured by AFM desensitize Piezo1 activation (31). In addition, the activation of Piezo1 in response to altered membrane properties was explored in the presence of polyunsaturated fatty acids. The *activation* of Piezo1 was not affected by the presence of different polyunsaturated fatty acids, which had similar AFM measurements (31). However, channel *inactivation* was affected by EPA and DHA differently where EPA increased inactivation sensitivity and DHA reduced this sensitivity, prolonging the open state of the channel (Figure 2.5) (31, 32). Piezo1 has also been demonstrated to be activated by cytoskeletal forces, supporting an *activation* mechanism which is modulated by cellular mechanics (105). AFM measurements could not delineate the differences observed for Piezo1 *inactivation* between EPA and DHA suggesting that overall cell stiffness does not mediate this effect. In contrast, micropipette aspiration of model membranes containing a phospholipid and cholesterol demonstrated differing area expansion moduli between EPA and DHA (46) suggesting that the membrane area expansion modulus may be important for Piezo1 *inactivation*, however, these effects will

need to be confirmed in cellular membranes. Together, these results suggest that channel *activation* may be sensitive to cell stiffness which has a large cytoskeletal contribution, while channel *inactivation* may be more sensitive to lipid mechanical properties.

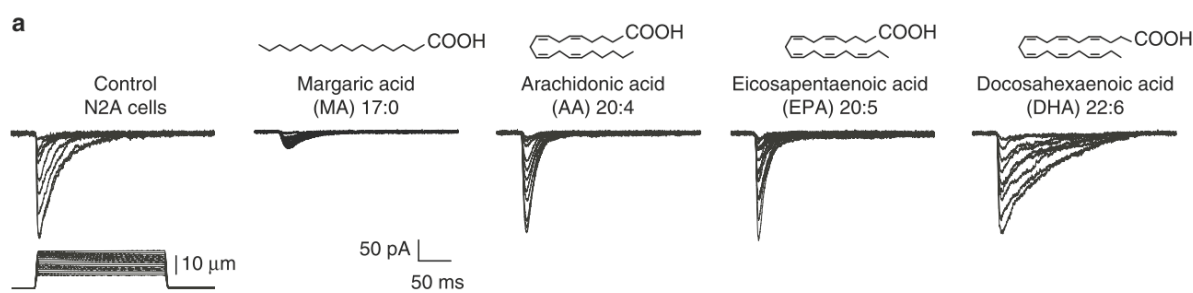


Figure 2.5 Piezo1 inactivation sensitivity is modulated by PUFAs

Various fatty acids were incubated with N2A cells expressing Piezo1. A saturated fatty acid (MA) reduced Piezo1 activation while PUFAs did not affect activation but exhibited differential effects on Piezo1 inactivation (reproduced with permission under CC-BY-4.0 <https://creativecommons.org/licenses/by/4.0/> original source: Romero *et al. Nat. Comm.* 2019).

Recent work by the Martinac group also proposed an effect of membrane mechanics on Piezo1 behavior as they determined that Piezo1 is sensitive to cholesterol organization within the membrane. Upon cholesterol removal or after redistribution of cholesterol, Piezo1 is less sensitive to forces which activate and later inactivate the channel and these features of channel behavior may be functionally linked (32). Similarly, the polyunsaturated fatty acid DHA decreased the inactivation sensitivity of Piezo1 suggesting a similar effect as cholesterol removal on channel desensitization. The observations of Piezo1 activity by the Martinac group (32) in comparison to the results by the Vasquez group (31) suggest that Piezo1 inactivation sensitivity may be a more reliable measurement in response to membrane mechanics rather than cytoskeletal forces and this measurement may predict overall sensitivity of the channel in differing membrane environments. Taken together, these results suggest that the membrane area expansion modulus may impact Piezo1 sensitivity where membranes which are softer after cholesterol removal reduce the sensitivity of Piezo1 programmed *inactivation*.

Despite the similarities between mechanosensitive channels, the membrane properties important for channel activation differ between each channel. For instance, MscL and MscS, which are bacterial mechanosensitive channels exhibit sensitivity to distinct membrane properties. In addition, more work needs to be performed on eukaryotic mechanosensitive channels to determine how membrane mechanical properties without cytoskeletal contributions alter eukaryotic mechanosensitive channels. Based on the research that has been performed in cellular membranes, the impact of membrane mechanical properties alone is difficult to elucidate however the results using AFM which measures overall cell stiffness and estimates of expected membrane mechanical properties can demonstrate that eukaryotic mechanosensitive channel behavior is more complex than bacterial mechanosensitive channels. As an example, Piezo1 behavior is characterized in two parts and each part may be fine-tuned where cell stiffness (bending rigidity and cytoskeletal contributions) may impact activation (31), however, other mechanical properties such as area expansion modulus may modulate the behavior of channel inactivation where lower area expansion moduli are expected in desensitize Piezo1 (31, 32, 46). Together, the studies of all mechanosensitive channels to date demonstrate that channels which are sensitive to bending stiffness are sensitized by reductions in bending stiffness and hydrophobic thickness (24, 27, 104). In contrast, channels which may be more sensitive to area expansion modulus are desensitized by membranes that are expected to have reductions in area expansion modulus (31, 32, 46).

2.4 The relationship between optimal membrane composition in membrane protein folding and activity

The impact of membrane mechanical properties of mechanosensitive channels from folding to function highlights a connection between these processes. There is a trend where membrane thickness and bending stiffness are important for both mechanosensitive channel folding and behavior. This could be due to the requirement for helix tilting during mechanosensitive channel activation (106) and helix insertion during folding (13). This observation suggests that in the environment of the ER, where the membrane is thinner

than the plasma membrane, some mechanosensitive channels may activate more frequently. Hydrophobic thickness may be the best predictor for folding and activity because thinner membranes allow a protein fold as well as promote mechanical activation of some mechanosensitive channels.

Mechanosensitive channels are required for cell viability, however, improving activation may not be beneficial in all circumstances. For example, Piezo1 prolonged activation is known to result in xerocytosis, a form of hemolytic anemia. This effect is also known to be lethal to bacterial cells where prolonged activation of MscL leads to a critical loss in cell volume (107). This trend suggests that the membrane composition surrounding a mechanosensitive channel is important for the tuning of channel activation. As discussed in the previous section, the optimal membrane composition for each mechanosensitive channel likely differs as different mechanosensitive channels are more sensitive to different membrane properties. To achieve different membrane environments, cells use protein sorting to localize proteins in an environment that is best suited for their function.

The observation of protein sorting into distinct membranes or rafts within a membrane has been increasingly demonstrated. To ensure membrane proteins are localized to their ideal membrane composition, cells have biological protein sorting mechanisms such as vesiculation and transport from the ER to the Golgi then plasma membrane (108). In addition, there are physical sorting mechanisms where proteins have been observed to sort based on transmembrane domain length and organelle membranes become thicker along the protein sorting pathway (Figure 2.6) (64, 109–112). The finding that GPCR raft localization can be changed upon addition of polyunsaturated fatty acids supports a physical sorting mechanism (77).

While most proteins fold in similar membrane environments, the optimal membrane composition for mechanosensitive protein activity varies. Segregation of protein folding events to a specific region of a membrane, or a specific organelle may benefit the cell by preventing premature protein activity, especially in the case of mechanosensitive channels. It is logical that there is a reason that the ER is used to fold

membrane proteins while most proteins are utilized in the plasma membrane or other organelles. In addition, each organelle has a unique membrane composition (36), suggesting that the composition used for protein folding may not be optimal for protein activity, and the protein must be sorted to a membrane with a composition more suited for its behavior. As an example, cholesterol is found at low concentrations in the ER and this is important for membrane protein folding (10), however, when cholesterol is removed, Piezo1 functionality is impaired suggesting a role for cholesterol in Piezo1 activity (32). This observation also highlights the possible importance of protein folding within the ER rather than the plasma membrane, as the optimal folding environment would promote channel activation and the cell would be vulnerable to lysis during mechanosensitive channel folding. In addition, the sorting of a membrane protein may be important for protein stability. In a study by the Booth group, one membrane protein preferentially folded into membranes with specific compositions while another protein did not exhibit a preference to any specific composition (12). This observation may indicate that timely sorting of membrane proteins may be required for their stability after folding.

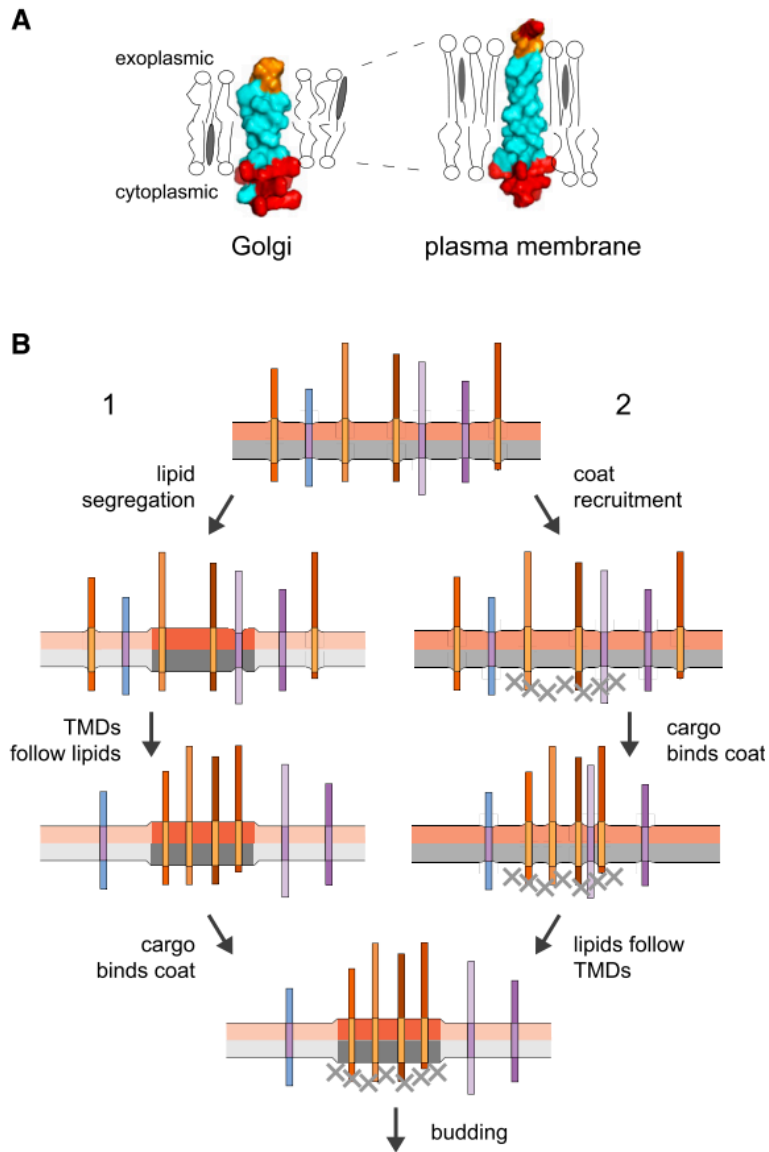


Figure 2.6 Protein trafficking is determined by transmembrane domain length

A) Proteins in the Golgi reside in thinner membranes than the plasma membrane and have relatively shorter TMD lengths. B) Two potential mechanisms of cellular organization. Either (1) lipids separate first and then proteins follow based on hydrophobic mismatch or (2) proteins are sorted through biological mechanisms which directs lipids towards these proteins to reduce hydrophobic mismatch (reproduced with permission under CC-BY-4.0 <https://creativecommons.org/licenses/by/4.0/> original source: Sharpe *et al. Cell* 2010).

Protein sorting is expected to be important for all proteins. Various examples of this phenomenon have been demonstrated in different biological systems. For example, KcsA channels localize to L_d domains (106). In addition, many bacterial signaling pathways are localized to L_o domains (75). Sorting has been demonstrated to be important for mechanosensitive channels too. For example, Piezo1 is believed to be clustered with cholesterol (L_o domains) and requires cholesterol for normal activation and programmed inactivation which are key features of this channel (32). Additionally, MscL is curvature-sensitive and as a result it clusters in areas of high membrane curvature such as the bacterial poles (113). These observations suggest that membrane protein sorting is critical to the functioning of mechanosensitive channels.

Mechanosensitive channel activation through force-from-lipids may also be affected when these channels reside within lipid rafts. The connection between mechanosensitive channel behavior, membrane mechanical properties and lipid rafts may be demonstrated by the previously determined relationship between mechanosensitive channel activation and cholesterol. Cholesterol was demonstrated to increase the force required to activate MscL (24). In contrast, cholesterol is required for Piezo1 activation and domain disruption prevents Piezo1 activation (32). These seemingly opposite behaviors could be connected by their localization within lipid rafts. For example, as rafts suppress mechanical noise (27) and the membrane may stretch around lipid rafts (46), channel activation may be protected from membrane perturbation and may be excluded from membrane stretching. However, when rafts are disrupted, or in the case of channels which reside in the non-raft phase, the channel is sensitive to membrane perturbations and relies on the global membrane properties and tension propagation to the channel. In addition, this model may also be important for perturbations which occur within a lipid raft by direct cytoskeletal attachment interactions (114) which may discern local activation from global activation of mechanosensitive channels. Together, these observations demonstrate that the relationship between mechanosensitive channel behavior and membrane properties are complex, and the presence of dynamic lipid rafts further complicates this relationship.

2.5 Conclusion

Membrane composition is heterogeneous throughout the various membranes of a cell and even within the same membrane. This heterogeneity gives rise to various physical features across and between membranes which serve unique roles in biological processes. One process which leverages this heterogeneity is membrane protein folding from translation to oligomerization and function. Evidence suggests that a membrane composition which is optimal for protein folding will not be optimal for the function of most proteins and cells use various trafficking mechanisms to relocate proteins after production. This observation may explain why biological systems developed specialized organelles for folding in comparison to function. This observation, however, poses a question for bacterial protein folding and sorting. Do bacteria have more robust folding behaviors amenable to different environments because they do not have specialized organelles for compartmentalization? In addition, the role of intramembrane sorting through lipid rafts remains a question for folding and activity behaviors which may allow bacteria to fold proteins in non-raft domains and shuttle the folded protein into rafts for its proper function.

Chapter 3

3. Methods for lipid/polymer hybrid membrane preparation and co-translational insertion of a membrane protein

This chapter is published as

Jacobs M.L., Kamat N.P. (2022) Cell-Free Membrane Protein Expression into Hybrid Lipid/Polymer Vesicles. In: Karim A.S., Jewett M.C. (eds) Cell-Free Gene Expression. Methods in Molecular Biology, vol 2433. Humana, New York, NY. https://doi.org/10.1007/978-1-0716-1998-8_16

The works in this chapter is reproduced with permission (5278980905393)

Abstract

Hybrid membranes comprised of diblock copolymers and phospholipids have gained interest due to their unique properties that result from blending natural and synthetic components. The integration of membrane proteins into these synthetic membranes is an important step towards creating biomembrane systems for uses such as artificial cellular systems, biosensors, and drug delivery vehicles. Here, we outline a technique to create hybrid membranes composed of phospholipids and diblock copolymers. Next, we describe how membrane proteins can be co-translationally integrated into hybrid lipid/ polymer membranes using a cell-

free reaction. We then outline a method to monitor insertion and folding of a membrane-embedded channel protein into the hybrid membrane using a fluorescent-protein reporter and dye release assay, respectively. This method is expected to be applicable for a wide range of membrane proteins that do not require chaperones for co-translational integration into vesicles and provides a generalized protocol for expressing a membrane protein into a membrane mimetic.

3.1 Introduction

Hybrid-membrane vesicles, self-assembled from phospholipids and diblock copolymers, display an array of unique properties. These properties can include increased stability of the vesicle and enhanced and directed integration of cell-free expressed membrane proteins (115–117). Together, these properties should enhance the performance of biosensors, drug delivery vehicles, as well as artificial cellular systems (118–124). While membranes serve as a critical scaffold to incorporate a variety of amphiphiles and proteins, the membrane proteins themselves allow a range of functionalities to be introduced through behaviors such as the transport of specific molecules, inducible permeability, and enzymatic activity (125).

To add to the functionalities imparted by proteins to membrane systems, non-natural molecules such as diblock copolymers have recently gained interest as a membrane mimetic. These synthetic molecules offer increased stability and chemical flexibility compared to natural lipids (117, 126–129). Diblock copolymers can be blended with phospholipids to form hybrid membranes that display both the biocompatibility of a lipid membrane and the increased stability of a polymer membrane (130, 131). Recently, diblock copolymers have also been shown to impart unique physical properties to phospholipid membranes that, in turn, enhance the integration of certain channel proteins (115).

Cell-free protein expression enables the co-translational integration of membrane proteins into synthetic membrane mimetics such as synthetic vesicles. Unlike traditional protein purification and reconstitution techniques required to integrate membrane proteins into vesicles, this system requires limited equipment

and is faster and less labor intensive than traditional expression and purification techniques. The cell-free expression of membrane proteins has the additional benefits of reduced aggregation of proteins and decreased cytotoxicity that results when the desired protein is made within live cells prior to purification (132). The PURExpress system for in vitro protein expression is particularly useful as it is commercially available and is extremely user-friendly (133). In addition, the PURExpress system lacks proteases, which allows for the production of proteins that would typically be signaled for degradation in a cellular context (134). Cell-free expression systems offer ease-of-use and have the ability to overcome many challenges in membrane protein production.

Traditional, reconstitution-based techniques to integrate membrane proteins into synthetic vesicles require detergent solubilization of both proteins and lipids followed by reconstitution and removal of excess detergent. While methods using detergent-based reconstitution are more commonly used to integrate membrane proteins, complete detergent removal after protein insertion into vesicles is not possible and residual detergent in the membrane would affect membrane physical properties and subsequently may interfere with protein activity and membrane stability (135–137). Similarly, the cell-free expression of membrane proteins in cell-free systems made from crude cellular extract is subject to lipid contamination from residual cellular lipids. However, the PURExpress system lacks significant lipid contamination. This purity allows the user to better control the composition of membrane mimetics to which they will co-translationally integrate membrane proteins, ultimately providing more control over experimental studies of protein functionality assays.

An added benefit to using cell-free protein expression techniques to integrate membrane proteins into synthetic vesicles is the detection of proteins as they are being produced. Green fluorescent protein (GFP) can be used as a protein tag for the observation of protein folding in a cell-free reaction (138, 139). In this method, we outline the use of green fluorescent protein as a c-terminal tag on a membrane protein of interest, the mechanosensitive channel of large conductance (MscL). This tag enables the detection of

protein production and folding through a fluorescent readout (115, 138) and could be included as a chimera on a wide variety of proteins to detect protein expression and folding during the reaction.

Here, we outline a protocol for the formation of these hybrid membranes that can be used for any application. Cell-free membrane protein expression into polymer or lipid vesicles has been used to reconstitute a variety of membrane proteins. However, many of the applications of such systems have yet to be realized. This protocol outlines a streamlined method to insert membrane proteins into hybrid lipid/polymer membranes and observe protein production, while the reaction is taking place. In addition, we outline a method to demonstrate the functional folding of a channel protein by observation of dye transport through an open channel. This method can be applied to the formation of hybrid vesicles for any application and can be used to assess the expression of membrane proteins into any membrane mimetic. Together, these methods should help scientists rapidly assess the assembly of hybrid vesicle membranes containing integral membrane proteins for a variety of subsequent applications.

3.2 Materials

All organic solvents should be handled in a fume hood using glass syringes and containers.

3.2.1 Hybrid vesicle preparation

1. 1,2-dioleoyl-sn-glycero-3-phosphocholine (DOPC) (786.1 g/mol): 50 mg/mL (63.6 mM) in HPLC-grade chloroform (see Note 1).
2. Poly(1,2-butadiene)-b-poly(ethyleneoxide) (PEO14-b-PBD22) (1800 g/mol): 40 mM in HPLC-grade methylene chloride (see Note 2).
3. 20 mL glass vial.
4. Nitrogen gas.
5. Vacuum oven (see Note 3).
6. Ultrapure water.

7. Calcein: 100 mM Calcein in ultrapure water (see Note 4).
8. 60 °C oven.
9. Vortex.
10. Miniextruder set: 2 O-rings, 2 gastight syringes, heat block, filter supports (Avanti Polar Lipids #610000).
11. Polycarbonate membrane filters: 100 nm pore size (Avanti Polar Lipids #610005).

3.2.2 Vesicle purification

1. Gravity flow purification column: chromatography column (Bio-Rad 731-1550) packed with 4 mL Sepharose 4B resin (Sigma Aldrich), hydrated in water (see Note 5).
2. 96-well plates.
3. Fraction collector, compatible with 96-well plates (see Note 6).

3.2.3 Cell-free expression of a GFP-membrane protein into hybrid vesicles

1. Membrane protein expression plasmid: Any bacterial expression plasmid containing a T7 promoter and membrane protein of interest, 200 ng/ μ l in ultrapure water (see Note 7). A C-terminal GFP fusion may be included for the observation of protein expression (see Note 8).
2. PURExpress kit (see Note 9).
3. Microplate reader with fluorescence and kinetic scan capabilities.
4. Glass bottom 384-well plate.
5. Plate sealers.

3.2.4 Assessment of membrane protein activity

1. Osmometer.

2. 800 mOsm PBS: Phosphate buffered saline (PBS tablets) dissolved to 800 mOsm (see Note 10).
3. MTSET solution: (2-(Trimethylammonium)ethyl methanethiosulfonate Bromide)) dissolved in ultrapure water to 21 mM.
4. Glass bottom 96-well plate.
5. Triton-X 100: 10% by volume in ultrapure water.

3.3 Methods

Carry out all procedures at room temperature unless otherwise specified.

3.3.1 Hybrid vesicle preparation

1. Using a glass syringe (see Note 11), mix 369.2 μL of DOPC stock (63.6 mM) and 65 μL of PEO-b-PBD stock (40 mM) (see Note 12) into a large (~20 mL) glass vial. Gently swirl the vial to mix. This will later equate to vesicles with 26.09 mM total amphiphile concentration in 1 mL (90 mol% DOPC, 10 mol% PEO-b-PBD) (see Note 13).
2. Dry chloroform from the sample by tilting at a 45° angle and slowly rotating the vial under a nitrogen stream until no chloroform is visible. An even, thin film should be deposited on the wall of the vial (see Note 14).
3. Remove residual chloroform by incubating the sample in a vacuum oven at -0.8 Pa for > 4 hours at room temperature.
4. Add 1 mL of ultrapure water to the dried film, being careful not to disturb the film. Cap tightly to limit evaporation of water and incubate at 60 °C overnight (see Note 15).
5. Vortex hydrated films until homogenous (5-10 seconds).
6. Assemble the miniextruder (140). Hydrate filter supports in water and place on either side of the open mini extruder inside the O-ring. Place a 100 nm polycarbonate filter over one side of the extruder O-ring and filter support. Close the extruder with the O-rings facing each other, separated by the filter. Hydrate

the extruder cavity by filling one of the extruder syringes with water and inserting on the right side of the extruder. Use a kimwipe to catch the water on the left port and push the water through the extruder.

7. Extrude vesicles. Fill the syringe with your sample and place the syringe in the right extruder port. Place an empty syringe in the left extruder port. Slowly push the sample through the extruder into the other syringe, this equals one pass. Repeat for 7 passes so the sample is removed on the opposite side of the extruder from where it began, remove the left syringe from the extruder and collect extruded vesicles in a 1.5 mL Eppendorf tube (see Note 16).

3.3.2 Vesicle purification

3.3.2.1. Purification with an automated fraction collector

1. Rinse fraction collector column connectors and tubing with 3 mL of water then reattach to the bottom of the columns.
2. Use a drop-to-drop connection and connect a gravity size exclusion column to the line. Raise the column above the collector to initiate gravity flow (Figure 3.1A), rinse the column with one column volume of purification solution (see Note 17).
3. Lower the column height below the fraction collector and add 100 μ L of calcein-containing vesicles carefully to the resin (Figure 3.1B).
4. Move the column height above the fraction collector and start collecting fractions. Collect drops at 0.4 min/well into one row of two 96-well plates.
5. Add buffer dropwise to the resin until the calcein has completely entered the column and a clear layer of resin is visible above the calcein.
6. Gently fill the column with 1 column volume of water and collect 24 fractions.
7. When all fractions are collected, rinse with 1 column volume of buffer. Lower the columns below the fraction collector height to stop gravity flow and cap both ends of each column to store.

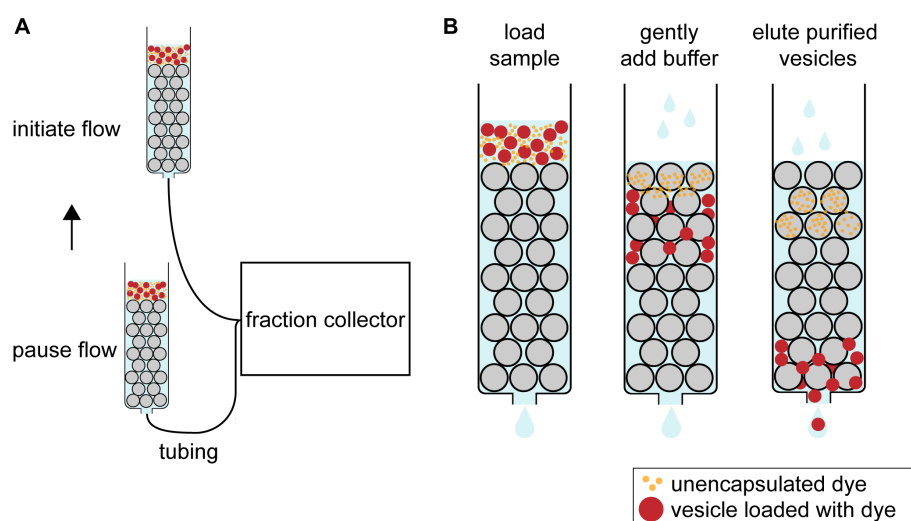


Figure 3.1 Vesicle purification schematic

A) Gravity size exclusion chromatography using a fraction collector. Altering the height of the column relative to the fraction collector controls flow within the column. Fraction collector use is optional, and samples can be collected manually by placing a tube under a dripping column as described in **method 3.3.2**. B) Vesicles are isolated from unencapsulated dye using gravity size exclusion chromatography as described in **method 3.3.2**.

8. To determine which fractions contain vesicles, measure the fluorescence of each well using a plate reader (Figure 3.2) with Excitation 480 nm, Emission 520 nm (see Note 18).

3.3.2.2. Purification without the assistance of a fraction collector

1. Secure the column by clamping onto a stand or placing in holder such that a 96-well plate can be moved easily underneath the column. Add vesicle samples as described above and collect an equivalent number of drops (3-4 drops) per well (see Note 19).

3.3.3 Cell-free expression of a GFP-membrane protein into hybrid vesicles

1. Heat a plate reader to 37 °C.
2. Thaw all PURExpress kit components on ice for 30 min. Mix tube A from the PURExpress kit by vortexing for several seconds, if precipitation does not dissolve, mix by pipetting. Do not vortex tube B from the PURExpress kit. Briefly centrifuge tubes A and B.

3. Add 10 μL of tube A, 7.5 μL of tube B, 1 μL (200 $\text{ng}/\mu\text{L}$) of DNA (see Note 20), and 11.5 μL of extruded vesicles to a 0.5 mL tube. Mix by pipetting 15 times (see Note 21).
4. Aliquot each sample into a glass bottom 384-well plate and seal with a plate sealer. Insert the plate into the plate reader and begin reading GFP fluorescence.
5. Allow the reaction to incubate for 3.5 h at 37 $^{\circ}\text{C}$ while reading GFP fluorescence every 5 minutes (see Note 22). GFP fluorescence should increase over time as protein is produced in the presence of vesicles (Figure 3.3). If vesicles contain calcein for non-selective channel activity, proceed to method 3.3.4, GFP fluorescence will not be able to be detected in the presence of calcein.

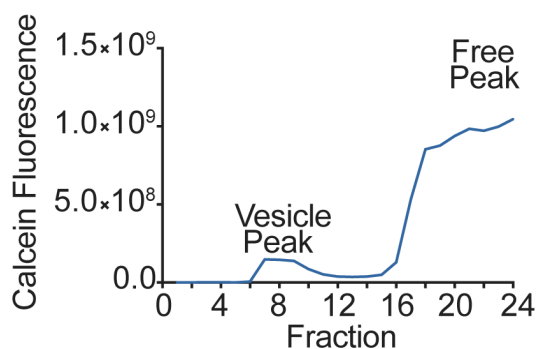


Figure 3.2 Sample vesicle purification elution curve

After calcein encapsulation, vesicles are purified to remove free calcein. The vesicle fraction is detected first, in the column void fraction, followed by the free calcein peak. Calcein fluorescence is plotted against the collected fraction number.

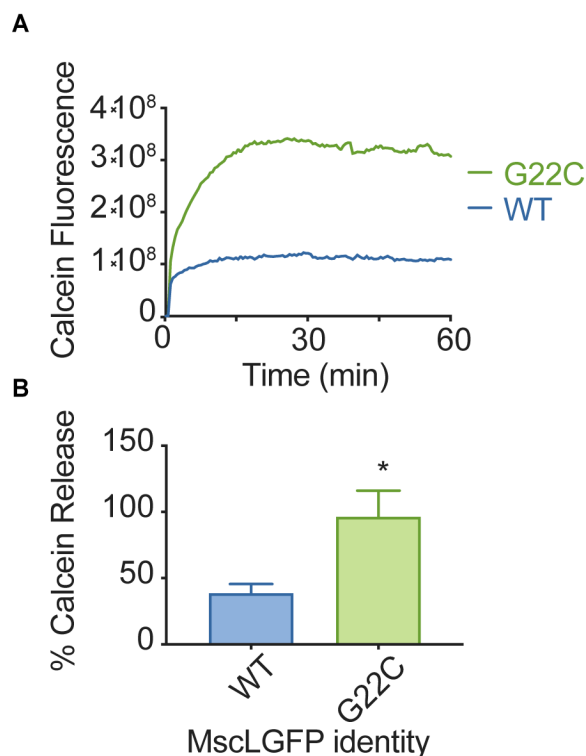


Figure 3.3 MTSET calcein release assay

A) MscLGFP is activated by the addition of MTSET to initiate channel opening and activity is observed using calcein fluorescence activation upon release from vesicles. Increased calcein fluorescence demonstrates release from vesicles in the presence of an activatable mutant (G22C) and a wild-type negative control. B) Calcein release is greater in the presence of chemically activatable MscL compared to wild type. Final % calcein release is compared to the wild type negative control, * $p < 0.5$, significance values are determined by the student's unpaired t-test. $n=3$, error bars represent standard error of the mean.

3.3.4 Assessment of membrane protein activity

1. Re-purify vesicles as described in method 3.3.2, using 800 mOsm PBS as a purification buffer instead of water (see Note 23). Equilibrate the prepared column that was used for the initial vesicle purification in 800 mOsm PBS by washing with 2 column volumes (see Note 24).

2. Using the vesicle fraction from step 1 with the highest amount of calcein (Figure 3.2), transfer 75 μL of each sample in duplicate into a glass bottom 96-well plate (see Note 25).
3. Read the background calcein fluorescence of the aliquoted samples using a plate reader with Excitation 480 nm, Emission 520 nm.
4. Add 3.57 μL of ultrapure water or 3.57 μL of 21 mM MTSET to each sample for a final concentration of 1 mM MTSET (see Note 26).
5. Observe calcein release immediately by measuring fluorescence on a plate reader with Excitation 480 nm, Emission 520 nm, taking measurements every 30 sec for a total release time of 30 min (Figure 3.4A) (see Note 27).
6. To determine calcein fluorescence upon complete release from vesicles, add 1 μL of 10% triton-X 100 solution to each well and mix using a shaker for 5 min to ensure total destruction of vesicles.
7. Measure total calcein release on a plate reader with Excitation 480 nm, Emission 520 nm.
8. Calculate channel activity through percent calcein release using the following equation, $(F_{\text{MTSET}} - F_{\text{initial}}) / (F_{\text{triton}} - F_{\text{initial}})$ (Figure 3.4B).
9. Compare % release between MTSET and control samples and perform an unpaired t-test to determine if the channel is active.

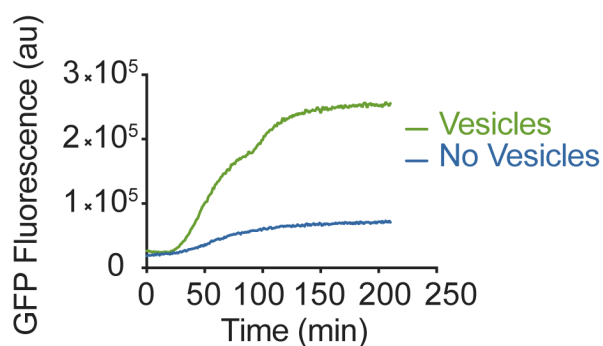


Figure 3.4 GFP fluorescence allows the observation of protein production and folding.

MscLGFP expression is monitored during a cell free reaction by observation of GFP fluorescence. A comparison of MscLGFP expression in the presence of hybrid lipid/polymer (10 mol% PEO-b-PBD, 90 mol% DOPC) vesicles compared to no vesicles.

3.4 Notes

- Using a metal spatula, weigh 100 mg DOPC powder in a glass vial (see Note 11). Add 2 mL HPLC-grade chloroform with a glass syringe and vortex to dissolve. If the lipids are pre-dissolved in chloroform from the manufacturer the solution may be dried under a stream of N₂ and rehydrated to the proper concentration. It is helpful to use small volumes of chloroform stock solution when drying mixtures of lipids and polymers into a thin film.
- Weigh 144 mg PEO-b-PBD on a balance. Using a metal spatula, transfer polymer to a glass vial by scraping small amounts of polymer from a pure stock of polymer and depositing the polymer on the inside of the glass vial near the bottom. The polymer should be viscous and sticky. Add 2 mL HPLC-grade methylene chloride with a glass syringe, cap and vortex for 3-5 seconds to dissolve.
- A vacuum that can hold up to -0.8 mPa is preferred, use at room temperature.
- Add 1245 mg calcein powder to ~18 mL ultrapure water, Add NaOH or KOH pellets, one at a time, until calcein is dissolved. This step may take longer than expected and should be performed in advance to calcein usage. Adjust pH to 8.0 using HCl. Adjust final volume to 20 mL with ultrapure water. The pH

measurements will likely dye your pH probe. If possible, it is nice to designate a pH probe in the lab for measurements in fluorescent solutions such as this. Prepared calcein may be stored at 4 °C for 6 months and should be discarded if aggregates are observed.

5. Snap the stopper off the end of a Biorad poly-prep chromatography column and wash with one column volume of ultrapure water. Add 7 mL of Sepharose 4B resin slurry and let the ethanol flow out by gravity as the resin settles. The resin rapidly settles-be sure to mix the Sepharose 4B slurry in its original container well before addition to the column to ensure you are extracting approximately the same amount each time you prepare a column. The final column volume will settle to ~4 mL. Wash with 3 column volumes of ultrapure water to remove residual ethanol by gravity flow. To wash a column, it is best to add a small layer of liquid above the column first, let that liquid fully enter the column, then add a larger volume of water or buffer. To add 1 column volume of water (4 mL in this case), you would add ~ 200 μ L of water to the column, let that water enter the column completely but not allow the column to remain dry for more than 5 seconds, and then add the remaining 3.8 mL of water. Repeat 2X. Allowing the resin to remain dry for more than 5-10 seconds will cause cracking of the column, however, not allowing column solutions to completely enter the column prior to the addition of more water/buffer results in continual dilutions of that solution opposed to its complete removal.

6. We use a Gilson FC204 fraction collector; however, fractions may be collected manually as well.

7. Any plasmid containing a T7 promoter is suitable for protein expression in the PURExpress system (ex. Addgene #165097).

8. A membrane protein fused with GFP at the C-terminus may be used to observe expression and folding of most proteins (138). This tag must be fused C-terminally to ensure the full length of the desired membrane protein is translated when GFP is detected. However, this tag is a large soluble protein that is expected to impact protein orientation. If a protein with a different desired orientation is required, alternate methods may be used to assess expression and folding (ex. Western Blotting, CD spectra, NMR, EPR).

9. Any cell-free protein synthesis system can be used, however, PURExpress contains purified transcription and translation machinery and does not contain lipid contamination, which is preferred for

downstream applications including assaying the effect of membrane composition on membrane protein behavior.

10. If an osmometer is not available, 3x PBS is acceptable to use as a purification buffer to prevent vesicle bursting after exposing the vesicles to the cell-free reaction.

11. Glass syringes are necessary when handling organic solvents since plastic is soluble in chloroform. Wash glass syringes at least three times in clean chloroform prior to handling samples and between each sample.

12. To determine an optimal molar ratio of lipids and polymers, a range of ratios may be tested. We have used 10, 15, 25, 50, 75, and 100% PEO-b-PBD and formed bilayer membranes. Some diblock copolymers may not form bilayers depending on the size of their hydrophobic and hydrophilic blocks, the polymer we use was purchased from Polymer Source and contains ~14 PEO groups linked to 22 PBD groups. PEO-b-PBD polymers with a similar ratio of hydrophilic to hydrophobic regions should form bilayers. The successful formation of bilayers can be determined by observing giant vesicles using microscopy techniques, more coarsely by performing dynamic light scattering techniques to measure particle size, and most accurately by performing cryoTEM analysis. DLS should never be used as the sole method to assess vesicle formation as aggregates also form particles in the size range of vesicles. Unextruded vesicles should be visible using phase contrast microscopy with a 20x objective or higher and can range from <1 – 80 μm . If bilayers do not form, the amphiphiles may form micelles, which are too small to visualize using microscopy (see Note 13) but can result in a DLS peak around 10 nm.

13. When using microscopy for the determination of bilayer formation, a larger vial and a lower concentration of lipids should be used during the thin film hydration procedure. For example, we find that 20 mL glass vials containing 1 mL of a 150 μM solution of amphiphiles is best. It is also important to dilute vesicles in an osmolarity matched, but less dense solution to aid imaging after vesicle formation. For example, we hydrate our vesicles in ~300 mOsm sucrose and dilute these vesicles in PBS. Pipette a small amount of formed vesicles into a larger microscope chamber containing equiosmolar PBS. The vesicles should sink to the bottom of the chamber and be more readily visible.

14. It is important to be careful while drying mixtures of lipid and polymer films. If a uniform film is not distributed with maximum surface area within the vial, we have observed visible aggregation of the amphiphiles after hydration. Aggregation is also an indication that the amphiphile concentration needs to be reduced. Thin film formation is critical for hybrid lipid/ polymer vesicle formation as some methods may cause independent lipid and polymer vesicles or domain formation (131, 141). By slowly spinning the vial as the solvent is removed, a uniform and visible thin film will coat the glass surface of the vial and the lipids and polymers should remain mostly mixed upon rehydration. Other inert gasses such as argon are also acceptable for drying lipids and polymers.

15. For fluorescent protein detection, hydrate vesicles in ultrapure water. For channel activity assays, hydrate vesicles in 100 mM calcein. Vesicle addition to the cell-free reaction takes the place of water, it is important to avoid the introduction of excess salt to the reaction during the addition of vesicles as salt changes affect PURExpress reaction efficiency. Accordingly, the vesicles must be hydrated in water, or hydrated in calcein, then purified in water. Calcein release from vesicles is a straightforward method to measure channel activity. This method is applicable to any nonselective membrane channel protein that can be activated using a chemical additive. We used a chemically activatable mutant of the mechanosensitive channel of large conductance, MscLGFP (G22C), which opens with the addition of MTSET (142). Upon channel opening, calcein is released from the vesicles to the external solution, which increases calcein fluorescence and provides a fluorescent readout for channel activity.

16. Vesicles may be stored at 4 °C for up to two weeks. If vesicles were hydrated in calcein, purification is required immediately prior to protein expression, proceed to method 3.3.2 for vesicle purification. If vesicles were hydrated in water, proceed to method 3.3.3.

17. Purification solution for calcein vesicles prior to expression is ultrapure water. After protein expression, the purification solution may be any buffer near 800 mOsm, such as 3x PBS. Once the buffer is level with the top of the resin, being careful not to allow the resin to dry and crack, lower the column height to below the fraction collector to pause the column flow. It is easiest to add samples to multiple columns while gravity flow is paused.

18. The vesicle peak should be within the first 10 fractions and the free peak should be present after fraction 12. The vesicle peak should exhibit less fluorescence than the free peak since calcein is present at a self-quenching concentration within the vesicles. If high concentrations of vesicles are used, calcein in the vesicle and free fractions will be visible by eye as well.

19. Purification without a fraction collector is useful if a fraction collector is not available (143). As this method requires the user to manually collect samples it is more prone to user error and it may be helpful to tune the number of drops per well to the desired elution volume. We find that 200-300 μ l elution volume per well is optimal for vesicle purification.

20. The optimal plasmid concentration varies and may be optimized. Any plasmid containing a T7 promoter is suitable for expression using the PURExpress system. Many membrane proteins display the ability to fold into their native conformation without the need for chaperones (12, 15, 144). This phenomenon may allow for the production of difficult-to-express membrane proteins (145). Therefore, the present method is likely applicable to a wide range of membrane proteins for the functionalization of model membranes. A method to determine the optimal phospholipid for a given protein is to form pure lipid vesicles at equal concentrations and observe fluorescence during expression. The composition which exhibits the highest fluorescence should be used as the phospholipid in a lipid/polymer blended vesicle.

21. Vesicle addition to the PURExpress reaction takes the place of water, which differs from the manufacturer's protocol. The volume of vesicles is limited to 11.5 μ l per reaction in order to maintain the proper concentration of reaction components. If more vesicles per reaction are desired, increasing the lipid concentration during vesicle preparation is preferred over adding more vesicle volume to the cell-free reaction. Vesicles composed of DOPC and diblock copolymer will form up to 60 mM, or higher if polymer is present at a lower mol%. If aggregation is observed after vesicle hydration, the concentration of amphiphile must be reduced. If a no-vesicle control is desired, the vesicle volume in the cell-free reaction should be replaced with ultrapure water.

22. A membrane protein expressed as a fusion protein with a c-terminal GFP tag may be used for the observation of protein expression and folding during the cell-free reaction (138, 146). While this protocol is

applicable to the expression of any membrane protein, tagged or untagged; using a GFP folding reporter allows the observation of protein production and allows the quantification of protein folding. If calcein is encapsulated in vesicles, GFP fluorescence will not be detected as calcein fluorescence occurs at a similar wavelength as GFP.

23. After protein expression, vesicle purification is necessary to remove any calcein that may have diffused out of the vesicles during protein insertion. In addition to removal of calcein, vesicle purification can also be used to purify the expressed membrane protein away from the PURExpress components that may disrupt downstream applications of the functional vesicles.

24. The osmolarity of the vesicle internal and external solutions must match to prevent vesicle bursting and to retain the remaining encapsulated components. In this step, in order to retain calcein for the activity assay, the osmolarity of the purification buffer solution after cell-free expression must be near 800 mOsm.

25. Free calcein will have higher fluorescence than encapsulated calcein. It is important to be careful to use the vesicle fraction which is the first small peak instead of the large peak of unencapsulated dye (Figure 3.2).

26. Ultrapure water is used as a control for the osmotic disruption of vesicles when MTSET is added, some calcein leakage is expected with water addition. An additional important control for studies like this is to include vesicles that do not have any membrane protein to evaluate the extent to which water or MTSET nonspecifically induces calcein release.

27. Calcein is a self-quenching dye. Fluorescence becomes increasingly quenched past a certain concentration of calcein, which we encapsulated in vesicles. Upon release from vesicles, the local concentration of calcein is reduced and an increase in fluorescence is observed. Depending on the ratio of the concentration of vesicles used compared to the volume of the extravesicular solution, the encapsulated concentration of calcein may be optimized to maximize the increased signal in calcein fluorescence upon vesicle disruption or permeabilization. The optimal range of calcein concentration for vesicle formation may range from 10 mM to 200 mM.

3.5 Acknowledgements

This work was supported by the Air Force Office of Scientific Research (AFOSR) YIP FA9550-19-1-0039 P00001 to NPK and NSF grant MCB-1935356 (NPK). M.L.J. was supported by Grant No. T32GM008382 from the National Institute of General Medical Sciences and The American Heart Association Predoctoral Fellowship under Grant No. 20PRE35180215.

Chapter 4

4. Determination of the role of membrane area expansion modulus and defects on the folding of the mechanosensitive channel of large conductance using hybrid membranes composed of diblock copolymers and phospholipids

Parts of this chapter have been published as or are in preparation to be published as

Jacobs, M. L.; Boyd, M. A.; Kamat, N. P. "Diblock copolymers enhance folding of a mechanosensitive membrane protein during cell-free expression." *Proceedings of the National Academy of Sciences*. 2019.

Steinkühler, J.; Jacobs, M. L.; Boyd, M. A.; Loverde, S. M.; Kamat, N. P. "Addition of bioorthogonal diblock copolymer to phospholipid membranes controls membrane hydration and enhances peptide insertion rates." *in preparation*

Abstract

The expression and integration of membrane proteins into vesicle membranes is a critical step in the design of cell-mimetic biosensors, bioreactors, and artificial cells. While membrane proteins have been integrated

into a variety of non-natural membranes, the effects of the chemical and physical properties of these vesicle membranes on protein behavior remain largely unknown. Non-natural amphiphiles, such as diblock copolymers, provide an interface that can be synthetically controlled in order to better investigate this relationship. Here, we focus on the initial step in a membrane protein's life cycle: expression and folding. We observe improvements in both the folding and overall production of a model mechanosensitive channel protein, the mechanosensitive channel of large conductance (MscL), during cell-free reactions when vesicles containing diblock copolymers are present. By systematically tuning the membrane composition of vesicles through incorporation of a poly(ethylene oxide)-b-poly(butadiene) diblock copolymer, we show that membrane protein folding and production can be improved over that observed in traditional lipid vesicles. We then reproduce this effect with an alternate membrane-elasticizing molecule, C₁₂E₈. Our results suggest that global membrane physical properties, specifically available membrane surface area and the membrane area expansion modulus, significantly influence the folding and yield of a membrane protein. Furthermore, our results set the stage for new explorations into how non-natural membrane amphiphiles can be used to both study and enhance the production of biological membrane proteins.

4.1 Significance

Membrane protein folding is a critical step that underlies proper cellular function as well as the design of technologies like vesicle-based biosensors, and artificial cells. Membrane composition is known to play a role in membrane protein folding, however, the specific mechanical properties that govern protein folding remain unclear. Using a highly elastic non-natural amphiphile, we highlight the importance of a membrane mechanical property, membrane elasticity, on the spontaneous insertion and folding of a model α -helical membrane protein. Through this study, we gain a deeper understanding of cellular membrane protein folding and offer a potential approach to improve the production of membrane proteins through optimizing the mechanical properties of synthetic scaffolds present in cell-free reactions.

4.2 Introduction

Our ability to bridge the functionality of biological and synthetic molecules could lead to entirely new materials and biotechnologies (139). A striking example of this merger is the reconstitution of membrane proteins into synthetic vesicles, which have a wide range of potential applications, from the design of model cellular systems (118–120), to the development of biosensors (121, 122) and drug delivery carriers (123, 124). Nature has designed a variety of proteins with specific and useful functions that we can harness for the aforementioned applications (125). Likewise, recent advances in the creation of synthetic membrane mimetics have generated a variety of new amphiphiles (147, 148). Among these molecules, diblock copolymers have emerged as a new class of amphiphiles that expand the range of membrane properties beyond what is possible with biological lipids alone (117, 126, 128, 129).

Polymersomes, bilayer vesicles assembled from block copolymers, are highly promising for biotechnological applications due to their compositional flexibility and enhanced stability in comparison to lipid vesicles (126). In addition, these vesicles provide new opportunities as model membrane systems to investigate biological processes. While several membrane proteins have been incorporated into both pure polymeric and hybrid polymer/lipid membranes to date (116, 117, 124, 128, 129, 149, 150), the effect of membrane composition on a wide range of protein behaviors remains largely unexplored. In order to effectively use biological membrane proteins in synthetic vesicles, we must understand how properties of vesicles and any non-natural components they incorporate affect protein behavior from production to final activity.

Because protein expression and folding are the initial steps that ultimately dictate protein activity, it is important to understand how membrane composition and properties influence these critical processes. To date, protein unfolding and refolding studies have provided the most conclusive evidence that membrane composition influences the final structure and stability of a membrane protein (14, 92–95, 151). Importantly, these studies suggested that mechanical properties, such as the available volume of hydrophobic environments, can enhance the functional folding of a membrane protein. More recently, cotranslational

folding studies have provided a more biologically relevant technique to explore how membrane composition affects protein folding. In contrast to investigating denatured proteins, cotranslational folding studies allow us to investigate how a nascent peptide chain folds as it emerges unidirectionally from a ribosomal complex. Cell-free expression methods, which utilize cellular extracts or purified components for isolated protein expression, provide a promising new technique to investigate protein-membrane relationships during protein translation (132, 133, 145, 152). Cell-free methods enable the spontaneous, cotranslational integration of many membrane proteins into vesicles or amphiphilic scaffolds that are included in the reaction (12, 153). A variety of membrane proteins have been expressed into amphiphilic constructs such as lipid vesicles (15, 97, 154), polymer scaffolds and polymersomes (127, 129, 149, 155, 156), and nanodiscs (136, 157). While these studies suggest the presence of membranes is important for preventing protein aggregation, an open question remains as to how membrane properties affect protein folding.

Using a cell-free expression system and synthetic vesicles, we show that the production of a mechanosensitive channel protein (MscL) is affected by physical features of membranes present in the reaction mixture, including membrane concentration and membrane area expansion modulus. We use diblock copolymers to tune the chemical and mechanical properties of synthetic vesicle membranes present in the reaction mixture and show that protein folding is dependent on a balance of steric repulsive interactions at the membrane surface and available membrane surface area. Our study points to the unexplored role of available membrane surface area and membrane area expansion moduli in membrane protein folding.

4.3 Materials and Methods

Materials

Chemicals: 18:1 ($\Delta 9$) 1,2-dioleoyl-sn-glycero-3-phosphocholine (DOPC), Lissamine-Rhodamine PE (18:1 1,2-dioleoyl-sn-glycero-3-phosphoethanoamine-N-(lissamine rhodamine B sulfonyl) (ammonium salt), and 1,2-distearoyl-sn-glycero-3-phosphoethanolamine-N-[methoxy(polyethylene glycol) -550] (ammonium salt) (DSPE-PEG550) were obtained from Avanti Polar Lipids, Inc. Poly(ethylene oxide)-block-polybutadiene

copolymers (PEO9-b-PBD12, PEO14-b-PBD22, and PEO24-b-PBD36) were obtained from Polymer Source. Octaethylene Glycol Monododecyl Ether ($C_{12}E_8$), Phosphate-buffered Saline (PBS), sucrose, and Sepharose 4B were obtained from Sigma Aldrich. NBD PE (NBD-phosphoethanolamine, triethylammonium salt) was obtained from Thermo Fisher. 1,6-diphenyl-1,3,5-hexatriene (DPH) was obtained from Sigma Aldrich. Calcein dye and 2-(Trimethylammonium)ethyl methanethiosulfonate bromide (MTSET) were obtained from Thermo Fisher.

Plasmids: EcMscL gene (pADtet-His6-MscL was a gift from Allen Liu (Addgene plasmid # 83373) (28)), the pET19b backbone was a gift from Douglas Rees (Addgene plasmid # 79028) (158)), mEGFP-pBAD was a gift from Michael Davidson (Addgene plasmid # 54622). Channelrhodopsin (ChR2) (pAAV-EF1a-double floxed-hChR2(H134R)-mCherry-WPRE-HGHpA was a gift from Karl Deisseroth (Addgene plasmid # 20297)). ChR2GFP was cloned into the pET19b expression vector as described for EcMscLGFP.

Methods

Lipid and polymer vesicle preparation

Vesicles were prepared through thin-film hydration as described by Kamat et al (57). Briefly, DOPC lipids were dissolved in chloroform and mixed with PEO_x-b-PBD_y polymers of varying molecular weights, DSPE-PEG, or $C_{12}E_8$ in chloroform at varying mol% relative to DOPC prior to addition to glass vials. Chloroform was evaporated under a stream of nitrogen to create a uniform film, and films were placed under vacuum for > 4 hours. For studies with MscL expression, films were rehydrated in water and incubated at 60 °C overnight. The films were vortexed and vesicles were extruded to 100 nm by 7 passes through a polycarbonate membrane using a mini-extruder set (Avanti). For studies with hybrid vesicles and membrane additives, the total amphiphile concentration per sample (moles amphiphile/ solution volume) was kept constant and the effective concentration of amphiphiles after vesicle assembly, typically 10 mM, is reported in the text.

Cloning

Briefly, EcMscL was cloned into the pET19b backbone and mEGFP was cloned as a fusion protein C-terminal to EcMscL. To generate a chemically active construct as described by Yoshimura et al. (159), a point mutation was cloned (G22C) into the EcMscLGFP fusion.

PURExpress reactions

Protein expression was performed with the PURExpress *in vitro* Protein Synthesis kit (E6800, NEB) according to the manufacturer's protocol. Final reaction volumes were 30 μ L and contained PURExpress components, 200 ng plasmid (EcMscLGFP), and desired vesicle content (10mM final unless otherwise stated). The reactions were monitored in a Molecular Devices Spectra Max i3 plate reader at 37 °C, GFP fluorescence was measured at excitation 480 nm, emission 507 nm for 3.5 hours.

Quantitative Western Blotting: Using the WesternBreeze chemiluminescent kit for mouse antibodies (ThermoFisher Scientific), 12% SDS-Page gels were treated according to kit protocol with anti-GFP (Abcam). Blots were imaged using an Azure biosystems c280 imager. Densitometry quantification was performed in ImageJ (160), measuring band density and comparing relative levels within the same blot. n=3 averaged between blots.

Microscopy

Microscopy images were taken to observe vesicle formation in the presence of C₁₂E₈. Giant unilamellar vesicles (GUVs) were hydrated to 0.5 mM GUVs in a 298 mOsm solution of sucrose. Glass bottomed Lab-Tek II microscope chambers (Thermo Fisher Scientific) were blocked with 150 μ L Bovine Serum Albumin (1 mg/mL in PBS) and rinsed. Chambers were filled with 200 μ L of 298 mOsm PBS. 1 μ L of GUVs were added to the chamber. Images were acquired on a Nikon Eclipse Ti2 Inverted Microscope.

Determination of MscL activity

Calcein was included in the vesicle hydration buffer to promote encapsulation. Unencapsulated calcein was removed by gravity size exclusion chromatography using a column packed with Sepharose 4B. Vesicles were introduced into a PURExpress reaction and were re-purified using gravity size exclusion chromatography to remove reaction components following 3.5 hr in the reaction. MscLG22C opening was measured by 1 mM MTSET activation followed by the observation of calcein release. Calcein release was

measured by fluorescence (excitation 480 nm, emission 507 nm) at room temperature for 30 min in a Molecular Devices Spectra Max i3 plate reader. A maximal release value was calculated using the fluorescence after adding 0.1% Triton X-100, which destroys vesicles. Percent calcein release was calculated as $(F_{\text{MTSET}} - F_{\text{initial}}) / (F_{\text{Triton}} - F_{\text{initial}})$ where F_{MTSET} is the fluorescence after MTSET addition, F_{initial} is the initial sample fluorescence before treatment, and F_{Triton} is the fluorescence after Triton addition.

Electroformation of GUVs

Giant Unilamellar Vesicles (GUVs) were formed through electroformation using the Nanion Vesicle Prep Pro (Nanion Technologies) and standard prep protocol. 10 μL of a 20 mM stock of amphiphiles in chloroform were dried onto the conductive side of the Nanion slide and hydrated with 200 μL of 280 mOsm sucrose.

Elasticity measurements

Area expansion moduli were measured using micropipette aspiration techniques similar to those described by Kamat et al (161). Briefly, borosilicate pipettes were filled with a PBS solution with 1 wt% BSA and connected to an aspiration station mounted on the side of a Nikon inverted microscope, equipped with a manometer, Validyne pressure transducer (model DP 15-32, Validyne Engineering Corp), digital pressure read-outs, and micromanipulators (model WR-6, Narishige). Suction pressure was applied via a syringe connected to the manometer. GUVs were picked up by a micropipette and suction was applied in ~ 1 cm H_2O increments, allowing for 5 s of equilibration before subsequent aspiration steps. Images were analyzed in ImageJ to measure vesicle diameter and membrane extension, which were then used to calculate the average area expansion modulus, K_A , of each population of vesicles.

Determination of even membrane amphiphile mixing

NBD/Rhodamine conjugated lipid were incorporated into vesicle membranes with varying fractions of DOPC and PEO-b-PBD 1.8 kDa. Vesicles were extruded to 100nm and 100 μl vesicles were aliquoted in a glass bottom 96-well plate. Bulk Forster Resonance Energy Transfer (FRET) ratios were measured in a Molecular Devices Spectra Max i3 plate reader. NBD (donor) and Rhodamine (acceptor) fluorescence were excited using 463 nm light and the emission was measured at 517 nm (to determine f_{don}) and 590nm (to determine f_{acceptor}) respectively. FRET ratio is defined at $f_{\text{don}}/f_{\text{acc}}$.

Membrane anisotropy measurements

0.5 mM vesicles containing 0.5 mol% DPH and various fractions of PEO-b-PBD 1.8 kDa and DOPC were analyzed using an Agilent Technologies Cary Eclipse Fluorescence Spectrophotometer with the Automated Polarization Accessory. Fluorescence anisotropy (r) was calculated automatically by software provided with the instrument, according to $r = (I_{vv} - I_{vh}G) / (I_{vv} + 2I_{vh}G)$, where I_{vv} and I_{vh} are the intensities of the vertically and horizontally polarized components of the fluorescent light, respectively, after excitation with vertically polarized light. $G = I_{hv}/I_{hh}$ is a grating correction factor for the optical system. Fluorescence anisotropy was assessed at the following excitation and emission wavelengths: 360 nm and 435 nm for DPH.

Membrane stability measurements

100mM calcein was encapsulated in 10mM vesicles prepared with various fractions of C₁₂E₈ or PEO-b-PBD (1.8 kDa) with DOPC. Unencapsulated calcein was removed by gravity size exclusion chromatography using a column packed with Sepharose 4B resin. Calcein leakage was measured by fluorescence (excitation 480 nm, emission 507 nm) at 37 °C for 4 hours. A maximal release value was calculated using the fluorescence after adding 0.1% Triton X-100 which destroys vesicles. Percent calcein release was calculated as $(F_{\text{final}} - F_{\text{initial}}) / (F_{\text{triton}} - F_{\text{initial}})$ where F_{final} is the fluorescence after 4 hours, F_{initial} is the initial sample fluorescence before treatment, and F_{triton} is the fluorescence after Triton addition.

Dithionite NBD quenching membrane permeability assay

1 M Sodium Dithionite was prepared fresh immediately prior to experiments in 1x PBS, pH 7.4. Small unilamellar vesicles were diluted to 2.5 mM in PBS and NBD fluorescence was measured at excitation 463 nm, emission 536 nm using a kinetic scan on a Cary Eclipse Fluorescence Spectrometer (Agilent). Sodium Dithionite was added to a final concentration of 75 mM after 1 min of the kinetic scan. The scan was continued for 20 min further to measure the rate of NBD quenching in the membrane inner leaflet. Normalized NBD fluorescence was calculated by dividing fluorescence intensity by the fluorescence intensity immediately after outer leaflet quenching. NBD quenching rate was calculated as %/min.

4.4 Results

Lipid vesicles increase production of a membrane protein.

We first investigated the folding of the mechanosensitive channel of large conductance (MscL) in a standard 1,2-dioleoyl-sn-glycerol-3-phosphocholine (DOPC) lipid vesicle membrane. While vesicles have been shown to enhance the yield of membrane proteins in these reactions (146), the effect of vesicle concentration on this process has not been widely explored. To investigate this relationship, we used an *in vitro* transcription-translation system (PURExpress) with a construct expressing an MscL green fluorescent protein fusion (MscLGFP) with varying concentrations of DOPC vesicles (Figure 4.1A, B). Because monomeric enhanced green fluorescent protein (mEGFP) cannot dimerize (162) and because its folding and fluorescence is dependent on the proper folding of the N terminal fusion partner (138), this fusion protein is a useful marker for MscL folding during production. MscL is known to cotranslationally insert into lipid membranes without a chaperone, making it a useful model protein for membrane protein folding studies conducted in cell-free systems (15).

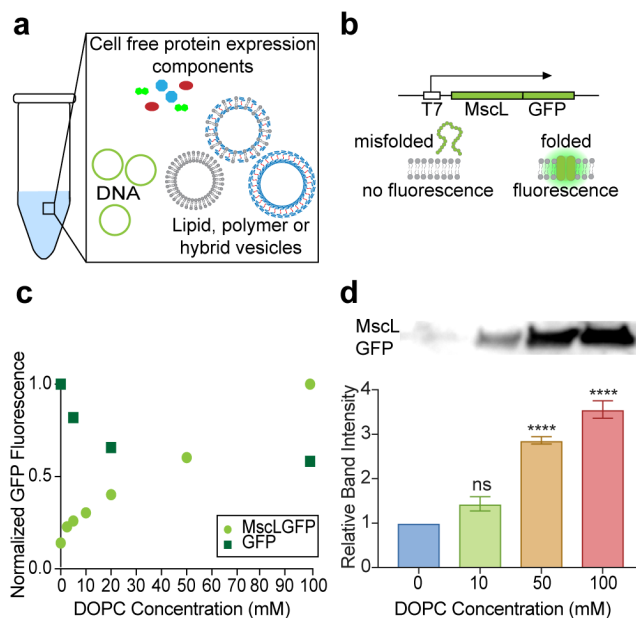


Figure 4.1 Lipid vesicles improve the production of MscL during cell-free protein synthesis.

a) Schematic of a cell-free reaction in which DNA and vesicles were mixed with PURExpress kit components. b) Schematic of the plasmid used to generate an MscL-GFP fusion protein. MscL is tagged C-terminally with mEGFP: the proper folding of MscL allows GFP folding and fluorescence (right) while the misfolding or aggregation of MscL does not permit GFP folding (left). c) Fluorescence of MscL-GFP and soluble GFP (GFP) 3.5 hrs after cell-free reactions with varying concentrations of DOPC vesicles, normalized to the maximum GFP fluorescence value observed for each protein. d) Quantitative western blot of MscL-GFP from cell-free reactions shown in (c). Densitometry values were normalized to reactions performed in water. **** $p \leq 0.0001$ (p values were generated by ANOVA using the Dunnett Test for multiple comparisons to the sample performed in water). $n=3$; error bars represent standard error of the mean.

We observed that MscL-GFP fluorescence increased in the presence of increasing DOPC vesicle concentration, leading to a 7-fold increase in GFP fluorescence at the maximum vesicle concentration with respect to protein production in the absence of vesicles (Figures 4.1C, 4.2A). The upper limit of vesicles used in our studies (100 mM) was constrained by the inability to form vesicles at high concentrations. We expect, however, that if MscL-GFP folding is dependent on available membrane surface area, protein folding should eventually plateau when available membrane surface area exceeds the surface area occupied by

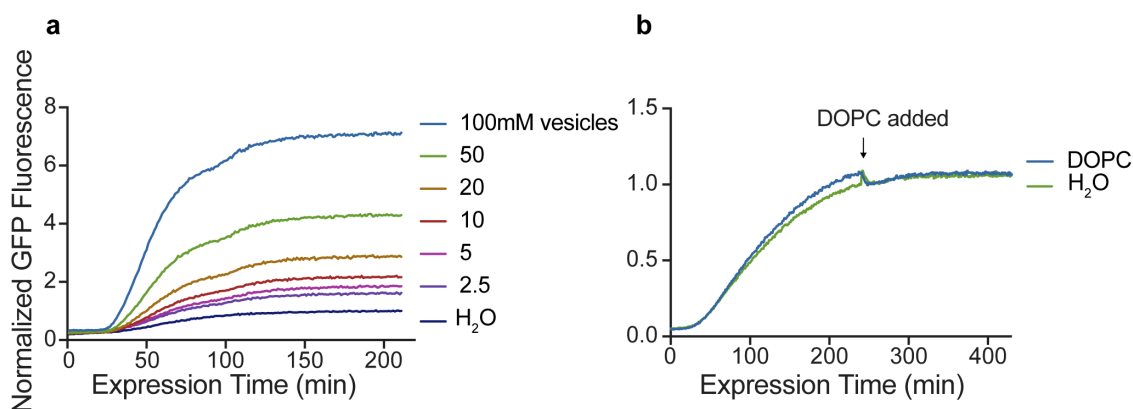


Figure 4.2 Lipid vesicles improve the folding of MscL during cell-free protein synthesis.

(a) Time course of MscLGFP fluorescence during a PURExpress cell-free reaction with varying concentrations of DOPC vesicles. Fluorescence values were normalized to the $t=0$ min initial read. (b) Time course of MscLGFP fluorescence in a PURExpress cell-free reaction with no vesicles. DOPC vesicles were added after 4 hours. GFP fluorescence did not significantly increase after this time indicating the vesicles were unable to rescue misfolded proteins.

expressed proteins. In contrast to MscL, the folding of soluble GFP decreased when expressed in solutions containing increasing vesicle concentrations (Figure 4.1C). These results suggest that lipid vesicles improve the folding of MscLGFP through direct interactions with the protein. When we added vesicles post-expression, we were unable to rescue misfolded proteins (Figure 4.2B), indicating that membranes act as chaperones to facilitate cotranslational folding of MscL. Protein fluorescence observed during cell-free reactions correlated monotonically with Western Blot densitometry analysis of the relative protein produced, indicating that lipid vesicles not only improve the functional folding of MscL, but also the overall production (Figure 4.1D). Finally, we assessed the functional integration of MscLGFP by assessing protein activity. Using a calcein dye release assay, we observed the activity of MscLGFP G22C, a chemically activatable mutant of MscL, after integration into vesicle membranes (Figure 4.3). Our results confirm that MscLGFP is functionally integrated into vesicle membranes present during cell-free protein synthesis.

Diblock copolymers enhance MscLGFP folding during cell-free protein synthesis.

Next, we used the poly (ethylene oxide)-b-poly (butadiene) (PEO-b-PBD) diblock copolymer to gain insight into how physical features of membranes affect membrane-assisted protein folding. Of the various diblock copolymers that have been studied, PEO-b-PBD is one of the best characterized within vesicle membranes. PEO-b-PBD has been particularly useful in providing insight into how chemical properties of individual amphiphiles affect the macroscopic properties of assembled membranes and how membrane physical properties affect biological processes of interest (9, 117, 163).

A unique feature of diblock copolymers in comparison to phospholipids is that chemical and physical features of the polymer can be systematically changed. For the PEO-b-PBD polymer, the molecular weight of the hydrophilic PEO chain and the hydrophobic PBD chain can be modified, resulting in a controlled shift in the hydrophilicity of membrane surface groups and membrane hydrophobic thickness, respectively, while maintaining the overall chemical identity of the polymer. While polymersomes have been successfully used as an insertion platform in the cell-free synthesis of membrane proteins (149), a systematic study of how diblock copolymers influence membrane protein folding has yet to be conducted.

We investigated the effect of diblock copolymer content in vesicles on MscLGFP production by preparing DOPC vesicles with increasing fractions of PEO₁₄-b-PBD₂₂ (Molecular weight (MW) = 1.8 kDa, hereafter referred to as PEO-b-PBD 1.8 kDa) in the membrane, and monitoring GFP fluorescence (Figure. 4.4A). The total amphiphile concentration was kept constant in these studies (10 mM), and we varied the ratio of lipid: polymer. The # amphiphiles / vesicle is expected to be similar across vesicle blends as DOPC lipids and PEO-b-PBD 1.8 kDa polymer chains are expected to have similar surface areas in a membrane, discussed further in the Discussion. We chose the 1.8 kDa polymer as it is expected to have a similar membrane thickness as lipid vesicles, estimated to be ~4-5 nm, thereby minimizing hydrophobic mismatch between the two amphiphiles (164). In addition, this polymer is expected to uniformly blend with certain phospholipids (117). Using a Förster resonance energy transfer (FRET) assay (165) and microscopy, we observed uniform mixing of DOPC and PEO-b-PBD 1.8 kDa polymers (Figure 4.5). We observed that

MscLGFP folding varied as a function of PEO-b-PBD 1.8 kDa content in the membrane, with maximum fluorescence

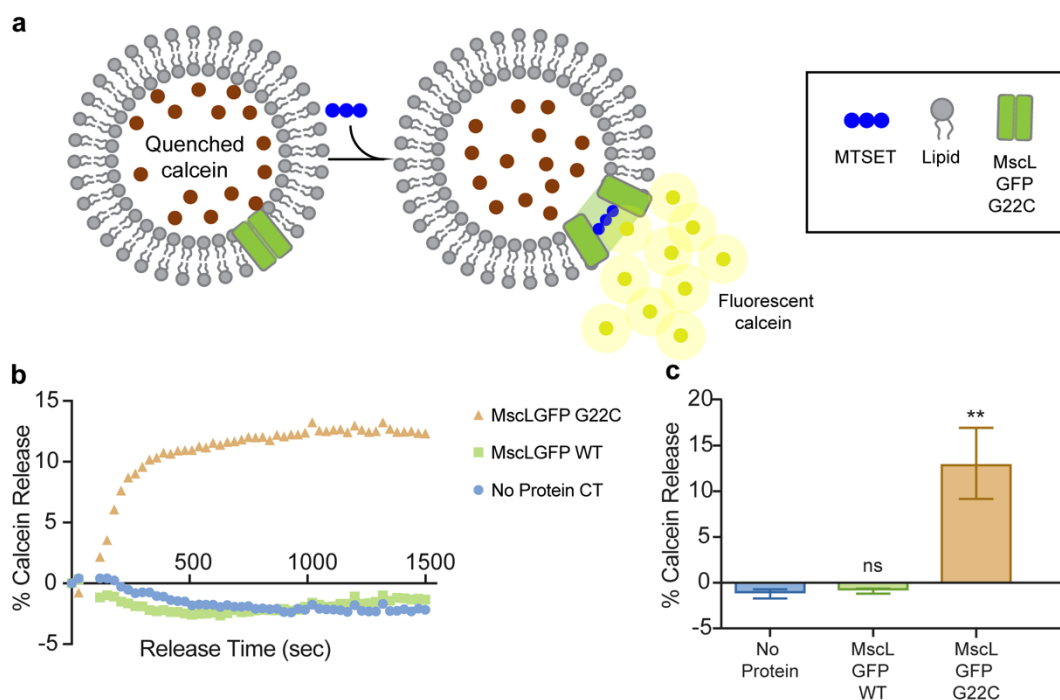


Figure 4.3 MscLGFP is active in lipid vesicles.

(a) Schematic of a calcein release assay used to assess channel activity. Calcein was encapsulated at self-quenching concentrations (100 mM) in lipid vesicles and unencapsulated calcein was purified away from vesicles through size exclusion chromatography. 10 mM vesicles were incubated in PURExpress reaction mixtures expressing MscLGFP G22C and re-purified after the reaction to remove reaction components. MTSET addition induces dye release from 1 mM vesicles containing MscL G22C, reported through a fluorescence increase. A representative release curve (b) and the mean final % release (c) are shown. Upon addition of MTSET, calcein dye release was observed with the G22C mutant as expected and was absent in both vesicles lacking MscLGFP and the inactive wild type MscLGFP (WT). ** $P \leq 0.01$, non-significant (ns) $P > 0.05$ (p values were generated by ANOVA using the Dunnett Test for multiple comparisons against the no protein control). $n=3$; error bars represent the standard error of the mean.

observed when vesicles contained 25 mol% PEO-b-PBD 1.8 kDa (Figure 4.4B). We confirmed this relationship between protein folding and PEO-b-PBD content using a smaller molecular weight analog PEO9-b-PBD12 (PEO-b-PBD 1.05 kDa) (Figure 4.6). Western Blot analysis again revealed that MscLGFP fluorescence varied monotonically with overall protein production (Figure 4.7).

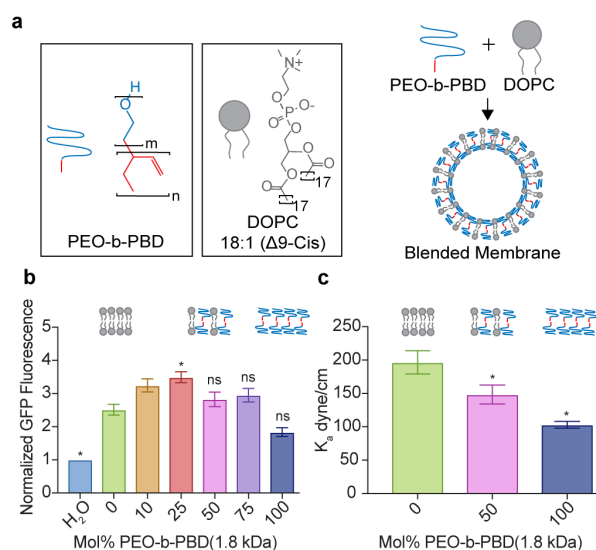


Figure 4.4 PEO-b-PBD 1.8 kDa polymers aid MscLGFP folding

a) Chemical structures of the amphiphiles used to generate vesicle membranes. **b)** MscLGFP fluorescence after cell-free reactions with varying fractions of PEO-b-PBD 1.8 kDa in DOPC vesicles normalized to reactions performed in water. The vesicle concentration was kept constant at 10 mM total amphiphiles. $n=3$; error bars represent standard error of the mean. **c)** K_a values for DOPC, PEO-b-PBD, and 1:1 DOPC:PEO-b-PBD vesicles, measured via micropipette aspiration. $n>15$ vesicles; error bars represent standard error of the mean. * $p \leq 0.05$, nonsignificant (ns) $p > 0.05$ (p values were generated by ANOVA using the Dunnett Test for multiple comparisons to the sample containing 0 mol% polymer).

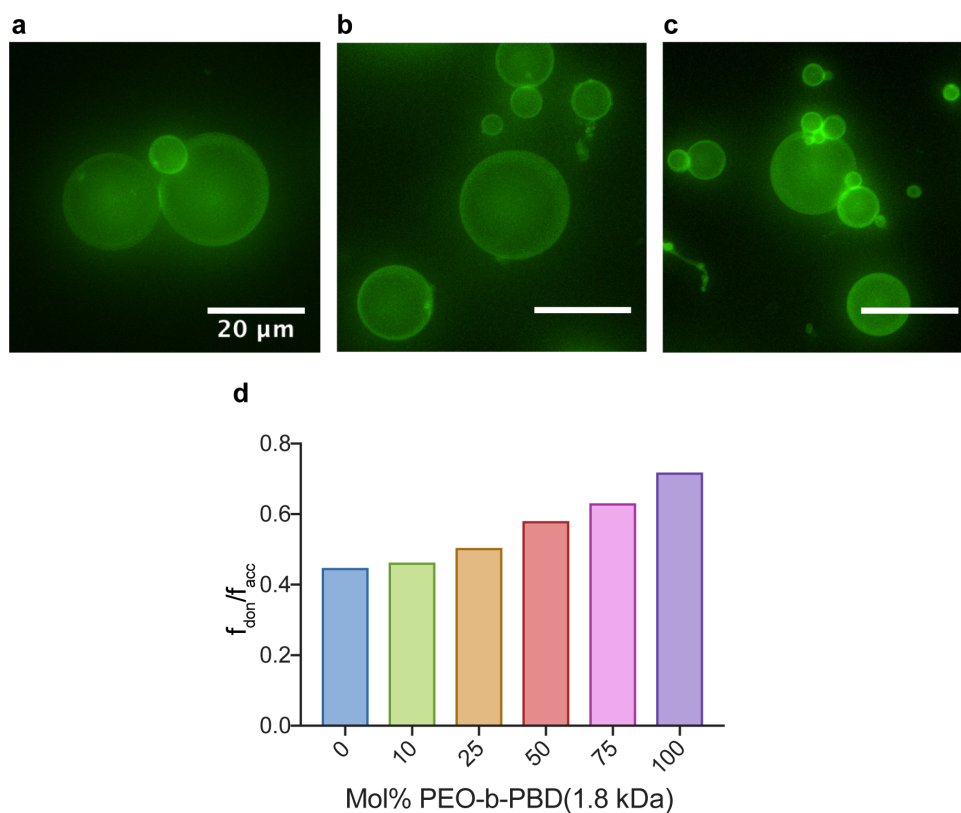


Figure 4.5 PEO-b-PBD 1.8 kDa and DOPC blend uniformly in hybrid vesicles.

(a-c) 25%, 50%, and 75% PEO-b-PBD 1.8 kDa in DOPC GUVs were prepared via electroformation with 0.1 mol% Lissamine-Rhodamine PE dye and imaged using fluorescence microscopy. A z-stack was collected with 0.5 μm step size and merged using Nikon VIS software. Dye fluorescence appears uniformly distributed across vesicles. Scale bar = 20 μm. (d) 1 mM DOPC/Polymer hybrid vesicles were prepared with 0.2 mol% each NBD and Rhodamine and various fractions of PEO-b-PBD 1.8 kDa and DOPC in PBS. The FRET donor (f_{don}) and acceptor (f_{acc}) emission intensity was measured and the f_{don}/f_{acc} ratio is reported. Increases in the f_{don}/f_{acc} ratio for vesicles that contain a constant concentration of FRET dyes indicate that the inclusion of diblock copolymers into vesicles increases the average distance between lipid molecules in vesicles.

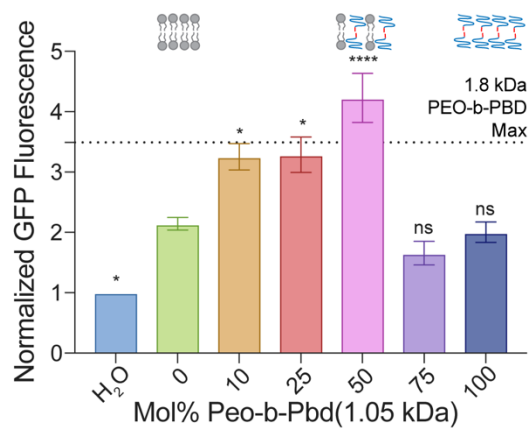


Figure 4.6 PEO-b-PBD 1.05 kDa improves MscLGFP folding in DOPC vesicles.

MscLGFP fluorescence after cell-free reactions conducted with DOPC vesicles containing varying fractions of 1.05 kDa PEO-b-PBD normalized to reactions performed in water. The total amphiphile concentration was maintained at 10 mM. **** $p \leq 0.0001$, * $p \leq 0.05$, non-significant (ns) $p > 0.05$ (p values were generated by ANOVA using the Dunnett Test for multiple comparisons to the 0 mol% polymer control). $n=3$; error bars represent standard error of the mean.

We wondered what features of the diblock copolymer was affecting MscLGFP production. PEO-b-PBD diblock copolymers assemble into highly elastic membranes in comparison to lipid vesicles. Specifically, PEO-b-PBD membranes can be stretched up to 50% of their initial area in comparison to lipid membranes which stretch to approximately 5% (163). The area expansion modulus (K_A) of PEO-b-PBD 1.8 kDa is ~ 90-110 dyne/cm versus the K_A of DOPC, which is ~200-250 dyne/cm (7, 9). We measured the K_A of several membrane compositions in our study using micropipette aspiration and observed that the K_A decreases as PEO-b-PBD 1.8 kDa polymers are blended into DOPC vesicle membranes (Figures 4.4C, 4.8, Table 4.1). Protein conformational changes that involve the protein-bilayer interface have an energetic cost associated with bilayer deformation (reviewed by Lundbaek et. al. (166)). Accordingly, membrane physical properties that affect the energy required to deform the bilayer would be expected to influence processes associated with membrane protein conformational changes, such as insertion and folding. Because the diblock copolymers we used are expected to have either an equivalent or higher bending rigidity than lipid vesicles (163) that would increase the cost of bilayer deformation, our findings suggested that a reduction in the membrane area expansion modulus could be responsible for the improved folding of MscL we observed.

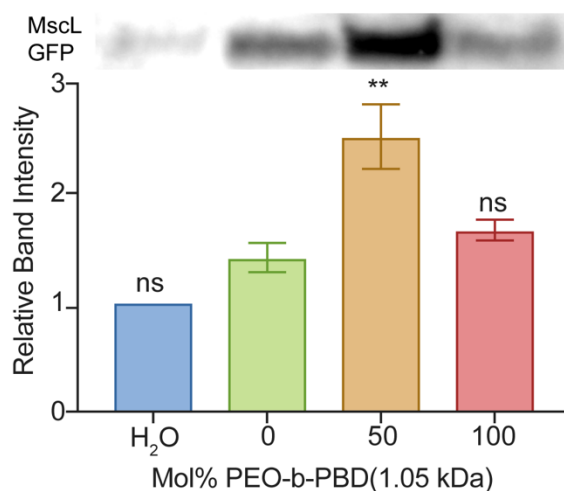


Figure 4.7 MscL GFP yield varies with MscL GFP folding in a cell-free reaction containing vesicles. Cell-free reactions containing blends of DOPC and PEO-b-PBD (1.05 kDa) were analyzed for total MscL GFP production using a quantitative western blot. Densitometry values were normalized to reactions performed in water. ** $P \leq 0.01$, non significant (ns) $P > 0.05$ (p values were generated by ANOVA using the Dunnett Test for multiple comparisons to the sample performed in 0 mol% PEO-b-PBD (1.05 kDa)). $n=3$; error bars represent standard error of the mean.

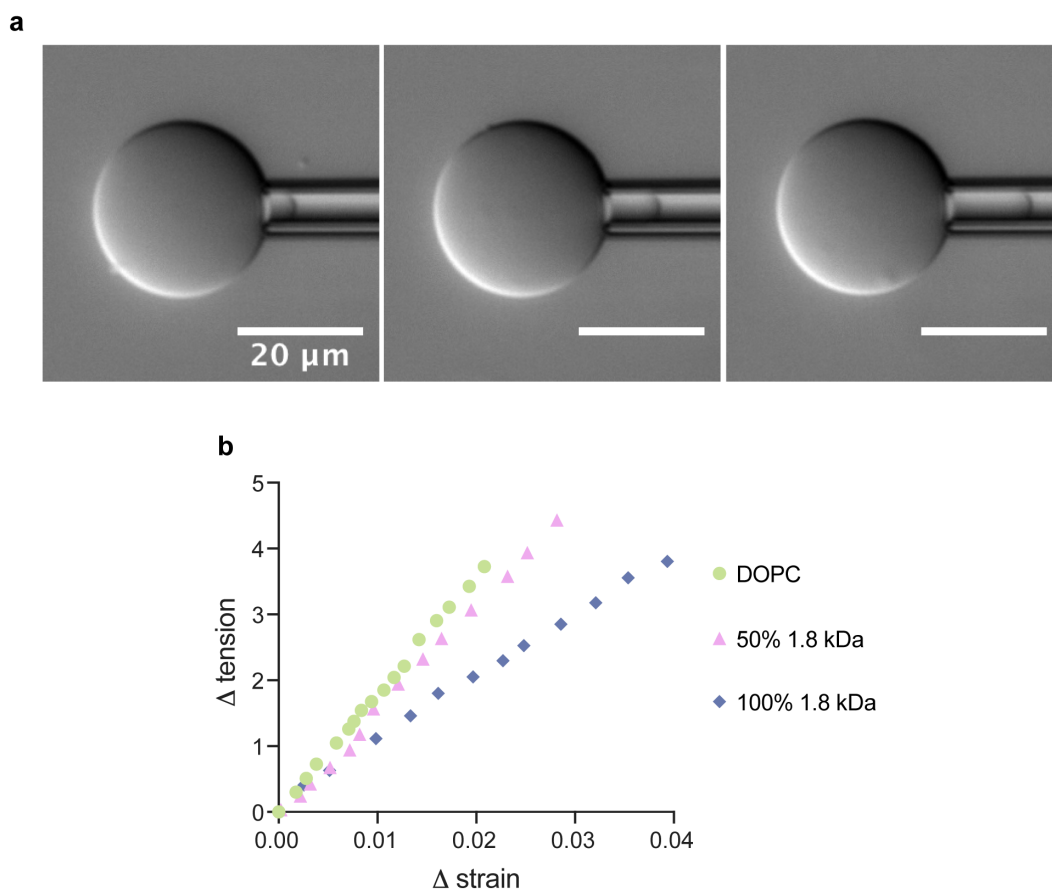


Figure 4.8 Micropipette aspiration of hybrid polymer/lipid vesicles.

(a) Micropipette aspiration of a DOPC GUV. DIC images were acquired every 10 seconds for 3 minutes as vesicles were aspirated in ~ 1 cm H₂O steps. Images were then loaded into Image J to measure vesicle size, pipette diameter, and membrane extension as a function of applied suction pressure. (b) Sample tension/strain curves for GUVs of varying compositions undergoing micropipette aspiration. The K_a is determined from the slope of this curve and average K_a values calculated for the membrane blends analyzed appear in Table S1.

| Sample | K_a (dyne/cm) +/- SEM |
|-----------------------------------|---|
| DOPC | 196.43 ± 17.37 |
| 50% PEO-b-PBD 1.8kDa | 148.34 ± 14.21 |
| 100% PEO-b-PBD 1.8kDa | 103.15 ± 5.163 |
| 25% PEO-b-PBD 1.05kDa | 100.50 ± 6.49 |
| 25% $C_{12}E_8$ | 113.80 ± 8.22 |

Table 4.1 Area expansion moduli of giant unilamellar vesicles.

Micropipette aspiration studies were used to determine the area expansion modulus (K_a) of various vesicle compositions.

Increasing membrane elasticity improves membrane protein folding.

To confirm the role of the membrane area expansion modulus on the cotranslational folding of MscL, we sought to change the area expansion modulus using alternate molecules. Specifically, we used membrane additives that would decrease and increase the K_A of DOPC vesicles by incorporating a detergent, $C_{12}E_8$, and cholesterol, respectively. The detergent $C_{12}E_8$ has been previously proposed to increase bilayer elasticity in lipid vesicles as a function of $C_{12}E_8$ content (167). We confirmed that $C_{12}E_8$ significantly reduced the area expansion modulus of DOPC vesicles, while maintaining membrane stability with respect to pure DOPC vesicles (Figure 4.9). We then prepared DOPC vesicles with increasing amounts of $C_{12}E_8$ while maintaining an overall constant amphiphile concentration and observed a commensurate increase in MscLGFP fluorescence when vesicles contained up to 25 mol% detergent (Figure 4.10). Typical methods for protein reconstitution use detergents to structurally alter lipid vesicles (e.g., forming micelles) or destabilize vesicles to a degree that results in membrane permeabilization (135). Our approach differs from these studies in that the concentrations of detergent that resulted in the most efficient protein folding (25 mol%), did not lead to significant permeabilization of vesicles (Figure 4.11), indicating membrane cohesion was maintained. To confirm MscLGFP fluorescence was due to interactions with the membrane and not free detergent micelles, we evaluated MscLGFP folding in the presence of $C_{12}E_8$ alone, in which $C_{12}E_8$ was added in comparable concentrations to that used in the studies with vesicles (Figure 4.12). We observed that detergent alone reduces protein folding relative to samples containing pure DOPC vesicles. In addition, we observed through microscopy that detergent added at 50 mol% or higher disrupted vesicle formation, helping to explain why MscLGFP fluorescence decreased in these samples.

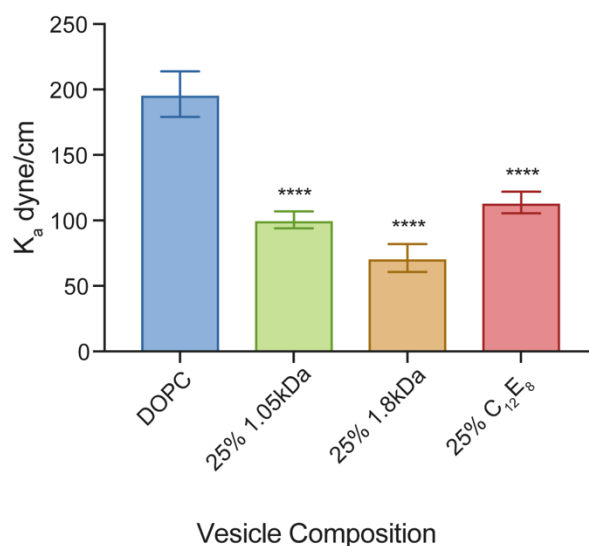


Figure 4.9 Elastic moduli of DOPC vesicles containing various amphiphiles.

Area expansion moduli (K_a) of GUVs in sucrose were determined using micropipette aspiration. 1 mM GUVs were prepared with 25 mol% PEO-b-PBD 1.05kDa, PEO-b-PBD 1.8 kDa, and C₁₂E₈. K_a values are compared to the K_a value determined for 100% DOPC vesicles. **** $p \leq 0.0001$ (p values were generated by ANOVA using the Dunnett Test for multiple comparisons to the 100% DOPC sample). $n > 20$; error bars represent standard error of the mean.

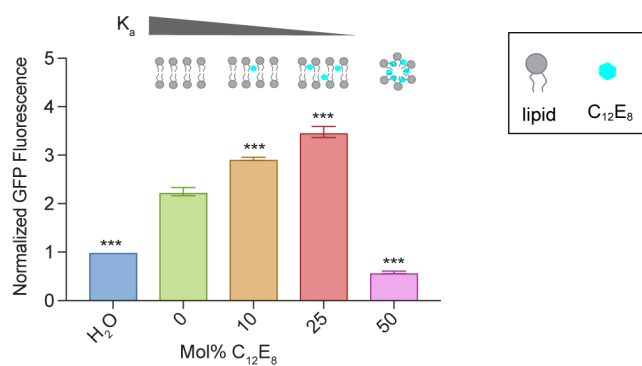


Figure 4.10 Increasing membrane elasticity with a membrane-additive improves MscLGFP folding.

MscLGFP fluorescence after cell-free reactions conducted with DOPC vesicles containing varying fractions of C₁₂E₈. MscLGFP fluorescence was normalized to reactions performed in water. *** $p \leq 0.001$. (p values were generated by ANOVA using the Dunnett Test for multiple comparisons to the DOPC vesicle sample containing 0 mol% C₁₂E₈. $n=3$; error bars represent standard error of the mean.

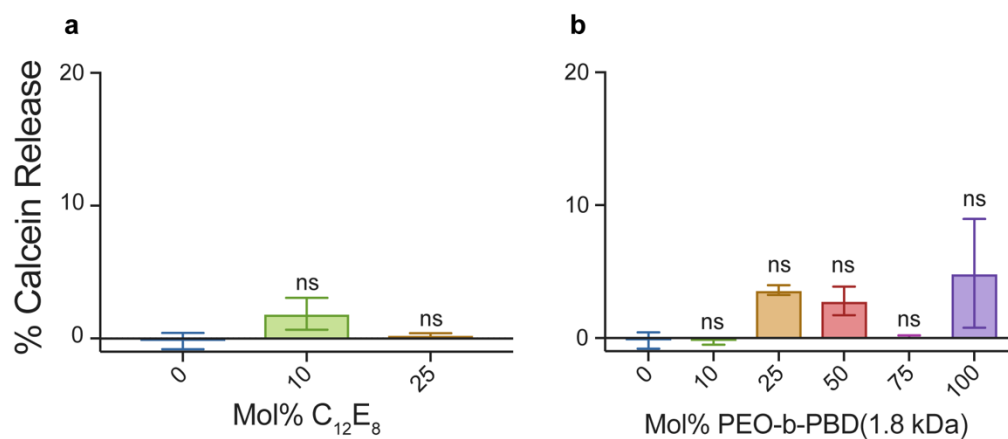


Figure 4.11 Calcein leakage assay to assess vesicle stability.

Calcein was encapsulated at self-quenching concentrations in lipid vesicles and free calcein was removed through size exclusion chromatography. 1 mM vesicles were incubated at 37 °C and the spontaneous release of calcein was monitored by measuring calcein fluorescence over 4h. The final % release is shown for DOPC vesicles containing various fractions of C₁₂E₈ (a) or PEO-b-PBD (1.8 kDa) (b) and show that no significant increases in calcein leakage was observed for all vesicle compositions tested. Non-significant (ns) $P > 0.05$ (p values were generated by ANOVA using the Dunnett Test for multiple comparisons against the 0% additive, DOPC, control). $n=3$; error bars represent the standard error of the mean.

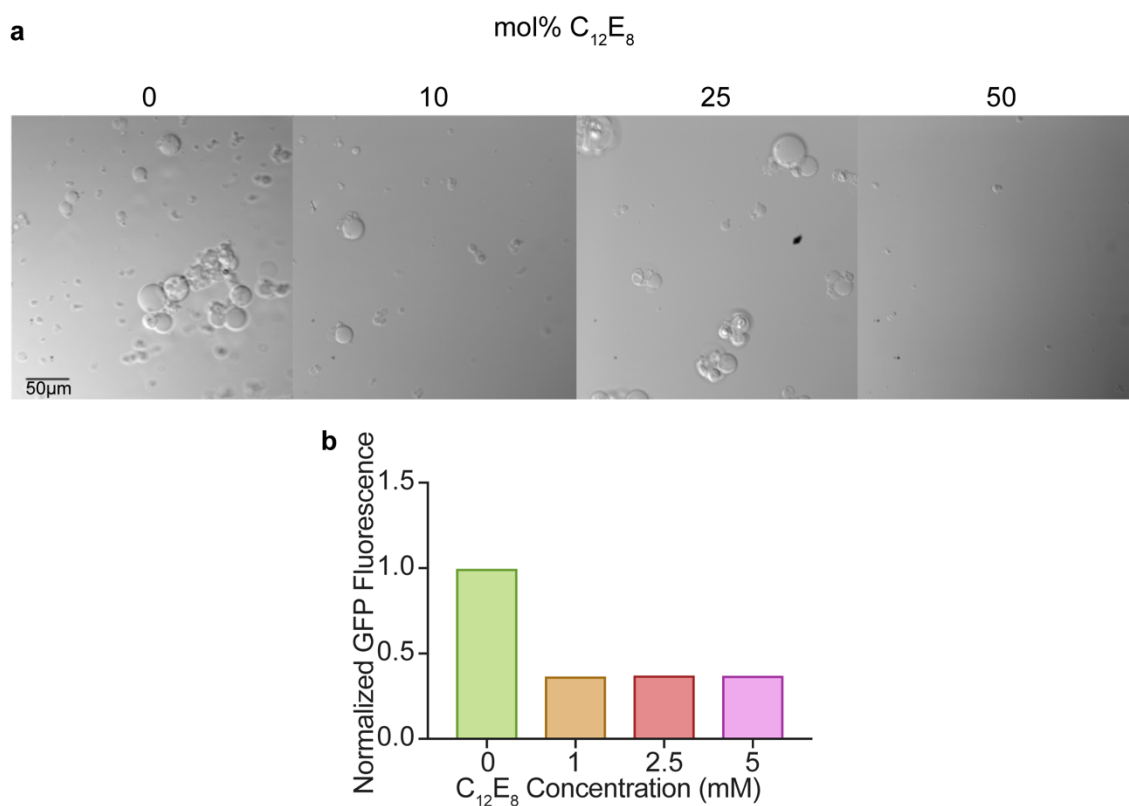


Figure 4.12 $C_{12}E_8$ alone does not facilitate membrane protein folding and at high concentrations disrupts vesicle formation.

(a) DIC microscopy shows that DOPC GUV formation is inhibited when $C_{12}E_8$ is mixed with DOPC lipids above 25 mol %. DOPC GUVs were prepared with increasing levels of $C_{12}E_8$ using thin film hydration. (b) MscLGFP fluorescence in PURExpress reactions after 3.5 h with varying concentrations of $C_{12}E_8$ micelles (that correspond to the amounts used when blended into DOPC vesicles) and normalized to reactions performed in water. The reduced GFP fluorescence in samples containing $C_{12}E_8$ indicate the detergent micelles alone are not responsible for the improved folding observed when DOPC vesicles contain $C_{12}E_8$.

We then observed how MscL folding was affected when membrane stiffness was increased. Cholesterol is known to increase the area expansion modulus of lipid membranes (168). For example, incorporation of 50% cholesterol into stearyloleoylphosphatidylcholine (SOPC) vesicles increased the K_A from ~193 to 781 dyne/cm (168). When we incorporated cholesterol into DOPC vesicles, we observed a decrease in MscLGFP folding relative to pure DOPC vesicles (Figure 4.13). Our observations with $C_{12}E_8$ and cholesterol indicate that using membrane additives that decrease the membrane area expansion modulus is a potential route to enhance MscL folding during cell-free reactions.

PEG headgroups prevent MscLGFP folding and insertion into membranes.

Finally, we explored what feature of PEO-b-PBD was inhibiting MscL folding when the polymer was present at higher concentrations (> 25 %) in vesicles. Diblock copolymers contain a hydrophilic PEO chain and PEO-modified amphiphiles can generate an effective steric barrier to prevent protein interaction with a membrane interface (169). To isolate the effect of PEO headgroups, otherwise known as PEG, in our cell-free expression system, we used a DSPE lipid with PEG modifications of three sizes: 550 kDa, 1000 kDa, and 2000 kDa. We performed cell-free reactions expressing MscLGFP in the presence of a constant amphiphile concentration (10mM) of DOPC vesicles containing 10 mol% DSPE-PEG, and monitored MscLGFP fluorescence. MscLGFP fluorescence decreased with increasing PEG chain length (Figure 4.14A). Our results are consistent with the expected steric behavior of PEG-modified amphiphiles or enhanced surface tension PEG chains can add to bilayers (170), which can prevent protein interaction with membranes.

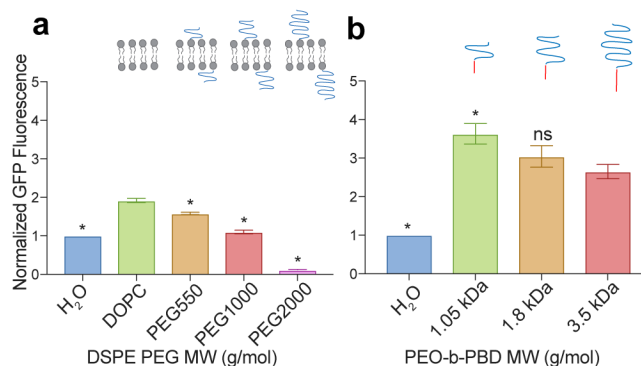


Figure 4.13 PEG-modified lipids decrease MscL-GFP folding efficiency.

a) MscL-GFP fluorescence after cell-free reactions conducted with vesicles containing 10 mol% DSPE PEG of varying molecular weights (550, 1000, and 2000 kDa) and 90% DOPC. **b)** MscL-GFP fluorescence after cell-free reactions conducted with vesicles containing 75 mol% DOPC and 25 mol% PEO-b-PBD of varying molecular weights normalized to reactions performed in water. All studies were conducted with 10 mM total concentration of amphiphiles. * $p \leq 0.05$, nonsignificant (ns) $p > 0.05$ (p values were generated by ANOVA using the Dunnett Test for multiple comparisons to the sample containing 100% DOPC in **(a)** and to the sample containing 3.5k MW PEO-b-PBD in **(b)**). $n=3$; error bars represent standard error of the mean.

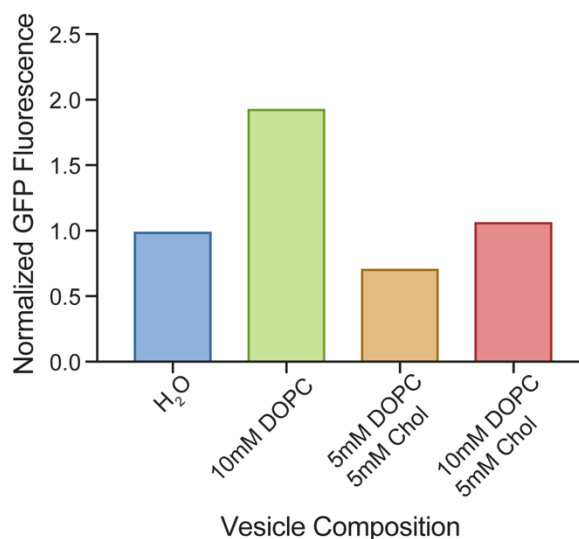


Figure 4.14 Cholesterol incorporation in DOPC vesicles decreases MscLGFP folding.

MscLGFP fluorescence after cell-free reactions conducted with DOPC vesicles containing varying amounts of cholesterol are reported normalized to reactions performed in water. Reactions were conducted with vesicles that maintained the total concentration of amphiphiles (5 mM DOPC/ 5 mM cholesterol) or that maintained the total concentration of DOPC (10mM DOPC/ 5 mM cholesterol) in a PURExpress reaction buffer. In either case, the addition of cholesterol reduces the yield of folded MscLGFP, measured through a reduction in GFP fluorescence.

We then confirmed the inhibitive role of PEG chains on membrane protein folding using a series of diblock copolymers. PEO-b-PBD amphiphiles of different molecular weights have similar area expansion moduli and chemical composition (9) but differing sizes of PEG and PBD groups. We performed cell-free reactions at a constant vesicle concentration (10 mM) with DOPC and 25 mol% PEO-b-PBD, but varied the molecular weight of the copolymer between 1.05 kDa (PEO9-b-PBD12), 1.8 kDa (PEO14-b-PBD22), and 3.5 kDa (PEO24-b-PBD46) (Figure 4.14B). As the MW of the diblock copolymer increased, protein folding decreased. Though changes in membrane thickness could also contribute to this decrease, diblock copolymers like those used in our study are expected to be more flexible and therefore more conveniently able to change conformation to accommodate membrane proteins, even with membrane thickness

mismatches (171). An additional property of diblock copolymers that could inhibit cotranslational protein folding is interdigitation of polymer segments in the hydrophobic core of the membrane. We would expect polymer interdigitation to increase with increasing polymer content in lipid vesicles and subsequently reduce protein insertion through increases in membrane bending rigidity. While diblock copolymers commonly interdigitate across assembled monolayers, smaller molecular weight diblock copolymers such as PEO-b-PBD 1.8 kDa are not expected to significantly interdigitate (172). Taken together, these results suggest steric interactions between MscL and diblock copolymer PEO groups are responsible for the reduced efficiency of MscL folding.

The role of membrane defects in protein folding

Hybrid lipid polymer membranes have increased packing defects which may enhance membrane protein folding. After demonstrating the interactions between membrane elasticity and protein folding, we studied the structural dynamics of blended lipid-polymer membranes. Specifically, we hypothesized that low amounts of PEO-b-PBD may introduce transient membrane packing defects. As studied previously for pure phospholipid systems (173, 174), density fluctuations in the headgroup region lead to transient exposure of the hydrophobic core to the solvent. On much longer length- and timescales, as probed in experiments, we expect that even larger defects protruding both leaflets (water filled pores) should occasionally form. Such transient pores would lead to an increase in membrane permeability for hydrophilic solutes. To confirm the presence of such large defects, we conducted experiments measuring liposome permeability to dithionite, which is a +2 charged hydrophilic molecule. Dithionite forms irreversible complexes with the lipid conjugated dye NBD which quenches NBD fluorescence. After a rapid quenching of NBD located in the outer liposomes surface, the following slow decreases in NBD fluorescence is indicative of permeability of the membrane to dithionite (175). Our measurements indicate an increase in membrane permeability at 10 mol% PEO-b-PBD and lowest permeability for dithionite in pure PEO-b-PBD (Figure 4.15-4.17).

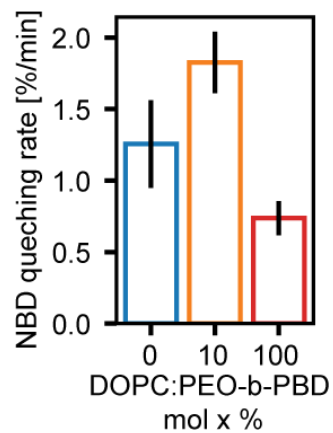


Figure 4.15 Hybrid membranes contain a larger fraction of membrane defects

Membrane permeability measured by NBD quenching by dithionite. Average NBD fluorescence decay rate measured for increasing fraction of PEO-b-PBD. Error bars represent standard error of the mean, $n = 5$.

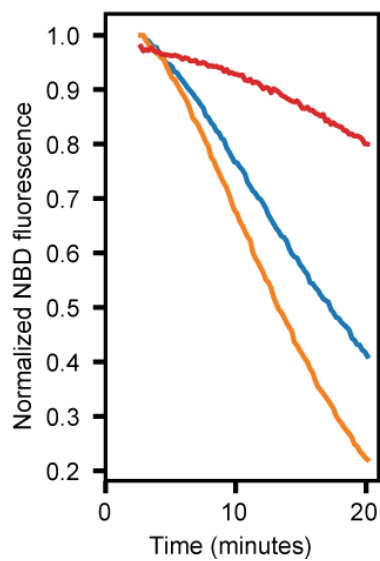


Figure 4.16 Example kinetic traces for NBD dithionite quenching membrane permeability assay DOPC (blue), 10 mol% (orange) and 100 mol% (red) PEO-b-PBD. NBD normalized fluorescence is plotted after initial quenching of the outer leaflet NBD fluorescence. Decreased fluorescence demonstrates increased membrane permeability to dithionite.

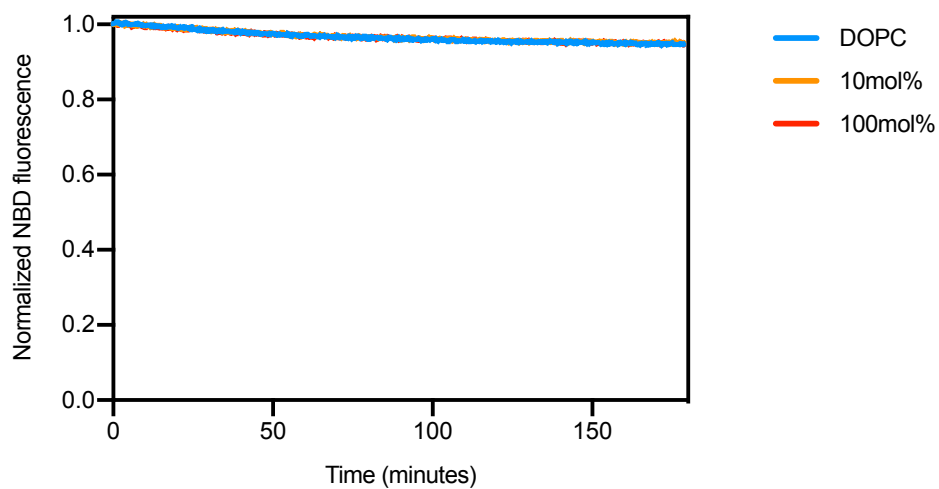


Figure 4.17 NBD photobleaching control in the absence of sodium dithionite

A kinetic scan of 18:1 NBD PE fluorescence was measured for each hybrid membrane composition to measure the rate of photobleaching. Photobleaching does not contribute to NBD quenching during the timescale of the dithionite quenching membrane permeability assay and is not dependent on membrane composition.

4.5 Discussion

Here, we have shown that the titer of a properly folded α -helical membrane protein can be increased by altering membrane concentration and composition in a cell-free reaction. While previous studies have shown that it is possible to cotranslationally fold membrane proteins into diblock copolymer membranes using cell-free expression techniques (127, 155, 156), to the best of our knowledge, we show for the first time that these synthetic membrane amphiphiles can enhance the cotranslational folding and synthesis of a membrane protein.

There are two major steps in membrane protein assembly: insertion into the membrane and folding. Bilayer membranes have a variety of mechanical properties that could influence either step, including bending rigidity, spontaneous curvature elasticity, hydrophobic thickness, area expansion moduli, and membrane fluidity/ viscosity. While it is difficult to vary any one of these parameters in isolation, diblock copolymers impart unique combinations of mechanical changes to membranes that are difficult to achieve with biological lipids alone, allowing us to examine the effect of these properties on folding in a new way. For example, the diblock copolymers we used are expected to have either an equivalent or higher bending rigidity and membrane thickness (163) and less fluid/ more viscous membranes (Figure 4.15) (176) compared to lipid vesicles. These parameters would be expected to decrease membrane protein folding efficiency, which is inconsistent with our observations (14, 92, 96). Additionally, unlike detergents used to solubilize membranes to allow protein reconstitution, diblock copolymers also do not appear to affect the stability of vesicles in our study (Figure 4.11). One of the remaining features of diblock copolymers that appear to be most relevant to protein folding efficiency in the current study are the chemical and structural features of the polymer chains. We are unable to exclude the role of membrane curvature or chemical interactions between MscL and PEO-b-PBD in enhancing protein folding at this time. However, our observation that small amounts of the polymer (10%) lead to significant increases in protein folding and the

reproducibility of this effect with $C_{12}E_8$, points to an important role of the global mechanical features of the hybrid polymer/lipid membrane in MscL folding. Our study suggests that membrane elasticity,

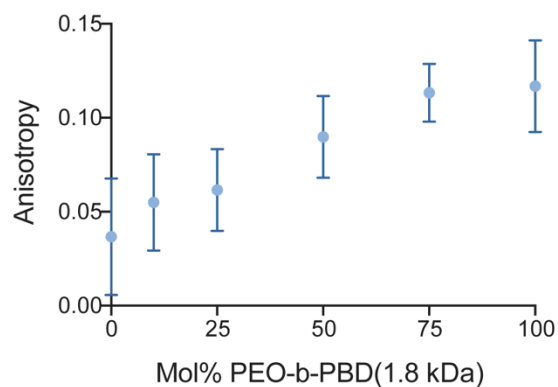


Figure 4.18 PEO-b-PBD 1.8 kDa decreases membrane fluidity

Fluorescence anisotropy measurements were conducted with 0.5mM vesicles containing 0.5 mol% DPH with varying fractions of PEO-b-PBD 1.8 kDa and DOPC. $n=10$; Error bars represent standard deviation.

specifically the area expansion modulus, which has not been widely considered in membrane protein folding studies, may be important.

The area expansion modulus is a membrane property that is commonly interconnected to other membrane physical properties, one of them being interfacial tension. Amphiphiles that integrate into vesicle membranes (diblock copolymers and $C_{12}E_8$) can reduce interfacial tension γ (161), which we can measure through the area expansion modulus ($K_A \sim 4\gamma$). Reduced interfacial tension has been shown to lead to two effects that should affect MscL folding: increased surface area per amphiphile and decreased energetic costs of membrane deformation. First, with reduced interfacial tension, the average surface area per amphiphile increases (161), leading to an increase in total membrane surface area available for membrane protein folding. This remains true even when total amphiphile density (amphiphiles/ vesicle or amphiphiles/ solution) is maintained. Our results with DOPC vesicles (Figure 4.1) show the importance of total membrane surface area, at a constant chemical composition and with constant membrane mechanical properties, on enhancing protein folding and yield. Similarly, the diblock copolymers used in our study are expected to provide increases in membrane surface area through native size and increased accommodation of strain. While the area per chain of PEO-b-PBD 1.8 kDa (expected to be $\sim 0.76 \text{ nm}^2$) (164) is similar to the area per lipid of DOPC (0.72 nm^2) (177) in a non-stretched/ relaxed membrane, we experimentally observed through FRET studies that polymers increase the average distance between lipids when blended into lipid vesicles (Figure 4.5D). Polymers could therefore increase available membrane surface area because they occupy more area per chain than lipids, by reducing interfacial tension of the membrane, which would increase the area per lipid chain, and by increasing the total strain that vesicles can experience.

A second consequence of reduced interfacial tension is that the energetic cost of bilayer compression and expansion will be reduced relative to the scenario where no elasticizing amphiphile is present. The energy required to create a vacancy in a bilayer membrane is proportional to the K_A (111). In studies with gramicidin, a channel whose function is regulated by elastic properties of the bilayer, Lundbaek et al. (178) showed that amphiphiles which increased membrane elasticity (here described as a combination of area expansion modulus, fluidity, and curvature) and reduced the free energy of membrane deformation shifted

the proportion of proteins in a dimerized, functional conformation. These results indicated that global changes in membrane elastic properties that lower the energy of membrane deformation can increase the conformational freedom of a protein in the bilayer, thereby increasing the probability of membrane protein assembly. We suggest that diblock copolymers decrease the area expansion modulus and increase available surface area in membranes with respect to the lipid used in this study, enabling more available membrane area as well as reduced energy costs to deform membranes (Figure 4.16). These effects should enhance protein folding by providing more surface area and more conformational freedom for protein segments

The extent to which our observations with MscL can be generalized to other membrane proteins is an important question. Towards answering this, we explored how the incorporation of PEO-b-PBD 1.8 kDa polymers affected the folding of another model α -helical membrane protein, channelrhodopsin (ChR2). We observed that the folding of ChR2 increased monotonically with increasing fraction of diblock copolymer, and a maximum level of folding was observed in the 100% polymer vesicles, in contrast to MscL, which exhibited maximum folding in 25% polymer vesicles (Figure 4.17). This may be due to differences in structure between MscL and ChR2. For example, ChR2 has seven transmembrane domains while MscL has two; this difference in structure could lead to differences in membrane affinity and folding thermodynamics. Overall, it appears that polymeric membranes could facilitate improved folding of different types of α -helical membrane proteins, and merits further investigation.

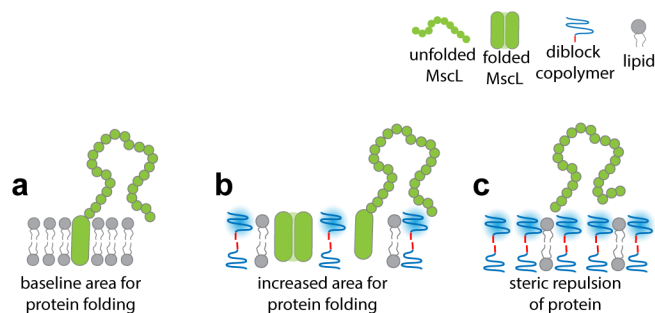


Figure 4.19 MscLGF folding into vesicle membranes depends on the available folding area and steric repulsion.

From our experimental observations and other reported studies, pure DOPC membranes have a baseline hydrophobic area available for protein folding **(a)**. An optimal blend of PEO-b-PBD and DOPC likely increases the available membrane area for protein folding and decreases the energy for membrane deformation **(b)**. Membranes composed of high levels of PEO-b-PBD may inhibit protein folding into the membrane due to steric interactions or increased surface tension between PEG headgroups and the nascent protein chain **(c)**.

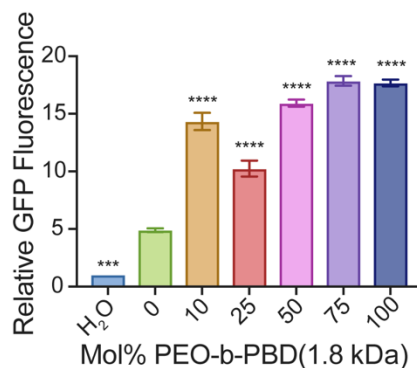


Figure 4.20 Channelrhodopsin-2 GFP (ChR2GFP) folding improves with PEO-b-PBD 1.8 kDa.

ChR2GFP fluorescence after cell-free reactions conducted with vesicles containing varying fractions of 1.8 kDa PEO-b-PBD and DOPC normalized to reactions performed in water. Reactions were conducted with 10 mM total concentration of amphiphiles in a PURExpress reaction buffer. **** $p \leq 0.0001$, *** $p \leq 0.001$ (p values were generated by ANOVA using the Dunnett Test for multiple comparisons to the sample containing 0 mol% PEO-b-PBD). $n=3$; error bars represent standard error of the mean.

Our findings have interesting implications for both biological systems and technological applications. Towards the former, our study contributes to mechanistic studies of cotranslational folding. Studies using cell-free systems have become an important tool to investigate this process and to date have revealed that several membrane proteins can be produced without translocase insertion machinery so long as vesicles are present (13, 15). A recently proposed model posits that transmembrane helices spontaneously insert into membranes, driven by the transfer of free energy between aqueous and lipid phases (179). Our study supports this thermodynamic model by showing that increasing the amount of membrane area increases both the rate of protein folding and the total amount of MscL expressed (Figure 4.1D).

Finally, our results have potential use in technological applications in order to increase the yield of membrane protein production in cell-free reactions. An important issue in membrane protein synthesis is improving the yield of protein or expanding the environments in which proteins are expressed (139). Cell-free expression methods have overcome a variety of issues associated with heterologous membrane protein expression and purification, yet membrane protein yield remains an area to be optimized (28). An emerging approach to address this problem is to change the reaction environment by using non-natural polymers as scaffolds or chaperones (117, 129, 149). Our use of non-natural amphiphiles that change membrane properties present in cell-free reactions should provide a new and complementary approach to protein design strategies in order to enhance the expression of membrane proteins that behave similarly to MscL.

4.6 Acknowledgements

The authors thank Monica Olvera de la Cruz and the members of the Kamat lab for helpful discussions. M.L.J. and M.A.B. were supported by Grant Number T32GM008382 from the National Institute of General Medical Sciences. This research was supported by the Searle Funds at The Chicago Community Trust.

Chapter 5

5. The effect of polyunsaturated fatty acids on membrane mechanical properties

This chapter is published as

Jacobs, M. L.; Faizi, H. A.; Peruzzi, J.P.; Vlahovska, P. M.; Kamat, N. P. "EPA and DHA differentially modulate membrane elasticity in the presence of cholesterol." *Biophysical Journal*. 2021.

Abstract

Polyunsaturated fatty acids (PUFAs) modify the activity of a wide range of membrane proteins and are increasingly hypothesized to modulate protein activity by indirectly altering membrane physical properties. Among the various physical properties affected by PUFAs, the membrane area expansion modulus (K_A), which measures membrane strain in response to applied force, is expected to be a significant controller of channel activity. Yet the impact of PUFAs on membrane K_A has not been measured previously. Through a series of micropipette aspiration studies, we measured the apparent K_A (K_{app}) of phospholipid model membranes containing non-esterified fatty acids. First, we measured membrane K_{app} as a function of the location of the unsaturated bond and degree of unsaturation in the incorporated fatty acids and found that K_{app} generally decreases in the presence of fatty acids with three or more unsaturated bonds. Next, we assessed how select ω -3 PUFAs, eicosapentaenoic acid (EPA) and docosahexaenoic acid (DHA), affect the K_{app} of membranes containing cholesterol. In vesicles prepared with high amounts of cholesterol, which should increase the propensity of the membrane to phase segregate, we found that inclusion of DHA

decreases the K_{app} in comparison to EPA. We also measured how these ω -3 PUFAs affect membrane fluidity and bending rigidity to determine how membrane K_{app} changes in relation to these other physical properties. Our study shows that PUFAs generally decrease K_{app} of membranes and that EPA and DHA have differential effects on K_{app} when membranes contain higher levels of cholesterol. Our results suggest membrane phase behavior, and the distribution of membrane elasticizing amphiphiles, impacts the ability of a membrane to stretch.

5.1 Introduction

Polyunsaturated fatty acids (PUFAs) are known to affect many biological processes in diverse cell types from T-cells and endothelial cells to deep-sea bacteria (40, 180). Mounting evidence supports the beneficial effects of certain ω -3 PUFAs, in particular, on cardiovascular and neurological systems (181, 182). Interestingly, PUFAs have been shown to alter cellular and tissue function by altering the activity of a diverse set of membrane proteins ranging from GPCRs and sodium-potassium pumps to mechanosensitive channels (8, 183). The mode of action of PUFAs is still unclear and may be driven through direct interactions of the fatty acids with a site on the membrane protein of interest or through indirect effects achieved through physical changes to membrane structure and properties (8, 184, 185).

PUFAs have the ability to change membrane composition and, in effect, membrane properties. Studies of both synthetic and model membranes have shown that PUFAs can rapidly insert into membranes at very fast timescales to alter membrane composition (186) and affect a variety of membrane properties (44, 60, 187). In particular, the ω -3 PUFAs, eicosapentaenoic acid (EPA) and docosahexaenoic acid (DHA), are two fatty acids that have been shown to affect the stability of phase-segregated domains (59, 79, 175, 188, 189), membrane fluidity (47), bending rigidity (31), and hydrophobic thickness (47, 77, 188) of membranes. Accordingly, PUFAs may impact a variety of biological functions through the modulation of these membrane properties.

Despite the chemical similarities of EPA and DHA, they have been shown to dissimilarly alter the activity of certain membrane proteins. In particular, PUFAs have been shown to differentially affect mechanosensitive channel protein activity (31). Many of these proteins follow the force-from-lipids principle which suggests that alterations in membrane forces influence the energy needed to drive conformational rearrangements required for protein activity, thus affecting protein function (190). Accordingly, changes in membrane properties that affect how a membrane deforms or transmits forces are likely to affect the activity of embedded mechanosensitive proteins (178). Proteins like Piezo1, TRPV4, and MscL, in addition to others, have been shown to be affected by ω -3 PUFAs, becoming activated or inhibited depending on fatty acid identity (31, 104, 183). Previous studies on membrane physical characterization focused on the impact of EPA and DHA on bending rigidity, fluidity, and hydrophobic thickness (31, 47, 77, 188, 191, 192), and had yet to uncover major differences in membrane properties that could be driving these PUFA-induced alterations in protein activity.

One membrane property that is important for membrane protein function is the ability of the membrane to stretch in response to tension. The area expansion modulus (K_A) describes the energy associated with a change in effective spacing between molecules in a lipid bilayer (193). Membrane K_A is likely an important property for mechanosensitive channel activity because it determines the extent of membrane deformation in the same plane upon which channel opening occurs (194, 195). However, the direct impact of PUFAs on K_A and the resulting impact on a wide class of mechanosensitive channels has not yet been characterized. In order to narrow this knowledge gap, it is important to first elucidate how various PUFAs affect membrane area expansion.

In the current study, we measure the apparent area expansion modulus (K_{app}) of model membranes containing PUFAs like EPA and DHA. Membrane K_{app} is similar to K_A but does not account for the contribution of residual thermal undulations as the bilayer stretches and is a more accurate term to use when reporting uncorrected micropipette aspiration area expansion data taken in the high tension regime

(7, 196). Using micropipette aspiration of model membranes composed of phospholipids, cholesterol, and non-esterified fatty acids, we demonstrate the impact of several PUFAs on membrane K_{app} . In particular, we take a closer look at how PUFAs affect membrane K_{app} in the presence and absence of cholesterol, which affects the propensity of membranes to phase segregate. Our study suggests that membrane phase-segregation behavior and the resulting distribution of membrane amphiphiles may impact the global mechanical properties of membranes, such as K_{app} . We propose that, in turn, these changes in membrane properties may be felt by a wide range of force-sensitive membrane proteins.

5.2 Materials and Methods

1,2-dioleoyl-sn-glycero-3-phosphocholine (DOPC), Cholesterol, and 18:1 1,2-dioleoyl-sn-glycero-3-phosphoethanolamine-N-(lissamine rhodamine B sulfonyl) ammonium salt (Liss-Rhod PE) were purchased from Avanti Polar Lipids, Inc (Alabaster, AL). NBD-phosphoethanolamine, triethylammonium salt (NBD-PE), Lipid peroxidation (MDA) assay, 1,6-diphenyl-1,3,5-hexatriene (DPH), and dipyrrometheneboron difluoride cholesterol (BODIPY-cholesterol), Triton X-100, Nonesterified fatty acid (NEFA HR-2) and Phospholipids-C Fujifilm quantitation kits were obtained from Thermo Fisher Scientific (Waltham, MA). Oleic acid (OA), alpha-linoleic acid (ALA), gamma-linoleic acid (GLA), steric acid (SDA), docosahexaenoic acid (DHA), eicosapentaenoic acid (EPA), phosphate buffered saline (PBS), β -casein, and D-sucrose were purchased from Millipore Sigma (St. Louis, MO). Fatty acid integrity was preserved to the best of our abilities via nitrogen treatment of buffers, storing fatty acids on ice, and limiting aspiration times at room temperature to one hour immediately following vesicle preparation. Aspiration measurements were conducted on the same day as vesicle preparation.

Thin film hydration

Small unilamellar vesicles (SUVs) were prepared using thin film hydration techniques as described previously (115). Phospholipid fatty acid blended vesicles can be prepared by mixing amphiphiles in a

chloroform stock solution (197). Briefly, lipid stocks in chloroform were prepared with the indicated mol% of lipids and fatty acids. Samples were dried under nitrogen then vacuum for 4 hours. To help maintain the integrity of the fatty acids, samples were rehydrated to 10 mM final total lipid in 300 mOsm PBS at 4 °C overnight then brought to 60 °C for 5 minutes. Vesicles were vortexed and extruded 7 passes to 100 nm and used immediately.

Electroformation

Giant unilamellar vesicles were prepared using electroformation techniques. A vesicle prep-pro (Nanion Technologies GmbH (Munich, Germany)) was used to generate giant unilamellar vesicles (GUVs) as described previously. Briefly, 0.05 μmol lipid dissolved in chloroform was dotted onto an ITO slide (Nanion Technologies GmbH (Munich, Germany)). Chloroform was dried under vacuum for 20 min. Films were hydrated with 250 μL of 300 mOsm sucrose to a final concentration of 200 μM total lipid and were electroformed using the standard setting (2:18:00 hr:min:sec, 3V, 5Hz, 45 °C). After electroformation, samples were diluted in equiosmolar PBS for microscopy studies to both allow vesicles to sink to the surface of the glass slide and ensure fatty acid concentration is below the critical micelle concentration.

Micropipette aspiration

Apparent membrane area expansion modulus (K_{app}) was measured using micropipette aspiration techniques (6, 198). Briefly, borosilicate glass capillaries (World Precision Instruments (Sarasota, FL)) were pulled to form long, thin tips with minimal change in thickness on the length scale visible during microscopy. Tips were further broken with a microforge to create a blunt end with a diameter of 5-8 μm . Pipettes and sample chambers were incubated in a blocking solution of 5 mg/mL β -casein for 1 hour. The pipette was filled with 300 mOsm PBS pH 7.4. An imaging chamber was assembled using two pieces of 50 x 25 no 1.5 cover glass spaced with vacuum grease. Blocked surfaces were rinsed with 1 mL of 300 mOsm PBS, pH 7.4 3 times and 1 mL was used to fill the imaging chamber. 200 μM total lipid was used to form GUVs. 1 μL of GUV solution was added to the chamber to an estimated final concentration of 0.2 μM lipid.

The total fatty acid concentration of vesicles in sample conditions used for micropipette aspiration was estimated to be no more than 0.05 μM fatty acid, which is below the critical micelle concentration (CMC) of oleic acid. Below the CMC, fatty acid is expected to favor partitioning into the bilayer (186, 199, 200). Notably, it appears that there is a significant reduction in the amount of fatty acid that actually resides in the membrane (~ 5 mol %) relative to the amount included in the original chloroform stock solution used to prepare lipid films (25 mol %) indicating fatty acid is lost to the surrounding solution during vesicle formation. Micropipette aspiration measurements were performed on 2-5 independent GUV samples and the total number of aspirated vesicles per composition is included in tabular results. Sucrose is known to affect membrane properties (201) but improves membrane contrast and decreases vesicle mobility in the imaging chamber. For these reasons, sucrose was required for micropipette aspiration to easily capture the vesicles and visualize the membrane within the glass micropipette. It is important to note that changing the salt and sugar conditions of micropipette aspiration conditions will alter the measured mechanical properties of bilayers. Our measurements of bending rigidity via fluctuation spectroscopy used sucrose free conditions. These measurements match the bending rigidity values extracted from micropipette aspiration conducted with sucrose-containing vesicles, indicating these particular solvents we used had little effect on the bending rigidity of vesicles relative to one another.

Using a Nikon inverted microscope (Nikon Inc. (Melville, NY)), connected to a Validyne pressure transducer and digital manometer (model DP 15-32, Validyne Engineering Corp) and a micromanipulator (model WR-6, Narishige International USA (Amityville, NY)), vesicles free of visible defects between 10-60 μm were gently aspirated with a micropipette prepared as described above. Membranes were carefully pre-stressed (7) for 30 seconds to approximately half-maximum tension (around 2-4 % areal strain) before bursting to remove any invisible membrane folds. Samples with visible membrane folds or other defects were not used as they tend to exhibit different responses to membrane stretching due to membrane reservoirs, resulting in artificially low K_A values. After pre-stress, suction pressure was reduced to baseline. If large amounts of

hysteresis occurred, vesicles were pre-stressed again or discarded as this indicates large amounts of excess membrane. Vesicles were then aspirated at 2 cm H₂O increments and imaged every 10 s. Images were analyzed using Fiji (160) to measure pipette diameter, vesicle area, and change in vesicle area within the pipette. Membrane K_{app} was calculated for each composition from the slope of the percent area dilation within the pipette ($\frac{\Delta A}{A_o}$) and membrane tension (τ).

$$K_{app} = \frac{\tau}{\frac{\Delta A}{A_o}} \quad (1)$$

Where ΔA is the change in area of membrane within the micropipette and A_o is the initial area of the aspirated vesicle within the pipette. The average K_{app} from at least 10 vesicles was used to calculate mean K_{app} values and actual N is reported with each mean K_{app} . Ordinary one-way ANOVA multiple comparisons tests were used to determine significance between compositions.

Fluctuation spectroscopy

GUVs formed using electroformation were analyzed using the flickering spectroscopy method (202) to measure membrane bending rigidity. The harvested vesicles were diluted 10 times in a slightly higher concentration of 270 mM Sucrose + 60 mM glucose solution to obtain deflated vesicles. This combination of sucrose and glucose provides a good optical contrast for contour detection (53) and avoids gravitational effects on vesicle fluctuations (203). The equatorial membrane fluctuations were recorded with phase contrast microscope (Axio-Observer A1 microscope Carl Zeiss AG (Oberkochen, Germany)) using a 63x/ Numerical Aperture (NA) 0.75 Ph2 (air) objective. The Focal depth, FD , was determined using the standard formula,

$$d = \frac{\lambda}{NA^2} \quad (2)$$

where wavelength, λ , of transmission light is 550 nm. This leads to $FD = 0.97 \mu\text{m}$ and the non-dimensionalized $\Delta = \frac{FD}{R_o}$ (vesicle size range of radius, R_o , 20-50 $97 \mu\text{m}$) smaller than 0.05 to avoid the averaging effect of out of focus optical projections on equatorial projections (204, 205). 8000-10000 images were recorded at 60 frames per second (fps) with Photron SA1.1 highspeed camera with a shutter speed

of 200 μs . The imaging acquisition speed was later adjusted to avoid time correlation between Fourier modes (206) for every specific vesicle. The contour in the equatorial plane of a quasi-spherical vesicle is decomposed in Fourier modes,

$$r(\phi, t) = R_0 \left(1 + \sum_{q=-q_{max}}^{q_{max}} u_q(t) \exp(iq\phi) \right), \quad (3)$$

where q is the resolved Fourier mode. In general, q_{max} is the maximum number of experimentally resolved modes that is dependent on the optical resolution of the camera. The mean square amplitude of the fluctuating amplitudes, u_q , yields the values of membrane bending rigidity κ and the tension σ since

$$\langle |u_q|^2 \rangle \sim kT / \kappa (q^3 + \bar{\sigma} q) \quad (4)$$

where $\bar{\sigma} = \sigma R_0^2$. To have good sensitivity with bending rigidity measurements, only vesicles with low tension value were chosen ranging from $10^{-8} - 10^{-9} \text{ N/m}$. This ensures a small cross over mode defined by

$$q_c = \sqrt{\bar{\sigma}} \quad (5)$$

from $q = 3-7$. Shape fluctuation modes $q < q_c$ are dominated by membrane tension while modes $q > q_c$ are controlled by bending rigidity.

Differential scanning calorimetry

Differential scanning calorimetry was performed to determine the phase transition temperature of vesicles using a Mettler Toledo Polymer DSC measurement system (56). Vesicles were prepared using thin film hydration methods and extruded to 100 nm using a mini-extruder (Avanti Polar Lipids (Alabaster, AL)). 30 μL of 20 mM vesicles in water were sealed into an aluminum pan. Scans were performed from -40 to 60°C with a ramp rate of 10°K/min under helium gas. Phase transition temperatures were determined using the Mettler STARe analysis software's glass transition tool.

Fluorescence Anisotropy

Membrane anisotropy measurements were performed as described previously (115). 0.5 mM small unilamellar vesicles prepared in 300 mOsm PBS containing 0.2 mol% DPH and various compositions of DOPC, fatty acid, and cholesterol, were analyzed using an Agilent Technologies Cary Eclipse Fluorescence Spectrophotometer with the Automated Polarization Accessory. Fluorescence anisotropy of DPH was assessed at the following excitation and emission wavelengths: 360 nm and 435 nm. Fluorescence anisotropy (r) was calculated automatically by software provided with the instrument, according to $r = (I_{vv} - I_{vh}G) / (I_{vv} + 2I_{vh}G)$, where I_{vv} and I_{vh} are the intensities of the vertically and horizontally polarized components of the fluorescent light, respectively, after excitation with vertically polarized light. $G = I_{hv}/I_{hh}$ is a grating correction factor for the optical system.

Fatty acid oxidation assays

Lipid oxidation levels were determined of electroformed samples. The detection of conjugated dienes was performed as described previously (7). Immediately following electroformation, 50 μ L of electroformed vesicles were diluted in pure ethanol to 1 mL. Oxidized positive controls were created by heating electroformed samples at 60 °C for 48 hours. Absorbance was measured at 230 nm using a Cary Eclipse spectrophotometer and values were normalized to pure, unoxidized DOPC.

Fatty acid membrane composition assays

Fatty acid incorporation into electroformed GUVs was determined as described previously (54) using a Fujifilm non-esterified fatty acid (NEFA) and phospholipid quantitation kit. Vesicles constructed using electroformation techniques were diluted in PBS to bring the fatty acid concentration below the CMC of oleic acid (199) to facilitate maximal partitioning of fatty acid into the bilayer and to mimic our micropipette aspiration study conditions (54). We then centrifuged our vesicles at 21,000xg for 30 min to pellet the vesicles. The supernatant was discarded to remove unincorporated fatty acids and the vesicle pellet was resuspended in PBS. We then disrupted the bilayer structure using 1% Triton X-100 and divided each sample into two. We incubated our samples with each kit activation reagent and measured non-esterified fatty acid and phospholipid concentrations in our vesicles using absorbance at 550 and 600 nm,

respectively. We constructed standard curves of fatty acids from 0.03 – 1.25 mM and phospholipids from 0 – 10 mM and measured absorbance at 550 and 600 nm, respectively after incubating with each kit activation reagent. Fatty acid and phospholipid sample concentrations were determined using these standard curves and molar ratios were calculated using $[FA] / [phospholipid]$. Mol% fatty acid was determined in binary mixtures of POPC and fatty acid by $[FA] / ([FA] + [phospholipid])$.

Cholesterol distribution determination

The cholesterol distribution in ternary mixtures of POPC, cholesterol and fatty acids were performed using BODIPY-cholesterol fluorescence microscopy. 0.5 mol% BODIPY-cholesterol was incorporated into lipid stocks containing 30 mol% POPC, 45 mol% cholesterol, and 25 mol% OA, EPA, or DHA. Vesicles were formed using electroformation and were immediately imaged using DIC phase-contrast and epifluorescence using a GFP filter set. To determine if cholesterol incorporates at similar amounts in the presence of different fatty acids, the fluorescence intensity in the membranes of GUVs was measured and quantified using Nikon eclipse software. Additionally, to determine if cholesterol was evenly distributed between different vesicles within each sample, fields containing multiple vesicles were imaged using phase-contrast and BODIPY-cholesterol fluorescence.

FRET Domain Disruption Assay

Fatty acid uptake and domain mixing measured to determine phase behavior of cholesterol-containing bilayers. Previous studies have demonstrated that fatty acid treatment leads to relatively even uptake of each fatty acid (54). Therefore, by inserting fatty acids into bilayers containing cholesterol domains, the phase behavior can be observed by a change in dye behavior. Briefly, Membranes containing 18:1 NBD-PE and 18:1 Liss-Rhod PE were used to determine surface area of L_d domains. 0.5, 1, 2, and 3 μ L of 100 mM non-esterified fatty acid dissolved in ethanol was added to 100 μ L 10 mM 50 mol% DOPC, 50 mol% cholesterol SUVs containing 0.1 mol% total fluorophore, prepared in 300 mOsm PBS, pH 7.4. Bulk Forster Resonance Energy Transfer (FRET) ratios were measured in a Molecular Devices Spectra Max i3 plate

reader. 18:1 NBD PE (donor) and 18:1 Liss-Rhod PE (acceptor) fluorescence were excited using 463 nm light and the emission was measured at 517 nm (to determine f_{don}) and 590nm (to determine $F_{acceptor}$) respectively. FRET ratio is defined at f_{don}/f_{acc} . Using a standard curve of mol% dye vs. FRET ratio, relative changes in surface area available to the dyes can be quantified by first calculating the local mol% dye. Then, a ratio of local mol% dye in untreated over FA-treated vesicle determines the local surface area available to the FRET dyes. When incubated with fatty acids, a large increase in surface area is expected when cholesterol domains are disrupted due to the homogenous dye content rather than being isolated to L_d domains.

Lipidomics Sample Preparation and Analysis

Lipidomic analysis was performed to determine membrane compositions during micropipette aspiration studies. Giant Unilamellar Vesicles (GUVs) were prepared using identical methods to GUVs prepared for micropipette aspiration. GUVs were purified by diluting below the CMC of the fatty acids. Samples were flash frozen in glass vials and stored at $-80\text{ }^{\circ}\text{C}$ prior to mass spectrometry. Lipidomic analysis and quantification was performed by the Lipidomics Core Facility at Wayne State University to quantify the amount of phospholipid, cholesterol, and non-esterified fatty acid in each sample. Liquid chromatography-mass (LC-MS) spectrometry was used to quantify these molecules. DOPC and POPC were quantified relative to DPPC-d62 standard, cholesterol was quantified relative to cholesterol-d7 standard, oleic acid was quantified relative to oleic acid-d17, EPA and DHA were quantified relative to arachidonic acid-d8, DHA oxidation was quantified relative to 15-HETE-d8 to measure a range of DHA oxidation analytes X-hydroxy-5E,7Z,10Z,13Z,16Z,19Z-docosahexaenoic acid (4-HDoHE, 7-HDoHE 8-HDoHE 10-HDoHE 11-HDoHE 13-HDoHE 14-HDoHE 16-HDoHE 17-HDoHE 20-HDoHE) and X-hydroperoxy-(4Z,7Z,11E,13Z,16Z,19Z)-docosahexaenoic acid (4-HpDoHE 7-HpDoHE 8-HpDoHE 10-HpDoHE 11-HpDoHE 13-HpDoHE 14-HpDoHE 16-HpDoHE 17-HpDoHE 20-HpDoHE) and the total amount of analyte detected was used to quantify %DHA oxidation. The mol % of phospholipids, fatty acids, and cholesterol

were determined from the concentrations of each component calculated via LC-MS and are reported in Table 5.1.

5.3 Results

ω -3 fatty acids increase membrane elasticity in the absence of cholesterol

We first set out to understand how non-esterified, or free fatty acids (FFAs), impact the membrane area expansion modulus of model 1,2-dioleoyl-sn-glycero-3-phosphocholine (DOPC) phospholipid membranes as a function of fatty acid content, identity, and the presence of varying amounts of cholesterol. We measured the apparent expansion modulus (K_{app}), which is the slope of tension versus apparent area dilation measured during micropipette pressurization of vesicles in the high tension regime (Figure 5.1A). Membrane K_{app} is similar to K_A but does not account for the contribution of residual thermal undulations as the bilayer stretches, and is a more accurate term to use when reporting uncorrected micropipette aspiration area expansion data taken in the high-tension regime (7, 196). Using electroformation techniques, we prepared multi-component giant unilamellar vesicles (GUVs) from chloroform stock solutions containing phospholipids, cholesterol, and non-esterified fatty acids. We were able to include up to 25 mol% FFA in the lipid solutions used to prepare vesicles: higher amounts of FFA in the lipid stock solution inhibited the formation of vesicles. We chose to incorporate FFAs into vesicles by premixing them with phospholipids in a chloroform solution before vesicle assembly (207) instead of adding them to preformed vesicles, as has typically been done (47). We used this alternate incorporation method to avoid the introduction of co-solvents, such as ethanol, that are typically required to solubilize fatty acids, but are also expected to change membrane properties. Using an absorbance-based lipid oxidation assay and mass spectrometry, we determined that under our experimental conditions, fatty acid oxidation is expected to be limited over the time scale of vesicle formation and aspiration (Table 5.1, Figure 5.2) (7, 208). We then used differential interference contrast (DIC) microscopy to visualize GUVs in the tip of a micropipette and measured the

changes in vesicle area within the pipette as pressure was applied (Figure 5.1B). This aspiration procedure provided us with a stress-strain response curve, the slope of which was used to determine the K_{app} (Eq.1) of various membrane compositions (Figure 5.3).

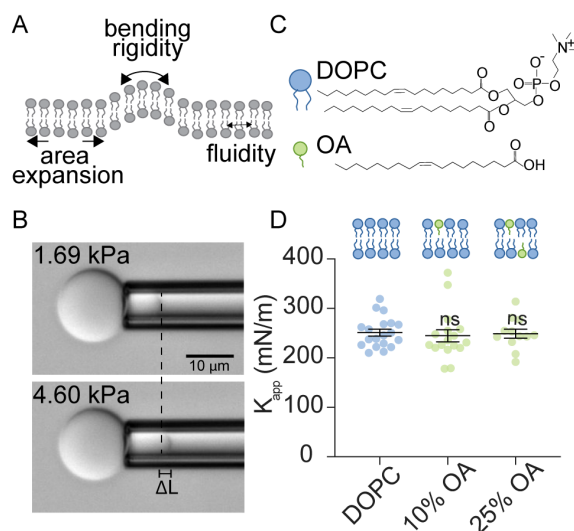


Figure 5.1 Apparent area expansion moduli (K_{app}) of model membranes containing non-esterified fatty acids.

A) In the course of this study, we measured three membrane mechanical properties including apparent area expansion modulus (K_{app}), bending rigidity (k_c), and fluidity. B) Example images of a micropipette aspiration study used to measure K_{app} . Giant unilamellar vesicles (GUVs) are aspirated into glass micropipettes where applied pressure induces membrane tension. Membrane stretching can be quantified by a change in vesicle projection length within the pipette (ΔL). Scale Bar = 10 μm . C) Chemical structures and schematics of DOPC and OA. D) Incorporation of OA does not alter the K_{app} of DOPC membranes. Increasing OA content in lipid stocks, from 0% OA (no FA) to 25% OA in DOPC membranes does not impact K_{app} . Dots represent K_{app} values from a single vesicle aspiration. Black lines represent mean K_{app} , error bars represent standard error of the mean, $n \geq 12$ vesicles were aspirated per composition. Vesicle assembly was disrupted above 25% OA incorporation. Micropipette aspiration studies were conducted in PBS, pH 7.4. P-values were generated by ANOVA using Dunnett's multiple comparisons test compared to no FA, non-significant (ns) $p > 0.5$.

Table 5.1 Lipidomic analysis quantifies membrane compositions used for micropipette aspiration.

Giant vesicles were prepared and purified using centrifugation to remove unincorporated amphiphiles. Samples were analyzed by liquid chromatography-mass spectrometry (LC-MS). In the absence of cholesterol, all fatty acids included at 25 mol% in chloroform mixtures with lipids subsequently incorporate similarly into DOPC vesicles (to a final concentration of ~6-8 mol %). Additionally, POPC/ cholesterol/ FA mixed at a ratio of 30: 45: 25 mol % in chloroform also exhibited similar incorporation of each polyunsaturated fatty acid (~ 3 mol %) as well as cholesterol (~10 mol%). Various possible DHA oxidation metabolites were quantified and the total mass of metabolites and the total amount of DHA present in the final sample were used to calculate % DHA oxidation. Nm indicates samples were not measured.

| DOPC/FA samples | phospholipid mol% | cholesterol mol% | fatty acid mol% | % DHA oxidation |
|------------------------|------------------------------|-----------------------------|----------------------------|----------------------------|
| DOPC/ OA | 93.5 | 0.0 | 6.5 | nm |
| DOPC/ EPA | 94.0 | 0.0 | 6.0 | nm |
| DOPC/ DHA | 92.3 | 0.0 | 7.7 | 0.3 |

| POPC/high chol/FA samples | phospholipid mol% | cholesterol mol% | fatty acid mol% | % DHA oxidation |
|--------------------------------------|------------------------------|-----------------------------|----------------------------|----------------------------|
| POPC/ chol | 92.9 | 7.1 | 0.0 | nm |
| POPC/ chol/ OA | 82.1 | 10.3 | 7.7 | nm |
| POPC/ chol/ EPA | 86.0 | 11.1 | 2.9 | nm |
| POPC/ chol/ DHA | 84.7 | 11.7 | 3.5 | 0.6 |

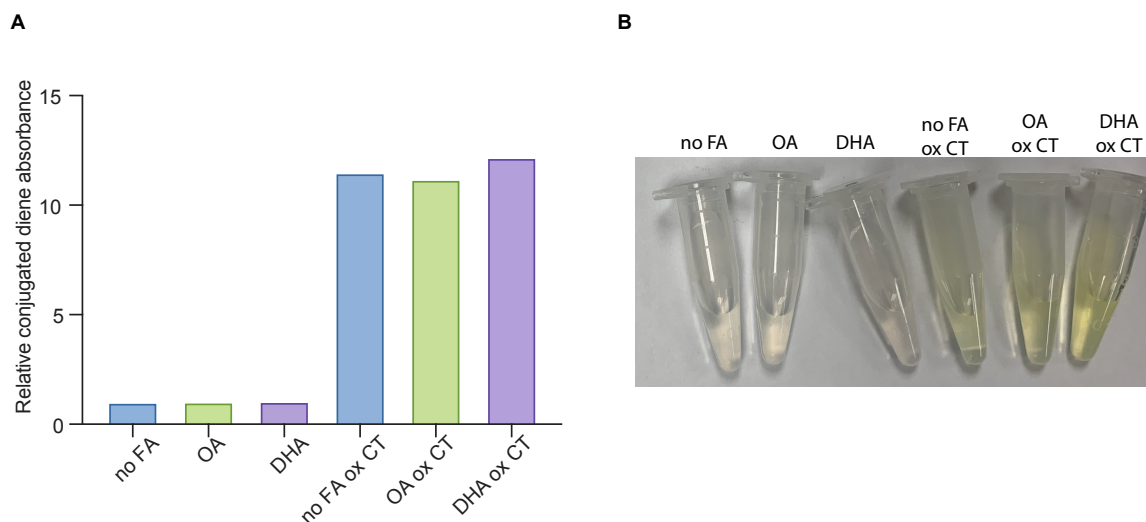


Figure 5.2 Spectroscopic analysis of fatty acid oxidation.

Fatty acid oxidation is minimal for PUFAs in our experimental conditions. A) Fatty acid oxidation, measured by conjugated diene presence, is low after electroformation. Immediately following electroformation, conjugated dienes were detected in samples containing only DOPC (no FA), 75 mol% DOPC/ 25 mol% OA (OA), and 75 mol% DOPC/ 25 mol% DHA (DHA) using absorbance at 230 nm in ethanol. Relative conjugated diene absorbance is reported with values normalized to DOPC, as DOPC is expected to be the most resistant to oxidation. We found that minimal oxidation occurred compared to samples subject to extreme heat and high levels of oxidation (ox CT). B) GUV samples are colorless after electroformation. Samples were photographed to demonstrate that they remained clear indicating that electroformed samples are minimally oxidized compared to oxidized samples which were brown.

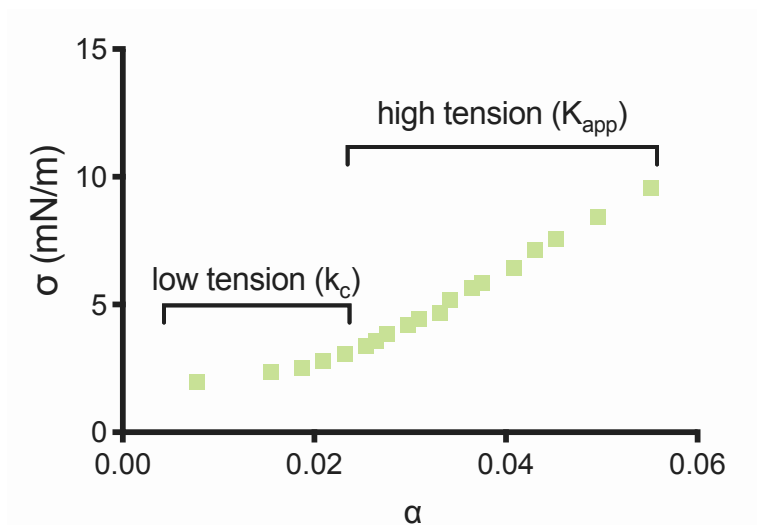


Figure 5.3 Sample micropipette aspiration stress/ strain curve.

Micropipette aspiration involves aspirating a vesicle at small intervals ~ 2 cm H₂O and observing a change in area within the pipette tip. K_{app} is calculated from the rate of change of the stress (σ) (equation S1) and the strain (α) (equation S2) in the high-tension regime, or the slope of this line.

$$\sigma = \frac{\Delta P * R_v * R_p}{R_v - R_p} \quad (\text{mN/m or dyne/cm}) \quad (\text{S1})$$

$$\alpha = \frac{\Delta A}{A(o)} \quad (\text{unitless}) \quad (\text{S2})$$

Where ΔP is the change in pipette pressure, and R_v and R_p are the vesicle and pipette radius, respectively. ΔA is change in vesicle area within the pipette, $A(o)$ refers to the original vesicle area within the pipette.

Next, we measured FFA incorporation into the DOPC membranes following vesicle formation. Fatty acid incorporation efficiency was dependent on fatty acid identity. Lipid stock solutions were made in chloroform to contain 75 mol% DOPC and 25 mol% of various fatty acids with differing hydrocarbon chain length and unsaturation. Using FFA and phospholipid quantification kits, we found that a monounsaturated fatty acid, OA, included in the chloroform stock solution at 25 mol% was subsequently incorporated into the bilayer at 15 mol%. Polyunsaturated FFAs such as EPA and DHA were incorporated around 5 mol% (Figure 5.4). In addition, we performed lipidomic analysis on our vesicles to further quantify our membrane compositions (Table 5.1). We found using the more sensitive method of mass spectrometry, that each FFA incorporated

around 7 mol% relative to DOPC. Because the polyunsaturated fatty acids, EPA and DHA, were incorporated into vesicle membranes at similar levels, we proceeded to compare changes in membrane properties between vesicles containing different polyunsaturated FFAs.

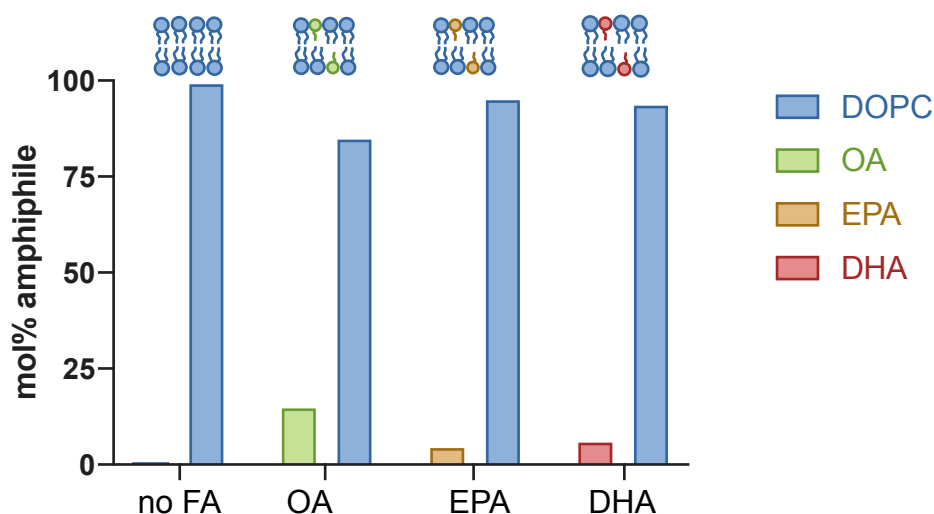


Figure 5.4 Fatty acid incorporation amounts differ based on fatty acid identity.

In order to confirm our membrane compositions after electroformation, we measured FA integration using phospholipid and fatty acid quantification kits. We mixed stock solutions containing 25 mol% fatty acid and 75 mol% DOPC in chloroform and created lipid films by removing solvent. The films were rehydrated in 300 mOsm sucrose and were subjected to electroformation to form GUVs. After electroformation, we diluted our GUVs below the fatty acid critical micelle concentration in PBS, pH 7.4, to mimic our micropipette aspiration conditions. We removed unincorporated fatty acids by centrifuging and removing the supernatant and measured the concentration of each class of amphiphile. As a control, we analyzed samples containing pure DOPC, which were found to not contain any fatty acids. We chose to analyze oleic acid (OA), eicosapentaenoic acid (EPA), and docosahexaenoic acid (DHA) because we focus the majority of our studies on these three fatty acids. We found that OA was present at 15 mol% while EPA and DHA were present at 5 mol%.

As fatty acids have differing hydrophilic headgroups and a smaller cross-sectional area compared to diacyl phospholipids, we first measured the impact of FFA headgroup on vesicle membrane K_{app} . FFAs consist of a carboxylic acid headgroup with a single hydrocarbon chain and phospholipid molecules consist of a phosphocholine headgroup and two hydrocarbon chains (Figure 5.1C). To isolate the effects of the carboxyl headgroup on K_{app} , we prepared DOPC (18:1) vesicles with increasing fractions of oleic acid (OA) (18:1) such that we retained the identity of hydrocarbon chains in the membrane (188). We observed that OA content did not impact membrane K_{app} when up to 25 mol% OA was included in the lipid stock solution (Figure 5.1D). These results indicate that the carboxylic acid headgroup and single-chain structure of FFAs do not alter the K_{app} of membranes with the same hydrocarbon chain composition.

We then wondered how the identity of the hydrocarbon chain of FFAs, including length, unsaturation content, and position of unsaturation, would impact membrane K_{app} . First, we compared gamma linoleic acid (GLA) (18:3) and alpha linoleic acid (ALA) (18:3), an ω -6 and ω -3 fatty acid, respectively (Figure 5.5). These fatty acids were selected because of their three unsaturated bonds and identical chain length, but differing location of their unsaturated bonds along their hydrocarbon chain, which allowed us to determine the effect of the location of unsaturated bonds in a fatty acid on membrane K_{app} . When OA, GLA, and ALA were included in DOPC lipid stock solutions at 25 mol%, we found that GLA and ALA reduced K_{app} (200 and 197 mN/m, respectively) to a similar extent compared to both OA-containing (249 mN/m) and pure DOPC membranes (245 mN/m) (Figure 5.5B, Table 5.2). These results indicate that for fatty acids containing three unsaturated bonds, the location of unsaturation at either ω -6 or ω -3 position does not impact the K_{app} of DOPC membranes. Next, we investigated how the chain length and degree of unsaturation of FFAs impact membrane K_{app} . Using ω -3 fatty acids ALA (18:3), stearidonic acid (SDA) (20:4), eicosapentaenoic acid (EPA) (20:5), and docosahexaenoic acid (DHA) (22:6), we analyzed how simultaneously increasing the degree of unsaturation as well as the chain length of a fatty acid affected membrane K_{app} (Figure 5.5C). We found that each polyunsaturated fatty acid decreased membrane K_{app} to a similar extent (~200 mN/m) compared to pure DOPC membranes (245 mN/m) (Figure 5.5D, Table 5.2).

Thus, increasing the extent of unsaturation and chain length in ω -3 fatty acids containing at least 3 unsaturated bonds appears to have no further effect on membrane area expansion moduli in DOPC model membranes. To the best of our knowledge, these results are the first K_{app} measurements of vesicles containing FFAs, and are consistent with previous findings performed with phospholipid-conjugated fatty acids (7, 45).

Table 5.2 K_{app} values of fatty acid/ DOPC blended membranes.

K_{app} values were measured using micropipette aspiration techniques. Vesicles were constructed from lipid stocks containing DOPC and varying mol percentages of each fatty acid, which are listed in the table. Values are represented as mean \pm standard error of the mean (SEM). The number of aspirated vesicles is included for each composition.

| | DOPC | 10% OA | 25% OA | 25% GLA | 25% ALA | 25% SDA | 25% EPA | 25% DHA |
|---------------------|-------------------------------|--------------------------------|-------------------------------|-------------------------------|-------------------------------|-------------------------------|--------------------------------|--------------------------------|
| K_{app} (mN/m) | 251 \pm 7 | 245 \pm 12 | 249 \pm 9 | 200 \pm 9 | 197 \pm 7 | 200 \pm 7 | 205 \pm 10 | 199 \pm 10 |
| n | 19 | 17 | 12 | 20 | 21 | 24 | 21 | 21 |

We next set out to validate the effect of FFAs on membrane fluidity, a property that has been studied more extensively in the presence of fatty acids. Using DPH fluorescence anisotropy of small unilamellar vesicles (SUVs), we measured the relationship between membrane fluidity and FFA identity in DOPC model membranes. We found that that FFAs generally increase membrane fluidity (Figure 5.6). This result is consistent with previous studies which measured the effect of unsaturated fatty acid integration, both when the FA was a phospholipid conjugate and as an FFA, on the fluidity of model and cellular membranes (31, 207, 209). However, in the current study, we expanded the range of FFA molecules explored. Furthermore, we observed that as the number of unsaturated bonds increases, fluidity is increased to a greater extent (Figure 5.6). Taken together, our results indicate that FFAs generally increase fluidity and decrease K_{app} of DOPC model membranes as a function of their unsaturated bond content.

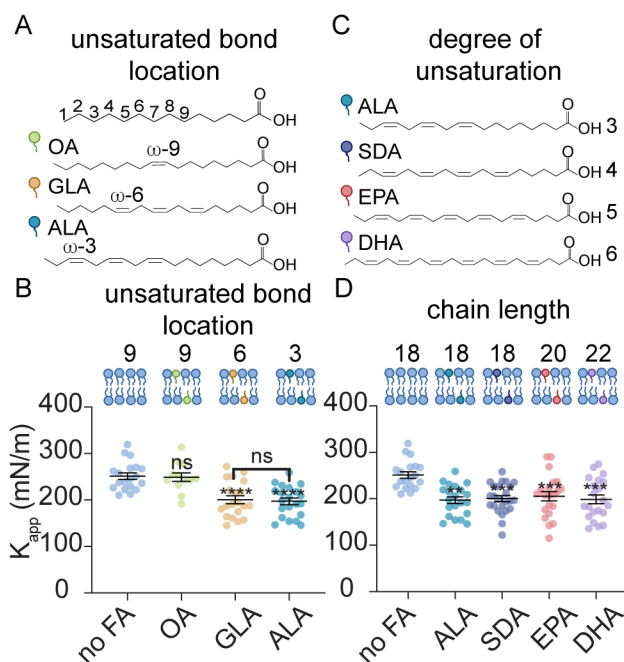


Figure 5.5 Effect of the number and position of unsaturated bonds in non-esterified PUFAs on K_{app}

A) Chemical structures and schematics of OA, GLA, and ALA. Selected fatty acids are ω -9, -6, and -3, respectively. B) Membrane K_{app} is reduced equally in the presence of GLA and ALA compared to no FA and OA. C) Chemical structures and schematics of polyunsaturated ω -3 fatty acids ALA, SDA, EPA, and DHA. D) K_{app} is reduced similarly in membranes containing ω -3 polyunsaturated fatty acids with 3 or more unsaturated bonds, regardless of the hydrocarbon chain length and number of unsaturated bonds. (B, D) Micropipette aspiration measurements were conducted on vesicles prepared using lipid stocks containing 100% DOPC (no FA) or 75 mol% DOPC, 25 mol% FA. Error bars represent standard error of the mean. P-values were generated by ANOVA using Dunnett's multiple comparisons test compared to no FA. $n \geq 12$ vesicles were aspirated per composition, **** $p \leq 0.0001$, *** $p \leq 0.001$, ** $p \leq 0.01$, non-significant (ns) $p > 0.5$.

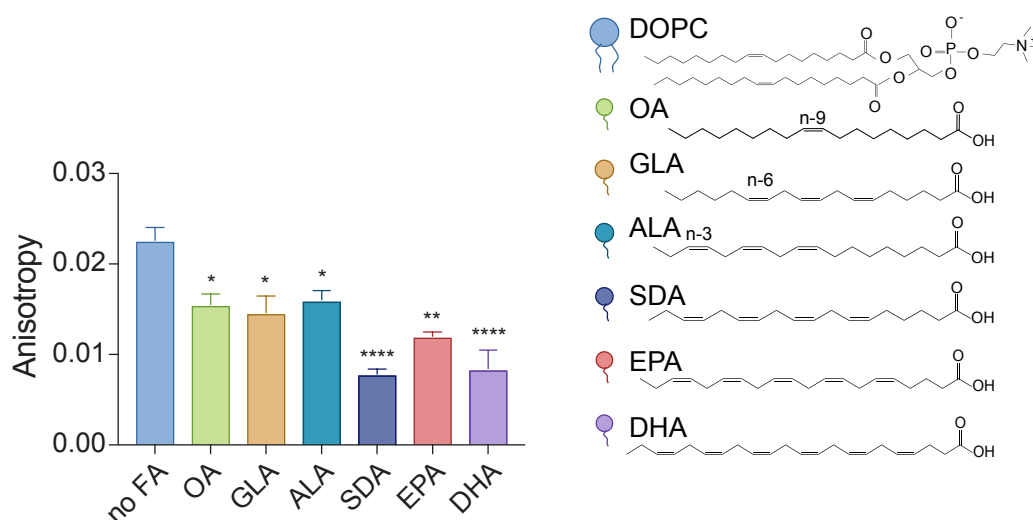


Figure 5.6 Fatty acids increase membrane fluidity.

Anisotropy studies were conducted with DOPC vesicles constructed from lipid stocks containing 25 mol% fatty acid and 0.2 mol% 1,6-Diphenyl-1,3,5-hexatriene (DPH) in 300 mOsm PBS, pH 7.4. $n=3$, P-values were generated by ANOVA using Dunnett's multiple comparisons test compared to no FA. **** $p \leq 0.0001$, ** $p \leq 0.01$, * $p \leq 0.05$, non-significant (ns) $p > 0.5$. Error bars represent standard error of the mean.

EPA and DHA differentially affect membrane elasticity in the presence of high levels of cholesterol

We next wondered how FFA inclusion would affect the K_{app} of membranes containing cholesterol. Cholesterol is a sterol found in all eukaryotic cell types and is critical for the proper function of a diverse array of membrane proteins. Among its many effects, this molecule promotes the formation of phase-segregated nanometer-sized crystalline domains, known as lipid rafts (50, 210) which have been found to affect the location and activity of membrane proteins (32, 77, 110, 178, 187). At low mole fractions, cholesterol is soluble and is dispersed through a bilayer membrane (47, 48). As the mole fraction of cholesterol increases to around 50 mol%, as in the lipid mixtures we investigated, the area fraction and number of cholesterol-rich crystalline domains also increases (47, 70, 80, 210). Using ternary mixtures of fatty acids, cholesterol at either a low (25 mol% stock solution) or high (45 mol% stock solution) amounts, and DOPC, we sought to determine how FFAs affected membrane K_{app} when cholesterol was present.

We first prepared vesicles containing a low amount of cholesterol from stock solutions containing 25 mol% fatty acid, 25 mol% cholesterol, and 50 mol% DOPC and performed micropipette aspiration studies (Figure 5.7A). At this concentration, we expected that cholesterol would not significantly affect lipid segregation and the membrane components would remain well mixed (47, 70). We chose to focus our studies on two FFAs, EPA and DHA, because of their biological relevance and distinct effect on membrane protein activity (8, 31, 187, 209, 211). As a control, we prepared vesicles with 25 mol% OA since this FFA had not impacted membrane K_{app} when mixed with DOPC in the absence of cholesterol (Figure 5.1D). In addition, we chose OA as an elasticity control because a previous study by Bruno and colleagues found that OA did not alter the activity of a mechanosensitive protein, Gramicidin (8). Furthermore, OA inclusion also allowed us to control for the smaller physical size of an FFA compared to a phospholipid and the potential physicochemical effects these FFAs may have on membrane properties (188). The inclusion of 25 mol% cholesterol in stock solutions with DOPC slightly increased the K_{app} relative to cholesterol-free membranes as expected (273 mN/m) (6). Our results using OA, EPA, and DHA mimicked those we observed in cholesterol-free membranes. We observed that OA had no effect on the K_{app} of membranes containing low

mol% cholesterol (264 mN/m). The subsequent addition of EPA and DHA reduced membrane K_{app} to similar levels (~240 mN/m) with respect to membranes lacking fatty acid (no FA) (273 mN/m) (Figure 5.7B, Table 5.3). These results demonstrated that the inclusion of the FFAs, DHA and EPA, in membranes containing low mol% cholesterol had a similar effect of reducing membrane K_{app} as they had in membranes without cholesterol (Figure 2.1, 5.5).

Table 5.3 K_{app} values for DOPC membranes containing fatty acids and cholesterol domains.

Sample names indicate the composition of lipid chloroform stocks used to create vesicles. Values are represented as mean \pm standard error of the mean (SEM).

| more domains | 50 mol% chol 50% DOPC | 25% OA 45% chol 30% DOPC | 25% EPA 45% chol 30% DOPC | 25% DHA 45% chol 30% DOPC |
|------------------------------------|----------------------------------|---|--|--|
| K_{app} (mN/m) | 339 \pm 8 | 479 \pm 18 | 463 \pm 13 | 357 \pm 15 |
| n | 23 | 34 | 51 | 46 |
| less domains | 25 mol% chol 75% DOPC | 25% OA 25% chol 50% DOPC | 25% EPA 25% chol 50% DOPC | 25% DHA 25% chol 50% DOPC |
| K_{app} (mN/m) | 273 \pm 9 | 264 \pm 9 | 244 \pm 6 | 237 \pm 5 |
| n | 18 | 21 | 25 | 23 |

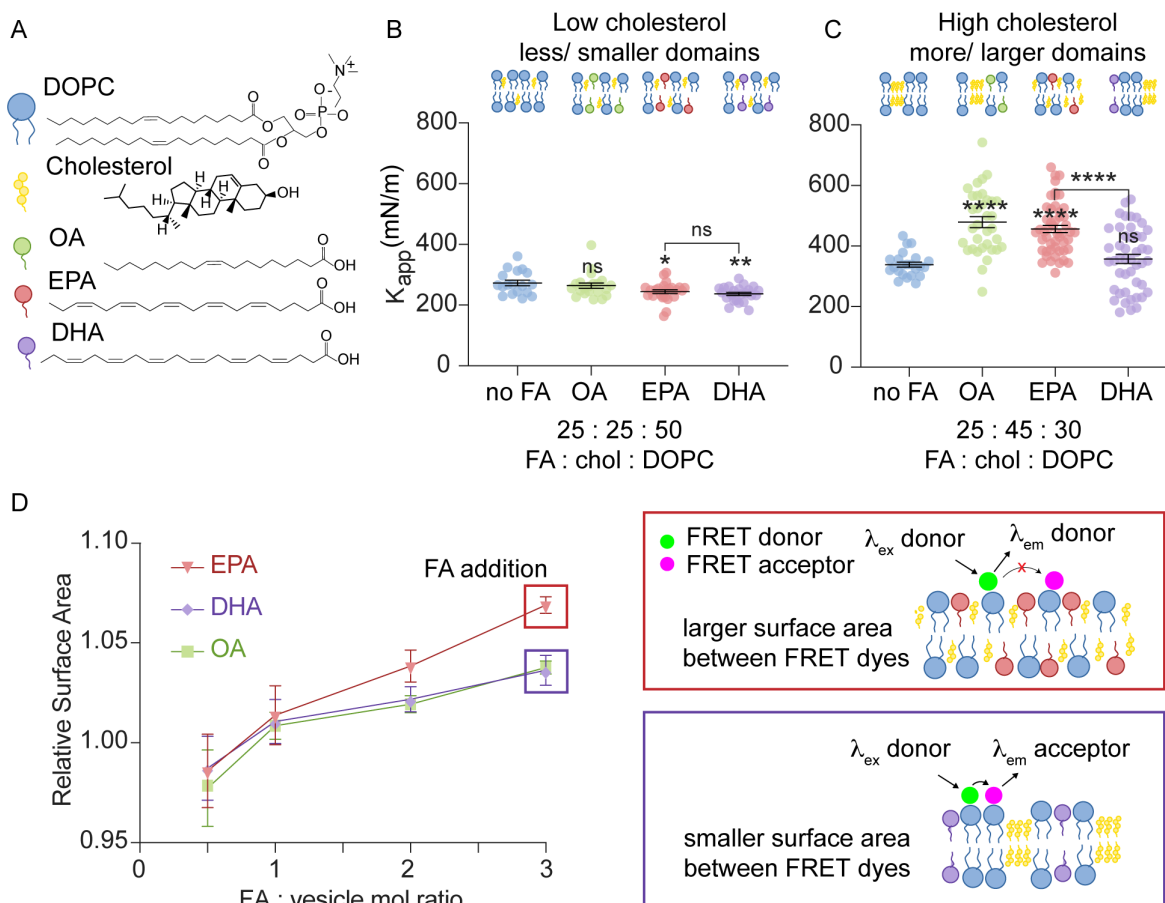


Figure 5.7 DHA and EPA have distinct effects on the K_{app} of membranes with cholesterol nanodomains

A) Chemical structures and schematics of cholesterol, DOPC, and select FAs. B) DOPC membranes have a reduced K_{app} in the presence of EPA and DHA compared to no FA when low amounts of cholesterol are present. Vesicles were constructed from lipid stocks composed of chol:DOPC 25:75 (no FA) and FA:chol:DOPC 25:25:50, $n \geq 18$. C) DHA decreases the K_{app} of membranes assembled with higher concentrations of cholesterol compared to EPA. Vesicles were constructed from lipid stocks containing chol:DOPC 50:50 (no FA), and FA:chol:DOPC 25:45:30. Error bars represent standard error of the mean, $n \geq 23$. P-values were generated by ANOVA using Dunnett's multiple comparisons test compared to no FA. **** $p \leq 0.0001$, ** $p \leq 0.01$, * $p \leq 0.05$, non-significant (ns) $p > 0.5$. D) Bulk FRET measurements of SUVs were used to determine the effect of EPA and DHA on nanodomain disruption. EPA inclusion increases the average distance between FRET labeled lipids to a greater extent than OA and DHA suggesting enhanced cholesterol redistribution with EPA. 10 mM 50 mol% chol, 50 mol% DOPC vesicles were prepared with different concentrations of equimolar 18:1 NBD PE and 18:1 Liss Rhod PE. The FRET ratio (f_{don}/f_{acc}) demonstrates energy transfer efficiency between the dyes after fatty acid addition. Relative surface area was determined by normalizing the fluorescence intensity of each sample to the fluorescence intensity in fatty acid-free PBS (data not shown). FRET studies were conducted in 300 mOsm PBS, pH 7.4, $n=3$ using independent vesicle samples.

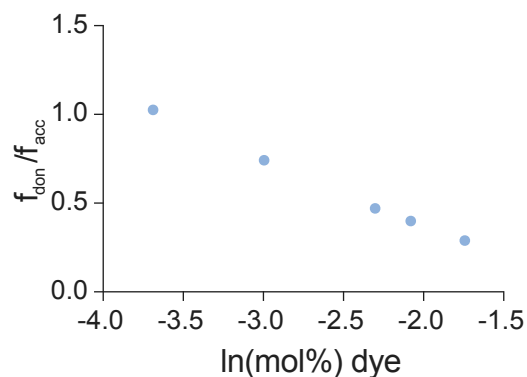


Figure 5.8 FRET standard curve used to calculate relative surface area changes in vesicles.

Increasing concentrations of equimolar 18:1 NBD PE and 18:1 Liss Rhod PE were added to 10 mM DOPC vesicles. The FRET ratio (f_{don}/f_{acc}) demonstrates the energy transfer efficiency of the dyes at different concentrations. FRET studies were conducted in PBS, pH 7.4.

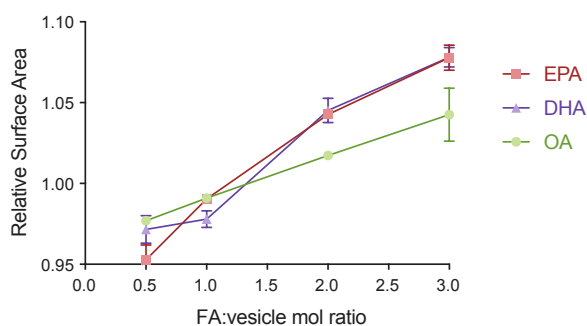


Figure 5.9 In the absence of domains, EPA and DHA affect vesicle surface area similarly.

When EPA and DHA are added to 25 mol% chol, 75 mol% DOPC vesicles, EPA and DHA exhibit similar changes in vesicle surface area, unlike vesicles that exhibit phase behavior (Fig 5.7C). Vesicles were prepared with different concentrations of equimolar 18:1 NBD PE and 18:1 Liss Rhod PE. The FRET ratio (f_{don}/f_{acc}) is used to measure energy transfer efficiency between the dyes after fatty acid addition. $n=3$, FRET studies were conducted in 300 mOsm PBS, pH 7.4. Error bars represent standard error of the mean.

We then investigated how FFA inclusion affected the K_{app} of phospholipid membranes when they contained higher levels of cholesterol that should form a greater amount of cholesterol-rich, crystalline nanodomains. Previous work by Mason et al. using X-ray diffraction analysis demonstrated that EPA and DHA can have distinct effects on cholesterol nanodomains: while EPA enhances cholesterol mixing and disrupts domains by integrating into both liquid-ordered and liquid-disordered domains, DHA increases the size and stability of membrane domains due to its exclusion from ordered domains (47, 48, 60, 61, 188, 211–213). Yet, we were unsure of how these structural changes would affect the bulk membrane property, K_{app} . We measured the K_{app} of DOPC membranes containing high amounts of cholesterol and either OA, DHA, or EPA. In the presence of fatty acids, we were able to include, at most, 45 mol% cholesterol in our lipid stocks as higher amounts of cholesterol prevented vesicle formation. Using GUVs constructed from lipid stocks containing ternary mixtures of 25 mol% fatty acid, 45 mol% cholesterol, and 30 mol% DOPC, we determined that membrane K_{app} of the resulting electroformed increased in the presence of OA (479 mN/m) and EPA (463 mN/m) compared to DOPC/cholesterol alone (339 mN/m) (Figure 5.7C, Table 5.3). We attribute this increase in K_{app} in the presence of OA to an increase in the cholesterol area fraction of the membrane because OA is a single hydrocarbon-chain lipid but DOPC contains two chains. When DOPC is replaced with OA, there is more cholesterol per hydrocarbon-chain, which is expected to increase K_{app} as if more cholesterol is present (6, 66). We expected EPA to reduce membrane K_{app} to a similar extent as DHA, resembling our observations with cholesterol-free and low-cholesterol content membranes. Surprisingly, we observed that EPA increased membrane K_{app} (463 mN/m) compared to DHA (357 mN/m) (Figure 5.7C, Table 5.3). These results indicate that in the presence of high mol% cholesterol, DHA and EPA affect the K_{app} of DOPC membranes differently, which has not been observed previously.

We wondered if the higher content of cholesterol was affecting the phase segregation behavior of DOPC model membranes and contributing to the differential effects of DHA versus OA and EPA on membrane K_{app} . We first confirmed that cholesterol inclusion at 50 mol% in preformed membranes exhibited

measurable increases in membrane phase segregation with DHA addition compared to EPA addition (Figures 5.7D, 5.8) We assessed changes in phase behavior by monitoring changes in membrane surface area. Using a bulk FRET assay we measured the average distance between fluorophore-labelled lipids. In the presence of 50 mol% cholesterol, the fluorophores conjugated to unsaturated phospholipids should colocalize with liquid disordered domains. Using this FRET assay, we observed larger differences in surface area changes with the external addition of EPA compared to OA and DHA. We attribute the greater FRET change in response to EPA to enhanced disruption of cholesterol domains, which increases the effective surface area of the dye-containing fraction of the membrane as cholesterol mixes with the phospholipids. This result indicated that EPA disrupted cholesterol domains to a greater extent than OA and DHA, leading to greater spacing between FRET labelled dyes as consistent with previous findings (47). In contrast, in membranes containing low mol% cholesterol, where nanodomains were not expected to occupy a significant fraction of the membrane, we observed no differences in membrane surface area change between EPA and DHA-containing membranes (Figure 5.9). These results supported our hypothesis that in membranes containing higher amounts of cholesterol, EPA disrupted phase segregated domains to a greater extent than DHA.

We set out to better understand why DHA reduced K_{app} relative to EPA when cholesterol was present at high levels in DOPC membranes but induced similar changes in K_{app} when cholesterol was at lower levels or absent. First, we wondered if the discrepancy in K_{app} values for membranes containing EPA or DHA was due to differential incorporation of either fatty acid. To test this, we used a phospholipid and a fatty acid quantitation assay to measure our true membrane compositions and found that EPA and DHA were present in similar amounts in their respective membranes (Figure 5.10). Interestingly, we observed OA was present at higher levels in electroformed vesicles than DHA or EPA. This difference in incorporation was expected as the partition coefficient of OA is 10 times larger than DHA in DOPC membranes, however previous studies have demonstrated the potent effects of DHA despite this lower incorporation efficiency (8). However, as OA did not reduce membrane K_{app} , we concluded the differential level of incorporation of this particular fatty acid did not have a significant impact on our observations. We next explored the possibility

that the presence of EPA or DHA differentially affected how much cholesterol was included in the membrane during formation and thereby affected the resulting K_{app} . We used fluorescence microscopy to compare cholesterol content in membranes containing different fatty acids by measuring the fluorescence of a boron-dipyrromethene (BODIPY) labelled-cholesterol. We found that fatty acid content did not affect cholesterol partitioning into electroformed GUVs, and that cholesterol was present in similar levels in the different vesicle samples we explored (Figure 5.11). We confirmed this result using lipidomic analysis of our vesicles and found that cholesterol incorporated around 10 mol% in the presence of each fatty acid (Table 5.1). While this incorporated amount is significantly less than what was included in the lipid stock solution (45 mol %), previous results from Stevens *et al* demonstrated that sterol solubility in electroformed membranes may be limited. While they observed up to 65 mol% cholesterol in assembled membranes, their studies included a different phospholipid, DPPC, which may have increased cholesterol solubility (214). In addition, we do not expect that a change in phase behavior due to force application (215) altered our aspiration results, as studies were performed at room temperature and the calculated phase transition temperature for these compositions is well below that (Table 5.4, Figure 5.12). Taken together, these results suggest that differences in K_{app} between membranes containing DHA versus EPA are not due to differences in molar ratios of the amphiphilic components.

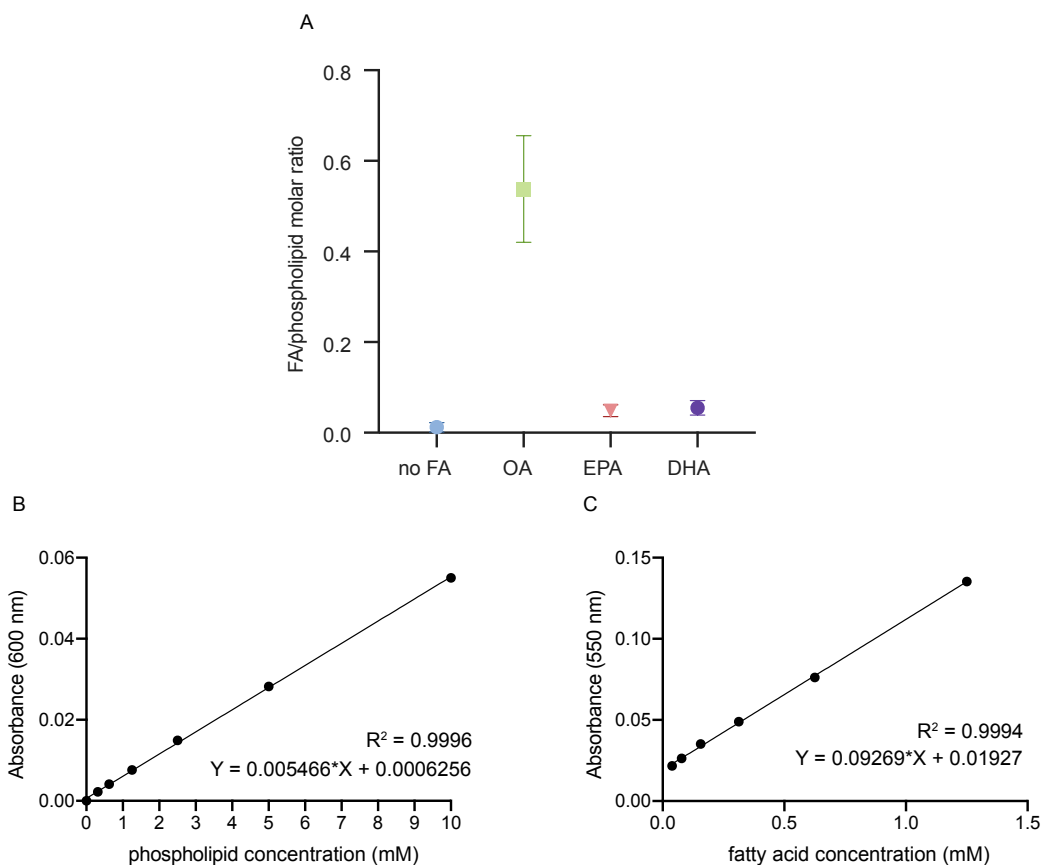


Figure 5.10 Determination of membrane fatty acid composition in ternary mixtures with POPC and cholesterol.

A) In order to confirm our membrane compositions of ternary mixtures of membranes constructed from lipid stocks containing 30 mol% POPC, 45 mol% cholesterol, and 25 mol% fatty acid, we used a phospholipid and a fatty acid quantitation kit to determine the mol% of each component. Molar ratios were calculated by dividing the concentration of fatty acid by the phospholipid concentration. POPC and cholesterol only (no FA) demonstrates the specificity of the free fatty acid kit to not detect phospholipids or cholesterol. OA, EPA, and DHA represent samples prepared from stocks containing 25 mol% of each respective fatty acid. Fatty acid and phospholipid concentrations were calculated from standard curves of phospholipid (B), and oleic acid (C).

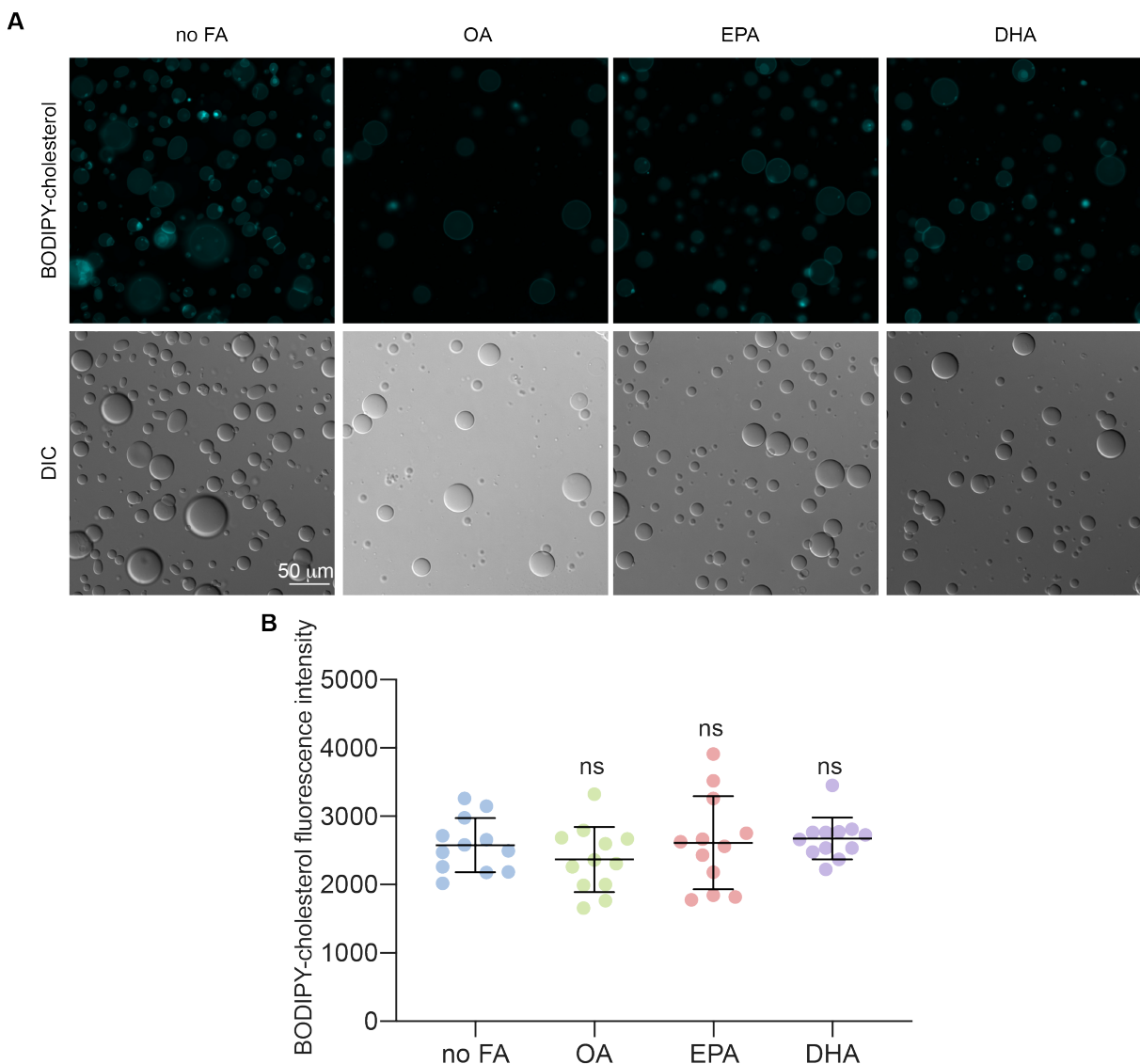


Figure 5.11 Cholesterol is similarly incorporated into membranes containing different fatty acids.

A) BODIPY-cholesterol images demonstrate similar incorporation of cholesterol in vesicle populations. BODIPY-cholesterol was incorporated into 30 mol% POPC, 45 mol% cholesterol, 25 mol% fatty acid lipid stocks and GUVs were formed using electroformation techniques. Epifluorescence images are false-colored in cyan and show BODIPY-cholesterol fluorescence at the membrane of all vesicles containing either no FA, OA, EPA, or DHA, scale bar = 50 μm . B) BODIPY-cholesterol fluorescence intensity values reveal no significant difference in cholesterol incorporation between membrane compositions. BODIPY-chol membrane fluorescence was calculated for 12 defect-free vesicles in each population and reported as single values. The center black line indicates mean fluorescence intensity. Error bars represent standard deviation, $n=12$. P values were generated by ANOVA using Dunnett's multiple comparisons test compared to no FA, non-significant (ns) $P > 0.5$.

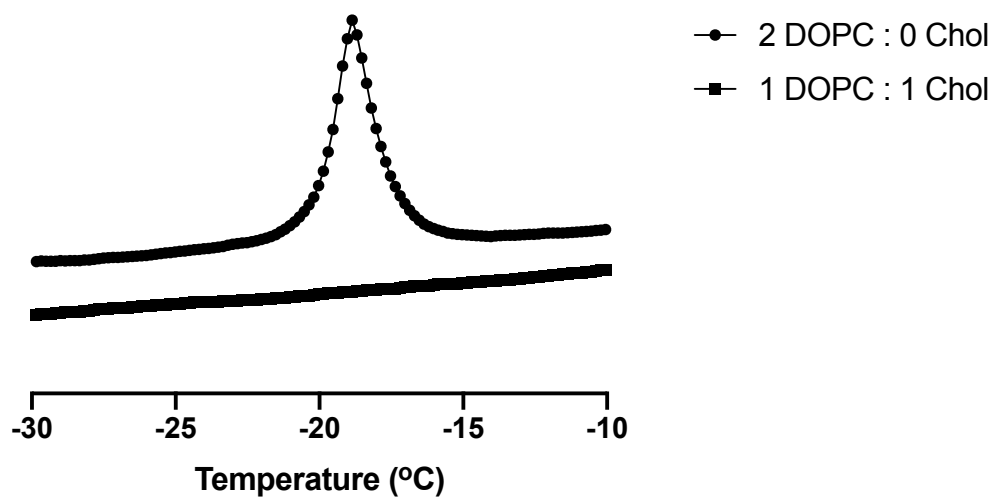


Figure 5.12 Melting temperature of membranes is below ambient temperature and a phase transition is not expected during aspiration measurements (Table 5.4). DSC thermogram for pure DOPC (2 DOPC: 0 chol) and 50 mol% chol, 50 mol% DOPC (1 DOPC: 1 chol) vesicles. Curves have been corrected using a water control.

Table 5.4 Comparison of phase transition temperatures for vesicles composed of DOPC and 1:1 DOPC and cholesterol

The phase transition temperature remains well below ambient temperature, where experiments were carried out. The addition of cholesterol decreases the phase transition temperature.

| <i>Sample</i> | <i>T_{transition} (°C)</i> |
|------------------------|------------------------------------|
| <i>2 DOPC : 0 Chol</i> | <i>-18.89</i> |
| <i>1 DOPC : 1 Chol</i> | <i>-20.96</i> |

We then investigated if these changes in phase behavior impacted other membrane physical properties beyond K_{app} . Using the flickering spectroscopy method, we measured the bending rigidity (k_c) of vesicles formed from lipid stocks containing 25 mol% fatty acid, 45 mol% cholesterol and 30 mol% DOPC. We found that EPA and DHA similarly increase k_c compared to OA and membranes without any FFAs (Table 5.5). This increase in bending stiffness in the presence of fatty acids is consistent with previous studies on model membranes, where FFAs alter the area per lipid of membrane amphiphiles and the resulting curvature strain increases k_c (207). In addition, our observation of no significant difference between the bending stiffness of EPA versus DHA-containing membranes is consistent with AFM measurements of cells enriched in EPA and DHA (31), though these studies observed a decrease in bending stiffness upon EPA and DHA addition. We were also able to extract k_c values from the low tension regime of our micropipette aspiration data. We compared k_c measured by the flickering spectroscopy method and micropipette aspiration and observed similar increases in bending rigidity (Table 5.6, Figure 5.3). Our finding of k_c being unaffected by the presence of cholesterol nanodomains suggest that membrane phase behavior does not impact bulk k_c measurements in a similar manner to K_{app} . This uncoupling of K_{app} and k_c changes was unexpected as a decrease in K_{app} is typically concurrent with a decrease in k_c (7). We also measured membrane fluidity in membranes with FFAs in the presence of high amounts of cholesterol. We found that in the presence of high levels of cholesterol, DHA increased membrane fluidity to a greater extent than EPA and compared to no fatty acid (Figure 5.13), consistent with previous findings (47). However, this result was also consistent with our findings in cholesterol-free membranes (Figure 5.6). Therefore, the K_{app} is the only membrane property that we measured which uniquely exhibits differences between EPA and DHA when in the presence of phase-segregated nanodomains. These results suggest that phase-segregated nanodomains have a pronounced effect on membrane K_{app} compared to k_c and fluidity.

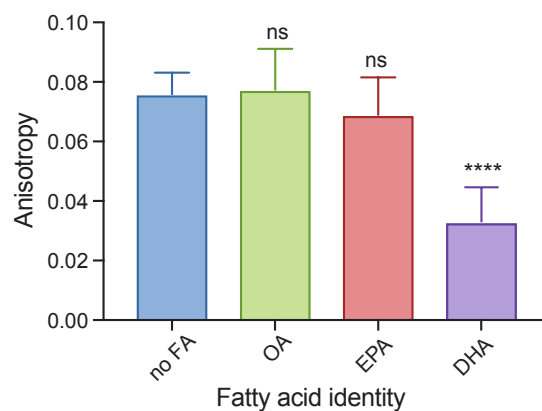


Figure 5.13 DHA increases the fluidity of membranes containing cholesterol.

Decreased fluorescence anisotropy occurs with increased membrane fluidity as observed in membranes containing DHA. Anisotropy studies were conducted with vesicles constructed from lipid stocks containing 50 mol% chol, 50 mol% DOPC (no FA) or 25 mol% FA, 50 mol% chol, 25 mol% DOPC and 0.2 mol% 1,6-Diphenyl-1,3,5-hexatriene (DPH) in 300 mOsm PBS, pH 7.4, n=3 independent vesicle preparations were measured. P-values were generated by ANOVA using Dunnett's multiple comparisons test compared to no FA. **** $p \leq 0.0001$, non-significant (ns) $p > 0.5$. Error bars represent standard error of the mean.

Table 5.5 k_c values for fatty acid and cholesterol-containing membranes.

k_c values were determined using the flickering spectroscopy method and are reported as mean \pm standard deviation, $n \geq 15$. Sample names indicate the composition of lipid stocks in chloroform.

| | 50 mol% chol 50% DOPC | 25% OA 45% chol 30% DOPC | 25% EPA 45% chol 30% DOPC | 25% DHA 45% chol 30% DOPC |
|--------------------------|----------------------------------|---|--|--|
| k_c (K _B T) | 30.4 \pm 2.6 | 20.8 \pm 2.1 | 33.4 \pm 4.3 | 37.6 \pm 3.2 |
| | 50 mol% chol 50% POPC | 25% OA 45% chol 30% POPC | 25% EPA 45% chol 30% POPC | 25% DHA 45% chol 30% POPC |
| k_c (K _B T) | 60.5 \pm 5.4 | 76.9 \pm 4.7 | 72.0 \pm 6.8 | 66.0 \pm 5.6 |

Table 5.6 Comparison of k_c measurements obtained by the flickering spectroscopy method and micropipette aspiration.

We compared k_c measurements from select samples using the flickering spectroscopy method and micropipette aspiration in the low-tension regime. We found that the flickering spectroscopy method was more sensitive (258), likely because micropipette aspiration utilizes membrane stretching to determine k_c while flickering spectroscopy does not use external membrane perturbation but both methods produced similar results. We chose to use the flickering spectroscopy method for the majority of our compositions for this reason.

| | Micropipette aspiration k_c ($k_B T$) | Flickering spectroscopy ($k_B T$) |
|------------------------------------|--|---|
| DOPC/ high cholesterol | 30.4 +/- 5.5 | 30.4 +/- 2.6 |
| POPC/ high cholesterol | 64.0 +/- 25 | 60.5 +/- 5.4 |
| DOPC/ high cholesterol/ DHA | 27.0 +/- 9.9 | 37.6 +/- 3.2 |
| DOPC/ high cholesterol/ EPA | 40.7 +/- 18.9 | 33.4 +/- 4.3 |
| DOPC/ high cholesterol/ OA | 50.4 +/- 13 | 20.8 +/- 2.1 |

Membrane phase-segregation behavior impacts elasticity with an alternate phospholipid composition

Finally, to investigate this proposal that EPA and DHA differentially alter membrane K_{app} through differentially altering cholesterol crystalline domain behavior, we used an alternate membrane composition that also forms cholesterol nanodomains: 1-palmitoyl-2-oleoyl-glycero-3-phosphocholine (POPC) (18:1, 16:0) and cholesterol. POPC is similar to DOPC except one of its 18-carbon monounsaturated chains is replaced with one 16-carbon saturated chain. We expected to observe similar relationships between cholesterol content and K_{app} values as a function of FFA identity as we observed in DOPC membranes. Additionally, we expected that the difference in K_{app} values between EPA and DHA-containing membranes would be more pronounced in POPC membranes because cholesterol has a greater stiffening effect on saturated lipids (6, 51). Using micropipette aspiration, we measured the K_{app} of GUVs formed from lipid stocks containing ternary mixtures of 25 mol% fatty acid, 45 mol% cholesterol, and 30 mol% POPC. In the POPC membranes made with high cholesterol content, we observed that K_{app} increased in the presence of OA (600 mN/m) and EPA (837 mN/m) compared to membranes containing POPC and cholesterol alone (545 mN/m) (Figure 5.14, Table 5.7). This result matched the general trends observed with DOPC and high cholesterol content membranes (Figure 5.7C). Similarly to DOPC samples, we found that the K_{app} of DHA-containing membranes (462 mN/m) was significantly reduced compared to membranes that contained EPA (837 mN/m). Lipidomic analysis of these samples revealed that in POPC membranes prepared with high concentrations of cholesterol, EPA and DHA incorporated at similar levels of 2.9 and 3.5 mol%, respectively, while OA incorporated at 7.7 mol % (Table 5.1). These results confirmed that in the presence of high amounts of cholesterol, which is believed to form cholesterol-rich domains, EPA and DHA have significantly different effects on membrane K_{app} . Taken together, our results in POPC/cholesterol and DOPC/cholesterol systems demonstrate that the FFAs, EPA and DHA, can differentially impact membrane area expansion moduli when cholesterol is present at high amounts.

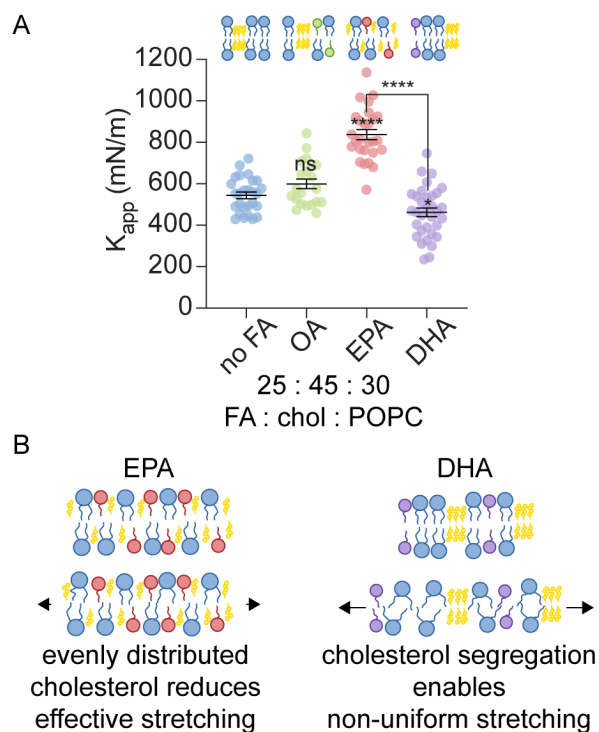


Figure 5.14 Assessing the generality of the effect of cholesterol content on FFA-induced changes in K_{app} .

A) POPC vesicles prepared with high (45 mol%) amounts of cholesterol confirm that EPA and DHA have differential effects on membrane K_{app} . K_{app} is reduced in DHA-containing vesicles compared to vesicles containing EPA. Vesicles were constructed from lipid stocks composed of chol:POPC 50:50 (no FA) and FA:chol:POPC 25:45:30 vesicles. Error bars represent standard error of the mean, $n \geq 18$. P values were generated by ANOVA using Dunnett's multiple comparisons test compared to no FA, **** $p \leq 0.0001$, * $p \leq 0.05$, non-significant (ns) $p > 0.5$. B) Proposed mechanism of decreased membrane K_{app} in the presence of phase-segregated cholesterol nanodomains.

Table 5.7 K_{app} values of POPC, cholesterol, and fatty acid membranes.

Sample names indicate lipid stock compositions in chloroform. Values are represented as mean \pm standard error of the mean (SEM).

| | 50% chol 50% POPC | 25% OA 45% chol 30% POPC | 25% EPA 45% chol 30% POPC | 25% DHA 45% chol 30% POPC |
|------------------|----------------------|--------------------------------|---------------------------------|---------------------------------|
| K_{app} (mN/m) | 545 \pm 16 | 600 \pm 24 | 837 \pm 24 | 462 \pm 21 |
| n | 27 | 21 | 27 | 33 |

5.4 Discussion

Here, we have shown the effect of FFAs on membrane K_{app} in phospholipid model membranes, which we believe are the first measurements of this nature. As FFAs are increasingly found to alter biological processes, the impact of FFA inclusion on membrane properties is important to understand. FFAs insert at fast timescales, much faster than metabolic-based membrane reorganization (186). Therefore, FFAs have the ability to transiently alter the local membrane composition (216) and impact biological function even prior to their incorporation in diacyl phospholipids. This would be especially prevalent in cells with malfunctioning machinery to control membrane composition or in cells lacking this machinery, such as red blood cells (217, 218). Therefore, understanding the specific role of FFAs on membrane physical properties is important to bridge the gap between FFA effects on membrane composition and their subsequent effects on cellular function.

Our K_{app} results with OA, which has the same hydrocarbon structure of DOPC lipids, indicate that the carboxylic headgroup and single chain structure of an FFA are not the dominant contributors to FFA-induced changes in K_{app} . Consistent with previous findings that explored the effect of unsaturation in diacyl lipids on the area expansion modulus (7, 45), it appears that the extent of hydrocarbon chain unsaturation is a key contributor to shifts in K_{app} . The structure of the fatty acid, whether it is in a monoacyl form or

incorporated into a phospholipid, does not appear to matter in this regard. Because introducing double bonds into an amphiphile chain causes thinning of the bilayer (7, 47) the membrane should exhibit an increased ability to stretch. This effect of membrane thinning and an increased area per lipid with the inclusion of polyunsaturated fatty acids reduces the energy required for elastic deformation (45). These previous results support our finding that FFA polyunsaturation reduces model membrane K_{app} .

Additionally, we explored how the increasingly investigated ω -3 fatty acids, EPA and DHA, affected membrane K_{app} in the absence and presence of cholesterol. These FFAs, which have similar effects on membrane K_{app} in the presence of no or low cholesterol, have different effects on K_{app} once cholesterol content is increased. For example, when EPA and DHA were added to DOPC membranes that lacked cholesterol, they had similar effects on membrane K_{app} , reducing the value from 251 mN/m to 205 and 199 mN/m, respectively. The addition of low levels of cholesterol (25 mol%) did not change this general trend. In contrast, when higher levels of cholesterol (45 mol%) were incorporated into DOPC membranes, we observed that EPA and DHA now had different effects on membrane K_{app} with EPA having a significantly higher K_{app} value (463 mN/m) than DHA (357 mN/m). This result demonstrates that cholesterol concentration alters the effect of EPA and DHA on the K_{app} of DOPC membranes.

Why might EPA and DHA differentially affect the propensity of a bilayer membrane to stretch when cholesterol is present in high concentrations? Cholesterol can have several effects on the physical properties of membranes that could explain this phenomenon. First, cholesterol increases the packing density of lipid chains and bilayer thickness, leading to increases in the bending rigidity and area expansion modulus of membranes (6, 53, 219). These effects appear to hold for both saturated as well as unsaturated membranes (220). DHA has one more unsaturated bond than EPA, and differential effects on membrane K_{app} that may not be apparent at low K_{app} values could become more obvious as the membrane is made stiffer (219). Second, cholesterol promotes phase segregation in model membranes and DHA and EPA are known to interact differently with phase-segregated domains (47, 60, 61, 188, 189, 213). Membranes

containing ordered and disordered lipids can phase segregate into raft-like (ordered) and nonraft-like (disordered) domains observed in cellular membranes (50, 76, 211, 221). Cholesterol typically associates with raft-like domains but can also induce nanodomain formation when incorporated into membranes containing only one phospholipid, like in POPC or DOPC (70, 80, 210, 222, 223). Experiments with model and cell-derived membranes have shown that DHA has highly unfavorable interactions with cholesterol and does not pack into ordered, raft-like phases, and instead segregates into disordered domains (47, 60, 61, 63, 79, 175, 212, 224). In contrast, EPA and other less disordered ω -3 fatty acids appear to inhibit or disrupt ordered domains relative to DHA (47, 213). These previous results suggest membrane organization may affect membrane K_{app} .

We hypothesize that the differences we observed in K_{app} when membranes contained high levels of cholesterol and either DHA or EPA were, in part, due to differences in molecular interactions between cholesterol and lipid acyl chains. When lipids and cholesterol are more evenly dispersed throughout the membrane there are increased van der Waals interactions between phospholipids and cholesterol, which can increase the apparent area expansion modulus, requiring more tension to stretch a membrane (6). In contrast, when cholesterol is sequestered into ordered domains, the net number of cholesterol interactions with phospholipids is reduced (59). In effect, we hypothesize the reduction of K_{app} of DHA-containing membranes, compared to EPA-containing membranes, is due to non-uniform membrane deformation because of reduced interactions between phospholipids and cholesterol when cholesterol is phase segregated. Put another way, it appears that by segregating a molecule (cholesterol) that typically stiffens a membrane, that molecule has less impact on long-range membrane properties than when it is well mixed into the membrane. In summary, we expect cholesterol phase segregation is reduced in the presence of EPA, leading to more cholesterol-lipid interactions and a higher K_{app} in this condition relative to DHA. For membranes with a significant level of cholesterol-rich domains, we hypothesize that in response to applied tension, the majority of membrane stretching occurred in the liquid disordered phase and reduced deformation was occurring in segregated, stiffer ordered domains. This effect of non-uniform stretching

would explain a net decrease in membrane K_{app} compared to membranes with homogeneously distributed cholesterol and lipids (Figure 5.14).

We further observed we could change lipid-cholesterol interactions by changing the diacyl lipids; by switching the phospholipid from DOPC to POPC, we increased cholesterol-lipid interactions and the differential effects of EPA and DHA on K_{app} further increased. Differences in K_{app} between membranes constructed from POPC or DOPC and containing high cholesterol concentrations may be explained by the increased content of saturated acyl chains in POPC membranes (Figures, 5.7, 5.14) (53). This increase in saturation is known to increase the stiffening effect of cholesterol, increasing membrane K_{app} (6). Our results demonstrate that cholesterol concentration (Figures 5.5, 5.7), and phospholipid identity (Figure 5.7C, Figure 5.14A) can affect how individual fatty acids change membrane K_{app} . These results highlight the potential for variability in lipid composition to affect how a given fatty acid will change membrane biophysical properties (189): if a membrane is fairly elastic, different fatty acids may have small effects on membrane elasticity, however, if a membrane is more stiff, small differences in fatty acid unsaturation and chain length may have significant effects on membrane elasticity.

Our findings also help explain why EPA and DHA may have differential effects on the behavior of membrane proteins. Previous studies have shown that EPA and DHA differentially impact membrane protein activity when the fatty acids were added to cells, but the mechanism was unclear (8, 31, 184). In these studies, the properties of bending rigidity and viscosity were investigated, which probe the propensity of a membrane to move out of plane or for lipids to move past one another. Both properties were similarly modified by EPA and DHA. In contrast, our study, which explored the propensity of a membrane to stretch in plane, identified differences between EPA and DHA-containing samples.

Finally, the current results contribute to the growing theory that certain changes in protein activity may be due to alterations of the physical membrane environment surrounding the protein rather than distinct

chemical binding effects of the fatty acid (178, 183, 185). FFAs that remodel membranes can alter membrane protein activity in two ways. First, FFAs may be able to alter the concentration of certain lipids around the protein. For example, DHA, which has been shown to shift cholesterol into crystalline nanodomains (47), could soften the local membrane area or reduce hydrophobic thickness through the removal of local cholesterol. This removal of cholesterol from and effective softening of a local membrane environment would in turn alter the activity of certain channel proteins, most obviously mechanosensitive channels (26, 225, 226). Second, membrane remodeling can alter membrane composition through altering the phase in which the protein resides (77, 187). Towards this possibility, membrane remodeling has been shown to alter membrane protein domain-localization and activity (32, 77, 104). Both of these potential mechanisms would change the local mechanical properties of the membrane surrounding a protein, affect how much that membrane stretches in response to applied force, and would in turn alter protein activity. By influencing the activation, enhancement, or sensitization of ion channel gating, these mechanical changes have the potential to affect a wide range of physiological responses from synaptic plasticity to cognitive functions.

5.5 Conclusion

Here, we demonstrated the effects of various FFAs on DOPC, DOPC/cholesterol, and POPC/cholesterol model membranes. We found that PUFAs generally reduce K_{app} of model membranes. When cholesterol membrane content is high, we found that the PUFAs EPA and DHA exhibit different effects on membrane K_{app} . This result can possibly be explained by the presence of cholesterol crystalline nanodomains, which are expected to be larger in the presence of DHA compared to EPA. This structural difference may alter global membrane force transmission, resulting in our observed differences of membrane K_{app} . Overall, our results demonstrated that FFAs can differentially alter membrane mechanical properties, to an extent that can be measured via micropipette aspiration and likely sensed by cellular components when incorporated into cellular membranes. The mechanistic understanding of this non-specific modulation of membrane-

embedded proteins has the potential to decipher the elusive effects of fatty acids on various membrane proteins and the broader alteration of biological processes.

5.6 Acknowledgements

We thank Prof. Robert Raphael for his experimental advice, helpful discussions, and careful reading of the manuscript. We also thank members of the Kamat Lab for thoughtful discussions. This work was supported by the Air Force Office of Scientific Research (AFOSR) YIP FA9550-19-1-0039 P00001 to NPK, the Searle Funds at The Chicago Community Trust (NPK), and NSF grant MCB-1935356 (NPK). M.L.J. was supported by Grant No. T32GM008382 from the National Institute of General Medical Sciences and The American Heart Association Predoctoral Fellowship under Grant No. 20PRE35180215. J.A.P. was supported by the NSF Graduate Research Fellowship and the Ryan Fellowship and International Institute for Nanotechnology at Northwestern University. PMV and HAF were supported by NSF grant CMMI-1748049. This work made use of IMSERC at Northwestern University. IMSERC has received support from the Soft and Hybrid Nanotechnology Experimental (SHyNE) Resource (NSF ECCS-1542205), the State of Illinois, and the International Institute for Nanotechnology (IIN). Wayne State Lipidomics Core Facility is supported in part by National Center for Research Resources, National Institutes of Health Grant S10RR027926.

Chapter 6

6. Methods of membrane protein integration into giant bilayer vesicles for patch-clamp electrophysiology and micropipette aspiration techniques

Micropipette aspiration and patch-clamp electrophysiology are complementary techniques in the determination of the relationship between channel behavior and membrane mechanical properties. These techniques require similar bilayer membrane samples with slight differences in sample preparation challenges. Micropipette aspiration and patch-clamp electrophysiology are techniques which utilize glass micropipettes to measure membrane mechanical properties and membrane protein activity, respectively. These techniques require similar membrane structures, but these structures may differ slightly due to differences in glass micropipette geometry and differences in the interactions between the membrane and the pipette. Micropipette aspiration utilizes a long, flat, straw-like micropipette with a blunt end that ranges from 6 -10 μM in diameter that is passivated to prevent interactions between the lipids and the glass surface. Because of this passivation, the vesicle must be larger than the diameter of the micropipette in order to prevent complete aspiration of a vesicle into the pipette. In contrast, patch-clamp electrophysiology techniques utilize a pointed glass micropipette which directly interacts with the membrane to form a seal with gigaohm electrical resistance. As the membrane interacts directly with the glass, vesicle size and

geometry are less important for this system, however, protein yield and membrane stability are important to allow for seal formation and the quantification of ion channel behavior.

6.1 Cell-free protein synthesis into synthetic giant unilamellar vesicles

The large size and ability to tune membrane composition key features of synthetic giant unilamellar vesicles (GUVs) that is attractive in studying how membrane mechanics affect mechanosensitive channel behavior. GUVs may be composed of any mixtures of lipids which form bilayers using various methods from electroformation and thin film hydration to microfluidic techniques. The variety of methods for formation and the ability to control membrane composition enable a range of studies of lipid and protein interactions and properties. In addition, the use of cell-free protein synthesis enables high-throughput protein expression and integration into model bilayers (Figure 6.1) without the use of detergents which are difficult to remove from lipid bilayers. A method which combines these complementary systems for membrane formation and protein integration is outlined in the following section of this chapter and the observation of challenges for electrophysiology are discussed.

Protein production

MscLGFP was expressed in 33 mM DOPC small unilamellar vesicles (SUVs) (100 mM vesicle stock) using one PURExpress reaction. The reaction was incubated at 37 °C in a 0.5 mL tube wrapped in foil for 4 hours. The sample was then dialyzed in a cold room on a rotator/shaker in 1.5 mL H₂O using a Slide-A-Lyzer MINI Dialysis Device in a 2mL Eppendorf tube. The dialysis device was transferred to 100 mL 10mM HEPES, pH 7.4 after 2 hours. The sample was dialyzed 2 hours further for 4 hours total dialysis.

GUV electroformation from SUVs containing protein

A glass syringe was used to apply dots of 10 μ l of dialyzed protein sample in a circle on a clean ITO slide compatible with a nanion vesicle prep pro. The slide was air dried under a box on the bench top for 30 min

or until completely dry. The sample chamber was assembled according to manufacturers instructions with a medium o-ring and the sample was hydrated with 200 μl of 300 mOsm sucrose. A protocol using a sine function of voltage oscillating at a magnitude of 5V was used to induce GUV formation over 2 hours. The device was covered in foil to protect the fluorescent protein from photobleaching.

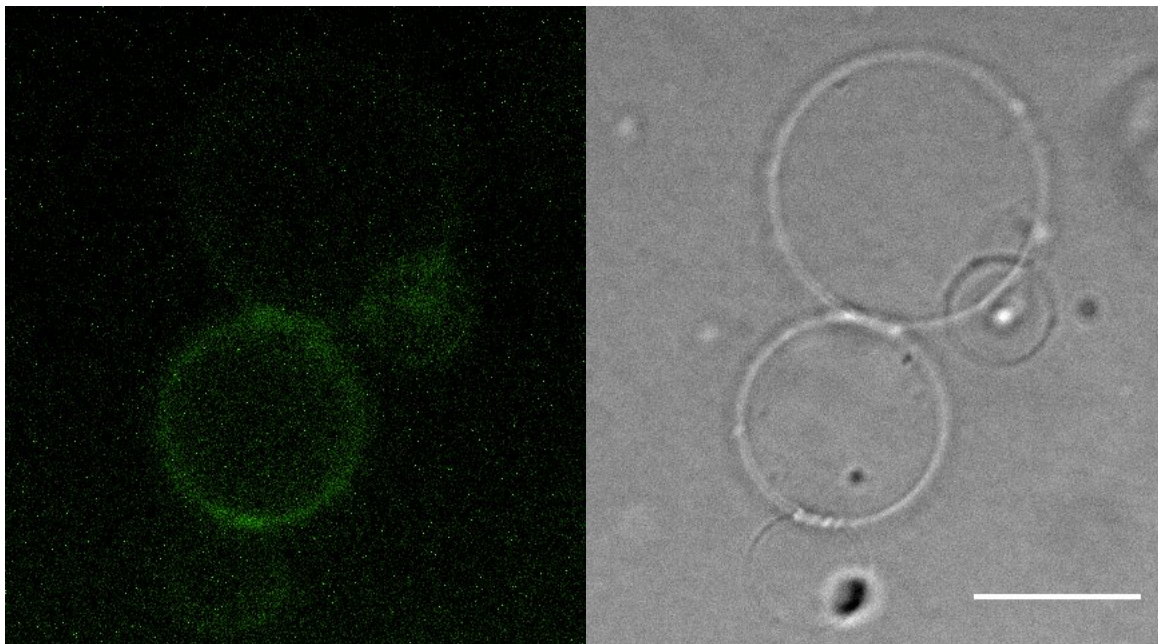


Figure 6.1 GUVs formed from the dry dot method incorporate proteins expressed into SUVs in cell-free reactions.

Large vesicles containing protein formed from SUVs. This method incorporated more protein than the methods where proteins are expressed into preformed GUVs. This method is very promising for the insertion of membrane proteins into GUVs. Images were captured using a 40x air objective, 20 μm scale bar.

Challenges of using GUVs in high-pressure patch-clamp electrophysiology applications

While the use of model membrane GUVs is optimal for studying the effects of membrane composition on mechanosensitive channel activation, the use of high pressures required to activate mechanosensitive channels are a limiting feature of this platform. We attempted to measure MscL activation in GUVs formed

from this method and we were able to readily form the gigaohm resistance seals necessary for electrophysiology recordings. However, upon application of high pressures, we observed vesicle lysis prior to channel activation. This observation demonstrated an additional challenge of the use of synthetic GUVs for mechanosensitive channel activation, a platform which is known to be difficult for use in electrophysiology applications (227). Because of these challenges, we chose to explore other systems for protein incorporation into giant vesicles in natural systems which have increased stability and improved protein incorporation.

6.2 Giant spheroplasts

One of the major challenges of performing patch-clamp electrophysiology techniques on GUVs are protein incorporation and membrane stability and these challenges can be overcome by using vesicles extracted from natural membranes. While the alteration of membrane mechanical properties is limited in giant spheroplasts, which are giant membranes formed from bacterial plasma membranes, this platform allows for protein overexpression which has a benefit of improved protein yield and improved membrane protein folding through cellular machinery. A protocol for spheroplast formation is outlined in the following section and the observation of challenges for electrophysiology are discussed.

Spheroplast formation methods

Bacterial Growth

This procedure is adapted from Martinac et al. (228). Bacteria containing a plasmid which expresses a MscLGFP under a T7 promoter was inoculated for an overnight growth in 5 mL of LB broth with appropriate antibiotics. The following day, 1 mL of culture was diluted into 10 mL fresh LB with antibiotics in a 125 mL flask and grown at 37 °C, 220 rpm to OD₆₀₀ 0.5 - 0.7. 3 mL of outgrown culture was diluted into 27 mL fresh LB without selective antibiotics with 60 µg/mL cephalixin and grown for 2 hours at 42 °C. Long rods should be visible using phase-contrast microscopy (Figure 6.2A). To induce the expression of MscL, 1 mM IPTG

was added to the culture and the temperature was adjusted to 37 °C and grown for 1 hour. The spheroplasts were incubated at 4 °C overnight to improve spheroplast quality.

Spheroplast extraction

The samples were kept on ice for the remaining procedure unless otherwise noted.

Bacterial cultures were centrifuged in a fixed-rotor at 1500 rcf for 5 min in a 50 mL falcon tube and the supernatant was removed. The pellet was rinsed with 1 mL of 800 mM sucrose solution and centrifuged again at 1500 rcf for 5 min. The supernatant was removed and the pellet was resuspended in 2.5 mL of 800 mM sucrose solution. Fresh lysozyme solution was prepared at 5 mg/mL in sterile water. 150 μ L 1 M Tris Cl pH 7.8, 120 μ L 5 mg/mL lysozyme solution, 30 μ L 5 mg/mL DNase I and 120 μ L 0.125 M Na EDTA pH 8.0 was added and gently swirled into the resuspended pellet solution. The solution was incubated 4 – 8 min at room temperature and spheroplast formation was observed using phase-contrast microscopy. 1 mL 20 mM MgCl₂, 700 mM sucrose, 10 mM Tris Cl (pH 7.8) solution was added slowly and gently swirled to stop spheroplast formation and the mixture was incubated at room temperature for 4 min then returned to ice. This solution was then slowly added to a 15 mL conical tube containing 10 mM MgCl₂, 800 mM sucrose, and 10 mM Tris Cl, pH 7.2. The tubes were then centrifuged at 1000 rcf at 4 °C and the supernatant was slowly removed and discarded leaving 1 mL. The spheroplasts were then collected from the bottom of the tube and aliquoted and frozen at -20 °C, not flash frozen as this damages spheroplast integrity. Spheroplasts were visualized using phase contrast microscopy and epifluorescence microscopy in 800 mOsm phosphate buffered saline solution to prevent osmotic lysis (Figure 6.2 B).

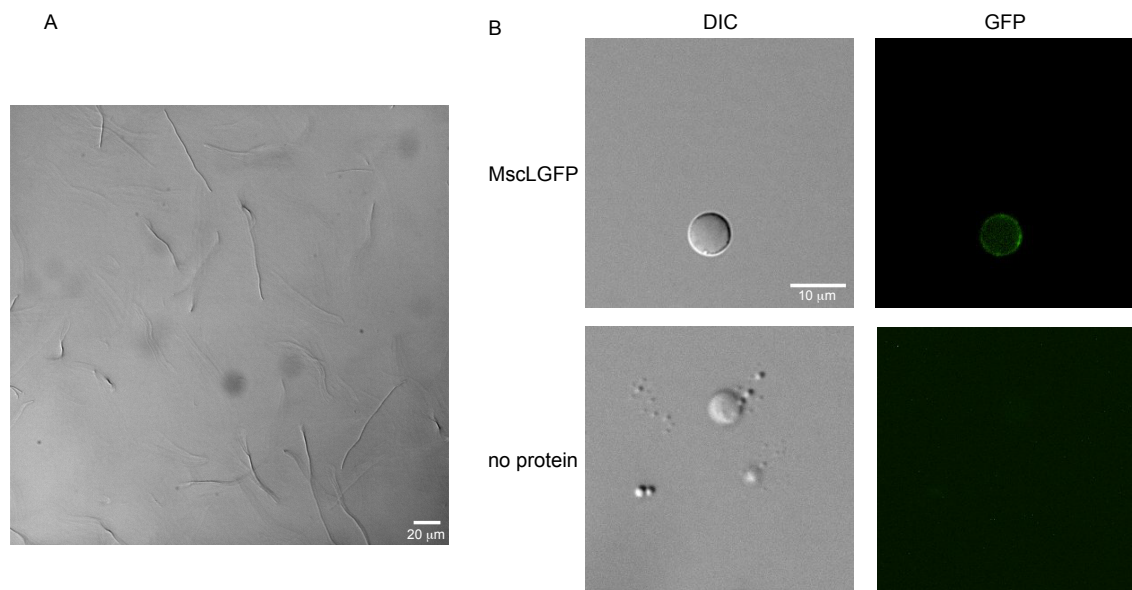


Figure 6.2 Fluorescence images of spheroplasts overexpressing MscLGFP.

A) MscLGFP was overexpressed in *E. coli* prior to spheroplast formation. Cephalixin treatment allowed *E. coli* to grow into large rod structures and lysozyme was added to form spherical vesicles. B) Left, images show spheroplasts that resemble model membrane vesicles. Right, fluorescence images show MscLGFP overexpression results in membrane-localized fluorescence indicating MscLGFP expression and membrane localization.

Patch-clamp electrophysiology with pressure control for mechanosensitive channel activity measurements

Patch clamp electrophysiology techniques were utilized to measure MscL activity with the addition of an integrated pressure-controller. The addition of a pressure-controller in electrophysiology systems is generally unique to the study of mechanosensitive channels and serves as both a modulator of pressure and a readout of protein activity as the study of mechanosensitive channel force-from-lipids activations generally relies on determining the magnitude of pressure or calculated membrane tension which is required to activate a channel. These measurements are commonly used to measure channel sensitivity and an example of the experimental data recorded in this type of system is outlined in Figure 6.3 A. Common to all ion channels, mechanosensitive channels undergo stochastic activation and the observation of “steps” of the same magnitude are observed as a channel opens and closes (Figure 6.3 B).

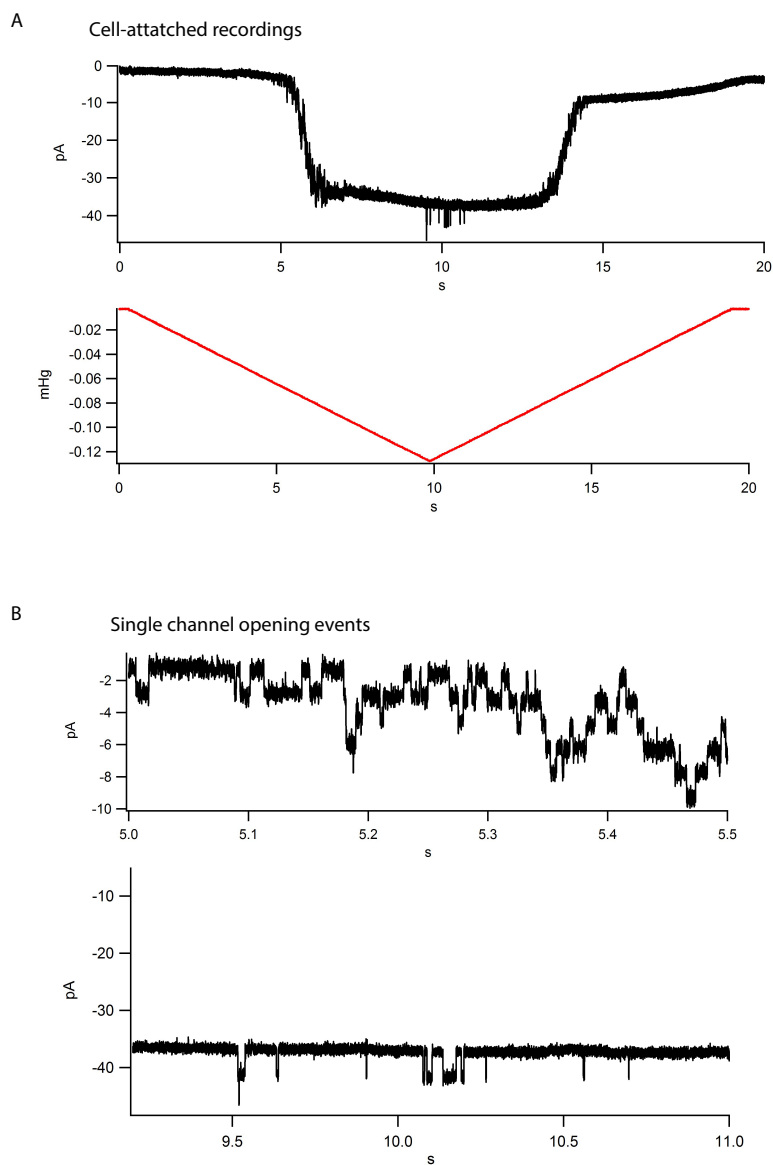


Figure 6.3 Patch clamp electrophysiology demonstrates activity of MscLGFP overexpressed in spheroplasts.

A) cell-attached patch clamp electrophysiology of spheroplasts shows many channels opening (black line) in response to a pressure ramp (red line). Channels open with negative pressure and re-close when pressure is released. B) Stepwise current traces indicate single channel resolution and show the signature “flickering” that occurs in MscL activity.

Challenges of measuring MscL activation in spheroplasts

While we were able to successfully observe MscL activation in spheroplasts, this sample type was challenging in patch-clamp electrophysiology applications in comparison to GUVs and mammalian cells. We found it difficult to form gigaohm seals in spheroplasts, specifically and we observed that seal formation, which usually occurred in seconds, took over an hour to form when patching spheroplasts. It is known that membranes extend into the patch pipette during long incubations and this extension alters membrane tension by altering membrane curvature. Because of this increase in tension, an increase in channel sensitivity and spontaneous mechanosensitive channel opening has been observed under long incubations (24), which makes the use of spheroplasts less sensitive in the quantification of the pressure required to activate a mechanosensitive channel. When measuring mechanosensitive channel activation using pressure alone it is important to limit incubation time within the patch pipette and to avoid repeating recordings which may cause spontaneous channel activation. For these reasons, we explored alternate systems for measuring mechanosensitive channel activation in response to membrane composition.

6.3 Giant plasma membrane vesicles

To overcome the challenges of micropipette aspiration and patch-clamp electrophysiology techniques on vesicles, we turned to mammalian Giant Plasma Membrane Vesicles (GPMVs). This platform is more suitable for these complementary methods as GPMV techniques leverage the high efficiency of protein expression and incorporation into cellular plasma membranes as well as the larger size of GPMVs in comparison to spheroplasts.

GPMVs are bilayer vesicles formed from the plasma membrane of a mammalian cell. GPMVs contain cytoplasm but lack other membranes, found by proteomics and looked for proteins found in other organelles, and cytoskeletal proteins. Their diameter and membrane composition are dependent on cell

type where larger cells produce larger GPMVs. As we intended to use these GPMVs for micropipette aspiration applications, we chose to use U2OS cells due to their large size.

Paraformaldehyde with DTT or N-ethylmaleimide (NEM) are vesiculation reagents used to form GPMVs. These reagents bind to sulfhydryl groups on proteins and promotes GPMV formation by inducing an effect on the membranes that causes membrane budding. This binding likely induces a change in membrane curvature or membrane preferred curvature when it binds to membrane surface structures that forces the plasma membrane to bud off of the cell, however, the exact mechanism of GPMV formation is not known. Paraformaldehyde is the more commonly used reagent for GPMV formation in the characterization of GPMV membranes (76). While paraformaldehyde is a common crosslinking reagent, NEM is non-crosslinking which has benefits for membrane protein applications. The details of GPMV formation and the use of this system in micropipette aspiration and patch-clamp electrophysiology techniques are outlined in **Chapter 7**.

Chapter 7

7. Probing the force-from-lipid mechanism with synthetic polymers

The work in this chapter is in preparation for publication as

Jacobs, M. L., Steinkühler, J., Larmore, M. J., Ng, L. C. T., DeCaen, P. J.,* Kamat, N. P.,* “Probing the force-from-lipid mechanism with synthetic polymers” *in preparation*

Abstract

Nanoplastic pollution is increasingly prevalent and cellular exposure to such particles has demonstrated deleterious effects on biological systems. These synthetic amphiphiles are hypothesized to directly interact with cellular membranes and may modulate membrane mechanical properties. However, the effect of this interaction on biological function remains largely unexplored. One class of proteins which are especially sensitive to changes in membrane composition and properties are mechanosensitive channels which are activated through *force-from-lipids*. Through this mechanism, amphiphiles which alter membrane properties are expected to impact the sensitivity of embedded mechanosensitive channels by changing force propagation through the bilayer. However, the roles of specific membrane properties in the force-from-lipids mechanism are poorly understood. Here, we employ poloxamers, which are one class of nanoplastic amphiphiles that may shed light on which membrane properties are important for mechanosensitive channel

function by altering membrane properties in unexplored ways. Using precise mechanical characterization techniques that have rarely been used in conjunction with electrophysiology techniques, we reveal the role of poloxamer on membrane properties and mechanosensitive channel activation. We directly measured membrane mechanical properties such as area expansion modulus (K_A) and bending rigidity (k_c) as a function of poloxamer concentration. Then, we compared these results to electrophysiology studies of mechanosensitive channel pressure sensitivity using an integrated pressure controller. These comparisons revealed that by decreasing membrane K_A and k_c , the pressure required to activate two mechanosensitive channels was increased. We then confirmed that our results could not be attributed to changes in bilayer thickness or pore occlusion, and this relationship was also observed in the presence of a chemically distinct detergent. Our results further elucidate the generality of the force-from-lipids gating mechanism to demonstrate that this mechanism is translatable to non-natural amphiphiles. These findings suggest a relationship between membrane mechanical properties, K_A and k_c , on the force-from-lipids activation of mechanosensitive channels which was unable to be observed using natural lipids alone. Our study also demonstrates implications for the effect of nanoplastic amphiphiles on biological function through the alteration of channel activation sensitivity and downstream signaling.

7.1 Introduction

Plastic waste degradation and dispersion has increasingly received attention as nanoplastic contamination has been found in various locations from seawater to food products, which poses a risk to wildlife and human health. Due to the hydrophobic or amphiphilic properties of these particles, micro- and nanoplastics have been demonstrated to interact with cellular membranes and may disrupt membrane stability (229–231). However, the effect of nanoplastics on cellular membrane properties and a mechanistic understanding of their effect on cellular function is largely unknown. Poloxamer is a class of nanoplastic which is commonly found in household products and is used as a cell culture additive to stabilize cell membranes. Through the observation that poloxamer strengthens cellular membranes in cell culture conditions, poloxamer is

presumed to directly interact with the membrane (232). Poloxamer was recently proposed to alter model membrane properties (11, 233). Yet, the impact of poloxamer on specific cellular membrane properties and biological function remains to be characterized. One area of concern in the effect of poloxamer on the membrane are membrane-embedded channels which are sensitive to the surrounding lipid environment (4).

Mechanosensitive channels are a class of membrane proteins which are found in all domains of life and play important roles ranging from cellular volume regulation to touch and hearing sensation (234–236). This class of channels works to transduce mechanical forces into biochemical signals by activating in response to membrane tension through *force-from-lipids* (2, 22, 27, 190). Because of this relationship with membrane tension, mechanosensitive channels are proposed to be affected by long-range mechanical forces in the membrane (8, 185, 237). Towards this idea, various studies have begun to demonstrate the relationship between membrane composition and mechanosensitive channel function as changes in membrane composition may modulate force propagation to embedded channels (24, 27, 34, 104, 195). However, the specific mechanical properties which exert this behavior are poorly understood.

The alteration of membrane properties through changes in membrane composition has been proposed to alter the behavior of various mechanosensitive channels (8, 26, 27, 31, 32, 104, 106, 166, 178, 237). Through these studies, the impact of various membrane properties such as area expansion modulus (K_A), bending stiffness (k_c), fluidity, and hydrophobic thickness have been proposed to play a role in mechanosensitive channel behavior (27, 31, 104, 195). Yet, the majority of these studies do not measure these membrane properties directly and use published estimates or rely on methods which measure the bulk property of a cell, which include cytoskeletal mechanics. Many mechanosensitive channel studies have focused on the bacterial mechanosensitive channel of large conductance (MscL) which serves as a model mechanosensitive channel to deepen the understanding of mechanotransduction. However, the effect of lipid composition on membrane elastic properties, K_A and k_c , on MscL function was unable to be

distinguished from the effects on membrane thickness (27). Furthermore, the direct role of membrane mechanical properties on mechanosensitive channel behavior has been difficult to discern in the presence of natural lipids. Despite the vast number of studies using lipids, the impact of non-natural amphiphiles, such as poloxamer, on mechanosensitive channel behavior is yet to be determined and may provide insight into the relationship between membrane properties and mechanosensitive channel behavior.

Here, we use complementary techniques to measure the impact of poloxamer on both membrane mechanical properties and mechanosensitive channel activation. Using Giant Plasma Membrane Vesicles (GPMVs) to harness the composition of a cellular bilayer and *E. coli* EcMscL as a model mechanosensitive channel, we measured the effect of poloxamer on MscL function with a voltage-clamp electrophysiology system with an integrated pressure controller. We found that poloxamer desensitizes MscL activation. In conjunction with our electrophysiology studies, we use micropipette aspiration techniques and a fluorescent probe to determine the relationship between membrane K_A , k_c , and fluidity on mechanosensitive channel activation in response to various poloxamer analogues and a chemically distinct detergent. We also demonstrated that this effect was translatable to a mechanosensitive channel found in eukaryotic neurons, mTrek1, which is implicated in vastly different mechanotransduction pathways. Through these studies, we directly demonstrate a general role of membrane properties in the force-from-lipids mechanism of mechanosensitive channel activation which extends beyond natural lipids. Our study shows that nanoplastics affect mechanosensitive channel function which may affect cellular studies which use poloxamer, as mechanosensitive channels play a role in cellular signaling. We also highlight the potential impact of nanoplastics on human health through channel inactivation with prolonged exposure.

7.2 Results

We first set out to characterize a platform that enables the measurement of both mechanosensitive ion channel activity and membrane mechanical properties. We chose Giant Plasma Membrane Vesicles

(GPMVs) for these applications due to their ability to incorporate membrane proteins, large diameter, and biological membrane composition. GPMVs are bilayer membrane vesicles derived from mammalian cells which consist of the plasma membrane and embedded membrane proteins, but exclude organelles and cytoskeletal structures (Figure 7.1A) (60, 238). The absence of these structures enables force-from-lipids activation of mechanosensitive channels as well as direct measurements of the lipid contribution of membrane properties. We chose to first focus on the Mechanosensitive Channel of Large Conductance (MscL), which serves as a model mechanosensitive channel. We created U2OS cell lines stably expressing MscL which was expressed as a fusion to green fluorescent protein (GFP) for expression detection (Figure 7.2), and induced GPMV formation by adding a vesiculation agent (Figure 7.3). The addition of this agent resulted in GPMVs containing MscLGFP and were an appropriate size for micropipette aspiration measurements (Figure 7.1B). This method also enables the incorporation of poloxamer, a microplastic amphiphilic triblock copolymer which we will use to probe the force sensitivity of MscL in response to changes in membrane composition (Figure 7.4).

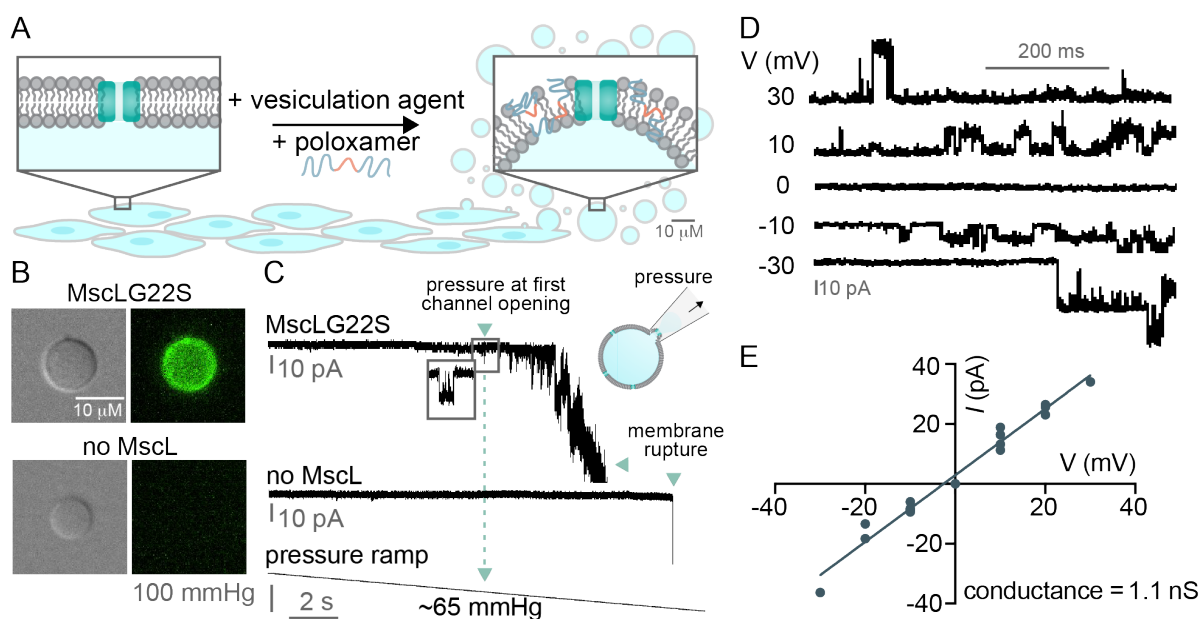


Figure 7.1 Patch-clamp electrophysiology of giant plasma membrane vesicles (GPMVs) measures MscL pressure sensitivity.

A) Schematic representation of GPMV formation. Human Bone Osteosarcoma Epithelial (U2OS) cells containing MscLGFP are treated with N-ethylmaleimide vesiculation agent and poloxamer to form GPMVs that contain MscLGFP and poloxamer in the membrane. B) Microscopy images of GPMVs that are untransfected (bottom) or contain MscL(G22S)GFP (top). DIC images (left) and GFP epifluorescence (right) are shown. 10 μM scale bar. C) Representative electrophysiology traces of MscL pressure sensitivity. MscLG22SGFP (top) recordings show MscL activation in response to pressure ramp (bottom). MscL activation sensitivity is defined as the pressure at which the first MscL channel activates. Untransfected GPMVs (no MscL) exhibit no change in current in response to pressure. MscL pressure response is determined by the pressure at first channel opening (~ 65 mmHg). Recordings are performed at -10 mV in 10 mM HEPES pH 7.3, 150 mM NaCl, 2 mM CaCl_2 . Pipette internal solution consists of 10 mM HEPES pH 7.3, 100 mM NaMES, 10 mM BAPTANa₄, 10 mM NaCl, 10 mM EGTA. D) Electrophysiology traces for the determination of MscL(G22S)GFP conductance in U2OS cells. Recordings were performed at holding potentials between -30 mV and $+30$ mV. E) Conductance calculations of MscL(G22S)GFP. The current amplitude at each voltage (shown in D) is plotted and the slope of the linear fit was used to determine channel conductance. MscL(G22S)GFP conductance is 1.113 nS (95% confidence 1.020 to 1.207 nS), $n = 17$ individual recordings at various holding potentials.

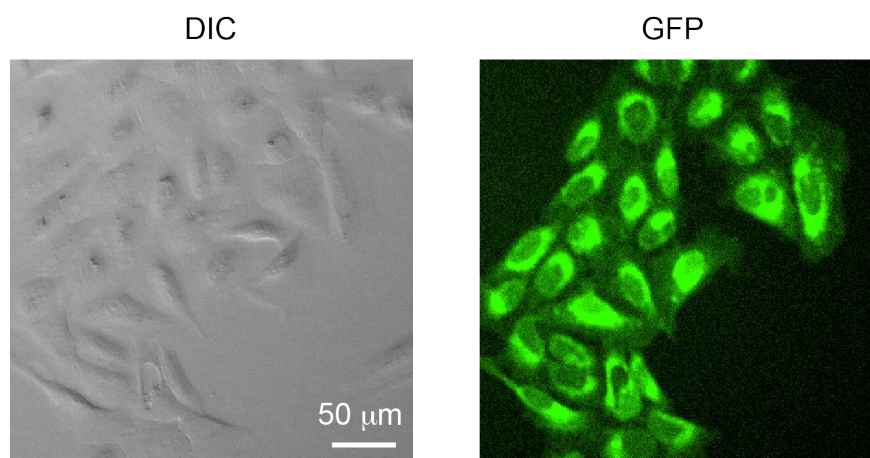


Figure 7.2 U2OS cell lines stably expressing MscLGFP

MscLGFP was transfected into U2OS cells and selected using geneticin for 4 weeks. MscL is localized to various membranes within the cell including the plasma membrane as demonstrated by dispersed GFP fluorescence.

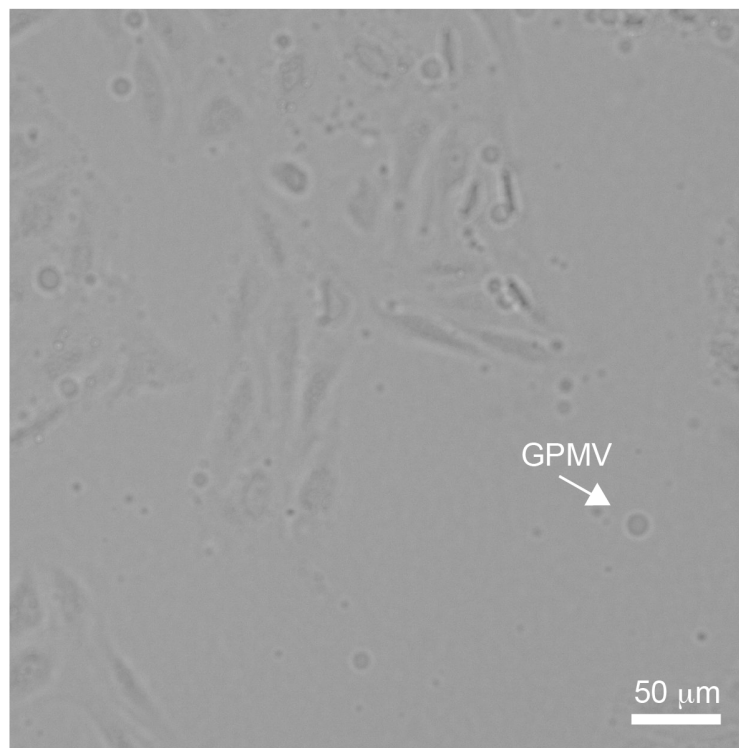
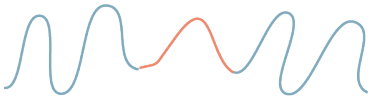


Figure 7.3 GPMVs budding off U2OS cells

DIC micrograph demonstrates Giant Plasma Membrane Vesicles (GPMVs) formation by budding off adherent mammalian cells. This process creates large diameter bilayer vesicles comprised of the cellular plasma membrane without cytoskeletal attachments or intracellular membranes.

Poloxamers



| | molecular weight | % hydrophobic blocks |
|--|------------------|----------------------|
| <p>poloxamer P124</p> $\text{H} \left[\text{O} \text{---} \text{CH}_2 \text{---} \text{CH}_2 \right]_6 \left[\text{O} \text{---} \text{C}(\text{CH}_3) \text{---} \text{CH}_2 \right]_{20} \left[\text{O} \text{---} \text{CH}_2 \text{---} \text{CH}_2 \right]_6 \text{OH}$ | 2000 g/mol | 60% |
| <p>poloxamer P188</p> $\text{H} \left[\text{O} \text{---} \text{CH}_2 \text{---} \text{CH}_2 \right]_{38} \left[\text{O} \text{---} \text{C}(\text{CH}_3) \text{---} \text{CH}_2 \right]_{29} \left[\text{O} \text{---} \text{CH}_2 \text{---} \text{CH}_2 \right]_{38} \text{OH}$ | 9000 g/mol | 20% |
| <p>poloxamer P184</p> $\text{H} \left[\text{O} \text{---} \text{CH}_2 \text{---} \text{CH}_2 \right]_9 \left[\text{O} \text{---} \text{C}(\text{CH}_3) \text{---} \text{CH}_2 \right]_{29} \left[\text{O} \text{---} \text{CH}_2 \text{---} \text{CH}_2 \right]_9 \text{OH}$ | 2900 g/mol | 60% |
| <p>poloxamer P407</p> $\text{H} \left[\text{O} \text{---} \text{CH}_2 \text{---} \text{CH}_2 \right]_{32} \left[\text{O} \text{---} \text{C}(\text{CH}_3) \text{---} \text{CH}_2 \right]_{131} \left[\text{O} \text{---} \text{CH}_2 \text{---} \text{CH}_2 \right]_{32} \text{OH}$ | 12500 g/mol | 30% |

Detergent

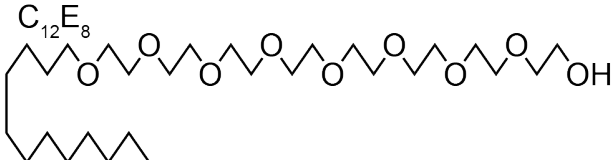
| | | |
|---|-----------|-----|
| <p>C_{12}E_8</p>  | 500 g/mol | n/a |
|---|-----------|-----|

Figure 7.4 Schematic and properties of amphiphiles used in this study

We used various synthetic amphiphiles to exogenously alter membrane mechanical properties. These amphiphiles belong to two classes, poloxamer (Pluronic) and small nonionic detergent. Poloxamer is a class of triblock copolymers which consist of and a polypropylene oxide hydrophobic block sandwiched by two polyethylene oxide hydrophilic blocks. Poloxamers have similar properties to surfactants in their ability to insert into bilayers but have much larger molecular weights. The detergent C_{12}E_8 we used has a much smaller molecular size in comparison to poloxamer.

We confirmed the presence of MscLGFP in our GPMV membranes using fluorescence microscopy (Figure 7.1B). Following this confirmation, we assessed MscL activation sensitivity using patch-clamp electrophysiology techniques with an integrated pressure controller and quantified MscL sensitivity using the pressure at first channel opening (Figure 7.5) (24). We applied a pressure ramp that reached suction pressures above 160 mmHg and observed pressure-induced channel activation in our GPMVs that contained MscLG22S, but no currents were observed in our no MscL control GPMVs (Figure 7.1C, 7.6). We used a gain of function mutation variant, MscLG22S as opposed to MscL wild-type (WT) due to the lower activation threshold which improved the number of GPMVs in which we observed MscL currents (Figure 7.7). Furthermore, we elected to use N-ethylmaleimide (NEM) rather than the more commonly used PFA/DTT formulation due to the non-crosslinking nature of NEM as crosslinking may prevent mechanosensitive channel activation (Figure 7.8). To characterize the behavior of MscL in our system, we measured channel conductance by quantifying the current through individual MscL channels under different voltages (Figure 7.1D). We found the conductance of MscLG22SGFP and MscLWTGFP to be ~ 1 nS in GPMVs (Figure 7.1E, 7.7), which is similar to published values of MscL conductance in mammalian cells (239) and bacterial membranes (240, 241). For the remaining studies we used MscLG22SGFP which will be referred to as "MscL". In addition, we confirmed that MscL is sensitive to membrane composition in our GPMV platform through the addition of a curvature-inducing amphiphile, lysophosphatidylcholine (LPC) as described previously (Figure 7.9) (24). These observations confirmed that the stochastic channel currents we observed were due to pressure-induced MscL activation and MscL is sensitive to membrane composition in GPMVs similar to other membrane platforms.

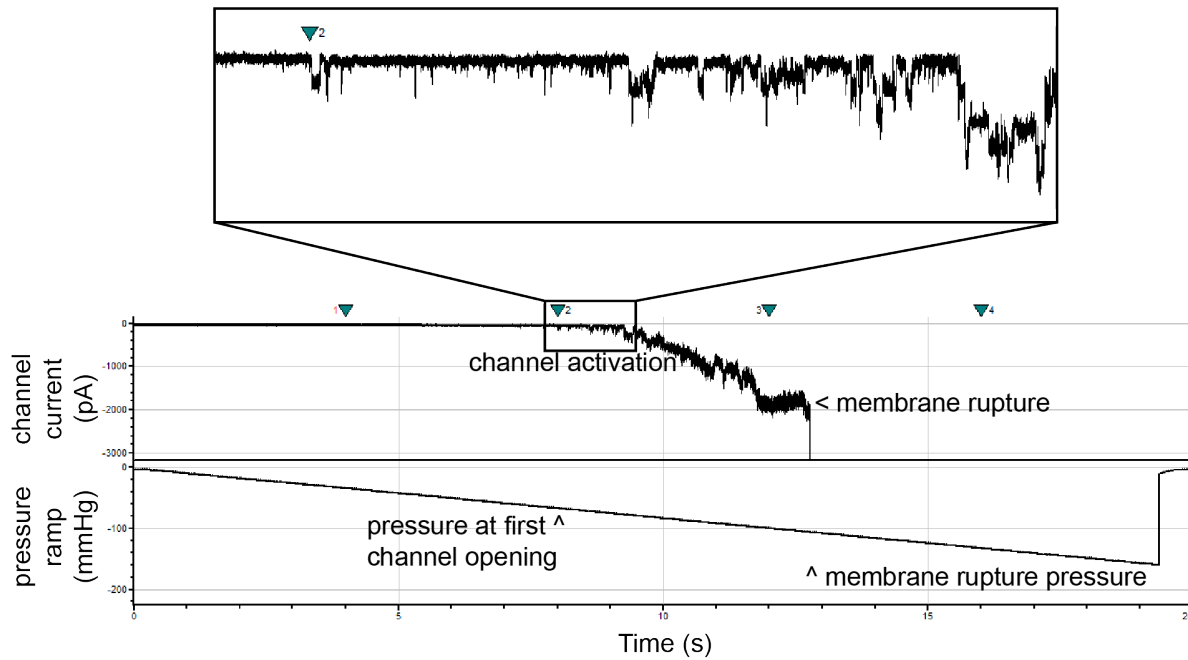


Figure 7.5 Sample data analysis workflow

We calculated MscL pressure sensitivity using an integrated pressure controller to quantify the pressure at which the first MscL channel activated. Higher pressures open more than one channel as demonstrated by multiples of original channel current. Inset demonstrates stochastic channel openings. We applied enough pressure to pop the GPMV membrane to ensure the pressure was high enough to activate mechanosensitive channels in the GPMVs and to enable the quantification of membrane stability.

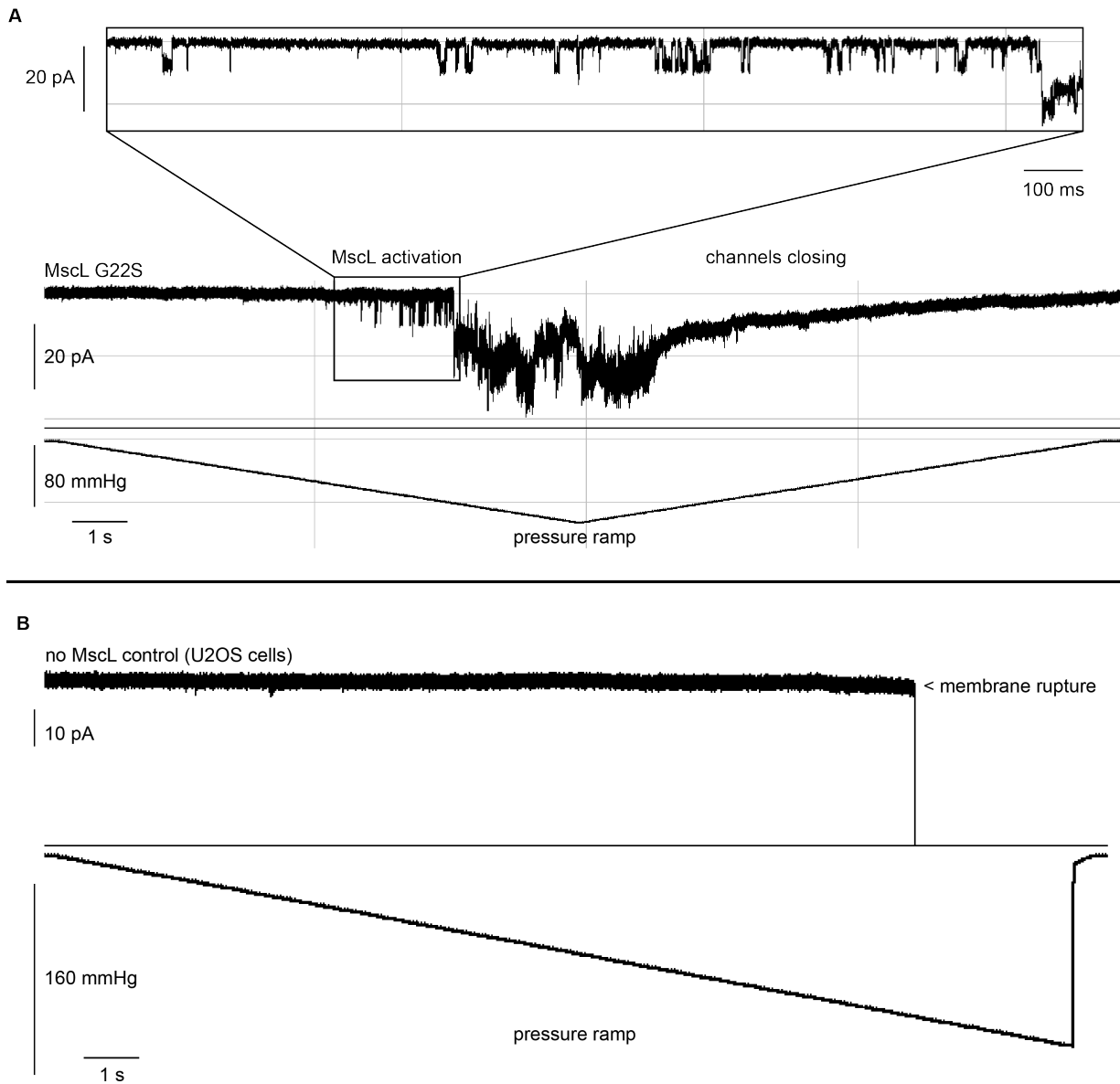


Figure 7.6 Example results of full traces of MscL and no MscL recordings

A) MscL exhibits stochastic activation behavior in response to pressure. When applied pressure is returned to 0 mmHg, MscL closes and current returns to baseline. This suggests that currents observed are due to channel activation and not membrane rupture. B) No MscL control demonstrates no channel currents under MscL activation conditions. Channel currents are not observed up to pressures high enough to rupture the membrane. The open/close pressure ramp in (A) was only used to demonstrate channel closure after pressure reduction, all recordings were performed using this rate of pressure change for all MscL activation calculations.

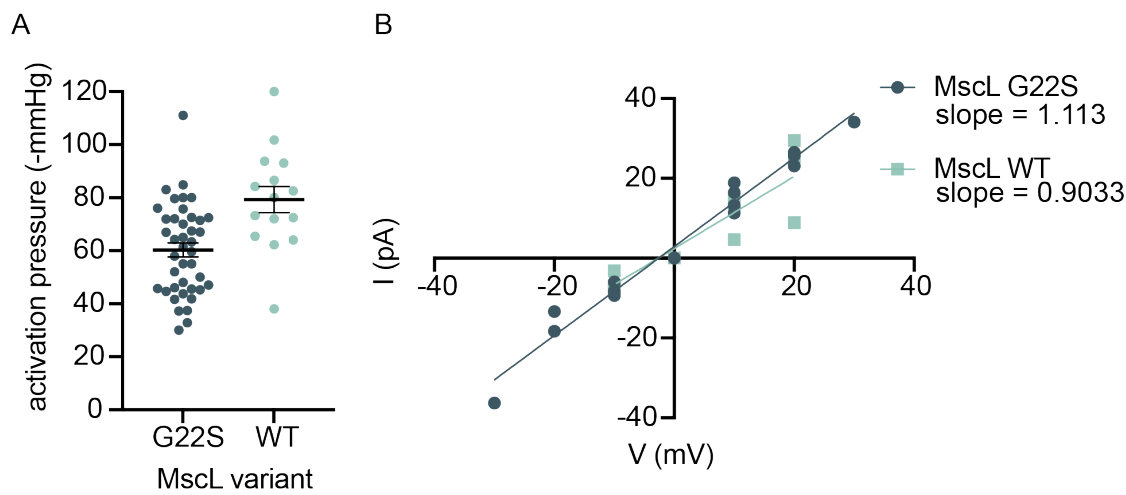


Figure 7.7 MscL(G22S)mEGFP reduces the pressure required for activation compared to MscLmEGFP (WT), but does not change channel conductance

A) MscL activation pressure is reduced in the G22C mutant. The pressure at first channel opening was measured for MscL in GPMVs. Individual points represent independent GPMV measurements. Mean is plotted with error bars which represent standard error of the mean. B) Conductance calculations for G22S and WT demonstrate that MscL channel size and selectivity is not affected by a G22S mutation. MscL(G22S)mEGFP conductance = 1.113 nS (95% confidence interval 1.020 – 1.207). MscLmEGFP (WT) conductance = 0.9033 nS (95% confidence interval 0.5761 – 1.231)

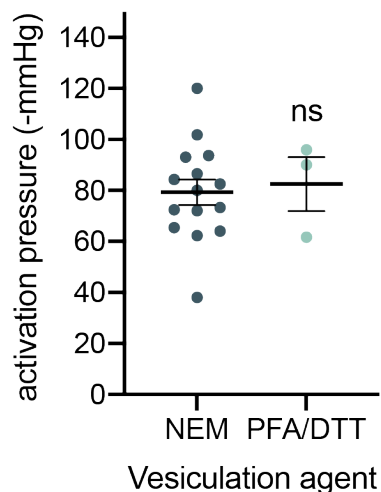


Figure 7.8 Differing GPMV formation methods yield similar MscL activation pressures, but crosslinking reagents reduce the probability of channel opening

GPMV formation is commonly performed using two different methods, NEM or PFA/DTT. While PFA/DTT is the most commonly used reagent mixture, this method induces crosslinking of lipids and proteins that is not amenable to mechanosensitive channel activation. In the presence of PFA/DTT, after >30 attempts over three independent GPMVs preparations, only three instances of MscL channels were observed. In contrast, NEM preparation allowed reliable observation of MscL activation. Both methods for GPMV formation did not demonstrate differing activation pressure thresholds of MscL. p-values to determine significance between means was measured using Student's t-test. non-significant (ns) $p > 0.05$, $n > 30$.

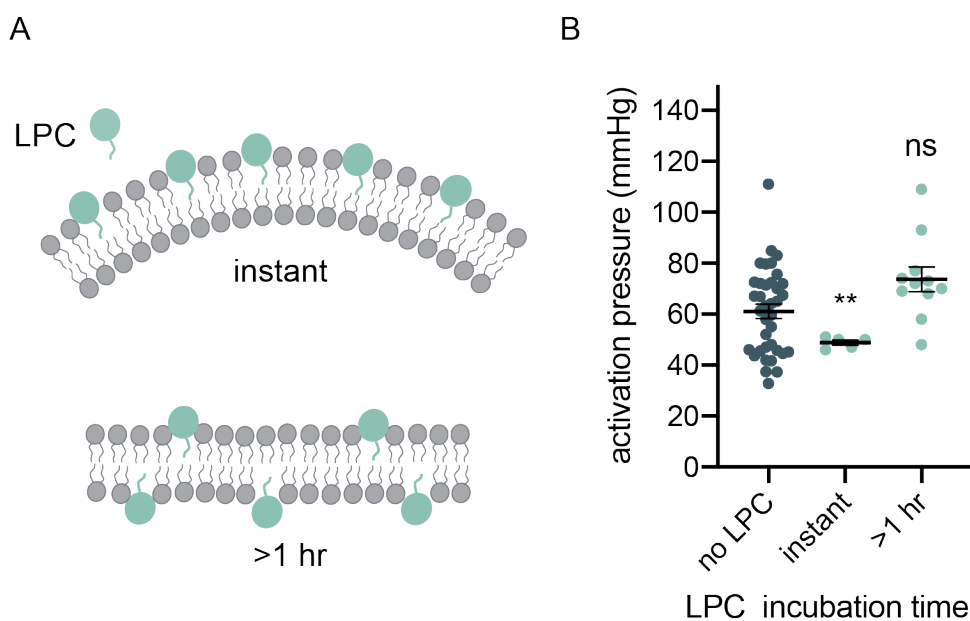


Figure 7.9 Lysophosphatidylcholine (LPC) activation confirms MscL behavior in GPMVs formed from U2OS cells

A) LPC inserts into membranes and induces local changes in curvature on short timescales. These changes in curvature are known to reduce the pressure required to activate MscL. On longer timescales, LPC flips and neutralizes curvature where there is no expected effect on MscL activation. B) MscL activation pressure is reduced upon LPC introduction. After incubation for >1hr, LPC does not alter MscL activation pressure as curvature is expected to be neutralized by LPC flip-flop. p-values were generated by ANOVA using Dunnett's multiple comparisons test compared to no poloxamer. ** $p \leq 0.01$, non-significant (ns) $p > 0.05$, $n > 10$.

Poloxamer P124 desensitizes MscL

After characterizing the behavior of MscL in GPMVs, we next set out to determine the effect of poloxamer on MscL activation sensitivity. Poloxamer is a triblock copolymer which can integrate into bilayer membranes and is expected to modulate their mechanical properties (Figure 7.10A) (11). We prepared GPMVs containing MscL in the presence of increasing amounts of poloxamer 124 (P124) in the buffer during GPMV formation (Figure 7.1A) and measured MscL activation pressure using patch-clamp electrophysiology. We found that MscL required higher pressures to activate in the presence of P124 and this response was monotonic with increasing poloxamer concentration, indicating that P124 decreased the sensitivity of MscL (Figure 7.10B). To further determine MscL sensitivity in the presence of P124, we quantified the percent of GPMVs that contained MscL currents out of all recorded GPMVs which exhibited GFP fluorescence and reached pressures above -80 mmHg, conditions under which we would expect MscL activation. We found in GPMVs with the highest buffer concentration of P124 (0.1% wt/vol), only ~20% of GPMV recordings contained active MscL currents, indicating that MscL was not activating in ~80% of GPMVs in high concentrations of P124 (Figure 7.11). Together, these results suggest that the pressure sensitivity of MscL is reduced in the presence of P124 through increasing the activation pressure and eventually leading to the prevention of channel activation.

We then investigated how P124 altered GPMV mechanical properties as mechanosensitive channels are expected to be sensitive to such properties. Using micropipette aspiration techniques, we measured the area expansion modulus (K_A) and bending rigidity (k_c) of GPMVs treated with P124 for greater than 4 hours (Figure 7.10C, 7.12, 7.13). We found that membrane K_A and k_c decreased with increasing P124 concentration in the buffer (Figure 7.10D, E). We then measured P124 fluidity using fluorescence anisotropy techniques and did not observe a significant change in membrane fluidity in the presence of P124 (Figure 7.14).

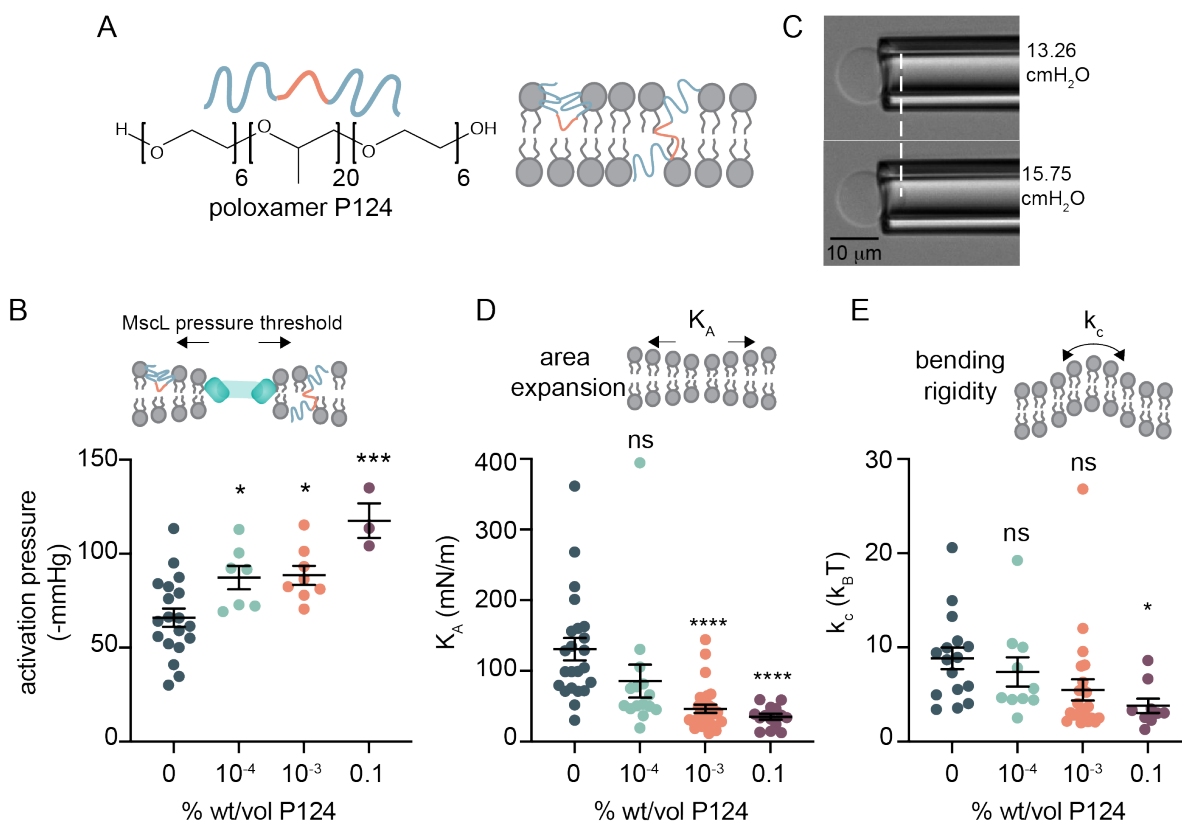


Figure 7.10 Poloxamer P124 decreases MscL sensitivity.

A) Schematic and chemical structure of poloxamer P124. Poloxamer may be found in a hairpin or transverse conformation within the membrane. B) MscL activation is desensitized in the presence of P124. MscL activation is defined here as the pressure where the first MscL channel is activated. The pressure at first channel opening was measured for GPMVs prepared in solutions containing 0 – 0.1% wt/vol P124, $n \geq 13$ independent GPMVs were recorded. C) Images of micropipette aspiration of GPMVs measuring membrane mechanical properties. Micropipette aspiration is used to measure membrane areal changes in response to applied tension. The area expansion modulus (K_A) and bending rigidity (k_c) of GPMV membranes treated with poloxamer were measured. D, E) K_A and k_c decrease in the presence of P124. GPMV K_A and k_c were measured using micropipette aspiration techniques after treatment of P124 in the GPMV formation buffer. k_c and K_A were calculated at low- and high-pressure regimes, respectively where K_A is corrected for relaxation of thermal undulations using mean k_c . P124 % wt/vol is as listed, pH 7.3. Bath and pipette solution consist of 10 mM HEPES pH 7.3, 150 mM NaCl, 2 mM CaCl_2 in micropipette aspiration studies. Mean activation pressure, K_A , k_c are plotted, error bars represent standard error of the mean. p-values in B, F, and G were generated by ANOVA using Dunnett's multiple comparisons test compared to no poloxamer. **** $p \leq 0.0001$, *** $p \leq 0.001$, * $p \leq 0.05$, non-significant (ns) $p > 0.05$, $n > 10$.

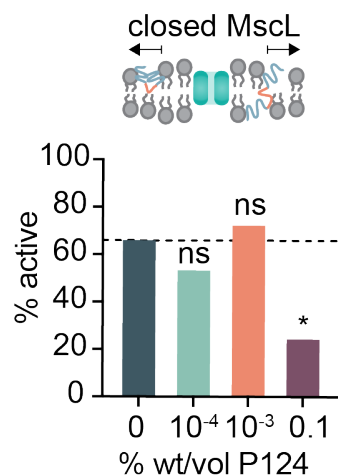


Figure 7.11 P124 prevents MscL activation at high concentrations

Some electrophysiology recordings contained membranes that remained stable in the presence of high pressure (> -80 mmHg) yet MscL did not activate. Recordings in which we observed activation of MscL are presented as % of all recordings for a given condition (% open). The number of recordings in which MscL activation was observed is reported above each bar, $n > 12$. The dashed line represents the percent of recordings in which MscL openings were observed in the absence of poloxamer. p-values were generated using Fisher's exact test comparing the distribution of values to 0% P124, * $p \leq 0.05$, non-significant (ns) $p > 0.05$, $n > 10$.

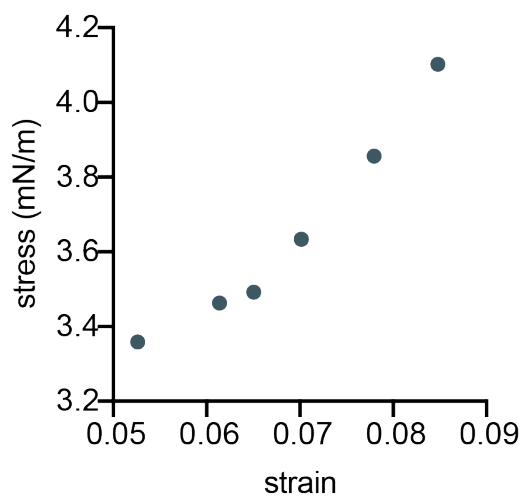


Figure 7.12 Micropipette sample aspiration curve of a GPMV membrane

A stress-strain curve was plotted to calculate K_{app} and k_c of GPMV membranes using micropipette aspiration techniques (7, 46). Adjusted strain values calculated by removing the smoothing of thermal undulations using k_c were replotted and K_A was calculated.

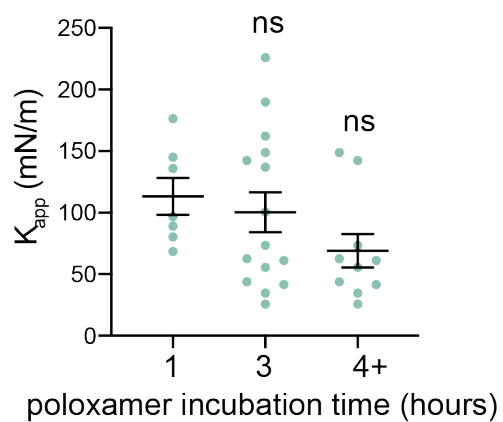


Figure 7.13 Poloxamer incubation time alters poloxamer effect on membrane properties

Incubations longer than 4 hours are required to alter membrane K_A . Samples were incubated with P188 at 4 °C for either 1, 3, or 4 hours and membrane K_A was measured using micropipette aspiration techniques. p-values were generated by ANOVA using Dunnett's test for multiple comparisons compared to 1 hour, non-significant (ns) $p > 0.05$, $n > 6$ independent GPMVs.

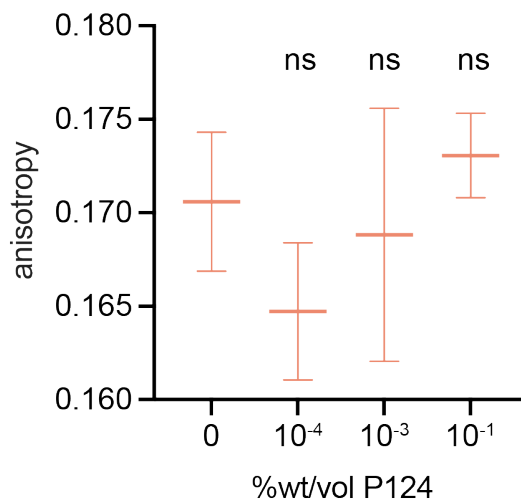


Figure 7.14 P124 Effect on membrane fluidity

Fluorescence anisotropy was used to measure relative differences in membrane fluidity between GPMV membranes containing various amounts of P124. Mean and standard error of the mean are plotted. p-values were generated by ANOVA using Dunnett's multiple comparisons test compared to no poloxamer, non-significant (ns) $p > 0.05$, $n > 10$.

We wondered how these changes in mechanical properties induced by P124 may affect mechanosensitive channel behavior. To assess this relationship, we plotted MscL activation pressure as a function of each of these membrane mechanical property measurements and found that decreases in membrane K_A and k_c correspond to commensurate increases in MscL activation pressure, $R^2 = 0.83$ and $R^2 = 0.66$, respectively (Figure 7.15A, B). However, we found no correlation between membrane fluidity and MscL activation sensitivity, $R^2 = 0.08$ (Figure 7.15C). These results suggest that MscL desensitization in the presence of P124 may be related to the alteration of specific membrane mechanical properties.

A detergent confirms the relationship between membrane properties and MscL activation

To confirm the relationship between membrane mechanical properties and MscL sensitivity, we sought to repeat these studies in the presence of an alternate molecule which is expected to alter membrane properties but is chemically distinct from poloxamer. We selected the detergent $C_{12}E_8$, which is known to decrease membrane K_A , (115) and measured the effect of this molecule on MscL activation sensitivity. Similar to our results in the presence of P124, $C_{12}E_8$ increased the pressure required to activate MscL (7.16A). We then measured the mechanical properties of GPMVs treated with $C_{12}E_8$ and confirmed that this molecule has a softening effect on membrane K_A and k_c , and fluidity (Figure 7.16B, C, D). Next, we compared our results measuring MscL activity to these mechanical property measurements and found a similar trend as we observed with P124, where decreased membrane K_A and k_c correspond to an increase in MscL activation pressure, $R^2 = 0.997$ and 0.90 , respectively (Figure 7.17A, B). In contrast to our results with P124, $C_{12}E_8$ exhibited a strong correlation ($R^2 = 0.98$) between membrane fluidity and MscL activation sensitivity (Figure 7.17C). These results suggest that MscL activation sensitivity may be modulated by alterations of membrane mechanical properties and this effect is likely not due to a chemical interaction between P124 and MscL.

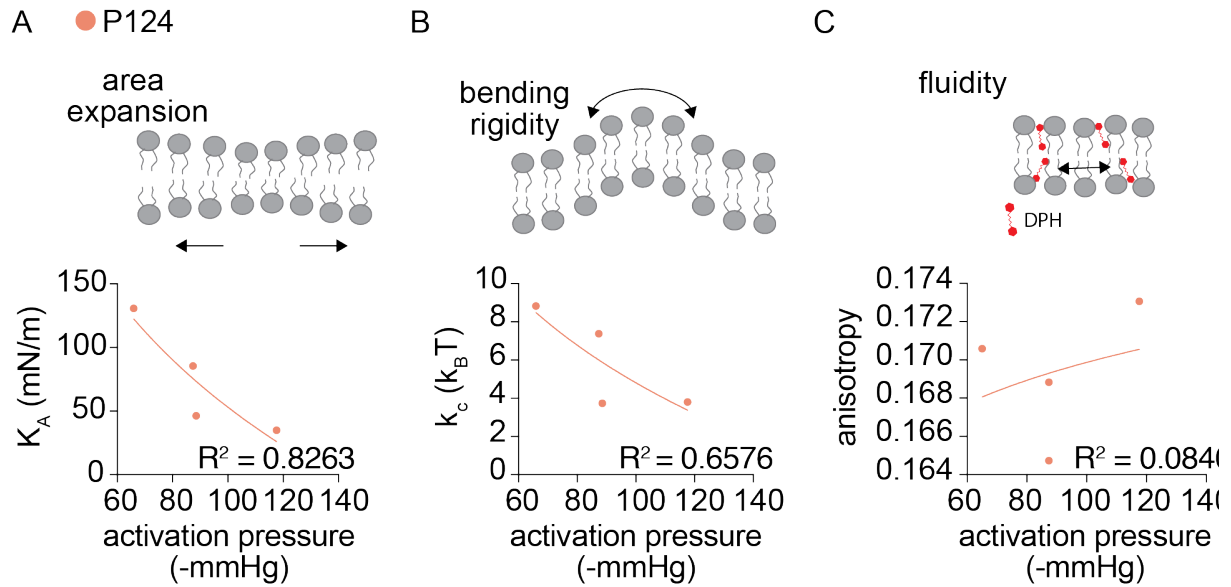


Figure 7.15 Poloxamer P124 alters GPMV mechanical properties

A) P124 decreases K_A and increases MscL activation pressure. K_A is plotted as a function of MscL activation pressure. B) P124 decreases k_c and increases MscL activation pressure. Mean k_c is plotted as a function of mean MscL activation pressure. C) Membrane fluidity does not correlate with MscL activation pressure. Membrane anisotropy was used to measure relative changes in membrane fluidity in the presence of P124. GPMVs were mixed with diphenylhexatriene (DPH) to a final concentration of 50 μM and fluorescence anisotropy was measured using a fluorimeter with fluorescence polarization capabilities. For all plots, R^2 was calculated from a non-linear fit where x is logarithmic and y is linear, $n > 10$.

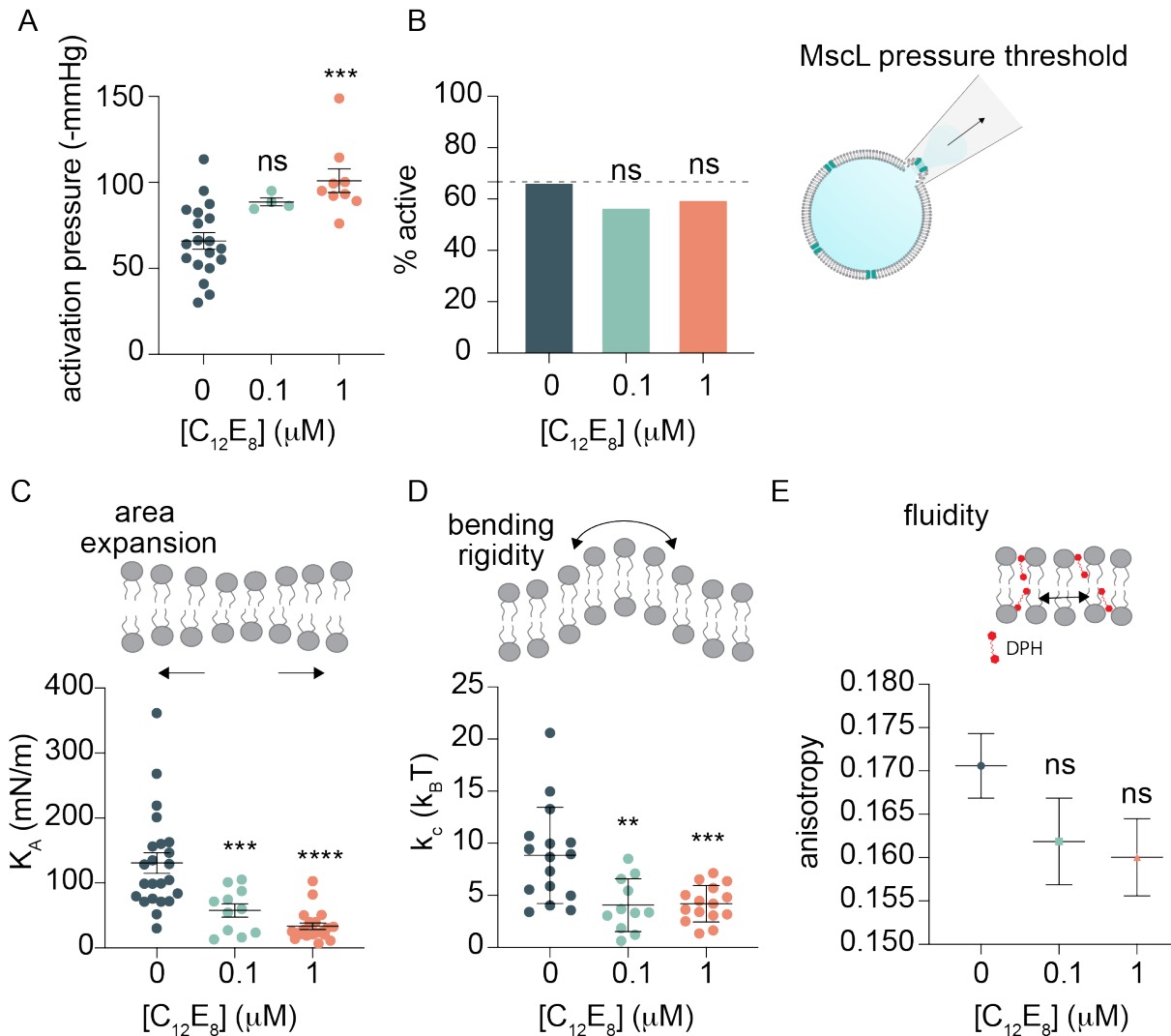


Figure 7.16 $C_{12}E_8$ effect on MscL activation pressure, K_A , k_c , and fluidity

A) $C_{12}E_8$ increases MscL activation pressure with increasing concentration. MscL activation pressure in the presence of $C_{12}E_8$ in the buffer during GPMV formation was measured using patch-clamp electrophysiology and quantified as the pressure at the first channel activation. B) $C_{12}E_8$ did not prevent MscL activation as described in Figure 7.11. The % of recordings which activated MscL were quantified. p-values were generated using Fisher's exact test compared to 0% $C_{12}E_8$. non-significant (ns) $p > 0.05$, $n > 10$. $C_{12}E_8$ decreased K_A (C), k_c (D) and measured by micropipette aspiration. Points represent individual GPMV measurements which were not repeated. E) $C_{12}E_8$ increased membrane fluidity as measured by fluorescence anisotropy (E). Mean and standard error of the mean for all plots is indicated by the bar and error bars p-values in (A), (C-E) were generated by ANOVA using Dunnett's test of multiple comparisons compared to no $C_{12}E_8$. **** $p \leq 0.0001$, *** $p \leq 0.001$, ** $p \leq 0.01$, non-significant (ns) $p > 0.05$, $n > 10$.

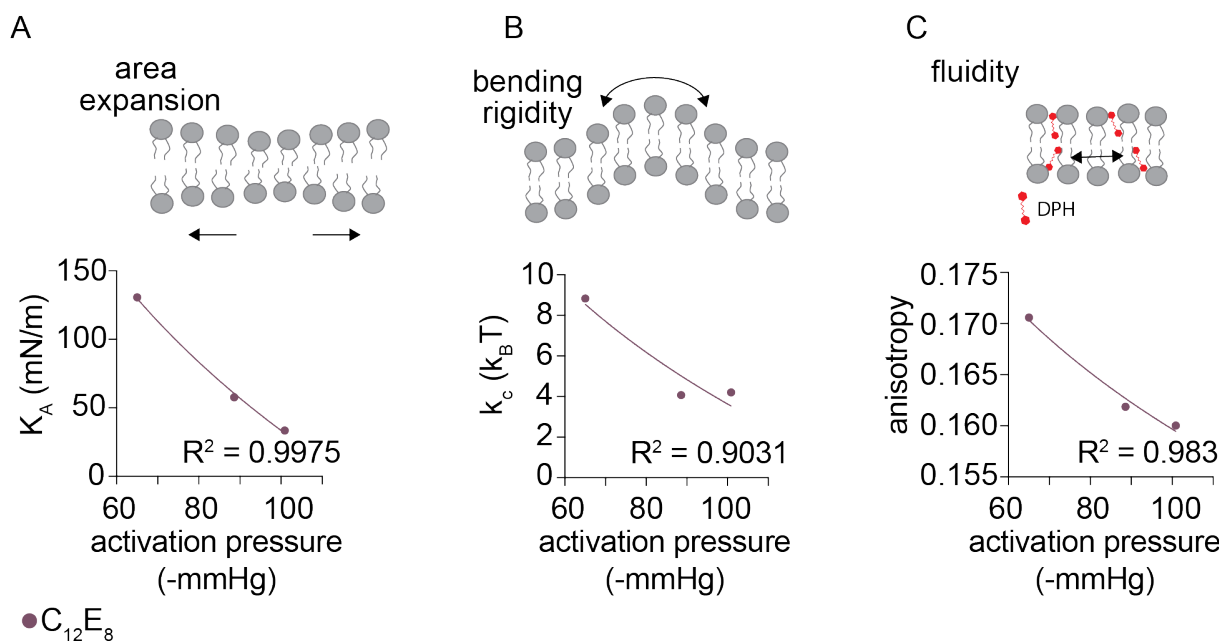


Figure 7.17 A non-ionic detergent decreases MscL sensitivity and alters membrane properties similar to poloxamer

A) $C_{12}E_8$ increases the pressure required to activate MscL. $C_{12}E_8$ was introduced to GPMVs during formation in buffer at the indicated concentration. Mean activation pressure and standard error of the mean is plotted. p-values were generated by ANOVA using Dunnett's multiple comparisons test compared to no poloxamer. non-significant (ns) $p > 0.5$, *** $p \leq 0.001$, $n > 10$. B) $C_{12}E_8$ decreases area expansion modulus and increases MscL activation pressure. K_a was measured using micropipette aspiration. Mean K_a is plotted as a function of mean MscL activation pressure for each concentration of $C_{12}E_8$. C) $C_{12}E_8$ decreases membrane k_c and increases MscL activation pressure. Mean k_c is plotted as a function of mean MscL activation pressure. B) Membrane fluidity and MscL activation pressure are increased in the presence of $C_{12}E_8$. Mean fluorescence anisotropy of DPH is plotted as a function of MscL activation pressure. Decreased anisotropy indicates a relative increase in membrane fluidity. For all plots, R^2 was calculated as a non-linear fit where x is logarithmic and y is linear, $n > 10$.

Various poloxamers reveal a relationship between K_A , k_c and MscL activation sensitivity

We then wanted to further explore the relationship between membrane mechanical properties and MscL activation sensitivity and wondered if these trends can be applied generally for various amphiphiles. We first measured the effect of other poloxamers with similar chemical structures but differing molecular weights on MscL pressure sensitivity and membrane mechanical properties (Figure 7.4, 7.18, 7.19, 7.20). We plotted the activation pressure of MscL as a function of K_A , k_c , and fluidity for each of the amphiphiles in which we measured both MscL activation and membrane properties and found similar trends as when we evaluated these relationships for each amphiphile individually (Figure 7.21, 7.17, 7.14). We found that membrane K_A ($R^2 = 0.53$) (Figure 7.21A) and k_c ($R^2 = 0.70$) (Figure 3B) correlated with MscL activation pressure, however, as we observed in the GPMVs containing P124, fluidity did not correlate with MscL activation pressure ($R^2 = 0.01$) (Figure 7.21C). Taken together, these results confirm that MscL behavior is sensitive to changes in membrane properties where membranes with reduced K_A and k_c generally decrease the pressure response of MscL (Figure 7.21D).

P124 does not alter MscL activity through pore occlusion or changes in membrane thickness

Next, we sought to rule out the possibility that P124 modulates MscL through a mechanism other than altering membrane mechanics. We first hypothesized that P124 could modulate MscL through pore occlusion (Figure 7.22A). As MscL conductance depends directly on pore size when measured in identical buffer conditions, a decrease in conductance would be expected if P124 resides within the MscL pore. We measured the conductance of MscL in the presence of increasing amounts of P124 and found that MscL conductance was not affected by P124 (Figure 7.22B, C). We included $C_{12}E_8$ as a control which would not be expected to extend out of the membrane due to its smaller molecular size and found that $C_{12}E_8$ also did not affect MscL conductance. Together, these observations demonstrate that P124 and $C_{12}E_8$ do not reside within the MscL pore while in the active conformation.

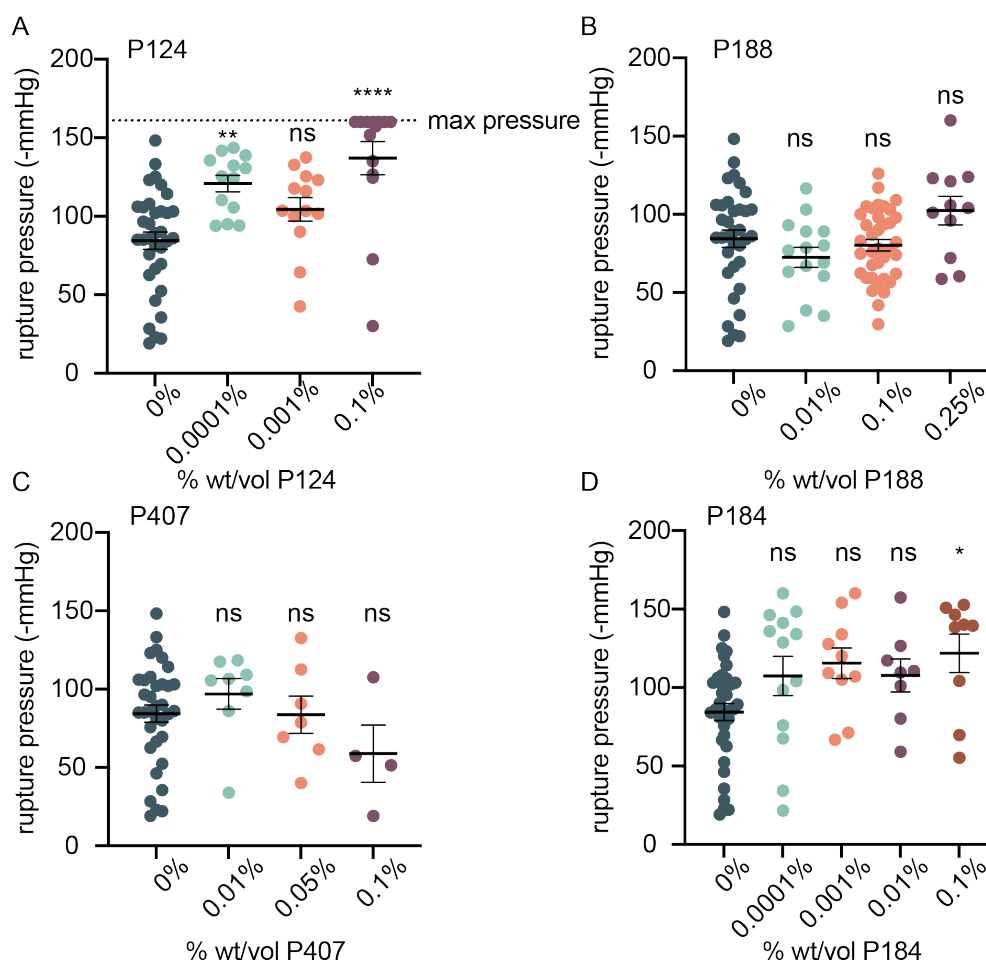


Figure 7.18 Poloxamer effect on membrane stability

We quantified membrane rupture pressure during our electrophysiology recordings of MscL activation to measure if various poloxamers exhibited a strengthening effect on the membrane as has been previously discussed (233). The effect of P124 (A), P188 (B), P407 (C), and P184 (D) were measured, and we observed a membrane strengthening effect in the presence of most poloxamers. However, 407 exhibited a decrease in membrane stability which we hypothesize is due to the large molecular weight of this poloxamer. Each point represents the rupture pressure of a single GPMV, mean is plotted and error bars represent standard error of the mean. p-values were generated by ANOVA using Dunnett's test for multiple comparisons compared to no poloxamer (0%). * $p \leq 0.05$, non-significant (ns) $p > 0.05$, $n > 10$ for most samples except P407 ($n > 3$) which was prone to popping prior to the initiation of the electrophysiology recording.

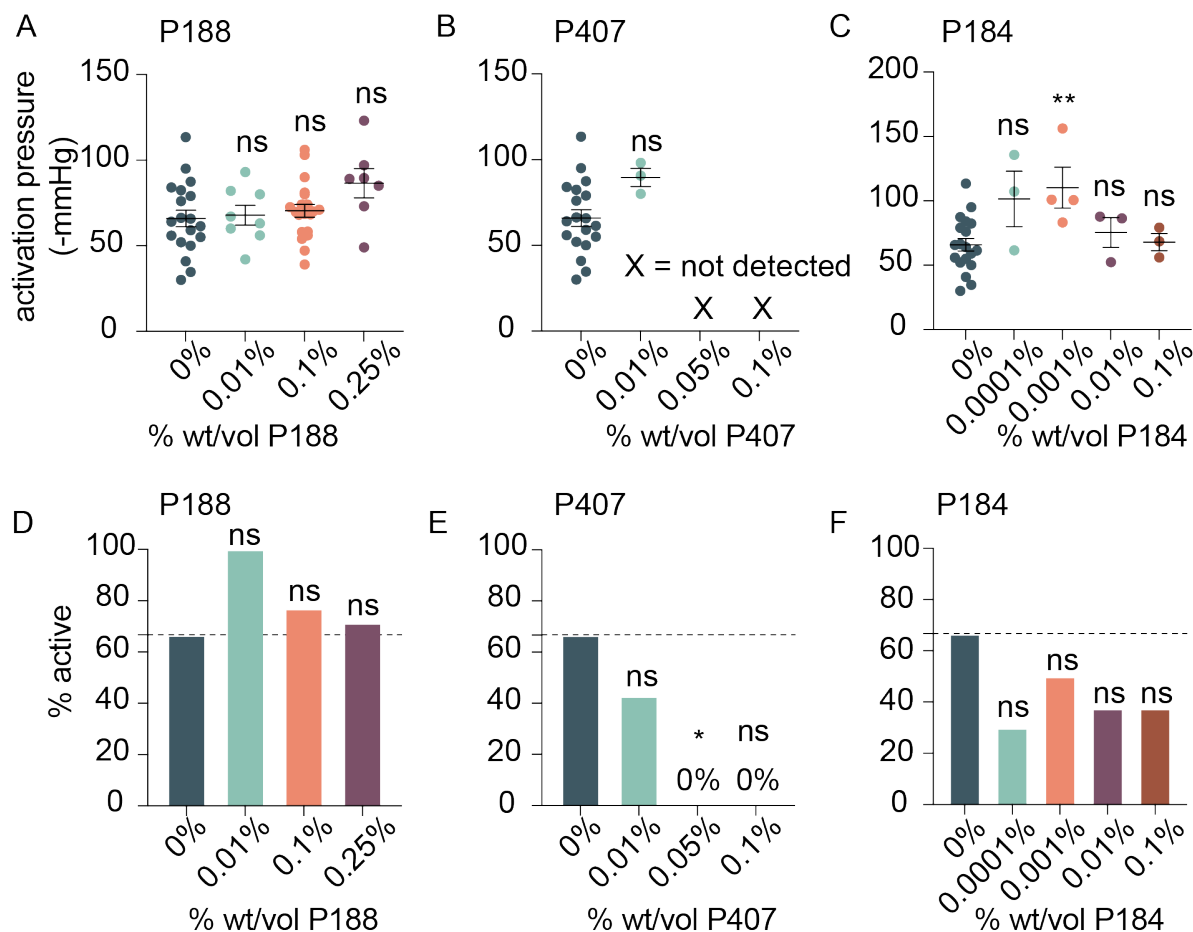


Figure 7.19 MscL activation sensitivity in the presence of various alternate poloxamers

A-C) MscL activation pressure is altered by poloxamer identity and concentration. The pressure of MscL first channel opening was calculated in the presence of various poloxamers at increasing concentration of poloxamer in the buffer P124 (A), P407 (B), and P184 (C). Individual points represent independent GPMV recordings. Higher concentrations of P407 (B) destabilized the membrane and led to rupture at pressures lower than the expected activation pressure of MscL. In the small number of P407 GPMVs which were successfully recorded, no active MscL currents were observed. Mean and standard error of the mean are indicated by the black bar and error bars. The amount of poloxamer in the GPMV formation buffer is indicated in the plot. p-values were generated using ANOVA Dunnett's test for multiple comparisons compared to no poloxamer (0%). ** $p \leq 0.01$, non-significant (ns) $p > 0.05$, $n > 10$ for all samples except for P407 which led to membrane instability which prevented MscL activation (B). D-E) MscL activation probability is prevented by some poloxamers. P188 (D) had no effect on MscL activation probability while P407 (E) and P184 (F) decreased MscL activation probability. p-values were generated using Fisher's exact test compared to 0% poloxamer. * $p \leq 0.05$, non-significant (ns) $p > 0.05$, $n > 3$.

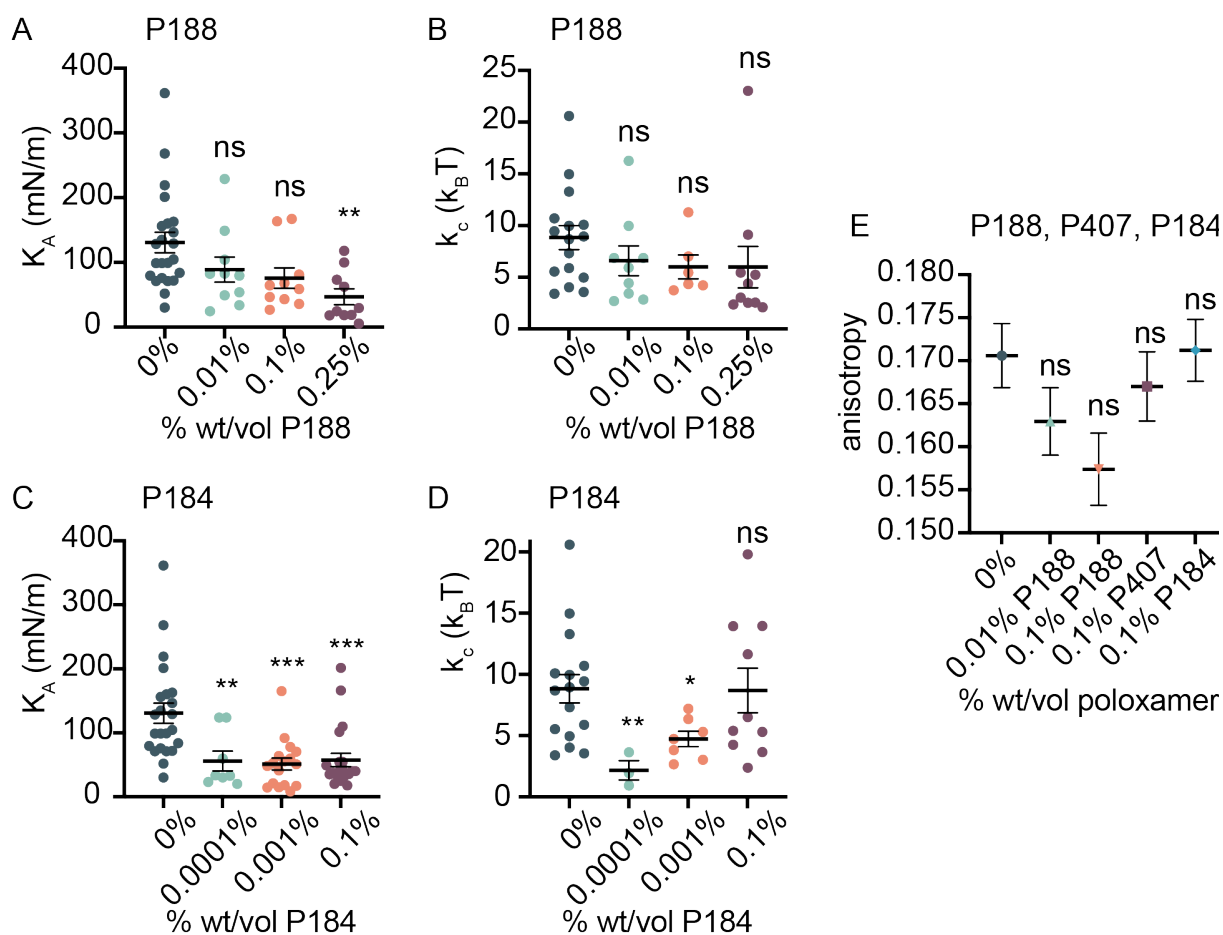


Figure 7.20 Other poloxamer effect on K_A , k_c and fluidity

Membrane mechanical properties were measured in the presence of alternate poloxamer molecules, P188 and P184. A, B) K_A and k_c are reduced with increasing P188 concentration. C) P184 generally decreases membrane K_A above 0.0001% wt/vol in the GPMV formation buffer. D) P184 exhibits a non-monotonic effect on membrane k_c where low concentrations decrease k_c but higher concentrations increase k_c . E) membrane anisotropy was measured in the presence of P188, P407 and P184. no significant differences in membrane fluidity were observed in the presence of these poloxamer molecules. Individual points represent single GPMV measurements, mean and standard error of the mean are plotted as a black bar with error bars, pH 7.4. p-values were generated using ANOVA Dunnett's test for multiple comparisons compared to no poloxamer (0%). *** $p \leq 0.001$, ** $p \leq 0.01$, * $p \leq 0.05$, non-significant (ns) $p > 0.05$, $n > 10$.

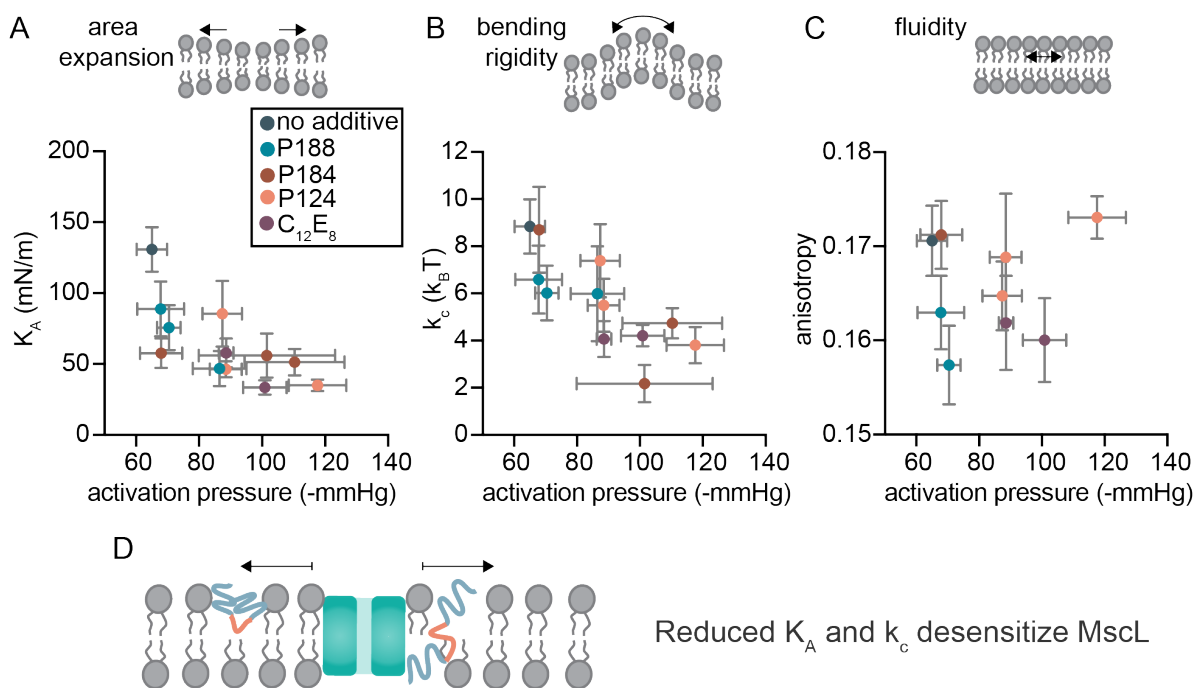


Figure 7.21 Membrane area expansion modulus and bending rigidity are good predictors for MscL pressure sensitivity

A, B, C) Membrane K_A and k_c , but not fluidity, predict MscL activation pressure. GPMVs were treated with various poloxamers and a detergent ($C_{12}E_8$) during formation and membrane properties (K_A , k_c , and fluidity) and MscL pressure sensitivity were measured. Mean K_A (A), k_c (B), and fluidity (C) are reported as a function of MscL activation pressure. R^2 was calculated as a logarithmic fit where x is logarithmic and y is linear, error bars represent standard error of the mean, $n > 10$. D) Potential Mechanism for MscL sensitivity reduction in the presence of membrane softening molecules. MscL serves as a membrane property sensor where changes in K_A and k_c alter membrane force propagation and softer membranes desensitize MscL.

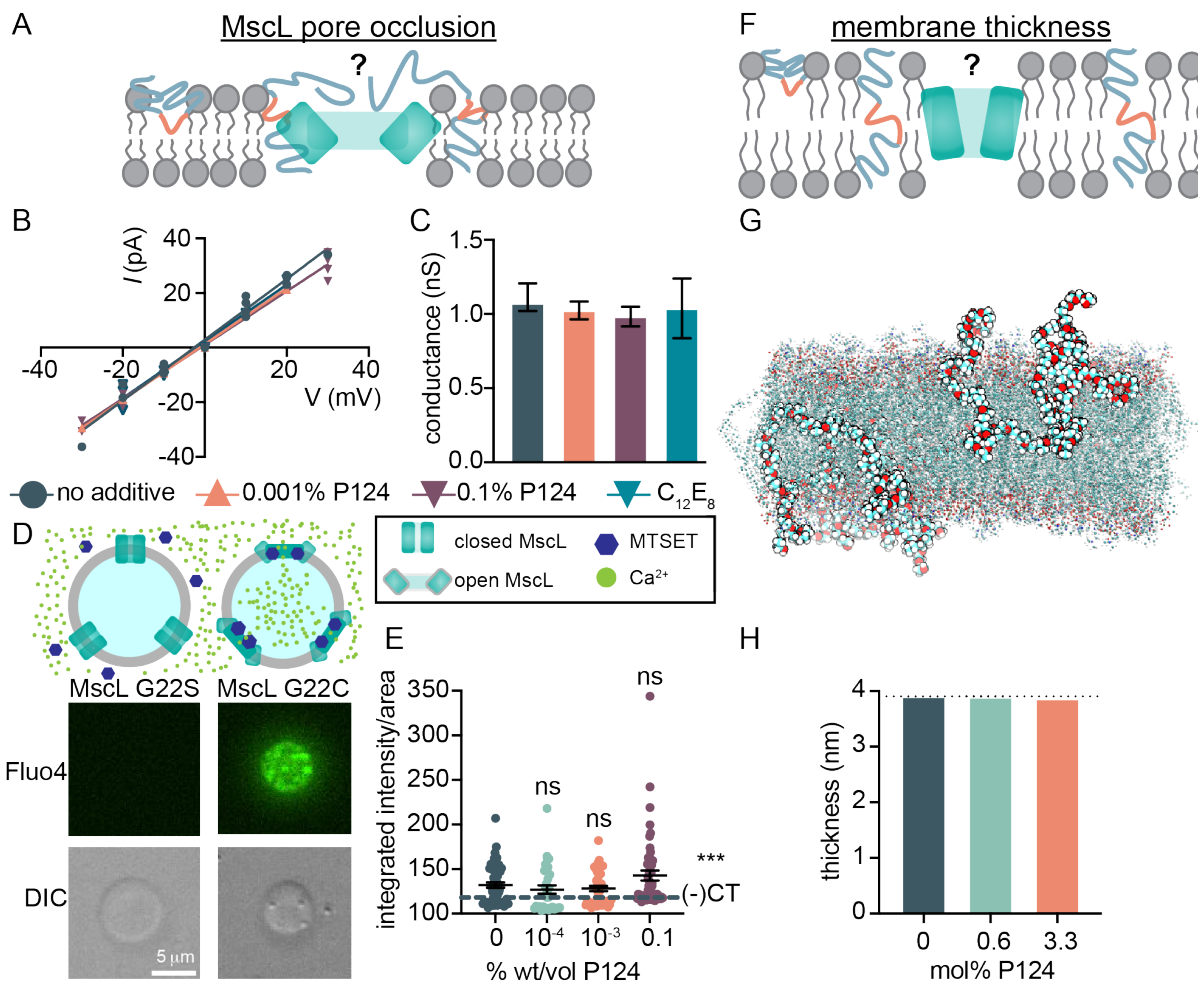


Figure 7.22 Poloxamer does not impact MscL through pore occlusion or membrane thickness changes

A) Poloxamers may prevent MscL activation by preventing pore hydration through channel occlusion. B) MscL pore size does not change in the presence of P124. MscL conductance in the presence of P124 is plotted. The current amplitude at each voltage is plotted and the slope of the linear fit was used to determine channel conductance. $C_{12}E_8$ serves as a non-polymeric membrane-additive control. C) MscL conductance quantification in the presence of P124 and $C_{12}E_8$. Mean conductance and 95% confidence interval are plotted from the linear fit shown in panel B. D) Chemical activation of MscL to determine if pore hydration is prevented by poloxamer presence. MscL(G22C)GFP is a chemically-activatable mutant of MscL which opens in the presence of MTSET. Fluo4 Ca^{2+} imaging of the internal space of the vesicle reveals that Ca^{2+} influx can be detected when MscL(G22C) is activated with MTSET but not in the presence of MTSET-insensitive MscL(G22S). DIC images show vesicle outline. E) P124 does not prevent MscL pore hydration. GPMVs containing MscL(G22C)GFP were formed in the presence of various P124 concentrations as indicated. Fluo4 fluorescence was quantified after GPMV incubation with MTSET and 5 mM Ca^{2+} and is plotted as integrated intensity/ vesicle area. Mean is plotted with error bars which represent standard error off the mean. Dashed line (control) indicates MscL(G22S)GFP mean fluorescence, *** $p \leq 0.001$ determined by student's t-test. p-values were generated by ANOVA using Dunnett's multiple comparisons test compared to no poloxamer. non-significant (ns) $p > 0.5$, $n > 30$ vesicles per condition. F) Poloxamers may prevent MscL activation by increasing membrane thickness, preventing MscL helix tilt required for activation. G) Schematic of coarse-grain molecular dynamics simulations of DOPC bilayers containing P124. H) Membrane thickness does not change with P124 concentration.

To further address the possibility that P124 alters MscL activation through pore occlusion we measured the propensity of P124 to inactivate a variant of MscL which is activated through chemical binding but is insensitive to physical stimuli. A mutation within the pore of MscL serves as a hydrophobic gate (G22C) which can be activated by the addition of a chemical which forcibly hydrates the pore by introducing charge, [2-(trimethylammonium)ethyl] methanethiosulfonate bromide (MTSET) (159). If P124 occludes the MscL pore, MTSET would be expected to be shielded from MscL and we would expect to observe no activation of MscL. In conjunction with this chemical activatable mutant of MscL, we developed a calcium influx assay which can detect MscL activation by the increase in fluorescence within the GPMV upon MTSET binding within the MscL pore. We first validated this assay by ensuring that internal vesicle fluorescence increased only in the presence of the chemically activatable mutant of MscL when MTSET was present (Figure 7.22D, 7.23). We also confirmed the behavior of this mutant through electrophysiology and observed MscL pressure sensitivity only in the presence of DTT as has been demonstrated previously (Figure 7.24) (107).

We then determined if MscLG22C chemical activation was altered by P124 addition by quantifying the internal fluorescence of GPMVs containing P124 in the presence of MTSET. This assay showed that P124 did not inhibit MscL activation relative to the no P124 control (Figure 7.22E) where all conditions activated significantly relative to the MTSET-insensitive control. This result demonstrated that P124 does not shield MscL to prevent pore hydration. This assay also confirmed that MscL is modulated through an alteration in membrane properties as we would expect MscL chemical activation to be sensitive to pore occlusion but not to changes in membrane properties. Taken together, these results suggest that P124 does not occlude the MscL pore during activation as demonstrated by MscL conductance and does not prevent activation by pore occlusion as demonstrated by calcium influx.

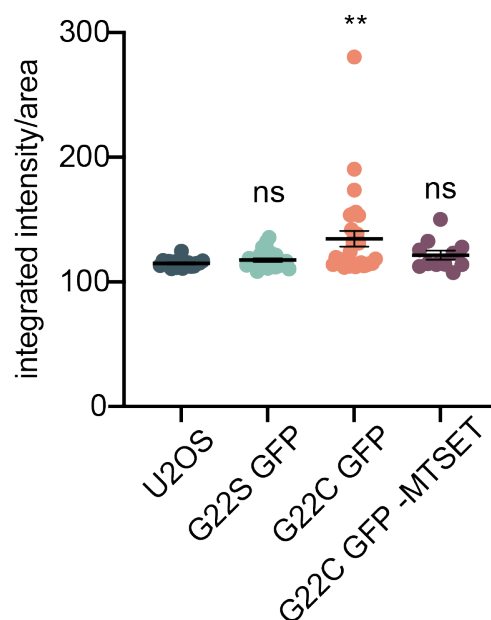


Figure 7.23 Validation of GPMV calcium influx assay

MscL(G22C)GFP is a chemically-activatable mutant of MscL which opens in the presence of MTSET through binding to cysteine groups which induces forced hydration of the hydrophobic gate of MscL. Calcium and MTSET were added to GPMVs formed from cells incubated with Fluo4 Ca^{2+} indicator and Ca^{2+} influx was detected as an increase in Ca^{2+} fluorescence and was quantified as integrated intensity/area. The GPMVs formed from untransfected cells (U2OS) and G22SGFP treated with MTSET, and MscL(G22C)GFP GPMVs not treated with MTSET (G22CGFP(-MTSET)) did not exhibit increases in fluorescence in response to Ca^{2+} . p-values were generated by ANOVA compared to no MscL (U2OS). ** $p \leq 0.01$, non-significant (ns), $p > 0.05$, $n > 10$ independent GPMVs.

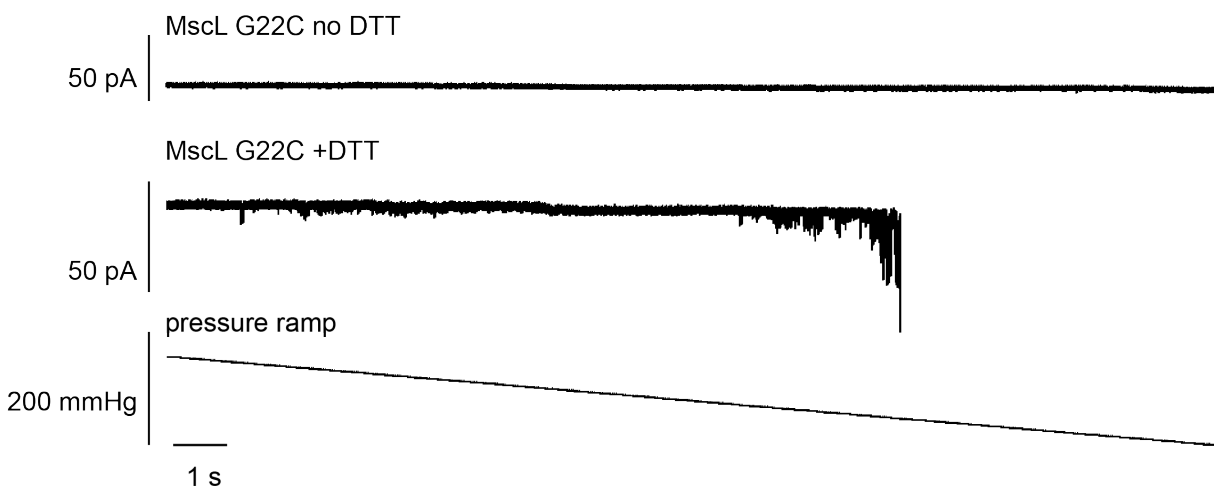


Figure 7.24 MscL(G22C)GFP pressure sensitivity is restored in the presence of DTT

The chemically activatable mutant used in Ca^{2+} imaging assays was further characterized using patch-clamp electrophysiology to confirm channel activity. Without DTT (top) the channel is not mechanically activatable as described previously (107) due to disulfide bonds which prevent channel opening. In the presence of DTT, channel mechanosensitivity is restored and stochastic channel activation is observed with increasing pressure.

Another potential mechanism by which MscL activation could be altered in the presence of P124 is through increasing membrane thickness (Figure 7.22F). MscL is known to be sensitive to membrane thickness where thinner membranes reduce the gating threshold of MscL (27). Although we do not expect membrane thickness to be increased based on our bending rigidity measurements (Figure 7.21B) we performed molecular dynamics simulations measure changes in membrane thickness after P124 incubation and found that membrane thickness did not change in the presence of P124 due to its unordered flexibility within the bilayer (Figure 7.22H). These findings demonstrate that P124 does not reduce MscL sensitivity through increasing membrane thickness.

To ensure that the changes we observed in MscL sensitivity and membrane properties were due to poloxamer effects within the membrane, we confirmed that poloxamer integrates into GPMV membranes. Our molecular dynamics simulations demonstrated that P124 inserts into bilayers when incubated in the buffer surrounding a membrane and this integration increases membrane surface area (Figure 7.22G). We confirmed this result through microscopy and found that poloxamer addition increases GPMV surface area (Figure 7.25). In addition, our finding that P124 increases GPMV stability has been observed in other systems and further suggests membrane integration (7.18). Together, these results suggest that poloxamer alters membrane mechanical properties through insertion into the bilayer structure.

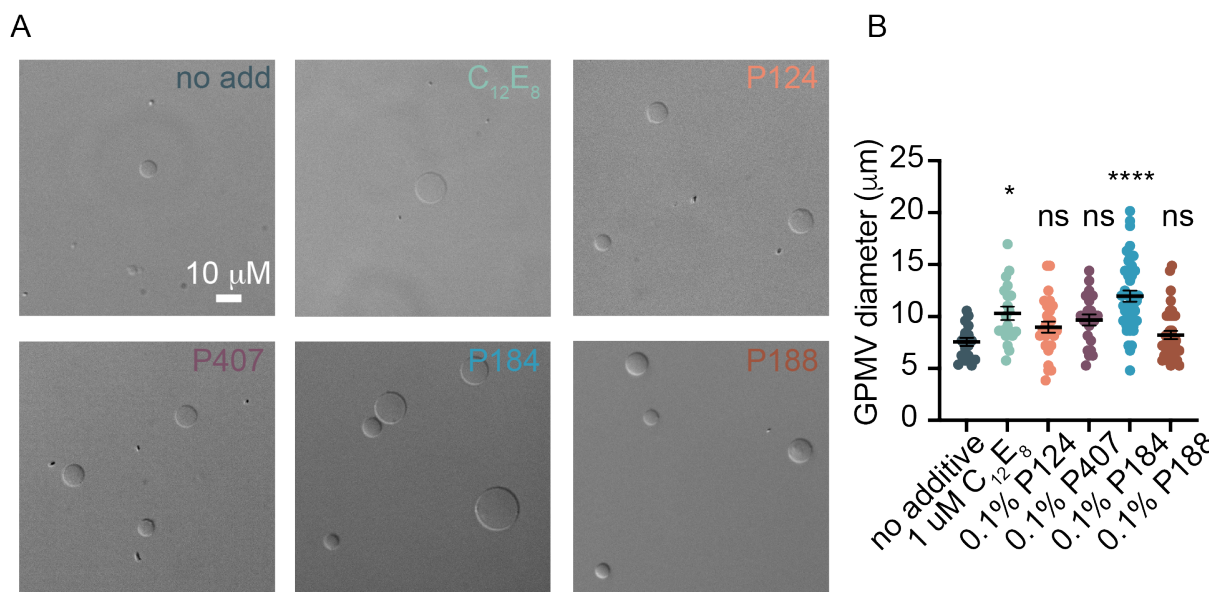


Figure 7.25 GPMV diameter increases in the presence of various poloxamers and a detergent

A) DIC phase contrast micrographs demonstrate the effect poloxamer and detergent ($C_{12}E_8$) on GPMV size. B) GPMV diameter was quantified for all GPMVs large enough to quantify. individual points represent the diameter of a single GPMV, mean and standard error of the mean are plotted. p-values were generated using ANOVA Dunnett's test of multiple comparisons compared to no poloxamer. **** $p \leq 0.0001$, * $p \leq 0.05$, non-significant (ns) $p > 0.05$, $n > 10$.

Trek1 confirms the relationship between K_A , k_c and *force-from-lipids* gating of mechanosensitive channels

Finally, we aimed to demonstrate the application of this model to another mechanosensitive channel to assess the generality of the effect of poloxamer on mechanosensitive channel behavior. We chose to measure the effect of P124 on the mouse potassium channel subfamily K member 2 (mTrek-1), a mechanosensitive channel found in neurons which has been demonstrated to be activated by force-from-lipids and is sensitive to changes in membrane composition (Figure 7.26) (34). Using a similar expression scheme as MscL, we created stable cell lines of mTrek1mEGFP (Figure 7.27) which was retained in the membrane after GPMV formation (Figure 7.28). We observed mTrek1 single-channel currents in response to a pressure gradient using an integrated pressure controller and similar currents were not observed in untransfected cells exposed to the same experimental conditions (Figure 7.26A, 7.29). We measured mTrek1 conductance using voltage-clamp electrophysiology measuring the respective current through a single channel and observed an outward conductance of 140 pS, similar to the conductance of mTrek1 in cellular systems (Figure 7.26B) (242, 243). The inward conductance was undetectable below +50 mV, suggesting a primarily outward rectifying channel, as has been observed previously (243). We next aimed to determine if Trek1 activation pressure responded to P124. We treated mTrek1-containing GPMVs with P124 and used $C_{12}E_8$ as a membrane-softening control and observed an increase in the pressure to activate the first mTrek1 channel under both conditions (Figure 7.26C), similar to our results with MscL (Figure 7.10B, 7.16A). Finally, we wondered if mTrek1 activation could be predicted by membrane properties. We plotted K_A , k_c , and fluidity as a function of mTrek1 activation pressure. Similar to MscL, we observed a strong correlation between mTrek1 activation pressure and K_A ($R^2 = 0.99$) and k_c ($R^2 = 0.96$) (Figure 7.26D, E). As we observed in the presence of MscL, there was not a correlation between membrane fluidity and mTrek1 activation pressure ($R^2 = 0.21$) (Figure 7.26F). These results suggest a relationship between membrane elastic properties, K_A , and k_c , and mTrek1 activation sensitivity. Taken together, our observations suggest that these properties play a role in mechanosensitive channel force-from-lipids

activation as exhibited by the effect of various poloxamer analogs and a chemically distinct detergent on mechanosensitive channel activation pressure.

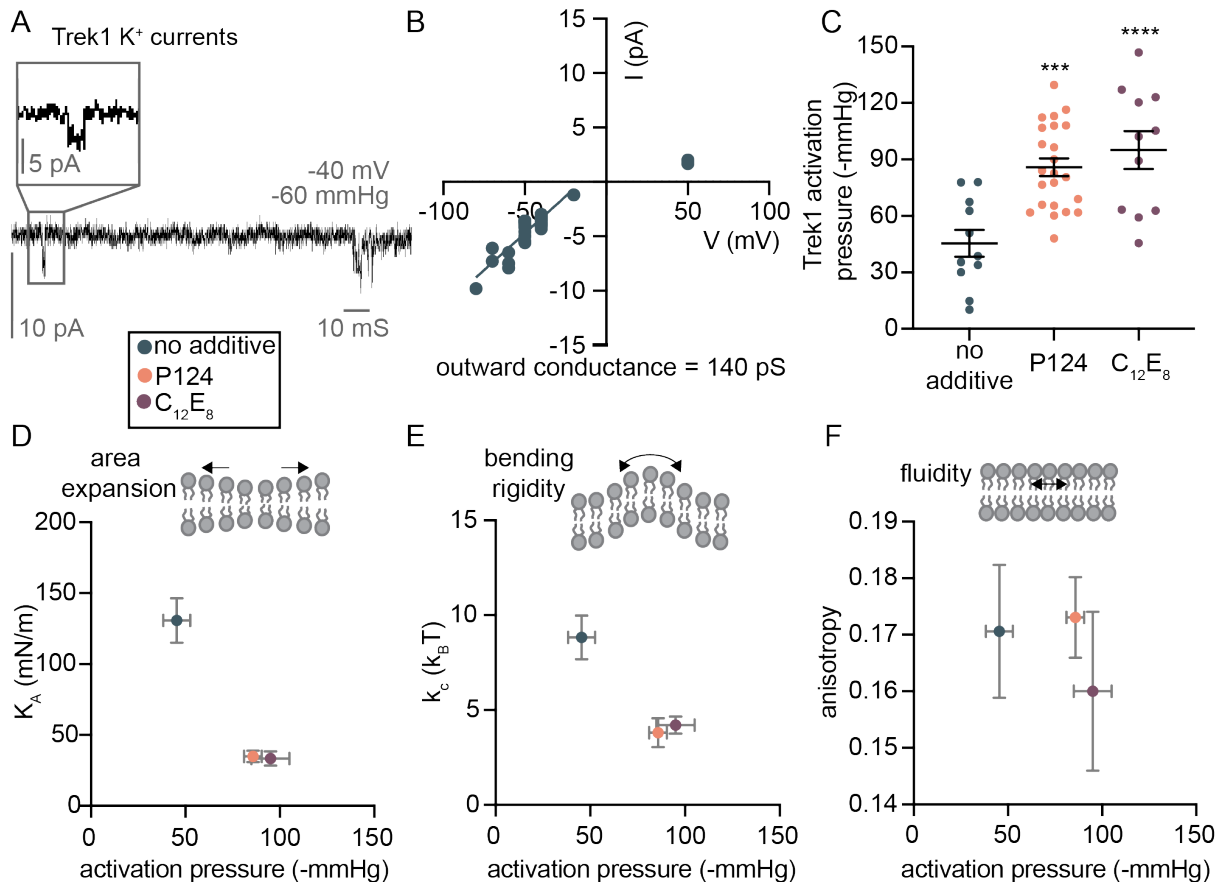


Figure 7.26 Trek-1 activation is also predicted by membrane properties.

A) Mouse Trek1 single channel potassium currents are observed GPMVs in response to pressure. Trek1 currents were measured using patch-clamp electrophysiology with an integrated pressure controller in asymmetric potassium conditions, pH 7.3. B) Trek1 is outward rectifying with a conductance of 140 pS. Trek1 current was quantified under various holding potentials. Trek1 currents were larger under negative voltages and the slope of the I/V relationship under negative voltages was used to measure outward rectifying conductance. Individual electrophysiology measurements are plotted, $n > 15$. C) Trek1 activation pressure is increased in the presence of a poloxamer (P124) and a detergent (C₁₂E₈). Mean activation pressure is plotted and dots represent individual measurements, error bars represent standard error of the mean. p-values were generated by ANOVA using Dunnett's multiple comparisons test compared to no poloxamer. **** $p \leq 0.0001$, *** $p \leq 0.001$, $n > 10$. D, E) Membrane K_A and k_c predict Trek1 activation pressure. GPMVs were treated with P124 or C₁₂E₈ at the highest concentration and Trek1 activation or membrane mechanical properties were measured. Mean K_A or k_c and Trek1 activation pressure were plotted. F) Membrane fluidity does not predict Trek1 activation pressure. Mean membrane anisotropy and Trek1 activation pressure were plotted. R² in (D-F) was determined from a logarithmic fit where x is logarithmic and y is linear, error bars represent standard error of the mean, $n > 10$ for each measurement.

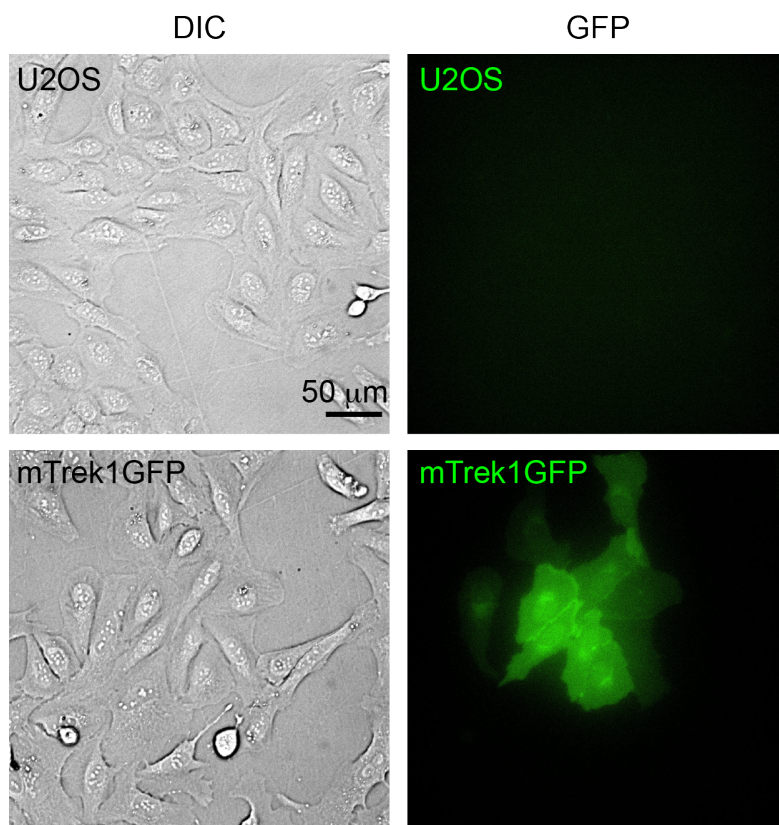


Figure 7.27 U2OS cells stably expressing mTrek1
mTrek1GFP localizes to the membrane as shown in GFP images. DIC images are shown to demonstrate cell boundary and confluency.

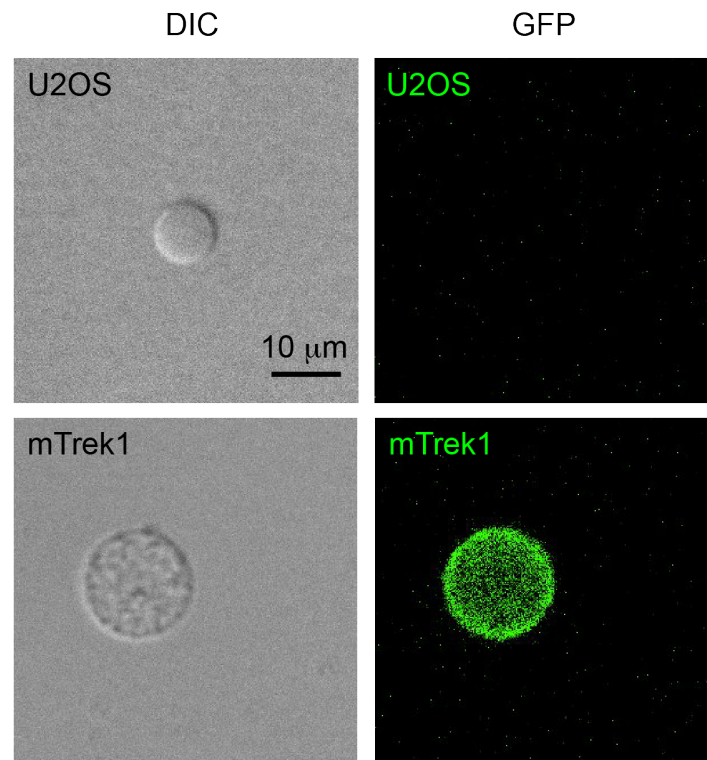


Figure 7.28 Trek1 GFP is retained in GPMV membranes

Trek1GFP is localized to the GPMV membrane. no GFP signal is detected in untransfected cells (U2OS).

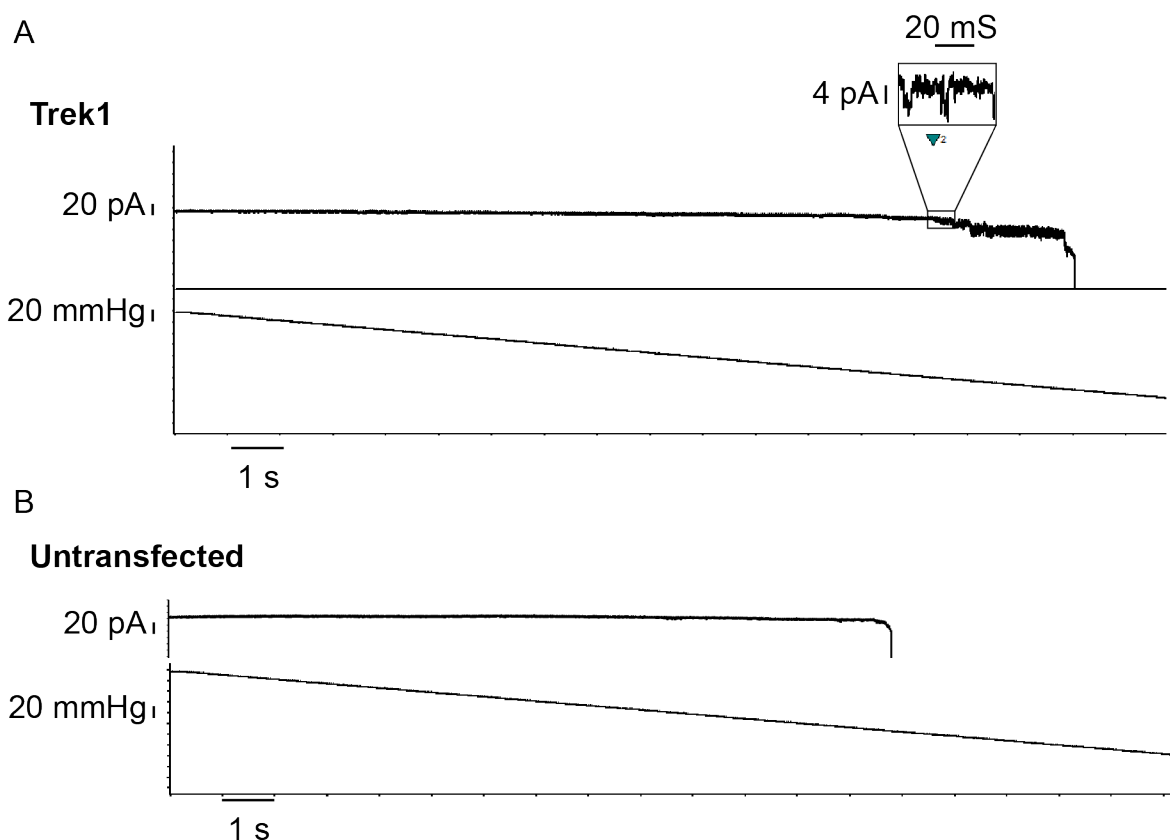


Figure 7.29 Trek1 mechanosensitive currents are only observed in GPMVs formed from stable cells expressing Trek1

A) We observed Trek1 activation where single channel currents were ~ 4.5 pA at -50 mV. Trek1 activation was observed in most patches above -30 mmHg. B) To further confirm that we observed Trek1 channels in our electrophysiology recordings, we performed patch-clamp electrophysiology on GPMVs formed from U2OS cells that were untransfected, referred to as untransfected GPMVs, under identical conditions as our Trek1 recordings which required higher holding potentials to observe single channels due to the smaller conductance of Trek1 compared to MscL. We applied enough pressure to pop the GPMV membrane to ensure the pressure was high enough to activate any native mechanosensitive channels in the GPMVs. We did not observe any channels in untransfected GPMVs before membrane popping. Recordings are performed at -50 mV in asymmetric potassium buffer conditions. Bath solution was composed of 10 mM HEPES, 150 mM KCl, 2 mM $MgCl_2$ for excised-patch recordings on Trek1 with outward rectifying potassium currents. $n > 6$ recordings on independent patches.

7.3 Discussion

Through a series of micropipette aspiration and patch-clamp electrophysiology studies, we have determined the effect of various poloxamers on membrane properties and mechanosensitive channel behavior. By measuring these properties directly, we found that membrane K_A and k_c correlate with MscL activation sensitivity while membrane fluidity does not. We then confirmed the role of membrane properties on MscL sensitivity using a chemically distinct detergent. Next, we demonstrated that membrane thickness and MscL pore occlusion did not contribute to our observations of MscL desensitization. Finally, we determined that K_A and k_c may also affect the behavior of more complex mechanosensitive channels in higher organisms by assessing the behavior of mTrek1 in response to changes in membrane properties. Our findings suggest that by decreasing membrane K_A and k_c , the force required to activate MscL and mTrek1 is increased. To our knowledge, our study is the first to directly measure multiple membrane properties to directly implicate K_A and k_c in MscL and Trek1 activation sensitivity.

Mechanosensitive channel activation sensitivity is an important feature of all mechanosensitive channels. Overactive mechanosensitive channels may lead to deleterious effects ranging from a loss in cell volume in bacteria or red blood cells (107, 236) to persistent itch disease in higher organisms (244). Membrane composition has been increasingly shown to modulate the force-from-lipids activation of mechanosensitive channels and this effect is hypothesized to be due to changes in global membrane properties (8). We demonstrated recently that membrane amphiphiles can impact membrane properties in unpredictable ways (46) which supports the importance of measuring membrane properties directly when drawing comparisons. While a number of studies discuss the effects of membrane properties on mechanosensitive channel activation (24, 26, 27), few have directly measured membrane properties (31, 104, 195). Moreover, no studies to date have used the classical micropipette aspiration technique in conjunction with patch-clamp electrophysiology to directly determine the relationship between membrane properties and mechanosensitive channel function. Accordingly, the body of research to date leaves an unexplored gap

between membrane mechanical properties and mechanosensitive channel behavior. In the present study, we contributed to this body of research by precisely measuring various membrane mechanical properties and mechanosensitive channel behavior under identical conditions (Figures 7.10, 7.21). To our knowledge, we have demonstrated, for the first time, direct measurements of membrane K_A , k_c and mechanosensitive channel activity.

Non-natural amphiphiles can reveal new aspects of the mechanism of mechanosensitive channel activation through the alteration of global membrane properties. Previous studies have shown that MscL activation is sensitive to membrane thickness where thicker membranes desensitize MscL (24, 27). Membrane elastic properties were also hypothesized to be important in this behavior, however, the amphiphiles used in these studies were expected to alter membrane thickness to an extent which would explain the effect on MscL activation. Therefore, the role of the membrane properties K_A and k_c in mechanosensitive channel activity have not been isolated from membrane thickness in using natural lipids alone. Our results demonstrate the power of using non-natural amphiphiles, which can alter membrane elastic properties without altering hydrophobic thickness to reveal the effect of K_A and k_c on MscL activation (Figure 7.21, 7.22F-H). We further demonstrated this effect using a small detergent, $C_{12}E_8$, which was expected to decrease membrane thickness (167), yet we observed an increase in MscL activation pressure as predicted by membrane K_A and k_c (Figure 7.17). Together, these results suggest that decreasing membrane K_A and k_c decreases MscL sensitivity. These findings also suggest a general role of the force-from-lipids mechanism which extends beyond interactions with natural lipids to systems with synthetic amphiphiles.

Although most poloxamers we studied exhibited a linear effect on membrane properties and channel activation, we observed a non-monotonic effect of P184 concentration on MscL activation and k_c . The presence of P184 induced a slight decrease in K_A at all concentrations while k_c decreased at low concentrations then increased at higher concentrations (Figure 7.21) which differed from our results with other poloxamers (Figure 7.10, 7.18, 7.19). Interestingly, we observed a similar pattern between membrane

k_c and MscL activation pressure as MscL activation pressure increased then decreased with increasing P184 concentration (Figure 7.19). This observation highlights that the influence of k_c may be stronger than K_A on MscL activation. We are unsure of the mechanism of this non-monotonic effect of P184 on k_c but attribute it to the large number of hydrophobic blocks relative to the small number of hydrophilic blocks which may increase membrane stiffness at higher concentrations through interdigitation (172) or through changing the depth of P184 insertion in the membrane at high concentrations (233).

While our results highlight a potential role of K_A and k_c in MscL activation, we cannot discount the possibility that poloxamer alters the lipid pressure profile or accommodates hydrophobic mismatch in unique ways. MscL is known to be sensitive to lipid pressure profile as demonstrated by activation upon insertion of LPC, a single-chain amphiphile with a large headgroup (Figure 7.9) (24, 245). However, we observed a similar effect on MscL function in the presence of various poloxamers (Figure 7.21) despite the differing hydrophobic/hydrophilic ratio of the various poloxamers we used, which would be expected to alter the lipid pressure profile differently (Figure 7.4). In addition, as hydrophobic mismatch is one of the key activators of MscL (27), our results may be explained by the ability of polymeric amphiphiles to support protein hydrophobic mismatch to a greater extent than natural lipids (171, 246). However, the distinct molecular features of poloxamer and $C_{12}E_8$ highlight that their effect on MscL function is more readily explained by membrane mechanical properties rather than membrane pressure profile or accommodation of membrane hydrophobic mismatch, as these amphiphiles have distinct chemical features and vary greatly in molecular size (Figure 7.4). Moreover, it is unlikely that a detergent (500 g/mol) which is smaller than a phospholipid (~700 g/mol) has the ability to accommodate hydrophobic mismatch like a large poloxamer may be able to (2,000 – 12,5000 g/mol). Together, our results support a mechanism where various poloxamers and $C_{12}E_8$ alter MscL function through membrane K_A and k_c .

Our observations of poloxamers interacting with membranes and altering mechanical properties and mechanosensitive channel activity highlight a potential unwanted effect of poloxamers and other

nanoplastic particles. The concentrations of poloxamer we chose to assess in the present study are commonly used in laboratory cell culture applications to prevent cell sticking and improve cell integrity and are also found at these concentrations in household products (232). Our findings suggest that poloxamers used at these concentrations may alter the behavior of membrane-embedded ion channels which in turn may affect environmental and human health or may affect biophysical studies in unexplored ways. In addition, these findings propose one potential mechanism for the alteration of biological function in response to nanoplastic pollution which has remained elusive (231). Our results suggest that nanoplastics which have been increasingly shown to interact with cellular membranes (229, 231, 247), may alter biological function through modulating embedded channel behavior.

7.4 Conclusion

In conclusion, we observed that various poloxamers and a detergent generally decrease membrane K_A and k_c , and increase the force required to activate mechanosensitive channels. Our study is the first to our knowledge to measure mechanosensitive channel activation in a polymeric environment. By harnessing the unique features of polymeric amphiphiles, we probed the relationship between membrane K_A , k_c , fluidity, and mechanosensitive channel activation independent of membrane thickness. These observations using two distinct mechanosensitive channels highlight a direct connection between the membrane physical environment and mechanosensitive function to show that K_A and k_c are important for force-from-lipids activation of mechanosensitive channels. In addition, our study highlights the power of non-natural amphiphiles while studying biological systems as they can alter membrane properties in unique ways to probe the physicality of biological interactions. These findings have implications for mechanosensitive channel function in various systems which are prone to changes in membrane properties such as cancerous cells, and cells which are exposed to fatty acids or nanoplastics.

7.5 Materials and Methods

Materials

Gibco G418 (geneticin), McCoy's 5A medium, Opti-MEM transfection medium, Fetal Bovine Serum (FBS), CaCl₂, MES sodium salt, BAPTA NA₄ Poloxamer 188, 124, and 184, diphenylhexatriene, and polyethylenimine were obtained from Thermo Fisher Scientific. HEPES, NaCl, N-ethylmaleimide, and EGTA was purchased from Millipore Sigma. Human Osteosarcoma U-2 OS HTB-96 cell line was purchased from ATCC.

Methods

Mammalian expression plasmid cloning

EcMscLGFP was amplified using polymerase chain reaction (PCR) and inserted into a mammalian pCDNA3.0 vector using restriction digest. A G22C mutation was introduced in the *mscL* gene using primers with a point mutation and the entire plasmid was amplified using PCR. The cloned plasmids were transformed into Top10 electrocompetent cells and amplified and functional gene insertion was verified using sanger sequencing. mTrek1 was amplified with using PCR and cloned into the pCDNA3.0 vector as a fusion to GFP by removal of EcMscL using restriction enzymes. Insertion and GFP fusion of mTrek1 was confirmed using sanger sequencing. pET19b:EcMscLGFP was used previously as an *in vitro* membrane protein folding reporter (Addgene plasmid # 165097) (115). pGEMHE:mTREK-1(K271Q) was a gift from Dan Minor (Addgene plasmid # 133270) (248).

Stable cell line transfection and selection

U2OS cells were plated in a 6-well plate and grown to 70% confluency on the day of transfection. Mammalian expression vectors containing EcMscLGFP or mTrek1GFP were transfected into U2OS cells using polyethylenimine (PEI). 500 ng DNA was mixed with 100 μ L Opti-MEM transfection media and 2.5

μg PEI. This solution was incubated for 15 minutes then added dropwise to U2OS cells in McCoy's 5A media with 10% FBS. The transfection media was replaced with fresh McCoy's 5A with 10% FBS and 300 $\mu\text{g}/\text{mL}$ geneticin after overnight incubation. Transfected cells were selected using 300 $\mu\text{g}/\text{mL}$ geneticin in McCoy's 5A media with 10% FBS for 1 month or until the cells reached confluency in a T-75 75 cm^2 flask. Cells were further propagated in McCoy's 5A with 10% FBS and 100 $\mu\text{g}/\text{mL}$ geneticin. Selection efficiency was confirmed using the GFP tag attached to the protein of interest.

GPMV formation and treatment with poloxamer

GPMV formation was performed using established techniques (249). Briefly, U2OS cells were plated at least one day prior to GPMV formation and grown to 70% confluency at the time of GPMV formation. GPMV buffer was used for all GPMV preparations and consisted of 10 mM HEPES, pH 7.4, 150 mM NaCl, and 2 mM CaCl_2 . N-ethylmaleimide (NEM) was prepared at 0.25 M in sterile water and stored in 300 μL aliquots. 30 μL NEM was added to 1 mL of GPMV buffer containing the indicated concentration of pre-dissolved poloxamer or detergent and mixed using a vortex. Cells were washed twice with GPMV buffer and removed by aspiration. The NEM-GPMV buffer solution was added gently to the U2OS cells and incubated at 37 $^\circ\text{C}$ for 1 hour. GPMVs were observed then removed from adherent cells by gentle aspiration and were incubated for 3 hours at 4 $^\circ\text{C}$ prior to experiments to ensure poloxamer equilibration.

Fluorescence and phase-contrast microscopy

Cells and GPMVs were imaged using epifluorescence and phase-contrast microscopy to confirm transfection and protein transfer to GPMV membranes. Glass bottom 96-well plates were passivated by incubating β -casein solution at 5 mg/mL in 10 mM Tris, pH 7.4 in each well for 30 minutes. This solution was replaced with GPMV buffer, pH 7.4 and GPMVs were diluted to a concentration suitable to observe single GPMVs. GPMV area was images using differential interference contrast (DIC) phase contrast and Transfection efficiency and membrane protein integration were confirmed using epifluorescence with a GFP

filter. All images being compared were brightness/contrast adjusted with identical settings and imaged at 20% light with identical exposure times.

Micropipette aspiration

GPMV membrane area expansion modulus (K_A) and bending rigidity (k_c) were measured using micropipette aspiration techniques (193). Micropipettes were constructed from borosilicate glass capillaries (World Precision Instruments) pulled using a P-1000 micropipette puller (Sutter instruments). The end was blunted and polished to an inner diameter of 5–8 μm using a microforge. The micropipette and sample chamber surfaces were passivated using 5 mg/mL β -casein for 1 hour and were filled with GPMV buffer, pH 7.4. 10 μL GPMVs prepared in the presence of poloxamer or detergent were diluted in a 1 mL glass chamber in GPMV buffer, pH 7.4. Imaging was performed on a Nikon inverted microscope connected to a Validyne pressure sensor and digital manometer (model DP 15-32; Validyne Engineering, Northridge, CA). A Narishige micromanipulator was used to control the micropipette (model WR-6; Narishige). GPMVs free of visible defects were aspirated and the membrane areal response to a change in pressure was measured using a series of DIC images with pressure recordings. Membrane K_{app} is calculated from the slope of the percent area dilation within the pipette ($\Delta A/A_o$) and membrane tension (τ),

$$K_{app} = \frac{\tau}{\frac{\Delta A}{A_o}}$$

where ΔA is the change in area of GPMV membrane within the micropipette and A_o is the initial area of the aspirated GPMV within the pipette. Bending elastic modulus, k_c is calculated from the same aspiration measurements through the following equation in the low-tension regime (<0.5 mN/m),

$$\frac{\ln(\tau)}{\frac{\Delta A}{A_o}} = \frac{8\pi k_c}{k_B T}$$

where k_B is the Boltzmann constant, and T is temperature. Membrane K_A is calculated through correction of K_{app} with k_c by subtraction for relaxation of thermal undulations measured by k_c (7, 196). For each

stress/strain measurement in the area expansion regime, the contributions of thermal undulations ($\Delta\alpha(i)$) was subtracted from the areal strain ($\Delta A/A_0$),

$$\Delta\alpha(i) = \frac{k_B T}{8\pi k_c} \ln\left(\frac{\tau(i)}{\tau(1)}\right)$$

where $\tau(1)$ is the initial tension. The corrected areal change was then plotted against τ and the slope of this plot was used to calculate K_A .

Patch Clamp electrophysiology of stretch-activated ion channels

Channel activity measurements were performed in identical conditions as micropipette aspiration. GPMVs containing EcMscL and mTrek1 prepared under indicated poloxamer conditions were added to an open-air bath on an Olympus IX73 phase-contrast microscope. Electrophysiology pipettes were pulled using a Sutter P-1000 micropipette puller and fire polished using a microforge to 5-8 M Ω resistance. Voltage-clamp measurements were recorded on a Molecular Devices Axon Instruments system including an amplifier and digitizer Low-Noise Data Acquisition System plus Hum silencer along with an ALA Scientific Instruments High Speed Pressure Clamp pressure controller which was used to apply a pressure ramp during electrophysiology recordings, all signals were integrated using Clampex software and pressure and current values were recorded temporally. A pressure ramp from 0 mmHg to -160 mmHg was applied at a constant rate for all recordings. EcMscL and mTrek1 recordings were performed at -10 mV and -40 mV, respectively unless channel conductance calculations were being measured. Current and pressure were recorded through these experiments using and were used to calculate pressure sensitivity and channel conductance, respectively. Each pressure sensitivity recording was performed on an independent GPMV and pressure ramps were never repeated as a decrease in pressure sensitivity is observed after repeat pressure ramps because of an increase in membrane tension when the membrane patch diffuses up the pipette (24). All electrophysiology recordings were performed at 25 °C Bath solution was composed of 10 mM HEPES, pH 7.4, 150 mM NaCl, 2 mM CaCl₂ for MscL and 10 mM HEPES, pH 7.4, 150 mM KCl, 2 mM CaCl₂ for mTrek1. The pipette solution was composed of 10 mM HEPES, pH 7.4, 100 mM NaMES, 10 mM BAPTA Na₄, 10

mM NaCl, 10 mM EGTA. All recordings were performed in the cell-attached or excised-patch configuration. A seal $> 8 \text{ G}\Omega$ was required for reliable single-channel observations.

Electrophysiology data analysis

Electrophysiology experiments were quantified using Clampfit software which displayed the current and pressure during the voltage-clamp recording. EcMscL and mTrek1 channel activation sensitivities were quantified using the pressure at first channel opening which has been described previously (24). Many recordings only contained one channel, and this first channel was clearly distinguished from electrical noise. However, some recordings contained many channels which could not be distinguished from membrane unsealing making maximum current an unreliable measurement. Membrane rupture pressure was calculated by the pressure at which a very large current change occurred, indicating complete membrane rupture. Single channel conductance was measured by calculating the current through single channels at various voltages and was independent from pipette pressure. Each current and voltage measurement was recorded from an independent GPMV and this measurement was not repeated by any single GPMV to mimic pressure sensitivity measurement conditions. The slope of many of these I/V relationships was used to calculate channel conductance. mTrek1 was observed to behave similarly to previous studies and had a short dwell time and was potassium selective with a much smaller conductance than MscL (243).

Anisotropy

Fluorescence anisotropy measurements were used to determine relative membrane fluidity as described previously (46). GPMVs were prepared and unbound poloxamer micelles were removed from solution through centrifugation and GPMVs were rehydrated in 1 mL GPMV buffer. A diphenylhexatriene (DPH) stock solution was prepared by adding dry DPH to GPMV buffer at $100 \mu\text{M}$. This solution was mixed 1:1 with purified GPMVs and anisotropy was measured using an Agilent Technologies Cary Eclipse Fluorescence Spectrophotometer with an Automated Polarization Accessory. Fluorescence anisotropy was

assessed at excitation 360 nm and emission 435 nm and was calculated by software provided with the instrument,

$$\text{anisotropy} = \frac{I_{vv} - I_{vh}G}{I_{vv} + 2I_{vh}G}$$

where I_{vv} and I_{vh} are the intensities of the vertically and horizontally polarized light, respectively, after excitation with vertically polarized light. $G = I_{hv}/I_{hh}$ which is a grating correction factor for the optical system.

Chemical activation of MscL and calcium imaging

Fluo4, a calcium indicator which has been used previously to sense mechanosensitive channel behavior (236), was used to determine if P124 inhibits MscL activation through inhibition of pore hydration. Briefly, Fluo4 was mixed with GPMV buffer to a 1x dye concentration. GPMV formation solution was prepared by adding 30 μL of 0.25 M NEM to 1 mL of diluted Fluo4 solution in GPMV buffer. Cells were washed twice with GPMV buffer and incubated in GPMV formation solution for 1 hour at 37 °C. Free-floating GPMVs were isolated by transferring formation solution to an eppendorf tube and incubated for 3 additional hours. A glass-bottom 96-well plate was passivated by incubating with a β -casein solution in 10 mM Tris, pH 7.4 for 30 min. The wells were rinsed 3 times with GPMV buffer and 100 μL GPMV buffer with 5 mM CaCl_2 was added to each desired well. 10 μL GPMVs were added to the bottom of each well. 5 μL of 21 mM MTSET was added to each well and GPMVs were incubated for 30 min. Ca^{2+} influx through MscL opening was quantified from raw images by a fluorescence increase in the GFP channel for each GPMV visible in the DIC channel.

7.6 Acknowledgements

We thank Prof. Paul DeCaen for his experimental advice and thorough training in patch-clamp electrophysiology, helpful discussions, and careful reading of the manuscript. We also thank members of

the Kamat Lab for thoughtful discussions. This work was supported by the Air Force Office of Scientific Research (AFOSR) YIP FA9550-19-1-0039 P00001 to NPK, the Searle Funds at The Chicago Community Trust (NPK), and NSF grant MCB-1935356 (NPK). M.L.J. was supported by Grant No. T32GM008382 from the National Institute of General Medical Sciences and The American Heart Association Predoctoral Fellowship under Grant No. 20PRE35180215.

Chapter 8

8. Conclusions and future work

8.1 Specific Aims

The work in this thesis addressed major questions regarding membrane composition and mechanical properties and their effects on the behavior of a mechanosensitive channel from folding to function. Through our various studies, we aimed to further the understanding of the effect of the area expansion modulus, K_A in these processes. These questions aimed to first, demonstrate how membrane K_A directly impacts membrane protein folding, which has not been observed previously. This aim was achieved using non-natural amphiphiles which allowed us to isolate K_A away from other membranes properties previously implicated in protein folding. Second, we aimed to determine how natural lipids may modulate this membrane property using polyunsaturated fatty acids. Finally, we wondered how K_A impacts the function of mechanosensitive channels which has not been able to be isolated from membrane thickness previously.

The following aims were discussed within this thesis to address these outstanding questions:

1. Measure MscL folding in response to changes in membrane composition and properties altered by diblock copolymers.
2. Quantify the effects of non-esterified fatty acids and cholesterol on membrane mechanical properties.

3. Measure changes in mechanosensitive channel activity and membrane mechanical properties in response to membrane composition altered by the incorporation of synthetic amphiphiles.

8.2 Conclusions

Membrane elasticity is important for membrane protein folding

Membrane protein folding is a key step in the synthesis and functionality of all membrane proteins where the malfunction of this process is associated with various pathologies. The membrane is hypothesized to play a large role in membrane protein folding and may assist chaperones in this process. Using non-natural amphiphiles, we were able to modulate the properties of model membranes to elucidate the role of membrane mechanical properties in membrane protein folding. In **Chapter 3** we developed a method to measure co-translational membrane protein folding in hybrid lipid/polymer vesicles, then used these methods in **Chapter 4** to determine the relationship between protein folding and membrane area expansion modulus (K_A), a metric of membrane elasticity. We demonstrated a connection between membrane K_A and membrane defects in membrane protein folding where decreased K_A and more defects enhance MscL folding. These findings demonstrate the impact of non-natural amphiphiles in understanding membrane elastic properties as they alter the membrane in unique ways which gives rise to findings which reveal how these properties influence biological function. In addition, non-natural amphiphiles are not expected to directly interact with proteins in the same way as lipids which further probes the effect of global membrane properties on protein folding rather than specific, local binding interactions.

Our results highlight the importance of an optimized membrane environment for protein folding, which supports the presence specialized organelles found in cells which have unique membrane compositions (64). The endoplasmic reticulum (ER) of eukaryotic cells is proposed to have relatively low cholesterol concentrations, which is expected to lead to a softer membrane (6). This observation highlights the potential importance of membrane elasticity in membrane protein folding within the ER, which supports our findings

outlined in **Chapter 4**. In conclusion, we used non-natural amphiphiles to elucidate the role of membrane K_A and membrane defects in co-translational membrane protein folding, which may mimic the effect of membrane properties on protein folding in ER.

Polyunsaturated fatty acids reduce membrane elastic moduli

Cellular membrane composition is important for cellular function and membrane properties are proposed to play a general role in the concerted behaviors of a cell. Although the membrane-stiffening effect of cholesterol is well-characterized (6, 178), the presence and importance of an amphiphile which has the opposite effect on membrane properties is yet to be determined. To address this question, we turned to polyunsaturated fatty acids, which are often found in bacteria and sea life that inhabit environments with low temperature conditions (40, 207). Polyunsaturated fatty acids are proposed to play a role in maintaining fluid membranes at extreme cold temperatures, yet the impact of these amphiphiles on membrane properties has not been characterized. In **Chapter 5**, we demonstrated the effect of fatty acids on three membrane properties, the apparent area expansion modulus (K_{app}), bending stiffness (k_c), and fluidity. We determined that the single-chain nature and small carboxyl headgroup of fatty acids or the location of unsaturated bonds along the carboxyl chain do not impact K_{app} . Next, we found that fatty acids with three or more unsaturated bonds decrease membrane K_{app} in membranes without cholesterol or with low concentrations of cholesterol. These results suggest that polyunsaturated fatty acids generally soften membranes through chain polyunsaturation.

Finally, we demonstrated that when membranes contained high amounts of cholesterol, the identity of the fatty acid was important in the effect on K_{app} but not k_c or fluidity. These findings revealed a relationship between lipid-lipid phase separation within the membrane which was induced by a specific polyunsaturated fatty acid. These results revealed that in the presence of phase separation, the overall K_{app} of the membrane is more similar to a membrane without cholesterol, suggesting an importance of cholesterol distribution in

global membrane properties. Together, our findings highlight the importance of fatty acids in decreasing membrane K_{app} and implicating them in a role of promoting or decreasing cholesterol phase separation within the membranes. In addition, our results highlight that membrane properties are not always equal to the sum of their parts and demonstrate a role of lipid heterogeneity in cellular membranes for the regulation of membrane properties.

Membrane elastic properties are important for mechanosensitive channel function

Mechanosensitive channels are activated by force-from-lipids mediated by membrane tension, which is proposed to be modulated by membrane mechanical properties. Despite the connection between membrane properties and membrane tension, the impact of specific membranes properties in force-from-lipids activation has not been demonstrated directly. The challenge of elucidating this relationship is likely due to the confounding changes in membranes properties that are induced by natural lipids. Studies using natural lipids were unable to isolate the role of membrane elastic properties away from membrane hydrophobic thickness, which is currently the dominating membrane feature implicated in mechanosensitive channel activation (24, 27, 250). We overcame this challenge in **Chapter 7** using a non-natural amphiphile, poloxamer, to demonstrate a role between membrane mechanical properties, K_A and k_c , and mechanosensitive channel activation.

We first determined the relationship between poloxamer concentration and MscL activation and found that increasing poloxamer concentration desensitized MscL. We then directly measured membrane K_A and k_c using micropipette aspiration techniques and determined that poloxamers generally decrease these moduli. This was an important finding as most studies of mechanosensitive channels which discuss the implications of membrane mechanics in channel function do not measure membrane properties directly. In these studies, we also demonstrated that poloxamer increases membrane surface area but not membrane thickness, which directly implicates K_A and k_c in MscL activation for the first time. We then demonstrated

that this relationship also affects the activation of a neuronal mechanosensitive channel, mTrek1. These findings demonstrate a connection between bacterial and eukaryotic mechanosensitive channels which are modulated by membrane K_A and k_c . Our findings also support the developing hypothesis that global membrane properties (8), rather than local binding interactions, are important for cellular mechanosensation.

8.3 Future work

Membrane composition and membrane mechanical properties

Although a basic understanding of how membrane lipids modulate model membrane mechanical properties has been established over decades, the effect of specific lipids in membranes with compositional complexity like cell membranes needs to be further elucidated. Our work in **Chapter 5** along with recent evidence suggests that combinations of lipids can lead to unique membrane properties due to lipid phase separation within the bilayer (46–48). Future work will continue to determine how mixtures of lipids alter membrane properties, using classical techniques such as micropipette aspiration of model and cell-extracted membranes such as GPMVs (249, 251).

Membrane properties are hypothesized to be important for force-transmission to embedded channels. Recent evidence suggests the propagation of membrane tension differs based on cell type and location within the cell. This relationship is believed to be driven by the organization of membrane proteins within the plasma membrane (1, 252). One feature of the membrane that remains to be explored further is the propagation of membrane tension in the presence of lipid rafts and to what extent lipid rafts mediate tension propagation. We demonstrated that in a system which is expected to cluster cholesterol, the effective change in membrane properties was altered in the presence of seemingly similar membrane compositions

(46). This observation suggests a role of lipid rafts in membrane mechanical properties and tension propagation in a similar manner as the observations in protein clustering.

The role of membrane properties in membrane protein folding

Mounting evidence suggests that membrane properties play a role in membrane protein folding in the presence and absence of chaperones. This relationship suggests that interactions between the membrane and a folding protein are important for folding. Eukaryotic cells compartmentalize this process and it is hypothesized that the membrane composition of the endoplasmic reticulum is specialized for protein folding and oligomerization (72). However, the understanding of this process within cells remains poorly understood. Future work on protein folding will begin to assess how this process functions within cells and more directly demonstrate how the membrane mediates protein folding within eukaryotic cells. Some studies that could begin to address membrane protein folding *in vitro* could involve the cell-free expression of proteins in a more native-like ER membrane composition either using model membranes or Giant Endoplasmic Reticulum Vesicles (GERVs) (253). These future studies should begin to address the question of the importance of ER membrane composition through altering the membrane composition of the ER using amphiphiles which can insert externally such as cholesterol and non-esterified fatty acids or by producing GERVs from cells of disease models which exhibit inefficient protein folding or have changes in metabolic processing of membrane lipids. In conclusion, future studies of Eukaryotic protein folding will address outstanding questions of how membrane composition impacts protein folding through concerted behaviors with chaperones.

While eukaryotic cells compartmentalize the process of protein folding, bacteria lack this level of organization. Without compartmentalization, the question of how bacteria are able to fold proteins efficiently in their plasma membranes remains an outstanding question as the ideal membrane composition for proper folding and function of a membrane protein is likely not the same. One possible way bacteria may facilitate

protein folding in their plasma membrane is through the organization of membrane lipids using lipid rafts (75). Like eukaryotic systems, a robust method to measure membrane protein folding within a bacterial cell has not been developed. Future studies of protein folding in bacteria will include the development of such a method for the detection of membrane protein folding *in vivo*. However, this has been a challenge to date as changes in protein folding rates are linked to changes in metabolism and the rate of protein production. These studies can also determine the localization of chaperones in either raft or non-raft domains in membranes to further uncover where and how membrane proteins fold in bacterial cells. In addition, bacteria may be the ideal system to determine the role of lipid rafts in protein folding. Together, future studies of membrane protein folding in bacteria will begin to outline a method for studying protein folding *in vivo* as well as elucidate the role of lipid rafts and local membrane composition during membrane protein folding.

The relationship between mechanosensitive channels and membrane mechanical properties

One major question yet to be answered is understanding if all mechanosensitive channels function through a conserved mechanism. It was proposed that mechanosensitive channels sense bilayer elasticity and tension which supports a mechanism which connects the behavior of mechanosensitive channels (23, 237). However, recent structural studies support various intermediate states of mechanosensitive channels such as closed, open, intermediate (254), and an inactivated state distinct from the closed state. In addition, some channels have programmed closing behavior such as Piezo1 and MscS which enter an inactivated state (255, 256), while other channels such as MscL, have not demonstrated this behavior. Despite these differences in channel inactivation, channels in either of these groups have been shown to be activated through pocket delipidation (25, 257). It is reasonable that while these channels have differences in their structural dynamics, there is a connection between these channels as they are all gated through membrane tension (178, 190). Remarkably, in **Chapter 7** we demonstrated that a simple bacterial mechanosensitive channel and a eukaryotic neuronal mechanosensitive channel are sensitive to changes in membrane properties. In

addition, similar findings have been observed in the presence of fatty acids and different eukaryotic mechanosensitive channels where polyunsaturated fatty acids activate various mechanosensitive channels (8, 27, 31, 34). These findings further connect mechanosensitive channel behavior across the domains of life. Future work should address these questions using various structural and biophysical techniques to determine if there is a true connection between all mechanosensitive channels through membrane tension and the mechanism behind these activation alterations. In addition, future studies will further probe the force-from-lipids mechanism in mechanosensitive channels which have cytoskeletal attachments (2) to determine if this mechanism applies to all mechanosensitive channels.

It is believed that the bilayer primarily regulates mechanosensitive channel behavior. When comparing the lipid environment of different cells, it is logical that they have different material properties as each cell type has specific functions and is exposed to different degrees of external stressors. For example, when comparing the function of a mechanosensitive channel in neuronal cells and endothelial cells, different systems may benefit from different membrane properties i.e., endothelial cells benefit from EPA, but neuronal cells benefit from DHA, and this may be due to preference for differing membrane thickness or preference to certain properties. A simple example of this idea was carried out in bacterial membranes and demonstrated that bacterial mechanosensitive channels have differing behavior based on bacterial cell type (195). An example of possible future studies on this topic may include demonstrating the effect of protein function in a neuronal cell compared to an endothelial cell or comparing neuronal mechanosensitive channels such as TRAAK to endothelial mechanosensitive channels, such as Piezo1 and demonstrating if each channel prefers certain membrane compositions. Furthermore, a lipidomic map and an understanding of the physical properties cell membranes based on cell type will advance the understanding of mechanosensation through this mechanism.

Membrane composition and the behavior of predominantly non-mechanosensitive membrane proteins

While all membrane embedded channels may not be mechanically gated, it is believed that all channels are sensitive to membrane properties to some extent (4). Membrane proteins are surrounded by a complex lipid environment and the lipid pressure profile is important to the structure and function of these channels. Therefore, it is possible that such proteins would react to changes in their environment which supports this structure. Towards this idea, GPCRs are hypothesized to alter raft location within the membrane depending on membrane fatty acid content (77). It remains to be answered whether this behavior has implications on GPCR function or if this sheds light on a preference for a specific lipid environment.

The example of GPCRs altering their raft localization highlights a physical preference for one protein to a certain lipid composition. One question that remains further to be answered is if protein organization alters membrane protein function through specific or non-specific interactions with lipids. Generally, to what extent do membrane global and local properties impact protein function. This question is largely unexplored due to challenges in isolating specific properties, but the micropipette aspiration technique has the power to answer a portion of this question. To address the local environment of the protein, there are various biophysical assays which can be used, including but not limited to, ITC or NMR and FRAP to probe direct binding of lipids or the mobility of certain lipids. In addition, as membrane and protein structural techniques continue to improve, these questions will increasingly be more straightforward to answer.

Finally, the question of the mechanism and importance of protein sorting within a cell remains to be further elucidated. As proteins fold and are trafficked to various locations within the cell, there is a general trend where membranes become thicker and more rigid (64, 111). There appears to be a physical and functional rationale behind protein sorting within cells, such as protein folding in softer membranes (10, 72), but the contribution of physical interactions compared to biological sorting mechanisms remain poorly understood. Various *in vitro* studies have begun to address these questions (56), and future studies will likely continue

to deepen our understanding of how cells control where proteins localize within a cell and why proteins are sorted to different membranes for their final function.

References

1. Shi Z, Innes-Gold S, Cohen AE (2022) Membrane tension propagation couples axon growth and collateral branching. *bioRxiv*:2022.01.09.475560.
2. Martinac B, et al. (2020) *Cell membrane mechanics and mechanosensory transduction* (Elsevier Inc.). 1st Ed. doi:10.1016/bs.ctm.2020.08.002.
3. Brown MS, Radhakrishnan A, Goldstein JL (2018) Retrospective on Cholesterol Homeostasis: The Central Role of Scap. <https://doi.org/10.1146/annurev-biochem-062917-011852> 87:783–807.
4. Yoshimura K, Sokabe M (2010) Mechanosensitivity of ion channels based on protein-lipid interactions. *J R Soc Interface* 7(SUPPL. 3). doi:10.1098/rsif.2010.0095.focus.
5. Symons JL, et al. (2021) Lipidomic atlas of mammalian cell membranes reveals hierarchical variation induced by culture conditions, subcellular membranes, and cell lineages. *Soft Matter* 17(2):288–297.
6. Rawicz W, Smith BA, McIntosh TJ, Simon SA, Evans E (2008) Elasticity, Strength, and Water Permeability of Bilayers that Contain Raft Microdomain-Forming Lipids. *Biophys J* 94(12):4725–4736.
7. Rawicz W, Olbrich KC, McIntosh T, Needham D, Evans E (2000) Effect of Chain Length and Unsaturation on Elasticity of Lipid Bilayers. *Biophys J* 79(1):328–339.
8. Bruno MJ, Koeppe RE, Andersen OS (2007) Docosahexaenoic acid alters bilayer elastic properties. *Proc Natl Acad Sci* 104(23):9638–9643.
9. Bermudez H, Brannan AK, Hammer DA, Bates FS, Discher DE (2002) Molecular Weight Dependence of Polymersome Membrane Structure, Elasticity, and Stability. *Macromolecules* 35(21):8203–8208.
10. Jacobs ML, Boyd MA, Kamat NP (2019) Diblock copolymers enhance folding of a mechanosensitive membrane protein during cell-free expression. *Proc Natl Acad Sci* 116(10):4031–4036.
11. Großkopf S, Fouquet P, Wiehemeier L, Hellweg T (2021) Pluronic-based lamellar phases: influence

- of polymer architecture on bilayer bending elasticity. *Mol Phys* 119(15–16). doi:10.1080/00268976.2021.1893400.
12. Harris NJ, et al. (2017) Structure formation during translocon-unassisted co-translational membrane protein folding. *Sci Rep* 7(1):8021.
 13. Cymer F, von Heijne G, White SH (2015) Mechanisms of Integral Membrane Protein Insertion and Folding. *J Mol Biol* 427(5):999–1022.
 14. Marsh D, Shanmugavadivu B, Kleinschmidt JH (2006) Membrane Elastic Fluctuations and the Insertion and Tilt of β -Barrel Proteins. *Biophys J* 91(1):227–232.
 15. Berrier C, et al. (2011) Coupled cell-free synthesis and lipid vesicle insertion of a functional oligomeric channel MscL. *Biochim Biophys Acta - Biomembr* 1808(1):41–46.
 16. Eaglesfield R, Madsen MA, Sanyal S, Reboud J, Amtmann A (2021) Cotranslational recruitment of ribosomes in protocells recreates a translocon-independent mechanism of proteorhodopsin biogenesis. *iScience* 24(5):102429.
 17. Ulmschneider MB, et al. (2014) Spontaneous transmembrane helix insertion thermodynamically mimics translocon-guided insertion. *Nat Commun* 5(1):4863.
 18. Allen SJ, Curran AR, Templer RH, Meijberg W, Booth PJ (2004) Controlling the Folding Efficiency of an Integral Membrane Protein. *J Mol Biol* 342(4):1293–1304.
 19. Van Meer G, Voelker DR, Feigenson GW (2008) Membrane lipids: Where they are and how they behave. *Nat Rev Mol Cell Biol* 9(2):112–124.
 20. Árnadóttir J, Chalfie M (2010) Eukaryotic Mechanosensitive Channels. *Annu Rev Biophys* 39(1):111–137.
 21. Chang G, Spencer RH, Lee AT, Barclay MT, Rees DC (1998) Structure of the MscL homolog from *Mycobacterium tuberculosis*: A gated mechanosensitive ion channel. *Science* (80-) 282(5397):2220–2226.
 22. Reddy B, Bavi N, Lu A, Park Y, Perozo E (2019) Molecular basis of force-from-lipids gating in the mechanosensitive channel mscs. *Elife* 8:1–24.

23. Cox CD, Zhang Y, Zhou Z, Walz T, Martinac B (2021) Cyclodextrins increase membrane tension and are universal activators of mechanosensitive channels. *Proc Natl Acad Sci U S A* 118(36). doi:10.1073/pnas.2104820118.
24. Nomura T, et al. (2012) Differential effects of lipids and lyso-lipids on the mechanosensitivity of the mechanosensitive channels MscL and MscS. *Proc Natl Acad Sci* 109(22):8770–8775.
25. Flegler VJ, et al. (2021) Mechanosensitive channel gating by delipidation. *Proc Natl Acad Sci U S A* 118(33):1–8.
26. Xue F, et al. (2020) Membrane stiffness is one of the key determinants of E. coli MscS channel mechanosensitivity. *Biochim Biophys Acta - Biomembr* 1862(5):183203.
27. Ridone P, et al. (2018) “Force-from-lipids” gating of mechanosensitive channels modulated by PUFAs. *J Mech Behav Biomed Mater* 79:158–167.
28. Heureaux J, Chen D, Murray VL, Deng CX, Liu AP (2014) Activation of a Bacterial Mechanosensitive Channel in Mammalian Cells by Cytoskeletal Stress. *Cell Mol Bioeng* 7(3):307–319.
29. Coste B, et al. (2010) Piezo1 and Piezo2 are essential components of distinct mechanically activated cation channels. *Science (80-)* 330(6000):55–60.
30. Beech DJ, Kalli AC (2019) Force Sensing by Piezo Channels in Cardiovascular Health and Disease. *Arterioscler Thromb Vasc Biol* 39:00–00(November):1–12.
31. Romero LO, et al. (2019) Dietary fatty acids fine-tune Piezo1 mechanical response. *Nat Commun* 10(1):1200.
32. Ridone P, et al. (2020) Disruption of membrane cholesterol organization impairs the activity of PIEZO1 channel clusters. *J Gen Physiol* 152(8). doi:10.1085/jgp.201912515.
33. Toft-Bertelsen TL, MacAulay N (2021) TRPping on Cell Swelling - TRPV4 Senses It. *Front Immunol* 12:3757.
34. Brohawn SG, Su Z, MacKinnon R (2014) Mechanosensitivity is mediated directly by the lipid membrane in TRAAK and TREK1 K⁺ channels. *Proc Natl Acad Sci* 111(9):3614–3619.
35. Van Meer G, De Kroon AIPM (2011) Lipid map of the mammalian cell. *J Cell Sci* 124(1):5–8.

36. Vance JE (2015) Phospholipid Synthesis and Transport in Mammalian Cells. *Traffic* 16(1):1–18.
37. Chwastek G, et al. (2020) Principles of Membrane Adaptation Revealed through Environmentally Induced Bacterial Lipidome Remodeling. *Cell Rep* 32(12). doi:10.1016/j.celrep.2020.108165.
38. Sampath H, Ntambi JM (2005) POLYUNSATURATED FATTY ACID REGULATION OF GENES OF LIPID METABOLISM. <http://dx.doi.org/10.1146/annurev.nutr.25051804101917> 25:317–340.
39. Magnuson K, Jackowski S, Rock CO, Cronan JEJ (1993) Regulation of fatty acid biosynthesis in *Escherichia coli*. *Microbiol Mol Biol Rev* 57(3):522–542.
40. Kawamoto J, et al. (2009) Eicosapentaenoic acid plays a beneficial role in membrane organization and cell division of a cold-adapted bacterium, *Shewanella livingstonensis* Ac10. *J Bacteriol* 191(2):632–640.
41. Levental KR, et al. (2020) Lipidomic and biophysical homeostasis of mammalian membranes counteracts dietary lipid perturbations to maintain cellular fitness. *Nat Commun* 11(1). doi:10.1038/s41467-020-15203-1.
42. Rowlett VW, et al. (2017) The impact of membrane phospholipid alterations in *Escherichia coli* on cellular function. *J Bacteriol* 199(13):1–22.
43. Sych T, Mély Y, Römer W (2018) Lipid self-assembly and lectin-induced reorganization of the plasma membrane. *Philos Trans R Soc B Biol Sci* 373(1747). doi:10.1098/RSTB.2017.0117.
44. Olbrich K, Rawicz W, Needham D, Evans E (2000) Water permeability and mechanical strength of polyunsaturated lipid bilayers. *Biophys J* 79(1):321–327.
45. Koenig BW, Strey HH, Gawrisch K (1997) Membrane lateral compressibility determined by NMR and X-ray diffraction: Effect of acyl chain polyunsaturation. *Biophys J* 73(4):1954–1966.
46. Jacobs ML, Faizi HA, Peruzzi JA, Vlahovska PM, Kamat NP (2021) EPA and DHA differentially modulate membrane elasticity in the presence of cholesterol. *Biophys J* 120(11):2317–2329.
47. Mason RP, Jacob RF, Shrivastava S, Sherratt SCR, Chattopadhyay A (2016) Eicosapentaenoic acid reduces membrane fluidity, inhibits cholesterol domain formation, and normalizes bilayer width in atherosclerotic-like model membranes. *Biochim Biophys Acta - Biomembr* 1858(12):3131–3140.

48. Sherratt SCR, Mason RP (2018) Eicosapentaenoic acid and docosahexaenoic acid have distinct membrane locations and lipid interactions as determined by X-ray diffraction. *Chem Phys Lipids* 212:73–79.
49. Demirbolat GM, Coskun GP, Erdogan O, Cevik O (2021) Long chain fatty acids can form aggregates and affect the membrane integrity. *Colloids Surfaces B Biointerfaces* 204(April):111795.
50. Schroeder F, Woodford JK, Kavecansky J, Wood WG, Joiner C (1995) Cholesterol domains in biological membranes. *Mol Membr Biol* 12(1):113–119.
51. Pan J, Tristram-Nagle S, Nagle JF (2009) Effect of cholesterol on structural and mechanical properties of membranes depends on lipid chain saturation. *Phys Rev E - Stat Nonlinear, Soft Matter Phys* 80(2):021931.
52. Kelley EG, Butler PD, Nagao M (2020) Scaling Relationships for the Mechanical Properties of Mixed Lipid Membranes. *Biophys J* 118(3):85a.
53. Gracià RS, Bezlyepkina N, Knorr RL, Lipowsky R, Dimova R (2010) Effect of cholesterol on the rigidity of saturated and unsaturated membranes: fluctuation and electrodeformation analysis of giant vesicles. *Soft Matter* 6(7):1472.
54. Onuki Y, Morishita M, Chiba Y, Tokiwa S, Takayama K (2006) Docosahexaenoic Acid and Eicosapentaenoic Acid Induce Changes in the Physical Properties of a Lipid Bilayer Model Membrane. *Chem Pharm Bull (Tokyo)* 54(1):68–71.
55. Vitkova V, et al. (2020) Elasticity and phase behaviour of biomimetic membrane systems containing tetraether archaeal lipids. *Colloids Surfaces A Physicochem Eng Asp* (April):124974.
56. Peruzzi JA, Jacobs ML, Vu TQ, Wang KS, Kamat NP (2019) Barcoding Biological Reactions with DNA-Functionalized Vesicles. *Angew Chemie - Int Ed* 58(51):18683–18690.
57. Clarke JH (2003) Lipid Signalling: Picking Out the PIPs. *Curr Biol* 13(20):815–817.
58. Unsay JD, Cosentino K, Subburaj Y, García-Sáez AJ (2013) Cardiolipin effects on membrane structure and dynamics. *Langmuir* 29(51):15878–15887.
59. Georgieva R, et al. (2015) Docosahexaenoic acid promotes micron scale liquid-ordered domains. A

- comparison study of docosahexaenoic versus oleic acid containing phosphatidylcholine in raft-like mixtures. *Biochim Biophys Acta - Biomembr* 1848(6):1424–1435.
60. Levental KR, et al. (2016) Polyunsaturated lipids regulate membrane domain stability by tuning membrane order. *Biophys J* 110(8):1800–1810.
 61. Kinnun JJ, Bittman R, Shaikh SR, Wassall SR (2018) DHA Modifies the Size and Composition of Raftlike Domains: A Solid-State ²H NMR Study. *Biophys J* 114(2):380–391.
 62. Mansilla MC, Cybulski LE, Albanesi D, De Mendoza D (2004) Control of membrane lipid fluidity by molecular thermosensors. *J Bacteriol* 186(20):6681–6688.
 63. Shaikh SR, LoCascio DS, Soni SP, Wassall SR, Stillwell W (2009) Oleic- and docosahexaenoic acid-containing phosphatidylethanolamines differentially phase separate from sphingomyelin. *Biochim Biophys Acta - Biomembr* 1788(11):2421–2426.
 64. Sharpe HJ, Stevens TJ, Munro S (2010) A Comprehensive Comparison of Transmembrane Domains Reveals Organelle-Specific Properties. *Cell* 142(1):158–169.
 65. Dorrance AM, Graham D, Webb RC, Fraser R, Dominiczak A (2001) Increased membrane sphingomyelin and arachidonic acid in stroke-prone spontaneously hypertensive rats. *Am J Hypertens* 14(11):1149–1153.
 66. Tierney KJ, Block DE, Longo ML (2005) Elasticity and phase behavior of DPPC membrane modulated by cholesterol, ergosterol, and ethanol. *Biophys J* 89(4):2481–2493.
 67. Ariola FS, Li Z, Cornejo C, Bittman R, Heikal AA (2009) Membrane fluidity and lipid order in ternary giant unilamellar vesicles using a new bodipy-cholesterol derivative. *Biophys J* 96(7):2696–2708.
 68. Heberle FA, Wu J, Goh SL, Petruzielo RS, Feigenson GW (2010) Comparison of three ternary lipid bilayer mixtures: FRET and ESR reveal nanodomains. *Biophys J* 99(10):3309–3318.
 69. Veatch SL, Keller SL (2003) Separation of Liquid Phases in Giant Vesicles of Ternary Mixtures of Phospholipids and Cholesterol. *Biophys J* 85(5):3074–3083.
 70. Suga K, Umakoshi H (2013) Detection of nanosized ordered domains in DOPC/DPPC and DOPC/CH binary lipid mixture systems of large unilamellar vesicles using a TEMPO quenching

- method. *Langmuir* 29(15):4830–4838.
71. Ernst R, Ejsing CS, Antonny B (2016) Homeoviscous Adaptation and the Regulation of Membrane Lipids. *J Mol Biol* 428(24):4776–4791.
 72. Braakman I, Hebert DN (2013) Protein folding in the endoplasmic reticulum. *Cold Spring Harb Perspect Biol* 5(5):a013201.
 73. Ammendolia DA, Bement WM, Brumell JH (2021) Plasma membrane integrity: implications for health and disease. *BMC Biol* 19(1):1–29.
 74. Lorent JH, et al. (2020) Plasma membranes are asymmetric in lipid unsaturation, packing and protein shape. *Nat Chem Biol* 16(6):644–652.
 75. Bramkamp M, Lopez D (2015) Exploring the Existence of Lipid Rafts in Bacteria. *Microbiol Mol Biol Rev* 79(1):81–100.
 76. Li G, Wang Q, Kakuda S, London E (2020) Nanodomains can persist at physiologic temperature in plasma membrane vesicles and be modulated by altering cell lipids. *J Lipid Res* 61(5):758–766.
 77. Javanainen M, et al. (2019) Reduced level of docosahexaenoic acid shifts GPCR neuroreceptors to less ordered membrane regions. *PLoS Comput Biol* 15(5):e1007033.
 78. Simons K, Sampaio JL (2011) Membrane organization and lipid rafts. *Cold Spring Harb Perspect Biol* 3(10):1–17.
 79. Wassall SR, Stillwell W (2008) Docosahexaenoic acid domains: the ultimate non-raft membrane domain. *Chem Phys Lipids* 153(1):57–63.
 80. Javanainen M, Martinez-Seara H, Vattulainen I (2017) Nanoscale Membrane Domain Formation Driven by Cholesterol. *Sci Rep* 7(1). doi:10.1038/s41598-017-01247-9.
 81. Oglecka K, Rangamani P, Liedberg B, Kraut RS, Parikh AN (2014) Oscillatory phase separation in giant lipid vesicles induced by transmembrane osmotic differentials. *Elife* 3:e03695.
 82. Breslow DK (2013) Sphingolipid homeostasis in the endoplasmic reticulum and beyond. *Cold Spring Harb Perspect Biol* 5(4):1–16.
 83. Ackerman DG, Feigensohn GW (2015) Lipid bilayers: clusters, domains and phases. *Essays*

- Biochem* 57(12):33–42.
84. Kollmitzer B, Heftberger P, Podgornik R, Nagle JF, Pabst G (2015) Bending Rigidities and Interdomain Forces in Membranes with Coexisting Lipid Domains. *Biophys J* 108(12):2833–2842.
 85. Tian A, Johnson C, Wang W, Baumgart T (2007) Line tension at fluid membrane domain boundaries measured by micropipette aspiration. *Phys Rev Lett* 98(20). doi:10.1103/PhysRevLett.98.208102.
 86. Hong H (2015) Role of Lipids in Folding, Misfolding and Function. *Lipids in Protein Misfolding*, pp 1–32.
 87. Engelman DM, Steitz TA (1981) The Spontaneous Insertion of Proteins into and across Membranes: The Helical Hairpin Hypothesis. *Cell* 23:411–422.
 88. Kamel M, Löwe M, Schott-Verdugo S, Gohlke H, Kedrov A (2022) Unsaturated fatty acids augment protein transport via the SecA:SecYEG translocon. *FEBS J* 289(1):140–162.
 89. Maurya SR, Chaturvedi D, Mahalakshmi R (2013) Modulating lipid dynamics and membrane fluidity to drive rapid folding of a transmembrane barrel. *Sci Rep* 3:1–6.
 90. Booth PJ, et al. (2001) In Vitro Studies of Membrane Protein Folding. *Crit Rev Biochem Mol Biol* 36(6):501–603.
 91. Harris NJ, Charalambous K, Findlay HE, Booth PJ (2018) Lipids modulate the insertion and folding of the nascent chains of alpha helical membrane proteins. *Biochem Soc Trans* 46(5):1355–1366.
 92. Booth PJ, et al. (1997) Evidence That Bilayer Bending Rigidity Affects Membrane Protein Folding. *Biochemistry* 36(1):197–203.
 93. Curran AR, Templer RH, Booth PJ (1999) Modulation of folding and assembly of the membrane protein bacteriorhodopsin by intermolecular forces within the lipid bilayer. *Biochemistry* 38(29):9328–9336.
 94. Sanders MR, Findlay HE, Booth PJ (2018) Lipid bilayer composition modulates the unfolding free energy of a knotted α -helical membrane protein. *Proc Natl Acad Sci* 115(8):E1799–E1808.
 95. Herrmann M, Danielczak B, Textor M, Klement J, Keller S (2015) Modulating bilayer mechanical properties to promote the coupled folding and insertion of an integral membrane protein. *Eur*

- Biophys J* 44(7):503–512.
96. Barrera FN, Fendos J, Engelman DM (2012) Membrane physical properties influence transmembrane helix formation. *Proc Natl Acad Sci* 109(36):14422–14427.
 97. Kalmbach R, et al. (2007) Functional Cell-free Synthesis of a Seven Helix Membrane Protein: In situ Insertion of Bacteriorhodopsin into Liposomes. *J Mol Biol* 371(3):639–648.
 98. Baumann A, et al. (2016) In-Situ Observation of Membrane Protein Folding during Cell-Free Expression. *PLoS One* 11(3):e0151051.
 99. Halbleib K, et al. (2017) Activation of the Unfolded Protein Response by Lipid Bilayer Stress. *Mol Cell* 67(4):673–684.e8.
 100. Robblee MM, et al. (2016) Saturated Fatty Acids Engage an IRE1 α -Dependent Pathway to Activate the NLRP3 Inflammasome in Myeloid Cells. *Cell Rep* 14(11):2611–2623.
 101. Katsov K, Müller M, Schick M (2004) Field theoretic study of bilayer membrane fusion. I. Hemifusion mechanism. *Biophys J* 87(5):3277–3290.
 102. Lei K, et al. (2021) Cancer-cell stiffening via cholesterol depletion enhances adoptive T-cell immunotherapy. *Nat Biomed Eng* 5(12):1411–1425.
 103. Nikolaev YA, et al. (2019) Mammalian TRP ion channels are insensitive to membrane stretch. *J Cell Sci* 132(23). doi:10.1242/JCS.238360/266180/AM/MAMMALIAN-TRP-ION-CHANNELS-ARE-INSENSITIVE-TO.
 104. Caires R, et al. (2017) Omega-3 Fatty Acids Modulate TRPV4 Function through Plasma Membrane Remodeling. *Cell Rep* 21(1):246–258.
 105. Bavi N, Richardson J, Heu C, Martinac B, Poole K (2019) PIEZO1-Mediated Currents Are Modulated by Substrate Mechanics. doi:10.1021/acsnano.9b07499.
 106. Balleza D (2012) Mechanical properties of lipid bilayers and regulation of mechanosensitive function: From biological to biomimetic channels. *Channels* 6(4):220–233.
 107. Levin G, Blount P (2004) Cysteine Scanning of MscL Transmembrane Domains Reveals Residues Critical for Mechanosensitive Channel Gating. *Biophys J* 86(5):2862–2870.

108. Yeaman C (2007) Protein Trafficking in the Exocytic Pathway of Polarized Epithelial Cells. *Protein Traffick Neurons* 11(12):271–303.
109. Heinrich M, Tian A, Esposito C, Baumgart T (2010) Dynamic sorting of lipids and proteins in membrane tubes with a moving phase boundary. *Proc Natl Acad Sci U S A* 107(16):7208–7213.
110. McIntosh TJ, Vidal A, Simon SA (2003) Sorting of lipids and transmembrane peptides between detergent-soluble bilayers and detergent-resistant rafts. *Biophys J* 85(3):1656–1666.
111. McIntosh TJ, Simon SA (2006) Roles of bilayer material properties in function and distribution of membrane proteins. *Annu Rev Biophys Biomol Struct* 35:177–98.
112. Gohrbandt M, et al. (2022) Low membrane fluidity triggers lipid phase separation and protein segregation in living bacteria. *EMBO J*:1–21.
113. Grage SL, et al. (2011) Bilayer-mediated clustering and functional interaction of MscL channels. *Biophys J* 100(5):1252–1260.
114. Dumitru AC, et al. (2021) Probing PIEZO1 Localization upon Activation Using High-Resolution Atomic Force and Confocal Microscopy. *Nano Lett* 21(12):4950–4958.
115. Jacobs ML, Boyd MA, Kamat NP (2019) Diblock copolymers enhance folding of a mechanosensitive membrane protein during cell-free expression. *Proc Natl Acad Sci* 116(10):4031–4036.
116. Kowal J, Wu D, Mikhalevich V, Palivan CG, Meier W (2015) Hybrid polymer-lipid films as platforms for directed membrane protein insertion. *Langmuir* 31(17):4868–4877.
117. Beales PA, Khan S, Muench SP, Jeuken LJC (2017) Durable vesicles for reconstitution of membrane proteins in biotechnology. *Biochem Soc Trans* 45(1):15–26.
118. Allen JP (2017) Design of energy-transducing artificial cells. *Proc Natl Acad Sci* 114(15):3790–3791.
119. Koike S, Jahn R (2017) Probing and manipulating intracellular membrane traffic by microinjection of artificial vesicles. *Proc Natl Acad Sci* 114(46):E9883–E9892.
120. Noireaux V, Libchaber A (2004) A vesicle bioreactor as a step toward an artificial cell assembly. *Proc Natl Acad Sci* 101(51):17669–17674.
121. Osaki T, Takeuchi S (2017) Artificial Cell Membrane Systems for Biosensing Applications. *Anal*

- Chem* 89(1):216–231.
122. Lentini R, et al. (2014) Integrating artificial with natural cells to translate chemical messages that direct *E. coli* behaviour. *Nat Commun* 5(1):4012.
 123. Ma X, Song Q, Gao X (2018) Reconstituted high-density lipoproteins: novel biomimetic nanocarriers for drug delivery. *Acta Pharm Sin B* 8(1):51–63.
 124. Kumar M, Grzelakowski M, Zilles J, Clark M, Meier W (2007) Highly permeable polymeric membranes based on the incorporation of the functional water channel protein Aquaporin Z. *Proc Natl Acad Sci* 104(52):20719–20724.
 125. Hediger MA, et al. (2004) The ABCs of solute carriers: physiological, pathological and therapeutic implications of human membrane transport proteins. *Pflugers Arch Eur J Physiol Arch Eur J Physiol* 447(5):465–468.
 126. Discher BM, et al. (1999) Polymersomes: Tough Vesicles Made from Diblock Copolymers. *Science* (80-) 284(5417):1143–1146.
 127. de Hoog H-PM, Lin JieRong EM, Banerjee S, Décaillot FM, Nallani M (2014) Conformational Antibody Binding to a Native, Cell-Free Expressed GPCR in Block Copolymer Membranes. *PLoS One* 9(10):e110847.
 128. Zaba C, et al. (2015) Functional Cell Adhesion Receptors (Integrins) in Polymeric Architectures. *ChemBioChem* 16(12):1740–1743.
 129. Hu Z, Ho JCS, Nallani M (2017) Synthetic (polymer) biology (membrane): functionalization of polymer scaffolds for membrane proteins. *Curr Opin Biotechnol* 46:51–56.
 130. Schulz M, Binder WH (2015) Mixed Hybrid Lipid/Polymer Vesicles as a Novel Membrane Platform. *Macromol Rapid Commun* 36(23):2031–2041.
 131. Lim SK, de Hoog HP, Parikh AN, Nallani M, Liedberg B (2013) Hybrid, nanoscale phospholipid/block copolymer vesicles. *Polymers (Basel)* 5(3):1102–1114.
 132. Shinoda T, et al. (2016) Cell-free methods to produce structurally intact mammalian membrane proteins. *Sci Rep* 6(1):30442.

133. Okano T, Matsuura T, Suzuki H, Yomo T (2014) Cell-free protein synthesis in a microchamber revealed the presence of an optimum compartment volume for high-order reactions. *ACS Synth Biol* 3(6):347–352.
134. Kuruma Y, Ueda T (2015) The PURE system for the cell-free synthesis of membrane proteins. *Nat Protoc* 10(9):1328–1344.
135. Geertsma ER, Nik Mahmood NAB, Schuurman-Wolters GK, Poolman B (2008) Membrane reconstitution of ABC transporters and assays of translocator function. *Nat Protoc* 3(2):256–266.
136. Fiori MC, et al. (2017) Polymer Nanodiscs: Discoidal Amphiphilic Block Copolymer Membranes as a New Platform for Membrane Proteins. *Sci Rep* 7(1):15227.
137. Seddon AM, Curnow P, Booth PJ (2004) Membrane proteins, lipids and detergents: not just a soap opera. *Biochim Biophys Acta - Biomembr* 1666(1–2):105–117.
138. Waldo GS, Standish BM, Berendzen J, Terwilliger TC (1999) Rapid protein-folding assay using green fluorescent protein. *Nat Biotechnol* 17(7):691–695.
139. Panganiban B, et al. (2018) Random heteropolymers preserve protein function in foreign environments. *Science (80-)* 359(6381):1239–1243.
140. Mini-Extruder Extrusion Technique *Avanti Polar Lipids*. Available at: <https://avantilipids.com/divisions/equipment-products/mini-extruder-extrusion-technique> [Accessed May 1, 2021].
141. Nam J, Beales PA, Vanderlick TK (2011) Giant Phospholipid/Block Copolymer Hybrid Vesicles: Mixing Behavior and Domain Formation. *Langmuir* 27(1):1–6.
142. Koçer A (2010) Functional Liposomal Membranes for Triggered Release. *Methods in Molecular Biology*, pp 243–255.
143. Kreimer S, Ivanov AR (2017) Rapid Isolation of Extracellular Vesicles from Blood Plasma with Size-Exclusion Chromatography Followed by Mass Spectrometry-Based Proteomic Profiling. *Extracellular Vesicles: Methods and Protocols. Methods in Molecular Biology*, eds Kuo WP, Jia S (Humana Press, New York, NY), pp 295–302.

144. Popot JL, Engelman DM (2016) Membranes Do Not Tell Proteins How to Fold. *Biochemistry* 55(1):5–18.
145. Klammt C, et al. (2006) Cell-free expression as an emerging technique for the large scale production of integral membrane protein. *FEBS J* 273(18):4141–4153.
146. Niwa T, et al. (2016) Comprehensive study of liposome-assisted synthesis of membrane proteins using a reconstituted cell-free translation system. *Sci Rep* 5(1):18025.
147. Vargo KB, Parthasarathy R, Hammer DA (2012) Self-assembly of tunable protein suprastructures from recombinant oleosin. *Proc Natl Acad Sci U S A* 109(29):11657–62.
148. Percec V, et al. (2010) Self-assembly of janus dendrimers into uniform dendrimersomes and other complex architectures. *Science (80-)* 328(5981):1009–1014.
149. Nallani M, et al. (2011) Proteopolymersomes: In vitro production of a membrane protein in polymersome membranes. *Biointerphases* 6(4):153–157.
150. Zhang X, Tanner P, Graff A, Palivan CG, Meier W (2012) Mimicking the cell membrane with block copolymer membranes. *J Polym Sci Part A Polym Chem* 50(12):2293–2318.
151. Findlay HE, Rutherford NG, Henderson PJF, Booth PJ (2010) Unfolding free energy of a two-domain transmembrane sugar transport protein. *Proc Natl Acad Sci* 107(43):18451–18456.
152. Rawlings AE (2016) Membrane proteins: always an insoluble problem? *Biochem Soc Trans* 44(3):790–795.
153. Henrich E, Hein C, Dötsch V, Bernhard F (2015) Membrane protein production in Escherichia coli cell-free lysates. *FEBS Lett* 589(15):1713–1722.
154. Nozawa A, et al. (2011) Production and partial purification of membrane proteins using a liposome-supplemented wheat cell-free translation system. *BMC Biotechnol* 11(1):35.
155. May S, et al. (2013) In vitro expressed GPCR inserted in polymersome membranes for ligand-binding studies. *Angew Chemie - Int Ed* 52(2):749–753.
156. Zapf T, et al. (2015) Synthesis and Functional Reconstitution of Light-Harvesting Complex II into Polymeric Membrane Architectures. *Angew Chemie Int Ed* 54(49):14664–14668.

157. Shenkarev ZO, et al. (2013) Lipid–protein nanodiscs promote in vitro folding of transmembrane domains of multi-helical and multimeric membrane proteins. *Biochim Biophys Acta - Biomembr* 1828(2):776–784.
158. Chang G, Spencer RH, Lee AT, Barclay MT, Rees DC (1998) Structure of the MscL Homolog from *Mycobacterium tuberculosis*: A Gated Mechanosensitive Ion Channel. *Science (80-)* 282(5397):2220–2226.
159. Yoshimura K, Batiza A, Kung C (2001) Chemically Charging the Pore Constriction Opens the Mechanosensitive Channel MscL. *Biophys J* 80(5):2198–2206.
160. Schindelin J, et al. (2012) Fiji: An open-source platform for biological-image analysis. *Nat Methods* 9(7):676–682.
161. Kamat NP, et al. (2010) A Generalized System for Photo-Responsive Membrane Rupture in Polymersomes. *Adv Funct Mater* 20(16):2588–2596.
162. Zacharias DA (2002) Partitioning of Lipid-Modified Monomeric GFPs into Membrane Microdomains of Live Cells. *Science (80-)* 296(5569):913–916.
163. Bermúdez H, Hammer DA, Discher DE (2004) Effect of Bilayer Thickness on Membrane Bending Rigidity. *Langmuir* 20(3):540–543.
164. Srinivas G, Discher DE, Klein ML (2004) Self-assembly and properties of diblock copolymers by coarse-grain molecular dynamics. *Nat Mater* 3(9):638–644.
165. Boyd MA, Kamat NP (2018) Visualizing Tension and Growth in Model Membranes Using Optical Dyes. *Biophys J* 115(7):1307–1315.
166. Lundbæk JA, Collingwood SA, Ingólfsson HI, Kapoor R, Andersen OS (2010) Lipid bilayer regulation of membrane protein function: gramicidin channels as molecular force probes. *J R Soc Interface* 7(44):373–395.
167. Otten D, Brown MF, Beyer K (2000) Softening of Membrane Bilayers by Detergents Elucidated by Deuterium NMR Spectroscopy. *J Phys Chem B* 104(51):12119–12129.
168. Needham D, Nunn RS (1990) Elastic deformation and failure of lipid bilayer membranes containing

- cholesterol. *Biophys J* 58(4):997–1009.
169. Yang Z, Galloway JA, Yu H (1999) Protein Interactions with Poly(ethylene glycol) Self-Assembled Monolayers on Glass Substrates: Diffusion and Adsorption. *Langmuir* 15(24):8405–8411.
 170. Rosilio V, Albrecht G, Okumura Y, Sunamoto J, Baszkin A (1996) Surface Properties and Miscibility of Monolayers of Dimyristoylphosphatidylcholine and Poly(Ethylene oxide) Lipids at the Water/Air Interface. *Langmuir* 12(10):2544–2550.
 171. Srinivas G, Discher DE, Klein ML (2005) Key roles for chain flexibility in block copolymer membranes that contain pores or make tubes. *Nano Lett* 5(12):2343–2349.
 172. Battaglia G, Ryan AJ (2005) Bilayers and interdigitation in block copolymer vesicles. *J Am Chem Soc* 127(24):8757–8764.
 173. Cui H, Lyman E, Voth GA (2011) Mechanism of membrane curvature sensing by amphipathic helix containing proteins. *Biophys J* 100(5):1271–1279.
 174. Vamparys L, et al. (2013) Conical lipids in flat bilayers induce packing defects similar to that induced by positive curvature. *Biophys J* 104(3):585–593.
 175. Wassall SR, Stillwell W (2009) Polyunsaturated fatty acid-cholesterol interactions: Domain formation in membranes. *Biochim Biophys Acta - Biomembr* 1788(1):24–32.
 176. Dimova R, Seifert U, Pouligny B, Förster S, Döbereiner HG (2002) Hyperviscous diblock copolymer vesicles. *Eur Phys J E*. doi:10.1007/s10189-002-8236-8.
 177. Kučerka N, Tristram-Nagle S, Nagle JF (2006) Structure of Fully Hydrated Fluid Phase Lipid Bilayers with Monounsaturated Chains. *J Membr Biol* 208(3):193–202.
 178. Lundbæk JA, et al. (2004) Regulation of Sodium Channel Function by Bilayer Elasticity: The Importance of Hydrophobic Coupling. Effects of Micelle-forming Amphiphiles and Cholesterol. *J Gen Physiol* 123(5):599–621.
 179. Pandey A, Shin K, Patterson RE, Liu X-Q, Rainey JK (2016) Current strategies for protein production and purification enabling membrane protein structural biology. *Biochem Cell Biol* 94(6):507–527.
 180. Brassard P, et al. (2007) Modulation of T-cell signalling by non-esterified fatty acids. *Prostaglandins*,

- Leukot Essent Fat Acids* 77:337–343.
181. Vásquez V, Krieg M, Lockhead D, Goodman MB (2014) Phospholipids that Contain Polyunsaturated Fatty Acids Enhance Neuronal Cell Mechanics and Touch Sensation. *Cell Rep* 6(1):70–80.
 182. Du Y, Taylor CG, Zahradka P (2019) Modulation of endothelial cell responses and vascular function by dietary fatty acids. *Nutr Rev* 77(9):614–629.
 183. Ridone P, et al. (2018) “Force-from-lipids” gating of mechanosensitive channels modulated by PUFAs. *J Mech Behav Biomed Mater* 79:158–167.
 184. Carrillo-Tripp M, Feller SE (2005) Evidence for a Mechanism by Which ω -3 Polyunsaturated Lipids May Affect Membrane Protein Function. *Biochemistry* 44(30):10164–10169.
 185. Cordero-Morales JF, Vásquez V (2018) How lipids contribute to ion channel function, a fat perspective on direct and indirect interactions. *Curr Opin Struct Biol* 51:92–98.
 186. Hamilton JA, Kamp F (1999) How Are Free Fatty Acids Transported in Membranes? Is It by Proteins or by Free Diffusion Through the Lipids? *Diabetes* 48:2255–2269.
 187. Stillwell W, Wassall SR (2003) Docosahexaenoic acid: Membrane properties of a unique fatty acid. *Chem Phys Lipids* 126(1):1–27.
 188. Leng X, et al. (2018) All n-3 PUFA are not the same: MD simulations reveal differences in membrane organization for EPA, DHA and DPA. *Biochim Biophys Acta - Biomembr* 1860(5):1125–1134.
 189. Williams JA, et al. (2012) Docosahexaenoic and eicosapentaenoic acids segregate differently between raft and nonraft domains. *Biophys J* 103(2):228–237.
 190. Teng J, Loukin S, Anishkin A, Kung C (2015) The force-from-lipid (FFL) principle of mechanosensitivity, at large and in elements. *Pflügers Arch - Eur J Physiol* 467(1):27–37.
 191. Vitkova V, Mitkova D, Staneva G (2014) Lyso- and omega-3-containing phosphatidylcholines alter the bending elasticity of lipid membranes. *Colloids Surfaces A Physicochem Eng Asp* 460:191–195.
 192. Georgieva R, et al. (2016) Phospholipase A2-Induced Remodeling Processes on Liquid-Ordered/Liquid-Disordered Membranes Containing Docosahexaenoic or Oleic Acid: A Comparison Study. *Langmuir* 32(7):1756–1770.

193. Evans EA, Waugh R, Melnik L (1976) Elastic area compressibility modulus of red cell membrane. *Biophys J* 16(6):585–595.
194. Wiggins P, Phillips R (2005) Membrane-protein interactions in mechanosensitive channels. *Biophys J* 88(2):880–902.
195. Nakayama Y, et al. (2018) Evolutionary specialization of MscCG, an MscS-like mechanosensitive channel, in amino acid transport in *Corynebacterium glutamicum*. *Sci Rep* 8(1):1–13.
196. Zhou Y, Raphael RM (2005) Effect of salicylate on the elasticity, bending stiffness, and strength of SOPC membranes. *Biophys J* 89(3):1789–1801.
197. Jin L, Kamat NP, Jena S, Szostak JW (2018) Fatty Acid/Phospholipid Blended Membranes: A Potential Intermediate State in Protocellular Evolution. *Small* 14(15):1704077.
198. Kamat NP, Lee MH, Lee D, Hammer DA (2011) Micropipette aspiration of double emulsion-templated polymersomes. *Soft Matter* 7(21):9863–9866.
199. Simard JR, Kamp F, Hamilton JA (2008) Measuring the adsorption of fatty acids to phospholipid vesicles by multiple fluorescence probes. *Biophys J* 94(11):4493–4503.
200. Høyrup P, Davidsen J, Jørgensen K (2001) Lipid membrane partitioning of lysolipids and fatty acids: effects of membrane phase structure and detergent chain length. *J Phys Chem B* 105(13):2649–2657.
201. Roy A, Dutta R, Kundu N, Banik D, Sarkar N (2016) A Comparative Study of the Influence of Sugars Sucrose, Trehalose, and Maltose on the Hydration and Diffusion of DMPC Lipid Bilayer at Complete Hydration: Investigation of Structural and Spectroscopic Aspect of Lipid-Sugar Interaction. *Langmuir* 32(20):5124–5134.
202. Fricke K, Sackmann E (1984) Variation of frequency spectrum of the erythrocyte flickering caused by aging, osmolarity, temperature and pathological changes. *BBA - Mol Cell Res* 803(3):145–152.
203. Henriksen JR, Ipsen JH (2002) Thermal undulations of quasi-spherical vesicles stabilized by gravity. *Eur Phys J E* 9(4):365–374.
204. Faizi HA, Reeves CJ, Georgiev VN, Vlahovska PM, Dimova R (2020) Fluctuation spectroscopy of

- giant unilamellar vesicles using confocal and phase contrast microscopy. *Soft Matter* 16(39):8996–9001.
205. Rautu SA, et al. (2017) The role of optical projection in the analysis of membrane fluctuations. *Soft Matter* 13(19):3480–3483.
206. Faizi HA, Frey SL, Steinkühler J, Dimova R, Vlahovska PM (2019) Bending rigidity of charged lipid bilayer membranes. *Soft Matter* 15(29):6006–6013.
207. Tyler All, Greenfield JL, Seddon JM, Brooks NJ, Purushothaman S (2019) Coupling phase behavior of fatty acid containing membranes to membrane bio-mechanics. *Front Cell Dev Biol* 7(SEP):187.
208. Zhou Y, Berry CK, Storer PA, Raphael RM (2007) Peroxidation of polyunsaturated phosphatidylcholine lipids during electroformation. *Biomaterials* 28(6):1298–1306.
209. Yang X, Sheng W, Sun GY, Lee JCM (2011) Effects of fatty acid unsaturation numbers on membrane fluidity and α -secretase-dependent amyloid precursor protein processing. *Neurochem Int* 58(3):321–329.
210. Tulenko TN, Chen M, Mason PE, Mason RP (1998) Physical effects of cholesterol on arterial smooth muscle membranes: Evidence of immiscible cholesterol domains and alterations in bilayer width during atherogenesis. *J Lipid Res* 39(5):947–956.
211. Duraisamy Y, Lambert D, O'Neill CA, Padfield PJ (2007) Differential incorporation of docosahexaenoic acid into distinct cholesterol-rich membrane raft domains. *Biochem Biophys Res Commun* 360(4):885–890.
212. Shaikh SR, Brzustowicz MR, Gustafson N, Stillwell W, Wassall SR (2002) Monounsaturated PE does not phase-separate from the lipid raft molecules sphingomyelin and cholesterol: Role for polyunsaturation? *Biochemistry* 41(34):10593–10602.
213. Lin X, et al. (2016) Domain Stability in Biomimetic Membranes Driven by Lipid Polyunsaturation. *J Phys Chem B* 120:39.
214. Stevens MM, Honerkamp-Smith AR, Keller SL (2010) Solubility limits of cholesterol, lanosterol, ergosterol, stigmasterol, and β -sitosterol in electroformed lipid vesicles. *Soft Matter* 6(23):5882–

- 5890.
215. Portet T, Gordon SE, Keller SL (2012) Increasing membrane tension decreases miscibility temperatures; An experimental demonstration via micropipette aspiration. *Biophys J* 103(8):35–37.
 216. Hilburger CE, Jacobs ML, Lewis KR, Peruzzi JA, Kamat NP (2019) Controlling Secretion in Artificial Cells with a Membrane and Gate. *ACS Synth Biol* 8(6):1224–1230.
 217. Revskij D, et al. (2019) Dietary Fatty Acids Affect Red Blood Cell Membrane Composition and Red Blood Cell ATP Release in Dairy Cows. *Int J Mol Sci* 20(11):2769.
 218. Bryk AH, Wiśniewski JR (2017) Quantitative Analysis of Human Red Blood Cell Proteome. *J Proteome Res* 16(8):2752–2761.
 219. Smaby JM, Momsen MM, Brockman HL, Brown RE (1997) Phosphatidylcholine acyl unsaturation modulates the decrease in interfacial elasticity induced by cholesterol. *Biophys J* 73(3):1492–1505.
 220. Chakraborty S, et al. (2020) How cholesterol stiffens unsaturated lipid membranes. *Proc Natl Acad Sci* 117(36):202004807.
 221. Owen DM, Neil MAA, French PMW, Magee AI (2007) Optical techniques for imaging membrane lipid microdomains in living cells. *Semin Cell Dev Biol* 18(5):591–598.
 222. Armstrong CL, Marquardt D, Dies H, Kučerka N, Yamani Z (2013) The Observation of Highly Ordered Domains in Membranes with Cholesterol. *PLoS One* 8(6):66162.
 223. Barrett MA, et al. (2013) Solubility of cholesterol in lipid membranes and the formation of immiscible cholesterol plaques at high cholesterol concentrations. *Soft Matter* 9(39):9342–9351.
 224. Soni SP, et al. (2008) Docosahexaenoic acid enhances segregation of lipids between raft and nonraft domains: 2H-NMR study. *Biophys J* 95(1):203–214.
 225. Rajagopalan L, et al. (2007) Tuning of the outer hair cell motor by membrane cholesterol. *J Biol Chem* 282(50):36659–36670.
 226. Kamar RI, Organ-Darling LE, Raphael RM (2012) Membrane cholesterol strongly influences confined diffusion of prestin. *Biophys J* 103(8):1627–1636.
 227. Garten M, et al. (2017) Whole-GUV patch-clamping. *Proc Natl Acad Sci* 114(2):328–333.

228. Martinac B, Rhode PR, Cranfield CG, Nomura T (2013) *Patch Clamp Electrophysiology for the Study of Bacterial Ion Channels in Giant Spheroplasts of E. coli* doi:10.1007/978-1-62703-245-2_11.
229. Hollóczy O, Gehrke S (2019) Can Nanoplastics Alter Cell Membranes? *ChemPhysChem*:9–12.
230. Bochicchio D, et al. (2022) Polystyrene perturbs the structure, dynamics, and mechanical properties of DPPC membranes: An experimental and computational study. *J Colloid Interface Sci* 605:110–119.
231. Fleury JB, Baulin VA (2021) Microplastics destabilize lipid membranes by mechanical stretching. *Proc Natl Acad Sci U S A* 118(31):1–8.
232. Guzniczak E, et al. (2018) Impact of poloxamer 188 (Pluronic F-68) additive on cell mechanical properties, quantification by real-time deformability cytometry. *Biomicrofluidics* 12(4):044118.
233. Zaki AM, Carbone P (2017) How the Incorporation of Pluronic Block Copolymers Modulates the Response of Lipid Membranes to Mechanical Stress. *Langmuir* 33(46):13284–13294.
234. Dave N, et al. (2021) A novel mechanosensitive channel controls osmoregulation, differentiation, and infectivity in trypanosoma cruzi. *Elife* 10:1–32.
235. Brohawn SG, et al. (2019) The mechanosensitive ion channel TRAAK is localized to the mammalian node of Ranvier. *Elife* 8:1–22.
236. Cahalan SM, et al. (2015) Piezo1 links mechanical forces to red blood cell volume. *Elife* 4(MAY). doi:10.7554/eLife.07370.
237. Anishkin A, Loukin SH, Teng J, Kung C (2014) Feeling the hidden mechanical forces in lipid bilayer is an original sense. *Proc Natl Acad Sci* 111(22):7898–7905.
238. Keller H, Lorizate M, Schwille P (2009) PI(4,5)P₂ Degradation Promotes the Formation of Cytoskeleton-Free Model Membrane Systems. *ChemPhysChem* 10(16):2805–2812.
239. Doerner JF, Febvay S, Clapham DE (2012) Controlled delivery of bioactive molecules into live cells using the bacterial mechanosensitive channel MscL. *Nat Commun* 3(1):990.
240. Sukharev SI, Sigurdson WJ, Kung C, Sachs F (1999) Energetic and spatial parameters for gating of the bacterial large conductance mechanosensitive channel, MscL. *J Gen Physiol* 113(4):525–

- 539.
241. Sukharev SI, Blount P, Martinac B, Blattner FR, Kung C (1994) A large-conductance mechanosensitive channel in *E. coli* encoded by *mscL* alone. *Nature* 368(March):265–268.
242. Heurteaux C, et al. (2004) TREK-1, a K⁺ channel involved in neuroprotection and general anesthesia. *EMBO J* 23(13):2684–2695.
243. Xian Tao Li, et al. (2006) The stretch-activated potassium channel TREK-1 in rat cardiac ventricular muscle. *Cardiovasc Res* 69(1):86–97.
244. LaMotte RH (2016) Allergic Contact Dermatitis: A Model of Inflammatory Itch and Pain in Human and Mouse. *Translational Research in Pain and Itch*, eds Ma C, Huang Y (Springer Netherlands, Dordrecht), pp 23–32.
245. Bavi O, Vossoughi M, Naghdabadi R, Jamali Y (2014) The effect of local bending on gating of MscL using a representative volume element and finite element simulation. *Channels* 8(4):344–349.
246. Itel F, Najer A, Palivan CG, Meier W (2015) Dynamics of Membrane Proteins within Synthetic Polymer Membranes with Large Hydrophobic Mismatch. *Nano Lett* 15(6):3871–3878.
247. Goodman KE, Hare JT, Khamis ZI, Hua T, Sang QXA (2021) Exposure of Human Lung Cells to Polystyrene Microplastics Significantly Retards Cell Proliferation and Triggers Morphological Changes. *Chem Res Toxicol* 34(4):1069–1081.
248. Lolicato M, et al. (2017) K2P2.1 (TREK-1)–activator complexes reveal a cryptic selectivity filter binding site. *Nature* 547(7663):364–368.
249. Sezgin E, et al. (2012) Elucidating membrane structure and protein behavior using giant plasma membrane vesicles. *Nat Protoc* 7(6):1042–1051.
250. Perozo E, Kloda A, Cortes DM, Martinac B (2002) Physical principles underlying the transduction of bilayer deformation forces during mechanosensitive channel gating. *Nat Struct Biol* 9(9):696–703.
251. Steinkühler J, Sezgin E, Urbančič I, Eggeling C, Dimova R (2019) Mechanical properties of plasma membrane vesicles correlate with lipid order, viscosity and cell density. *Commun Biol* 2(1):1–8.
252. Cohen AE, Shi Z (2020) Do Cell Membranes Flow Like Honey or Jiggle Like Jello? *BioEssays*

- 42(1):1–13.
253. Grimmer M, Bacia K (2020) Giant Endoplasmic Reticulum vesicles (GERVs), a novel model membrane tool. *Sci Rep* 10(1):1–8.
254. Liu Z, Gandhi CS, Rees DC (2009) Structure of a tetrameric MscL in an expanded intermediate state. *Nature* 461(7260):120–124.
255. Wang Y, et al. (2014) Single molecule FRET reveals pore size and opening mechanism of a mechano-sensitive ion channel. *Elife* 3:e01834.
256. Zhang Y, et al. (2021) Visualization of the mechanosensitive ion channel MscS under membrane tension. *Nature* 590(7846):509–514.
257. Wang B, et al. (2022) Pocket delipidation induced by membrane tension or modification leads to a structurally analogous mechanosensitive channel state. *Structure*:1–15.
258. Dimova R (2014) Recent developments in the field of bending rigidity measurements on membranes. *Adv Colloid Interface Sci* 208:225–234.